Ocean Optics & Biogeochemistry Protocols for Satellite Ocean Colour Sensor Validation

IOCCG Protocol Series Volume 7.0, 2021

Aquatic Primary Productivity Field Protocols for Satellite Validation and Model Synthesis (DRAFT)

Report of a NASA-sponsored workshop with contributions (alphabetical) from:

William M. Balch	**Bigelow Laboratory for Ocean Sciences, Maine, USA**
Magdalena M. Carranza	**Monterey Bay Aquarium Research Institute, California, USA**
Ivona Cetinic	**University Space Research Association, NASA Goddard Space Flight Center, Maryland, USA**
Joaquín E. Chaves	**Science Systems and Applications, Inc., NASA Goddard Space Flight Center, Maryland, USA**
Solange Duhamel	**University of Arizona, Arizona, USA**
Zachary K. Erickson	**University Space Research Association, NASA Goddard Space Flight Center, Maryland, USA**
Andrea J. Fassbender	**NOAA Pacific Marine Environmental Laboratory, Washington, USA**
Ana Fernández-Carrera	**Leibniz Institute for Baltic Sea Research Warnemünde, Rostock, Germany**
Sara Ferrón	**University of Hawaii at Manoa, Hawaii, USA**
E. Elena García-Martín	**National Oceanography Centre, Southampton, UK**
Joaquim Goes	**Lamont Doherty Earth Observatory at Columbia University, New York, USA**
Helga do Rosario Gomes	**Lamont Doherty Earth Observatory at Columbia University, New York, USA**
Maxim Y. Gorbunov	**Department of Marine and Coastal Sciences, Rutgers University, New Jersey, USA**
Kjell Gundersen	**Plankton Research Group, Institute of Marine Research, Bergen, Norway**

Kimberly Halsey	**Department of Microbiology, Oregon State University, Oregon, USA**
Toru Hirawake	**Faculty of Fisheries Sciences, Hokkaido University, Hakodate, Japan**
Tomonori Isada	**Akkeshi Marine Station, Field Science Center for Northern Biosphere, Hokkaido University, Hokkaido, Japan**
Lauren W. Juranek	**College of Earth, Ocean, and Atmospheric Sciences, Oregon State University, Oregon USA**
Gemma Kulk	**Earth Observation Science and Applications, Plymouth Marine Laboratory, Plymouth UK**
Chris Langdon	**Rosenstiel School of Marine and Atmospheric Science, University of Miami, Florida, USA**
Ricardo Letelier	**College of Earth, Ocean and Atmospheric Sciences, Oregon State University, Oregon, USA**
Daffne C. López-Sandoval	**Red Sea Research Center, King Abdullah University of Science and Technology, Thuwal, Saudi Arabia**
Antonio Mannino	**National Aeronautics and Space Administration, NASA Goddard Space Flight Center, Maryland, USA**
John F. Marra	**Earth and Environmental Sciences, Brooklyn College, New York, USA**
Patrick Neale	**Smithsonian Environmental Research Center, Maryland USA**
David. P. Nicolson	**Marine Chemistry and Geochemistry Department, Woods Hole Oceanographic Institution, Massachusetts, USA**
Greg Silsbe	**University of Maryland Center for Environmental Science, Maryland, USA**
Rachel H. Stanley	**Department of Chemistry, Wellesley College, Massachusetts, USA**
Ryan A. Vandermeulen	**Science Systems and Applications, Inc., NASA Goddard Space Flight Center, Maryland, USA**

Edited by:

Ryan A. Vandermeulen and Joaquín E Chaves

Correct citation for this volume:

IOCCG Protocol Series (2021). Aquatic Primary Productivity Field Protocols for Satellite Validation and Model Synthesis. Balch, W.M., Carranza, M., Cetinic, I., Chaves, J.E., Duhamel, S., Erickson, Z., Fassbender, A., Fernandez-Carrera, A., Ferrón, S., García-Martín, E., Goes, J., Gomes, H., Gorbunov, M., Gundersen, K., Halsey, K., Hirawake, T., Isada, T., Juranek, L., Kulk, G., Langdon, C., Letelier, R., López-Sandoval, D., Mannino, A., Marra, J., Neale, P., Nicholson, D., Silsbe, G., Stanley, R., Vandermeulen, R.A. IOCCG Ocean Optics and Biogeochemistry Protocols for Satellite Ocean Colour Sensor Validation, Volume 7.0, edited by R.A. Vandermeulen, J. E. Chaves, IOCCG, Dartmouth, NS, Canada. http://dx.doi.org/[DOI]

Acknowledgements:

We thank the Editorial Review Board Members for their constructive comments on this document:

Member 1	Affiliation
Member 2	Affiliation
Member 3	Affiliation
Member 4	Affiliation
Member 5	Affiliation
Member 6	Affiliation
Member 7	Affiliation
Member 8	Affiliation
Member 9	Affiliation
Member 10	Affiliation

http://www.ioccg.org

Published by the International Ocean Colour Coordinating Group (IOCCG), Dartmouth, NS, Canada, in conjunction with the National Aeronautics and Space Administration (NASA).

Doi: http://dx.doi.org/[DOI]

PREFACE

In 2018, a working group sponsored by the NASA Plankton, Aerosol, Cloud, and ocean Ecosystem (PACE) project, in conjunction with the International Ocean Colour Coordinating Group (IOCCG), European Organization for the Exploitation of Meteorological Satellites (EUMETSAT), and Japan Aerospace Exploration Agency (JAXA), was assembled with the aim to develop community consensus on multiple methods for measuring aquatic primary productivity used for satellite validation and model synthesis. A workshop to commence the working group efforts was held December 05-07, 2018 at the University Space Research Association headquarters in Columbia, MD U.S.A., bringing together 26 active researchers from 16 institutions. In this document, we discuss and develop the findings of the workshop as they pertain to measurements of primary productivity, including the essential issues, nuances, definitions, scales, uncertainties, and ultimately best practices for data collection across multiple methodologies.

Top row, left to right: Solange Duhamel, Mary Jane Perry, Helga Gomes, Maxim Gorbunov, Gemma Kulk, Greg Silsbe, Roo Nicholson, Rachel Stanley, Patrick Neale, John Marra, Mark Brzezinski, Barney Balch, Tomonori Isada, Laurie Juranek, SeungHyun Son, Toru Hirawake; Bottom row, left to right: Joaquim Goes, Ana Fernandez Carrera, Antonio Mannino, Ryan Vandermeulen, Ricardo Letelier, Kimberly Halsey, Priscila Kienteca Lange, Joaquín Chaves. Other workshop participants (not pictured): Joe Salisbury, Susanne Craig, Jeremy Werdell, Paula Bontempi.

Contents

1. Reconciling Estimates of Oceanic Primary Productivity from Cells to Satellites

Ryan A. Vandermeulen[1,2], Joaquín E. Chaves [1,2], Antonio Mannino [2]

[1]*Science Systems and Applications, Inc., Maryland, USA*
[2]*NASA Goddard Space Flight Center, Maryland, USA*

1.1. Why are we doing this?

The measurement of aquatic primary productivity (PP) is inarguably central to the quantitative understanding of the global biosphere, yielding critical insights into the role and magnitude of carbon, oxygen, and other bioactive element fluxes between the ocean, the geosphere and atmosphere. The accumulation of theoretical, methodological, and technological advances from this endeavor has resulted in the development of numerous approaches to measure oceanic PP, all with the common objective of quantifying the fluxes of reduced carbon into aquatic ecosystems. While these advances have furthered the understanding of carbon dynamics, from intracellular to global scales, it is notable that perhaps no single measurement in the suite of significant oceanographic observations exhibits as much methodological diversity as well as interpretive ambiguity (Marrra 2002, del Giorgio and Williams 2005).

Methods to derive estimates of PP include, but are not limited to, incubations to measure oxygen gas accumulation/consumption (Riley 1939, Collins et al. 2018), uptake of radioactive ^{14}C (Steeman Nielsen 1952), stable ^{13}C (Slawyk et al. 1977, Slawyk 1979; Hama et al. 1993; López-Sandoval 2019), and ^{18}O (Grande et al. 1989), the isotopic composition of atmospheric and dissolved oxygen (^{16}O,^{17}O, and ^{18}O; Luz and Barkan 2009), dilution growth and grazing incubation experiments (Calbet and Landry 2004; Landry et al. 2000), underway measurements of O_2/Ar ratios (Cassar et al. 2009), the use of temporally and spatially integrated time-series from gliders or buoys (Claustre et al. 1999; Nicholson et al. 2008, Alkire et al. 2014), as well as *in situ* methods that utilize instantaneous kinetic measurements of active fluorescence to derive primary productivity estimates from electron transport rates (Kolber et al. 1998, Gorbunov and Falkowski 2021).

An assessment of the oceanic carbon flux can be attained by the power of the discrete PP measurements accumulated over the years, but the capacity afforded by satellite observations of ocean biomass and its physical environment enables the scaling up of those data into a comprehensive, global picture (National Research Council 2008). Notably, ocean color remote sensing (i.e., measurements of passive water-leaving reflectance), no matter how well characterized, can only elucidate a limited portion of the multitude of degrees of freedom that impact daily, water-column integrated rates of primary productivity. The combination of field measurements, modeling efforts, and satellite observations, even if not explicit, is the only viable path to gauge the rate of marine carbon fixation at a global scale (Brewin et al. 2021), and thus it is critical to evaluate model outputs against accurate *in situ* measurements from diverse regions (Saba et al. 2011). Though PP measurements are ubiquitous within oceanographic research, an unfortunate impact of the variability in methodological approaches is that it can serve to hinder

the interoperability and scalability of existing measurements into synthesis efforts aimed at carbon cycle modeling and satellite algorithm development.

The various techniques and approaches used for measuring PP are dependent on multiple assumptions and are prone to artifacts that can introduce significant biases between measurements (Peterson 1980; Marra 2002; Regaudie-de-Gioux et al. 2014). Moreover, variations in results extend beyond the specific parameter used to estimate the rates of carbon fixation, and can often arise from environmental or experimental variability due to temperature (Eppley 1972), source and quality of light (Kirk 2011), filtration (Sharp 1977), bottle effects (Worrest et al. 1980), length and type of incubations (Lohrenz et al. 1992), inherent assumptions about respiration and dissolved losses, the depth of the photic zone (Geider and Osborne 1992; Marra 2015), grazing (Laws et al. 2000), regenerated production (Harrison 1980), quantum yield (Morel et al. 1996), as well as mixing and air-sea exchange (Duarte et al. 2013), among a multitude of other factors. Awareness of these uncertainties makes it little surprise that results from identical samples analyzed at different laboratories have shown an average coefficient of variation on the order of 25-40% (Richardson 1991).

If these uncertainties are not fully quantified or understood, it can lead to ambiguity in the interpretation and applicability of data for subsequent global PP model validation. However, systematic and random biases can be minimized by establishing a set of best practices, and through better understanding of the assumptions and limitations of each measurement approach. The reasons above highlight the motivation to develop community consensus on protocols for various PP measurement approaches, and define the uncertainty associated with each type of measurement. Accurate determination of carbon cycle parameters is central to priorities set by international space agencies and is required for the success of current and future programs in producing climate-quality data from sea-going platforms and space borne sensors.

1.2. One step beyond

Notably, the diverse range of measurements covered in this document are resolving an equally diverse spectrum of specific metabolic processes (see Chapter 2), which can become uncoupled from one another as environmental factors as well as taxonomic diversity directly impact the efficiency with which carbon is fixed and respired, as well as the intermediate pathways therewithin. These behaviors present formidable challenges when attempting to intercompare derived rates, as any discrepancies observed between two or more measurements may be real, methodological, or simply a result of inherent biases associated with the temporal and spatial scales of measurement (Regaudie-de-Gioux et al. 2014). In fact, differing methods of assessing primary productivity are rarely, if ever, simultaneously measuring the same quantity or process at the same spatial-temporal scales (Figure 1.1), thereby propagating the impacts of the metabolic disparities. This reasonably begs the question, why issue protocols for a broad set of rate measurements that represent varying metabolic processes, instead of focusing on one “gold standard” measurement for validation of models? Is more always better?

In short, each method or approach presented in this volume elucidates distinct processes that contribute to a holistic and integrated characterization of aquatic microbial energy and carbon dynamics on Earth. Our primary goal in presenting these protocols is to normalize a variety of emerging technologies, and thus improve our simultaneous understanding of larger scale spatial-temporal dynamics as well as smaller scale cell physiology, which are intrinsically linked. We

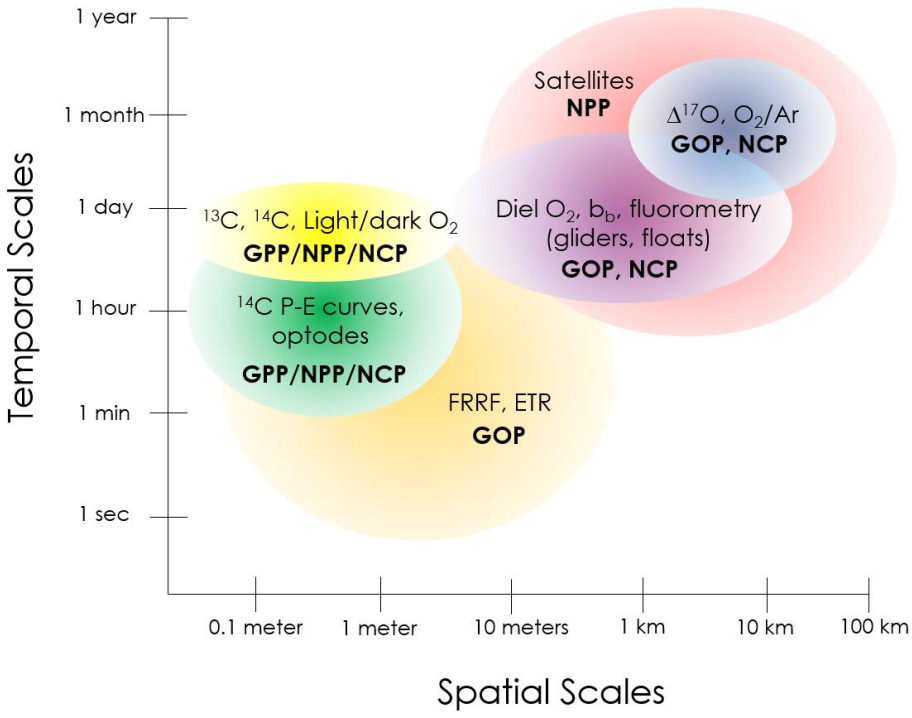

Figure 1.1. Different methods of assessing primary productivity rates in the ocean examine widely varying spatial-temporal scales as well as (potentially decoupled) metabolic processes. While integrating across scales can lead to ambiguity in absolute comparisons between methods and ecosystem processes, each approach yields valid information that contributes to a comprehensive understanding of microbial energetics and carbon dynamics.

intend for these protocols to be complementary, not competitive, to this understanding and by establishing best practices, we may leverage the assets and liabilities of each method. Thus, beyond establishing standardized best practices, we make every effort to be fully transparent about the capabilities, limitations, and impacts of the underlying assumptions inherent to each measurement.

An overarching goal of this effort is to encourage practitioners to consider their measurements in the context of recent and future advances in ocean color remote sensing technologies and their subsequent impact on understanding of primary production and associated ecosystem modeling efforts. With enhanced observational power gained from emerging sophistication in the capabilities of these technologies, there will be opportunities to directly validate what we only now empirically assume. Future geostationary orbits will make possible the measurement of diurnal changes in standing stocks of chlorophyll-*a* and phytoplankton carbon via backscatter, as well as changes in absorption efficiency throughout the day (Fishman et al. 2012). Globally-gridded hyperspectral data can yield a better understanding into the distribution of phytoplankton community composition (Werdell et al. 2019), and thus how taxonomically-dependent physiological variables are parameterized. Multi-angle polarimetry will allow the resolution of optical and microphysical properties of suspended oceanic particles, in a way that may help better determine the phytoplankton size spectra, and particle composition and morphology (Jamet et al.

2019). Sensors built with enhanced signal across the electromagnetic spectrum may enable greater practical use of natural fluorescence line height to help characterize phytoplankton physiology and nutrient stress (Behrenfeld et al. 2009) as well as elucidate global estimates of ultraviolet stress (Lee et al. 2013). Space-borne active remote sensing via LIght Detection And Ranging (LIDAR) can be optimized in such a way as to help resolve the three dimensional vertical structure of particles within the ocean (Lu et al. 2014) and vertical migration patterns (Behrenfeld et al. 2019). Future fleets of Bio-Argo floats and other autonomous platforms can provide greater *in situ* resolution of bio-optical parameters all around the globe (Johnson et al. 2009). The growing sophistication of machine learning, genetic programming, and neural networks can be robustly parameterized and tested as precisely as a laboratory experiment to help learn about subtle processes and trends in the ocean (D'Alelio 2020). To maximize the utility of current and future sensor technologies and computing power, it is imperative to examine and incorporate multiple dimensions of field data into the validation stream. We are hopeful that these protocols will prove useful to advance our conceptual understanding of global carbon dynamics in the ocean.

1.3. References

Alkire, M. B., C. Lee, E. D'Asaro, M. J. Perry, N. Briggs, I. Cetinić & A. Gray, 2014. Net community production and export from Seaglider measurements in the North Atlantic after the spring bloom. Journal of Geophysical Research: Oceans 119(9):6121-6139 doi:10.1002/2014JC010105.

Behrenfeld, M. J., Westberry, T. K., Boss, E. S., O'Malley, R. T., Siegel, D. A., Wiggert, J. D., ... & Moore, J. K. (2009). Satellite-detected fluorescence reveals global physiology of ocean phytoplankton. Biogeosciences, 6(5), 779.

Behrenfeld, M. J., Gaube, P., Della Penna, A., O'Malley, R. T., Burt, W. J., Hu, Y., ... & Doney, S. C. (2019). Global satellite-observed daily vertical migrations of ocean animals. Nature, 576(7786), 257-261.

Brewin, R. J., Sathyendranath, S., Platt, T., Bouman, H., Ciavatta, S., Dall'Olmo, G., ... & Walker, P. (2021). Sensing the ocean biological carbon pump from space: A review of capabilities, concepts, research gaps and future developments. Earth-Science Reviews, 103604.

Calbet, A. & M. R. Landry, 2004. Phytoplankton growth, microzooplankton grazing, and carbon cycling in marine systems. Limnology and Oceanography 49(1):51-57 doi:10.4319/lo.2004.49.1.0051.

Cassar, N., B. A. Barnett, M. L. Bender, J. Kaiser, R. C. Hamme & B. Tilbrook, 2009. Continuous High-Frequency Dissolved O_2/Ar Measurements by Equilibrator Inlet Mass Spectrometry. Analytical Chemistry 81(5):1855-1864 doi:10.1021/ac802300u.

Claustre, H., A. Morel, M. Babin, C. Cailliau, D. Marie, J.-C. Marty, D. Tailliez & D. Vaulot, 1999. Variability in particle attenuation and chlorophyll fluorescence in the tropical Pacific: Scales, patterns, and biogeochemical implications. Journal of Geophysical Research: Oceans 104(C2):3401-3422 doi:10.1029/98JC01334.

Collins, J. R., Fucile, P. D., McDonald, G., Ossolinski, J. E., Keil, R. G., Valdes, J. R., ... & Van Mooy, B. A. (2018). An autonomous, *in situ* light-dark bottle device for determining

community respiration and net community production. Limnology & Oceanography: Methods, 16(6), 323-338.

del Giorgio, P. & P. Williams, 2005. Respiration in Aquatic Ecosystems. Oxford University Press.

D'Alelio, D., Rampone, S., Cusano, L. M., Morfino, V., Russo, L., Sanseverino, N., ... & Lomas, M. W. (2020). Machine learning identifies a strong association between warming and reduced primary productivity in an oligotrophic ocean gyre. Scientific reports, 10(1), 1-12.

Duarte, C. M., A. Regaudie-de-Gioux, J. M. Arrieta, A. Delgado-Huertas & S. Agustí, 2013. The Oligotrophic Ocean Is Heterotrophic. Annual Review of Marine Science 5(1):551-569 doi:10.1146/annurev-marine-121211-172337.

Eppley, R. W., 1972. Temperature and phytoplankton growth in the sea. Fish Bull 70(4):1063-1085.

Fishman, J., Iraci, L. T., Al-Saadi, J., Chance, K., Chavez, F., Chin, M., ... & Eldering, A. (2012). The United States' next generation of atmospheric composition and coastal ecosystem measurements: NASA's Geostationary Coastal and Air Pollution Events (GEO-CAPE) mission. Bulletin of the American Meteorological Society, 93(10), 1547-1566.

Geider, R. J. & B. A. Osborne, 1992. Algal Photosynthesis: The Measurement of Algal Gas Exchange. Chapman and Hall.

Gorbunov, M. Y., & Falkowski, P. G. (2021). Using chlorophyll fluorescence kinetics to determine photosynthesis in aquatic ecosystems. Limnology and Oceanography, 66(1), 1-13.

Grande, K. D., P. J. L. Williams, J. Marra, D. A. Purdie, K. Heinemann, R. W. Eppley & M. L. Bender, 1989. Primary production in the North Pacific gyre: a comparison of rates determined by the 14C, O2 concentration and 18O methods. Deep Sea Research Part A Oceanographic Research Papers 36(11):1621-1634 doi:https://doi.org/10.1016/0198-0149(89)90063-0.

Hama, T., J. Hama & N. Handa, 1993. 13C Tracer Methodology in Microbial Ecology with Special Reference to Primary Production Processes in Aquatic Environments. In Jones, J. G. (ed) Advances in Microbial Ecology. Springer US, Boston, MA, 39-83.

Harrison, W. G., 1980. Nutrient Regeneration and Primary Production in the Sea. In Falkowski, P. G. (ed) Primary Productivity in the Sea. Springer US, Boston, MA, 433-460.

Jamet, C., Ibrahim, A., Ahmad, Z., Angelini, F., Babin, M., Behrenfeld, M. J., ... & Davis, A. B. (2019). Going beyond standard ocean color observations: lidar and polarimetry. Frontiers in Marine Science, 6, 251.

Johnson, K. S., Berelson, W. M., Boss, E. S., Chase, Z., Claustre, H., Emerson, S. R., ... & Riser, S. C. (2009). Observing biogeochemical cycles at global scales with profiling floats and gliders: prospects for a global array. Oceanography, 22(3), 216-225

Kirk, J. T. O., 2011. Light and Photosynthesis in Aquatic Ecosystems, Third edn. Cambridge.

Kolber, Z. S., O. Prášil & P. G. Falkowski, 1998. Measurements of variable chlorophyll fluorescence using fast repetition rate techniques: defining methodology and experimental protocols. Biochimica et Biophysica Acta (BBA) - Bioenergetics 1367(1–3):88-106 doi:http://dx.doi.org/10.1016/S0005-2728(98)00135-2.

Landry, M. R., J. Constantinou, M. Latasa, S. L. Brown, R. R. Bidigare & M. E. Ondrusek, 2000. Biological response to iron fertilization in the eastern equatorial Pacific (IronEx II) III. Dynamics of phytoplankton growth and microzooplankton grazing. Marine Ecology Progress Series 201:57-72.

Laws, E. A., M. R. Landry, R. T. Barber, L. Campbell, M.-L. Dickson & J. Marra, 2000. Carbon cycling in primary production bottle incubations: inferences from grazing experiments and photosynthetic studies using 14C and 18O in the Arabian Sea. Deep Sea Research Part II: Topical Studies in Oceanography 47(7-8):1339-1352.

Lee, Z., Hu, C., Shang, S., Du, K., Lewis, M., Arnone, R., & Brewin, R. (2013). Penetration of UV-visible solar radiation in the global oceans: Insights from ocean color remote sensing. Journal of Geophysical Research: Oceans, 118(9), 4241-4255.

Lohrenz, S. E., D. A. Wiesenburg, C. R. Rein, R. A. Arnone, C. D. Taylor, G. A. Knauer & A. H. Knap, 1992. A comparison of *in situ* and simulated *in situ* methods for estimating oceanic primary production. Journal of Plankton Research 14(2):201-221 doi:10.1093/plankt/14.2.201.

Lu, X., Hu, Y., Trepte, C., Zeng, S., & Churnside, J. H. (2014). Ocean subsurface studies with the CALIPSO spaceborne lidar. Journal of Geophysical Research: Oceans, 119(7), 4305-4317.

Luz, B. & E. Barkan, 2009. Net and gross oxygen production from O2/Ar, 17O/16O and 18O/16O ratios. Aquatic Microbial Ecology 56(2-3):133-145.

Marra, J., 2002. Approaches to the Measurement of Plankton Production Phytoplankton Productivity. Blackwell Science Ltd, 78-108.

Marra, J. F., 2015. Ocean productivity: A personal perspective since the first Liege Colloquium. Journal of Marine Systems 147:3-8 doi:https://doi.org/10.1016/j.jmarsys.2014.01.012.

Morel, A., D. Antoine, M. Babin & Y. Dandonneau, 1996. Measured and modeled primary production in the northeast Atlantic (EUMELI JGOFS program): the impact of natural variations in photosynthetic parameters on model predictive skill. Deep Sea Research Part I: Oceanographic Research Papers 43(8):1273-1304 doi:https://doi.org/10.1016/0967-0637(96)00059-3.

National Research Council, 2008. Earth Observations from Space: The First 50 Years of Scientific Achievements. The National Academies Press, Washington, DC.

Neale, P. J., Cullen, J. J., Lesser, M. P., & Melis, A. (1993). Physiological bases for detecting and predicting photoinhibition of aquatic photosynthesis by PAR and UV radiation. Photosynthetic responses to the environment, 33, 61-77.

Nicholson, D., S. Emerson & C. C. Eriksen, 2008. Net community production in the deep euphotic zone of the subtropical North Pacific gyre from glider surveys. Limnology and Oceanography 53(5part2):2226-2236 doi:10.4319/lo.2008.53.5_part_2.2226.

Peterson, B. J., 1980. Aquatic primary productivity and the 14C-CO2 method: a history of the productivity problem. Annual Review of Ecology and Systematics 11:359-385.

Regaudie-de-Gioux, A., S. Lasternas, S. Agustí & C. M. Duarte, 2014. Comparing marine primary production estimates through different methods and development of conversion equations. Frontiers in Marine Science 1:19.

Richardson, K., 1991. Comparison of ¹⁴ C primary production determinations made by different laboratories. Marine Ecology Progress Series 72(1/2):189-201.

Riley, G. A., 1939. Plankton studies II. the western North Atlantic, May-June, 1932. Journal Marine Research 2(1):145-162.

Saba, V. S., M. A. M. Friedrichs, D. Antoine, R. A. Armstrong, I. Asanuma, M. J. Behrenfeld, A. M. Ciotti, M. Dowell, N. Hoepffner, K. J. W. Hyde, J. Ishizaka, T. Kameda, J. Marra, F. Mélin, A. Morel, J. O'Reilly, M. Scardi, W. O. Smith Jr, T. J. Smyth, S. Tang, J. Uitz, K. Waters & T. K. Westberry, 2011. An evaluation of ocean color model estimates of marine primary productivity in coastal and pelagic regions across the globe. Biogeosciences 8(2):489-503 doi:10.5194/bg-8-489-2011.

Sharp, J. H., 1977. Excretion of organic matter by marine phytoplankton: Do healthy cells do it?1. Limnology and Oceanography 22(3):381-399 doi:10.4319/lo.1977.22.3.0381.

Slawyk, G., 1979. ¹³C and ¹⁵N Uptake by Phytoplankton in the Antarctic Upwelling Area: Results from the Antiprod I Cruise in the Indian Ocean Sector. Marine and Freshwater Research 30(4):431-448.

Slawyk, G., Y. Collos & J.-C. Auclair, 1977. The use of the 13C and 15N isotopes for the simultaneous measurement of carbon and nitrogen turnover rates in marine phytoplankton1. Limnology and Oceanography 22(5):925-932 doi:10.4319/lo.1977.22.5.0925.

Steeman Nielsen, E., 1952. The use of radio-active carbon (C^14) for measuring organic production in the sea. J Cons Int Explor Mer 18:117-140.

Werdell, P. J., Behrenfeld, M. J., Bontempi, P. S., Boss, E., Cairns, B., Davis, G. T., ... & Knobelspiesse, K. D. (2019). The Plankton, Aerosol, Cloud, ocean Ecosystem mission: status, science, advances. Bulletin of the American Meteorological Society, 100(9), 1775-1794.

Worrest, R. C., D. L. Brooker & H. V. Dyke, 1980. Results of a primary productivity study as affected by the type of glass in the culture bottles. Limnology and Oceanography, 25(2):360-364.

2. The Metabolic Continuum of Primary Productivity

Kimberly Halsey[1], Ricardo Letelier[2], Ryan A. Vandermeulen,[3,4]

[1] *Department of Microbiology, Oregon State University, Oregon, USA*
[2] *College of Earth, Ocean and Atmospheric Sciences, Oregon State University, Oregon, USA*
[3] *Science Systems and Applications, Inc., Maryland, USA*
[4] *NASA Goddard Space Flight Center, Maryland, USA*

2.1. Overview of components of photosynthesis

The marine ecosystem is wholly dependent on the activity of photosynthetic algae because within each algal cell most of the energy derived from light is subsequently used to convert carbon dioxide into organic material needed to build cell components (e.g., lipids, proteins, nucleic acids). Thus, photosynthetic processes initiate the marine carbon cycle. Furthermore, approximately half of the organic matter produced each day through photosynthesis is consumed by microzooplankton and other herbivorous grazers, initiating the complex marine food web. The global impacts of algae make the measurement and monitoring of their photosynthetic processes an imperative undertaking.

Photosynthesis refers to the biological conversion of light energy into chemical energy, which is used to fuel cell growth and division. There is no single metabolic step that defines photosynthesis. Rather, photosynthesis encompasses a wide range of processes initiated by light absorption by pigment complexes and transfer of energy to photosynthetic reaction centers, the site of electron excitation. In algae, the collection of photosynthetic processes includes: light energy transfer from pigments to the photosynthetic reaction centers, photosynthetic electron transport, carbon fixation via the Calvin Benson cycle, and subcellular carbon catabolism leading to cell division. Many of the fundamental biochemical processes and the connectivity of these processes are shared across algae, making it possible to characterize photosynthetic activities at the community scale.

Note that studies to dissect the tremendous diversity of bacterial and eukaryotic phytoplankton has revealed that photosynthetic activity is rarely confined to strict photoautotrophs. What this means is that while some photosynthetic algae can use light energy to fuel all of their growth processes (photoautotrophy), most algae are mixoplankton that can use dissolved organic carbon or phagocytize microbial prey in addition to photosynthesis. The ability to consume preformed organic matter ‘subsidizes’ the metabolic needs of mixoplankton. An extreme example of mixoplankton is kleptoplastidic protists that do not have the genetic capacity to produce their own chloroplasts and photosynthetic electron transport chains, but instead these organisms steal chloroplasts from their prey and use the stolen machinery for chemical energy generation. The spectrum of photosynthetic activities in aquatic microbes challenges interpretations of primary production because the relative reliance on photosynthesis vs. heterotrophy varies depending on species and environment (i.e., light, or nutrient availability). Unraveling these various activities is especially important for understanding how planktonic systems and the broader food web will respond to climate change.

2.2. Primary production: GPP to NCP

Because algae are the base of the marine food web, they are called the primary producers of the marine ecosystem. Thus, **primary production** *broadly* describes the photosynthetic activity of algae. Measurements of primary production aim to assess the rate at which energy or carbon is captured in the aquatic system. Akin to monetary accounting, the rate of light energy absorption by the algal community can be viewed as the gross energy budget that becomes available for algal growth and division over a period of time. This valuable ecosystem descriptor is called **gross primary production (GPP)**. Energy expenditures to carbon metabolism and respiration cause the remaining energy budget to be less than GPP. The extent to which energy expenditures deplete GPP in an ecosystem depends on algal physiology and the activity of the heterotrophic microbial community. The rate of carbon production after accounting for energy losses and carbon respiration by the entire microbial community is called **net community production (NCP)**. GPP and NCP describe the two endpoints of the primary production continuum (Figure 2.1).

To understand the approaches used to assess primary production requires a basic knowledge of the processes by which absorbed light energy becomes chemical energy and is then used by the cell to fuel growth and division. Here, we define the most commonly used descriptors of primary production. Note that these descriptors are not always clearly defined in the literature, challenging the interpretation of results. Thus, we hope that this document will assist in adoption of a common vocabulary for use by aquatic ecosystem scientists.

Within each algal cell, light energy is funneled to the photosystem II (PSII) reaction centers where the water-splitting reaction occurs. This canonical step in photosynthesis extracts electrons from water and simultaneously releases oxygen. The rate of oxygen evolution is thus a measure of the rate of energy (electrons) captured through the light-harvesting reactions of photosynthesis and is called **Gross Oxygen Production (GOP)**. The energized electrons are spontaneously passed through a series of electron carriers with decreasing electrochemical potentials, terminating at photosystem I (PSI). This process of photosynthetic electron transport converts electrochemical potential energy into chemical energy (ATP) through photophosphorylation.

Similar to PSII, PSI is surrounded by light absorbing pigments, which concentrate light energy at the PSI reaction center causing electrons to be re-energized to facilitate reduction of the key electron carrier, ferredoxin. There are several fates for reduced ferredoxin: (1) it is used to reduce NADP+ to form NADPH, or (2) it returns electrons to the photosynthetic electron transport chain, thus leading to continued ATP production, a process called cyclic electron transport, or (3) it can reduce O_2, which effectively promotes the proton motive force through light-dependent respiration. For biochemical and biophysical details on photosynthetic electron transport, the reader is referred to Molecular Mechanisms of Photosynthesis by Robert E. Blankenship (2014). Most of the chemical energy (ATP and NADPH) derived from photosynthetic electron transport is used for carbon fixation (CO_2 reduction into organic molecules).

Gross carbon production (GCP) is the rate at which CO_2 is converted into organic carbon by the Calvin Benson cycle. GCP is generally about 70-75% of GOP, with the difference between GOP and GCP reflecting losses of energy to rapid O_2 reduction, sometimes called water-water cycles because water was the source of the electrons delivered to the photosynthetic electron

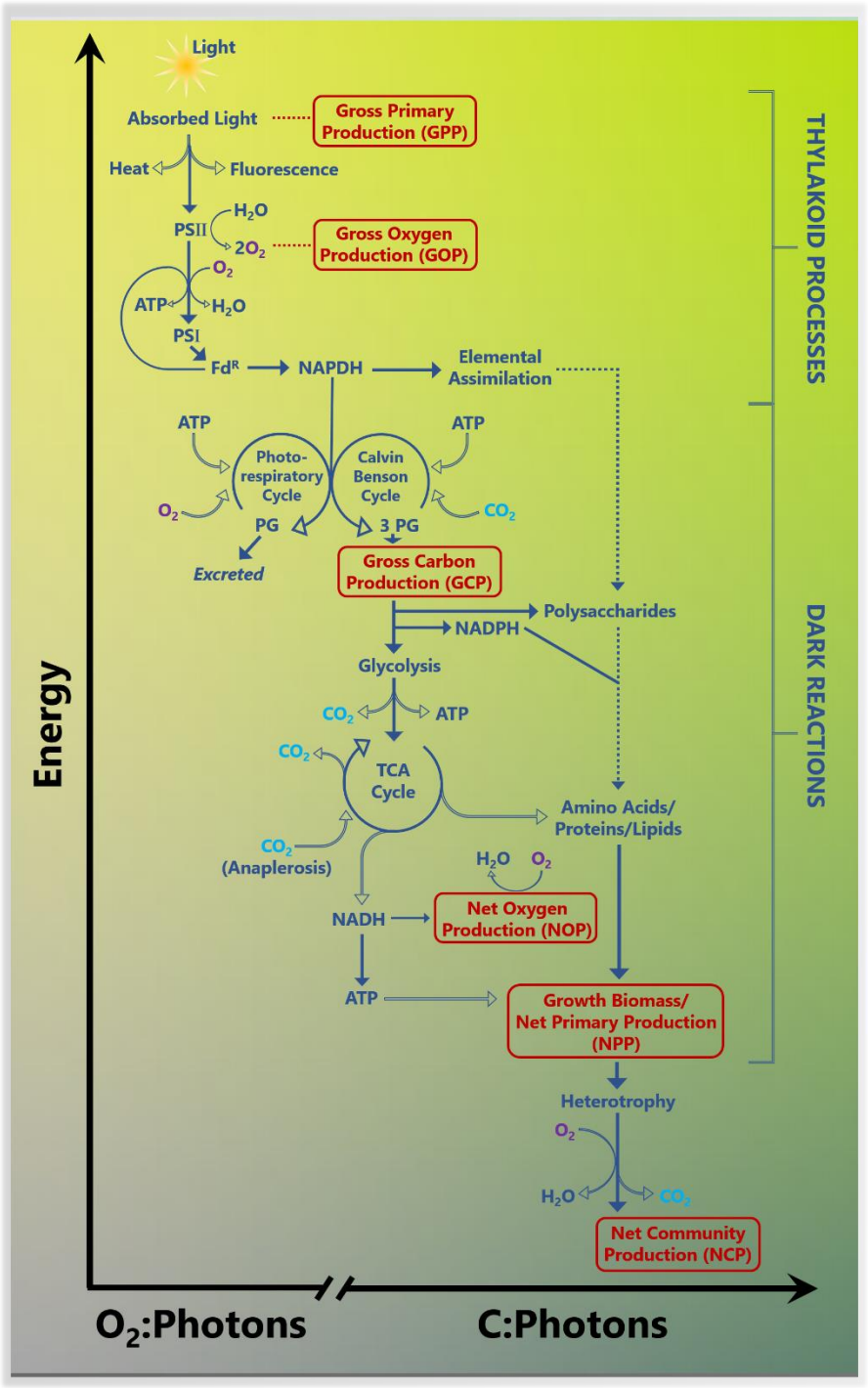

Figure 2.1: The metabolic processes contributing to the continuum of primary production are outlined as a function of solar energy utilization. The budgetary constraints on the two endpoints of this continuum, gross primary production and net community production, are dependent on varying factors influencing algal physiology and microbial heterotrophic activity.

transport chain and the return of electrons to O_2 produces water. These rapid cycles provide some cell protection from photoinhibition caused by absorption of light in excess of GCP by allowing for consumption of excess electrons. Water-water cycles are also important in maintaining proper balance in the cell's basic energetic currencies, ATP and NADPH. Some of the organic carbon produced by the Calvin Benson cycle is broken down to produce more chemical energy via glycolysis, the TCA cycle and respiratory electron transport. **Net oxygen production (NOP)** is the amount of O_2 produced after accounting for all O_2 reduced by respiration. The presence of heterotrophic microbes will further draw down the O_2 concentration, and NOP is commonly the measure used to obtain NCP (see below). Another fraction of the total organic carbon pool is catabolized to fuel biosynthesis of cell components or energy demanding processes such as DNA replication and cell division. **Net carbon production (NPP)** is the rate of organic carbon production after accounting for subcellular carbon catabolism and respiration. The relationships between GPP, GOP, GCP, NOP, and NPP can vary depending on the environment and species.

The preceding discussion largely centered on the algal cell and key descriptors of the starting points to aquatic carbon cycling. Of course, in nature algae coexist with a complex microbial community with each member taking up and respiring carbon that almost entirely originated from algal photosynthesis. Thus, in natural aquatic ecosystems, **Net community production (NCP)** is a valuable descriptor of the rate of carbon production that escapes degradation by the surface microbial community and is thus available for export into the twilight zone. NCP is commonly estimated by converting NOP determined from oxygen sensors into carbon units using an empirically-derived constant. While simple in concept, the complex milieu of dissolved organic carbon substrates and range of bacterial mechanisms employed to interact and metabolize with these substrates make accurate estimates of NCP a major challenge in aquatic ecosystem research.

2.3. Interconversions: $O_2 \rightarrow C$ via PQ and RQ

There is a suite of measurements commonly used to assess primary production. The value of these measurements depends on understanding what step in the primary production continuum is being targeted, and how cell physiology influences energy conservation. Theoretical considerations facilitate conversions between different measures of primary production. One of the most commonly applied conversions is the **photosynthetic quotient (PQ),** which refers to the molar ratio of oxygen produced to CO_2 assimilated into biomass. Thus, PQ can be used to convert oxygen production measurements to carbon production (i.e., the conversion of NOP, which is the difference between GOP and respiration, to NPP). PQ values ranging from 1.0 to 2.25 have been reported (reviewed in Williams and Robertson, 1991; Laws 1991), and a value of 1.4 is most commonly applied when nitrate is the primary source of nitrogen, while ammonia assimilation will lower the PQ because of the lower oxidation state of N in NH_4+. A range of environmental, taxonomic and metabolic factors interact to cause PQ to vary, even within a single species. For example, algae rich in lipids will have higher PQ values than those that are lipid deplete, and carbon composition is dependent on growth rate. Environments that cause growth to become imbalanced, such as rapid changes in light intensity, CO_2 or oxygen limitation, and iron limitation, may also decouple oxygen production from growth, increasing PQ beyond the canonical value of 1.4.

Another conversion factor to consider is the **respiratory quotient (RQ)**, which refers to the molar ratio of CO_2 produced per mole of oxygen consumed. Notably, the RQ varies with varying metabolic pathways, as well as the stoichiometric composition of the primary product. The value

of RQ is frequently assumed to be 1.0 (the theoretical value for complete oxidation of a simple carbohydrate), however, differing organic substrates can potentially yield RQ values ranging from 0.13–4 depending on their composition (Berggren et al. 2011). For example, substrates rich in lipid composition undergo both glycolysis and β-oxidation, and since the latter process does not yield CO_2, lipid metabolization will tend to yield a substantially lower RQ (del Giorgio and Williams 2005). If we consider a 'typical' algal cell containing 40% protein, 40% carbohydrate, 15% lipid, 5% nucleic acid ($C_1H_{1.7}O_{0.43}N_{0.12}P_{0.0046}$), this would yield a theoretical RQ of 0.89 based on stoichiometry alone (Williams and Robertson 1991, Hedges et al. 2002), and individual contributions from the above substrates would yield an RQ in the range of 0.71 – 1.23 (Rodrigues and Williams 2001). Of course, natural waters provide a more complicated reality, in which RQ values measured *in situ* can fall well below theoretical bounds (0.2 – 0.6; Münzner and Berggren 2019), perhaps as a result of additional complex biochemical processes such as nitrification or methane oxidation. In addition, not all oxygen consuming processes are directly linked with organic production/consumption (such as photorespiration or the Mehler Reaction - which is one of the "water-water cycles" described earlier) (del Giorgio and Williams 2005). Thus the RQ will ultimately vary as a function of cell physiology and environmental factors, and given the relative difficulty in executing a proper measurement of this value, researchers tend to settle on a constant RQ value, and accept a 20% margin of error (Robinson 2019).

Finally, there are a myriad of methodological considerations that can impact measurements of primary production and PQ. It appears that most artifacts are introduced during incubation-based techniques (e.g., bottle effects, intracellular and intercellular C and N recycling), and some of these are discussed with mitigating approaches later in this document. Future approaches that take advantage of incubation-independent measurements (e.g., optics, next-generation 'omics, dyes and imaging, or growth rate-dependent metabolite pools) will be of great benefit to constrain carbon fluxes on this changing planet.

Table 2.1.

Methods used to measure primary production. For methods that are not described in this protocol document, the reader is referred to the literature suggested in column four.

Ecosystem descriptor	Abbreviation	Methods	Chapter, Section, Reference
Gross primary production	GPP	Fluorescence	Chapter 9
		Chlorophyll	Chapter 10
Gross oxygen production	GOP	Triple oxygen isotopes	Chapter 7
		Membrane inlet mass spectrometry ($^{18}O_2$ and $^{16}O_2$)	Chapter 4, Kana et al. 1994, Ferron et al. 2016
		$H_2{}^{18}O$ bottle incubations	Chapter 4, Bender et al. 1987
		Fluorescence flash yields	Chapter 9
Gross carbon production	GCP	C-uptake (short incubation duration; 10-60 min for high biomass regions or ~2 h for oligotrophic regions)	Chapter 3
		By difference (GOP - light dependent respiration)	Chapters 5,6
Net oxygen production	NOP	Light-dark bottle incubations ($^{16}O_2$)	Chapter 5
		Oxygen electrodes/optodes	Chapter 6
Net primary production	NPP	C-uptake (24 h incubation, dawn-dawn)	Chapter 3
		Product of cell carbon (C_{phyto}) and growth rate (m)	C_{phyto}: Graff et al. 2012 m: Landry et al., 1995
		N-assimilation rate	Eppley et al. 1977
		Satellite and optics-derived models	Behrenfeld and Falkowski, 1997 Westberry et al. 2008 Silsbe et al. 2016 Fox et al. 2020
Net community production	NCP	O_2/Ar ratios	Chapter 8
		Optics or biogeochemcial sensor derived estimates	Chapter 10

2.4. References

Behrenfeld, M. J., & Falkowski, P. G. (1997). Photosynthetic rates derived from satellite-based chlorophyll concentration. Limnology and oceanography, 42(1), 1-20.

Bender, M., Grande, K., Johnson, K., Marra, J., Williams, P. J. L., Sieburth, J., ... & Heinemann, K. (1987). A comparison of four methods for determining planktonic community production 1. Limnology and Oceanography, 32(5), 1085-1098.

Berggren, M., Lapierre, J. F., & Del Giorgio, P. A. (2011). Magnitude and regulation of bacterioplankton respiratory quotient across freshwater environmental gradients. The ISME journal, 6(5), 984-993.

Blankenship, R. E. (2014). Molecular mechanisms of photosynthesis. John Wiley & Sons.

del Giorgio, P., & Williams, P. (Eds.). (2005). Respiration in aquatic ecosystems. OUP Oxford.

Eppley, R. W., Sharp, J. H., Renger, E. H., Perry, M. J., & Harrison, W. G. (1977). Nitrogen assimilation by phytoplankton and other microorganisms in the surface waters of the central North Pacific Ocean. Marine Biology, 39(2), 111-120.

Ferrón, S., del Valle, D. A., Björkman, K. M., Quay, P. D., Church, M. J., & Karl, D. M. (2016). Application of membrane inlet mass spectrometry to measure aquatic gross primary production by the 18O in vitro method. Limnology and Oceanography: Methods, 14(9), 610-622.

Fox, J., Behrenfeld, M. J., Haëntjens, N., Chase, A., Kramer, S. J., Boss, E., ... & Halsey, K. H. (2020). Phytoplankton growth and productivity in the Western North Atlantic: observations of regional variability from the NAAMES field campaigns. Frontiers in Marine Science.

Graff, J. R., Milligan, A. J., & Behrenfeld, M. J. (2012). The measurement of phytoplankton biomass using flow-cytometric sorting and elemental analysis of carbon. Limnology and Oceanography: Methods, 10(11), 910-920.

Hedges, J. I., Baldock, J. A., Gélinas, Y., Lee, C., Peterson, M. L., & Wakeham, S. G. (2002). The biochemical and elemental compositions of marine plankton: A NMR perspective. Marine Chemistry, 78(1), 47-63.

Kana, T. M., Darkangelo, C., Hunt, M. D., Oldham, J. B., Bennett, G. E., & Cornwell, J. C. (1994). Membrane inlet mass spectrometer for rapid high-precision determination of N2, O2, and Ar in environmental water samples. Analytical Chemistry, 66(23), 4166-4170.

Landry, M. R., Kirshtein, J., & Constantinou, J. (1995). A refined dilution technique for measuring the community grazing impact of microzooplankton, with experimental tests in the central equatorial Pacific. Marine ecology progress series. Oldendorf, 120(1), 53-63.

Münzner, K., & Berggren, M. (2019). *In situ* plankton community respiration measurements show low respiratory quotients in a eutrophic lake. Environmental microbiology, 21(4), 1425-1435.

Robinson, C. (2019). Microbial respiration, the engine of ocean deoxygenation. Frontiers in Marine Science, 5, 533.

Rodrigues, R. M., & Williams, P. J. L. B. (2001). Heterotrophic bacterial utilization of nitrogenous and nonnitrogenous substrates, determined from ammonia and oxygen fluxes. Limnology and oceanography, 46(7), 1675-1683.

Silsbe, G. M., Behrenfeld, M. J., Halsey, K. H., Milligan, A. J., & Westberry, T. K. (2016). The CAFE model: A net production model for global ocean phytoplankton. Global Biogeochemical Cycles, 30(12), 1756-1777.

Westberry, T., Behrenfeld, M. J., Siegel, D. A., & Boss, E. (2008). Carbon-based primary productivity modeling with vertically resolved photoacclimation. Global Biogeochemical Cycles, 22(2).

Williams, P. I., & Robertson, J. E. (1991). Overall planktonic oxygen and carbon dioxide metabolisms: the problem of reconciling observations and calculations of photosynthetic quotients. Journal of plankton Research, 13(supp1), 153-169.

3. Carbon-Based Incubations

^{14}C section:

Gemma Kulk[1], Ana Fernández Carrera[2], William M. Balch[3], John F. Marra[4], Patrick Neale[5], and Solange Duhamel[6]

[1]Earth Observation Science and Applications, Plymouth Marine Laboratory, Plymouth, UK
[2]Leibniz Institute for Baltic Sea Research Warnemünde, Rostock, Germany
[3]Bigelow Laboratory for Ocean Sciences, Maine, USA
[4]Earth and Environmental Sciences, Brooklyn College, New York, USA
[5]Smithsonian Environmental Research Center, Maryland USA
[6]University of Arizona, Arizona, USA

^{13}C section:

Tomonori Isada[1], Ana Fernández Carrera[2], Toru Hirawake[3], Joaquim Goes[4], Daffne C. López-Sandoval[5], Solange Duhamel[4,6]

[1]Akkeshi Marine Station, Field Science Center for Northern Biosphere, Hokkaido University, Hokkaido, Japan
[2]Leibniz Institute for Baltic Sea Research Warnemünde, Rostock, Germany
[3]Faculty of Fisheries Sciences, Hokkaido University, Hakodate, Japan
[4]Lamont Doherty Earth Observatory at Columbia University, New York, USA
[5]Red Sea Research Center, King Abdullah University of Science and Technology, Thuwal, Saudi Arabia
[6]University of Arizona, Arizona, USA

3.1. Introduction

This chapter deals with carbon-based primary production measurements using various incubation methods with the radioisotope ^{14}C and the stable isotope ^{13}C. First, a short history of the two tracer techniques is provided (section 3.1.1 and 3.1.2). Then, supplies and reagents are discussed in separate sections for ^{14}C (section 3.2.1) and ^{13}C (section 3.2.2) measurements, followed by a detailed explanation of shipboard sampling procedures (section 3.3.1) and three different incubation methods that can be used for both ^{14}C and ^{13}C measurements, i.e., *in situ* incubations (section 3.3.2), on-deck, simulated *in situ* incubations (section 3.3.3) and photosynthesis-irradiance incubations (section 3.3.4). Sample processing and analysis is discussed in separate sections for ^{14}C (section 3.4.1) and ^{13}C (section 3.4.2) measurements and these sections also provide information on the calculation of photosynthetic rates and the advantages, disadvantages, and caveats of both carbon tracer methods. Post-processing of carbon-based measurements, including photosynthesis-irradiance models and depth-integrated primary production calculations, is discussed in section 3.5. Additional methods for carbon-based measurements, including dissolved organic carbon (DOC) production, cell-specific techniques and calcification, micro-diffusion techniques are provided towards the end of this chapter (section 3.6). Finally, ancillary measurements that should be collected in addition to ^{14}C and ^{13}C measurements are discussed in section 3.7.

3.1.1. History of ^{14}C methods

In 1952, E. Steemann Nielsen published his "^{14}C technique" (Steemann Nielsen 1952). He submitted a first manuscript while conducting measurements aboard the Galathea expedition (1950-1952) to illustrate its efficacy and thereby introduced a new means to understand ocean productivity. ^{14}C had only been discovered about 10 years earlier and in the late 1940s was used by Calvin in his classic experiments on carbon pathways in photosynthesis (Barber and Hilting 2002). Steemann Nielsen's method was to add ^{14}C as labeled sodium bicarbonate to a sample of seawater and after an incubation period in the light, assay the amount of ^{14}C appearing in particulate matter filtered out of the sample. The rate of photosynthesis was defined as the proportion of ^{14}C in the organic matter relative to the amount of inorganic ^{14}C added, times the concentration of dissolved inorganic carbon in the seawater.

The advantage of the ^{14}C method for measuring photosynthetic carbon assimilation in the ocean is its extreme sensitivity. Earlier methods, notably the analysis of oxygen changes in incubated samples, simply cannot discriminate the small changes in O_2 characteristic of many regions of the ocean. The second advantage is the method's relative facility. It requires, in addition to the isotope, only a means to separate off the particulate matter from the seawater, and a means to assay the radioactivity. Handling ^{14}C at the activities used is safe, requiring no special equipment. Although aboard ship, precautions for all radioisotopes must be taken to ensure the ship itself does not become contaminated.

The "Carbon-14 Method," as it came to be known, heralded a new era in the study of ocean productivity. The measurement got to the source of primary productivity in the ocean, the rate of photosynthesis in phytoplankton. After some early controversy in the 1950s (Peterson 1980), the Carbon-14 Method became widely adopted and by the 1960s, global maps of primary productivity based on ^{14}C were being produced for publication (Koblentz-Mishke et al. 1970). One of the corollaries to the extreme sensitivity to the Carbon-14 Method is that it could not be validated or compared with other measurements. Perhaps that, and the ease with which the measurements could be made, is why it took a while to recognize significant concerns (Marra 2002). However, in the late 1970s, criticisms were being made regarding the effects of incubation, of respiration, the activities of heterotrophs, etc. Some of these concerns persist to this day.

Nevertheless, much progress has been made using the ^{14}C method for determining oceanic primary production and we can identify a series of 'milestones' in its use after its introduction by Steemann Nielsen (1952):

- 1957 Meeting of the International Council for the Exploration of the Sea produces the first map of the productivity of the ocean.
- 1970 Wide publication of the 'Koblentz-Mishke' map of ocean productivity (Koblentz-Mishke et al. 1970).
- 1979-1982 The VERTEX program establishes 'trace metal clean' methods for the measurement of plankton rate processes in the ocean (Fitzwater et al. 1982).
- 1982-1985 The program Planktonic Rate Processes in the Ocean (PRPOOS) establishes methodological comparisons among various measures of primary production and identifies errors associated with other than clean methods.

- 1989-1999 The Joint Global Ocean Flux Study (JGOFS) establishes international methodological protocols for measuring primary production.
- 2002 The conference "Plankton Production in Aquatic Environments" (and book by Williams et al., 2002) commemorates the 50th anniversary of the introduction of the ^{14}C technique.

It is important to note the contribution by JGOFS. Not only did that program establish international protocols, it produced a body of data that used a consistent method over a wide range of oceanic conditions (JGOFS 1992).

The ^{14}C method remains the pre-eminent means of measuring oceanic productivity. To be sure, there are now other means of estimating productivity, for example through measurements of fluorescence kinetics or the isotopic composition of surface waters.

3.1.2. History of ^{13}C methods

The ^{13}C tracer method, initially developed for phytoplankton cultures by Slawyk et al. (1977) and later modified by Hama et al. (1983) for natural seawater samples, has been employed to determine primary production rates of natural phytoplankton communities in a wide range of environments, including oligotrophic open ocean waters. The ^{13}C tracer method is based on the same principle as the radioactive carbon (^{14}C) labeling method (Steemann Nielsen 1952) in that the sample is enriched (with $NaH^{13}CO_3$) and the uptake of CO_2 into particulate organic matter (POC) is followed, in this case by tracking changes of the ^{13}C:^{12}C ratio of POC relative to the total inorganic carbon pool (Cullen 2001).

The main difference between both tracer techniques is that we measure a ratio of isotopic abundances in the sample with the ^{13}C tracer method, while we estimate an absolute amount of isotope with the ^{14}C tracer method (Collos and Slawyk 1985). Thus, the ^{13}C tracer technique requires information on the ^{13}C:^{12}C of POC before and after the incubation to estimate phytoplankton photosynthetic rates. Additionally, because mass-spectrometric methods used for quantifying stable isotopes are generally less sensitive than scintillation counters for radioactive compounds, the ^{13}C tracer method requires larger sample volumes and incubation times in excess of an hour. Yet, despite the inherent methodological differences, several studies have shown a good agreement between ^{13}C- and ^{14}C-sodium bicarbonate uptake rates (Slawyk et al. 1977, 1979, 1984; Hama et al. 1983; Sakamoto et al. 1984; Collos and Slawyk 1985; Mousseau et al. 1995; Regaudie-de-Gioux et al. 2014; López-Sandoval et al. 2018).

The recent introduction of the continuous–flow system of flash combustion for elemental analysis, coupled with a stable isotope ratio mass spectrometer (EA-IRMS) and the advent of new laser absorption techniques (e.g., cavity ring-down spectroscopy), now make it possible to measure the isotope ratio of a sample with a small amount of POC (Brenna et al. 1998) and accurately quantify aquatic primary production by using ^{13}C (López-Sandoval et al. 2019). Thus, with these advances in mass spectrometric methods, the ^{13}C labeling method is gaining importance as a reliable alternative to the ^{14}C method for measuring phytoplankton photosynthetic rates. Furthermore, because the ^{13}C tracer method does not involve the handling of radioactive substances, it does not suffer from restrictive regulations that are becoming a significant impediment for radioactive compound usage in some countries.

3.2. Supplies and reagents

Trace metal clean techniques should be used for primary production measurements wherever possible (JGOFS 1996; Cutter et al. 2010). Polyethylene gloves are recommended at all times, from the time of sample collection to sample preparation prior to incubation and filtration. Powder free latex and nitrile gloves can be used as well, but nitrile gloves should be rinsed with clean water prior to use.

3.2.1. ^{14}C measurements

3.2.1.1. Sampling and incubation bottles

The generally accepted containers for collecting water subsamples before ^{14}C incubation are 10 L opaque polycarbonate (PC) bottles, for example Nalgene™ round or rectangular PC ClearboyTM bottles with closure or spigot (2251-0020, 2317-0020; 2322-0020, DS2213-0020; Thermo Scientific). In order to prevent any contamination by trace metals that could enhance or diminish phytoplankton growth (Fitzwater et al. 1982), all sampling bottles are washed with a dilute solution of trace metal free, non-ionic detergent, followed by thorough rinsing with deionized water, and then soaking in 5-10% HCl solution for more than 24 hours. After that, the bottles are rinsed at least 3 times with MilliQ water. Different types of incubation bottles can be used for ^{14}C measurements, depending on the bottle characteristics and the aim of the study. An overview of the different incubation bottles is provided in Table 3.1. Incubation bottle volumes generally range from 10-250 mL, depending on the incubation method (*in situ*, on-deck, simulated *in situ* or photosynthesis-irradiance curves), available phytoplankton biomass and expected productivity. Trace metal-clean techniques should also be followed in the use of incubation bottles, i.e., (new and re-used) bottles are soaked overnight in 5-10% HCl and thoroughly rinsed 3 times with MilliQ water before use.

Table 3.1.

Overview of incubation bottles and their characteristics available for the use of ^{14}C primary production measurements. Volumes generally range from 10-250 mL.

Type of bottle or flask	UV transparent?	Price	Non-contaminating?	Comments
Polycarbonate bottles	Yes	$-$$	Yes, if cleaned properly with 5-10% HCl	
Polystyrene cell-culture flasks	No	$	Yes	Can be discarded after use
Polysulfone tissue-culture flasks	Yes	$	Yes	
Pyrex glass bottles	No	$$$	Yes, if cleaned properly with 5-10% HCl	Contamination with Si possible
Quartz bottles	Yes	$$$	Yes	
Teflon bottles	Yes	$$$	Yes	

3.2.1.2. Filters

The selection of the material, diameter and pore size of the filters used for ^{14}C measurements depends on the aim of the study and practicalities such as the size of the filtration setup. Options include Glass Fiber Filters (GF/F; ~0.7 µm pore size), polycarbonate or cellulose filters (from 0.2 µm pore size), with 25 and 47 mm being the most-used diameter for filtration funnels. Traditionally, ^{14}C samples would be filtered onto GF/F (JGOFS 1996) to conform to other methods, but there are two drawbacks that should prevent the use of this type of filters:

- Retention of autotrophic biomass may be lower compared to other filters due to the relative large pore size of traditional GF/F (~0.7 µm, Whatman) and GF-75 (0.35 µm, Advantec^{TM}). This is especially relevant in oligotrophic regions.
- An unknown amount of dissolved organic carbon, likely produced during the incubation and labelled with ^{14}C, can adsorb to the GF/F (Maske and Garcia-Mendoza 1994), which makes even GF-75 not suitable for ^{14}C measurements.

Polycarbonate or cellulose filters with small pore sizes (from 0.2 µm) are therefore recommended. The diameter of the filter depends on the size of the filtration setup, the incubation volume, and phytoplankton biomass in the sample, with the notion that 25 mm filters will require less scintillation cocktail (and therefore produce less waste).

3.2.1.3. Reagents

The following reagents and chemicals are required for ^{14}C-based primary production measurements:

- *^{14}C Sodium-bicarbonate ($NaH^{14}CO_3$)* is available in sealed glass ampoules containing 1 mCi (37 MBq) or 5 mCi (185 MBq) in aqueous solution from several vendors (including product NEC086H001MC from Perkin Elmer).
- *A high-capacity radioactive CO_2 absorber*, such as Ethanolamine, Phenethylamine or Carbosorb®, is used to trap ^{14}C labelled CO_2 for measuring activity in the working (stock) solution (available from Perkin Elmer, product 6013721).
- *Scintillation cocktail*, different types of scintillation cocktails can be used, including those that accommodate aqueous solutions (e.g., Ultima Gold XR, Perkin Elmer; Eco-Lume, MP Biomedicals) or dissolve membrane filters (Ultima Gold MV, Perkin Elmer). Other scintillation cocktails are suitable for long-term (1-2 months) storage of samples (e.g., InstaGel Plus, Perking Elmer). Each scintillation cocktail has different counting efficiencies and quench characteristics, which will have to be corrected for during scintillation counting (see section 3.4.1.2).
- *Hydrochloride acid (HCl)*, fuming 37% or 1 N, is used for trace-metal clean working and to vent off excess $NaH^{14}CO_3$ after incubation of the samples.
- *Sodium Hydroxide (NaOH)*, 1 N, is used to control the pH in the working solution and to (optionally) adjust the pH of the incubation samples after acidification.

Table 3.2.

Information is provided to determine the final concentration of ^{14}C for *in situ*, on-deck, simulated *in situ* or photosynthesis-irradiance incubations. As a general guidance, the final concentration of ^{14}C in the incubation sample is increased at low phytoplankton biomass, when low photosynthetic rates are expected (for example due to nutrient limitation or low temperatures) or when also measuring calcification in parallel.

Oceanic region	Phytoplankton biomass	Final concentration ^{14}C	
		$\mu Ci\ mL^{-1}$	$kBq\ mL^{-1}$
Coastal, upwelling	High	0.05-0.3	1.85-11.1
Oligotrophic	Low	0.1-0.4	3.7-14.8
Polar Regions	Variable	0.5-0.6	18.5-22.2

3.2.1.4. ^{14}C working solution

The specific activity of the ^{14}C bicarbonate working (stock) solution depends on the desired final activity during incubation, which is related to phytoplankton biomass and environmental conditions (Table 3.2). The content of the $NaH^{14}CO_3$ ampoule can be directly (undiluted) transferred to a non-contaminating, screw-cap Teflon bottle or diluted with MilliQ water (adjusting the pH to 8-9 with NaOH) and then transferred to a non-contaminating, screw-cap Teflon bottle. An activity of 100 $\mu Ci\ mL^{-1}$ is usually a good working solution for a variety of oceanic environments. The ^{14}C working solution should be stored at 4 ºC. Note that opening of the glass ampoule on ice (i.e., low temperatures) will prevent excess loss of radioactivity.

Total activity in the working solution is measured every time an experiment is performed. Approximately 1 µCi of the working solution (10 µL for a working solution of 100 $\mu Ci\ mL^{-1}$) is added to a pre-prepared scintillation vial with 100 µL of a high capacity radioactive CO_2 absorber. Scintillation cocktail is added (in the same volume of the incubation samples, section 3.4.1.1) and the vials are vigorously shaken to mix all reagents. Alternatively, for determining the total added activity in the incubation samples, a subsample from selected incubation samples could be collected and added to scintillation vials that contain an empty filter and a high-capacity radioactive CO_2 absorber, after which scintillation cocktail is added. Samples can be assayed by liquid scintillation counting after chemo-luminescence subsides (1-2 h).

3.2.1.5. Sample enrichment

The seawater sample is transferred to the incubation bottles in the desired volume (2-250 mL) and each incubation sample and the dark samples are enriched with ^{14}C bicarbonate (final concentration 0.05-0.6 $\mu Ci\ mL^{-1}$ or 1.85-22.2 $kBq\ mL^{-1}$; Table 3.2). Alternatively, the total volume for the incubation (including dark samples) can be enriched with ^{14}C bicarbonate and the enriched seawater samples can be transferred to incubation bottles afterwards. The latter method is more practical for low incubation volumes (<10 mL). Monochannel or repeating pipettes with sterile tips are recommended for enriching samples. After enrichment, samples are gently mixed. All handling of samples is performed under *in situ* temperatures (±2 ºC) and low light conditions.

3.2.2. ^{13}C measurements

3.2.2.1. Sampling and incubation bottles

The generally accepted containers for collecting water subsamples before ^{13}C incubation are 10 L opaque polycarbonate (PC) bottles, for example Nalgene™ round or rectangular PC Clearboy™ bottles with closure or spigot (2251-0020, 2317-0020; 2322-0020, DS2213-0020; Thermo Scientific). In order to prevent any contamination by trace metals that could enhance or diminish phytoplankton growth (Fitzwater et al. 1982), all sampling bottles are washed with a dilute solution of trace metal free, non-ionic detergent, followed by thorough rinsing with deionized water, and then soaking in 5-10% HCl solution for more than 24 hours. After that, the bottles are rinsed at least three times with MilliQ water.

For ^{13}C *in situ* and on-deck, simulated *in situ* incubations, we recommend acid-washed PC bottles, for example Nalgene™ Narrow-Mouth Square Bottle (2015-series) or Large Narrow-Mouth Round Bottle (2205-series). Larger volumes (>1 L) are preferred, but in case of water budgeting issues we recommend a volume of at least 0.25 L for coastal eutrophic waters, 2 L for oligotrophic waters and 4 L for ultra-oligotrophic ecosystems. For ^{13}C photosynthesis-irradiance incubations, non-treated polystyrene culture flasks and PC bottles are the preferred choice of incubation containers, but tissue polystyrene cell culture flasks are also acceptable. The volume of the flasks and bottles is typically 250 mL and can vary depending on the design of the incubator (section 3.3.4.3). All incubation bottles are to be acid washed and rinsed with MilliQ water similar to the procedure described for the sampling bottles.

3.2.2.2. Filters

Glass Fiber Filters (Whatman GF/F with ~0.7 pore size) with a diameter of 25 or 47 mm are recommended for all ^{13}C measurements. Advantec™ GF-75 (~0.3 µm pore size) is also acceptable. All filters should be pre-combusted at 450 ºC for 4 h before use.

3.2.2.3. Reagents

Sodium bicarbonate enriched to 99% with the stable isotope ^{13}C ($NaH^{13}CO_3$) is available from a variety of vendors, including Cambridge Isotope Laboratories Inc. (product CLM-441). Hydrochloric acid *(*HCl, fuming 37% or 1 N) is used for trace-metal clean working and to vent off excess $NaH^{13}CO_3$ after incubation of the samples.

3.2.2.4. ^{13}C working solution

The recommended solution is prepared by dissolving 0.1 g of ^{13}C-sodium bicarbonate in 25 mL of MilliQ water in a 25 mL acid-clean volumetric flask for a final concentration of 0.05 µM. The solution is then transferred to a 50 mL centrifuge tube (50 mL screw cap tube, SARSTEDT) and kept refrigerated at 4 ºC (do not freeze) until use.

3.2.2.5. Sample enrichment

A solution of ^{13}C-sodium bicarbonate roughly equivalent of ca. 5-10% of the total dissolved inorganic carbon (DIC) in the seawater is added to each incubation light and dark bottle. For example, assuming the DIC concentration of a sample is 2081 µM (~25,000 mg C m^{-3}), if 1 mL of the ^{13}C working solution described above is added to a 0.5 L of seawater by pipette (e.g., Eppendorf, Sartorius, etc.), then the atom percentage of ^{13}C in the total DIC is ca. 5.7%.

3.3. Incubation methods

3.3.1. Shipboard sampling procedure

Following trace-metal clean sampling techniques, Niskin-X bottles and silicone tubing should be cleaned with a 5-10% HCl solution before the start of the cruise or field campaign. To prevent inhibition of phytoplankton activity during sampling, toxic rubber (nitrile rubber for O-rings) and metals should not be attached to the Niskin-X bottles. Viton O-rings generally have less effect on phytoplankton than nitrile O-rings (Price et al. 1986; Williams and Robertson 1989; Matsumoto et al. 2012).

At each station, seawater samples are collected from selected depths using Niskin-X bottles attached to a CTD rosette. For *in situ* and on-deck, simulated *in situ* incubations, it is recommended to sample 8 depths distributed through the entire euphotic zone from the surface to ca. 0.2-1% of incident light at the surface (JGOFS 1996). For *in situ* incubations, the sampling and incubation depths can be evenly distributed or selected according to the profiles provided by the CTD (density, temperature, fluorescence, oxygen).

Prior to sampling for the primary production incubation, separate samples for dissolved inorganic carbon (DIC) analysis are to be carefully collected directly from the Niskin-X bottles with a clean silicon tube into 250 mL acid-cleaned and combusted borosilicate bottles (see section 3.2.1.1 and 3.2.2.1), leaving a headspace of 1% of the bottle volume to allow for water expansion. DIC samples are then poisoned with 50-100 µL of saturated mercuric chloride solution. Glass or quartz bottles are sealed with lightly silicone greased glass stoppers or some alternate gas-tight fashion and stored in a cool, dark location until analysis. Further details of the sampling and analytical procedure are described by Dickson et al. (2007). DIC measurements are particularly important in coastal ecosystems that come under the influence of river discharge or by melting sea ice in high latitude ocean ecosystems like the Arctic and Antarctic Oceans. If a CO_2 coulometer system or a closed-cell potentiometric titrator with pH meter is not available, DIC concentration could be empirically calculated by salinity.

After collection of the DIC samples, seawater for the primary production incubation is collected by gently draining the contents of the Niskin-X bottles into 10 L acid-clean PC carboys after triple rinsing. Alternatively, the incubation bottles can be filled directly from the Niskin-X bottles using acid-washed non-contaminating silicone tubing. In the case of the samples from depth, it is important to adequately shield the samples from the high irradiance and higher temperatures at the surface. This can be done by wrapping the 10 L PC carboys with black plastic bags and transferring the samples into coolers. Transfer of samples from the 10 L PC carboys into the incubation bottles followed by addition of the ^{14}C or ^{13}C labelled $NaHCO_3$ solution is done in the dark at *in situ* temperatures (±2 ºC).

Additionally, triplicate samples for time zero activity should be collected immediately after the sampling at the station. Details on filtration methods are provided in section 3.4.1.1 for ^{14}C and section 3.4.2.1 for ^{13}C methods. It is important to note the exact volume of water filtered for time zero activity in the ^{13}C method, this will depend on the system studied, but as a guidance, a distinctly colored filter should contain enough biomass of seston to define the ^{13}C:^{12}C ratio accurately. Any ancillary measurements (section 3.7) should also be collected at this time.

3.3.2. In situ incubations

In situ incubations with ^{14}C and ^{13}C are the closest representation of what happens in the ocean's euphotic zone and are recommended in the JGOFS protocol (JGOFS 1996). The advantages of the *in situ* incubation method are clear with temperature structure and light quality being adequately matched during the incubation. There is no need to obtain information on light or temperature at depth as would be the case for on-deck, simulated *in situ* incubations. Yet, care must be taken in interpretation of results if the physico-chemical structure of the water column changes throughout the day. The need for station-keeping near a drifting buoy must be weighed against other shipboard activities. However, such provisions should be made if productivity is a major objective for a field campaign.

3.3.2.1. Time of sampling

Water sampling should be carried out before sunrise if the incubation is conducted from dawn to dusk (~12-14 h). If ship operations are not flexible, water sampling could be done at any time of the day and enriched samples can be incubated for 24 h. In the latter case, it would also be possible to incubate from the time of sampling until dusk, assuming linearity in photosynthetic rates throughout the day, allowing for the calculation of a daily rate. This assumption was tested in some ocean regions (Marañón et al. 2005), but it should not be taken as a universal rule and test experiments in specific regions are strongly recommended. Alternatively, a correction factor can be applied (Moutin et al. 1999, Duhamel et al. 2007).

3.3.2.2. Incubation duration

The duration of the incubation is a critical factor in determining primary production with or without autotrophic respiration. JGOFS protocols (JGOFS 1996) originally advised 24 h, dawn to dawn incubations, whereas later protocols advised ~12-14 h, dawn to dusk incubations to estimate net primary production (Marra 2009). Both incubation periods can provide useful information and comparing the two methods allows for an estimate of autotrophic respiration (Marra and Barber 2004) which might otherwise not be amenable to direct measurement.

3.3.2.3. Sample incubation

At each depth, a total of 3 light and 1-2 dark bottles are recommended for the incubation. It is important to fill the bottles with the same volume of water, but the presence of a headspace does not affect the uptake of bicarbonate. There are several options for creating dark bottles, including wrapping bottles in several layers of black electrical or duct tape or aluminum foil or using a thick black cloth to prevent light penetration. If aluminum foil is used, bottles should be checked regularly for any damages to the foil as reflection of light inside the bottles can sustain relevant primary production.

Once samples have been enriched with ^{14}C- or ^{13}C-bicarbonate, the incubation bottles are securely hooked by plastic cable ties to the appropriate position of the mooring system in a coordinated fashion to match each sampling depth. The floats and strobe flash are attached to the top and the weights to the bottom of the mooring system. If the incubation is conducted from dawn to dusk, the system should be deployed before sunrise and recovered after sunset.

Figure 3.1. An example of an on-deck, simulated *in situ* incubator with re-circulating water baths (left) and the incubator covered with blue tarpaulin during the night (right).

3.3.3. On-deck, simulated **in situ** *incubations*

On-deck simulated *in situ* incubations with ^{14}C and ^{13}C are an alternative to *in situ* incubations when for example it is not possible to keep near drifting buoys due to other shipboard activities (Figure 3.1). On-deck, simulated *in situ* incubations require information on light and temperature throughout the water column prior to the start of the incubation, which is often collected the day before the incubation to allow enough time to adjust the incubator settings. As with *in situ* incubations, care has to be taken in interpretation of the results if the physico-chemical structure of the water column changes throughout the day.

3.3.3.1. Time of sampling

Water sampling should be carried out before sunrise if the incubation is conducted from dawn to dusk (~12-14 h). If ship operations are not flexible, water sampling could be done at any time of day and incubated for 24 h (see section 3.3.2.1 for more details).

3.3.3.2. Incubation duration

Samples are typically incubated for ~12-14 h from dawn to dusk or for 24 h from the time of sampling. The same considerations that have been discussed for *in situ* incubations (section 3.3.2.2) apply to on-deck, simulated *in situ* incubations.

3.3.3.3. On-deck incubator design

Incubator designs for on-deck, simulated *in situ* incubations can vary, but generally incubations are carried out in plexiglass containers that represent the water column conditions at each sampling depth (Figure 3.1). Temperature in the incubator is regulated by running surface seawater through the incubator for surface samples and adjusted using re-circulating water baths for the other sampling depths. Light levels reaching the incubation bottles can be adjusted by covering the incubation containers with a combination of blue and neutral photographic filters (Table 3.3, Figure 3.1) or by covering the incubation bottles with neutral density bags (no spectral correction for lower depths). If bottles are stacked in the incubator, the low irradiances bottles (1-5% of surface irradiance) are placed on the bottom and the high irradiance bottles (50-100% of surface

Table 3.3

Combination of Lee filters* for simulating the intensity (in percentage of surface irradiance) and spectral quality of light in an on-deck, simulated *in situ* incubator.

% Irradiance	# Layers of filter	
	Lee HT061 Mist blue	Lee 210 Neutral density
100	0	0
55	1	0
33	2	0
20	3	0
14	4	0
7	2	1
4.5	3	1
3	4	1
2	2	2
1	3	2
0.5	4	2

*http://www.leefilters.com/lighting/colour-list.html

irradiance) are placed on top. During 24 h incubations, it is recommended to cover the plexiglass incubators with a heavy duty thick black cloth or a plastic tarp overnight. This keeps samples shaded, regardless of the ship's operations and lights during the night. Additionally, photosynthetically active radiation (PAR, 400-700 nm) above the surface in the incubator should be regularly checked and preferably measured continuously using a quantum sensor connected to a data logger (e.g., the LI-190R/LI-1500 system, LI-COR). The achieved proportion of surface irradiance in the incubator should be checked during the set up of the system by comparing incident PAR with that inside the various incubation containers, which can be measured using a scalar PAR sensor (for example a QSL-2100 from Biospherical instruments or a US-SQS/L from Walz). This allows for the adjustment for the effects of reflection from surfaces near the incubator and refraction through the incubator walls.

3.3.3.4 Sample incubation

For each sampling depth, a total of 3 light and 1-2 dark bottles are recommended for the incubation. It is important to fill the bottles with the same volume of water. The presence of a headspace in the bottles does not affect the uptake of bicarbonate, but the incubation bottles will float if the headspace is large, and the bottles should be ballasted to stay underwater in the incubator. There are several options for creating dark bottles, including wrapping bottles in several layers of black electrical/duct tape or aluminum foil or using a thick black cloth to prevent light penetration. If aluminum foil is used, bottles should be checked regularly for any damages to the foil as reflection of light inside the bottles can sustain relevant primary production. Once samples

have been enriched with ^{14}C- or ^{13}C-bicarbonate, the incubation bottles can be placed in the on-deck incubator for the chosen incubation time.

3.3.4. Photosynthesis-irradiance incubations

Photosynthesis–irradiance (PE) incubations can provide a means of comparing the photosynthetic characteristics of marine phytoplankton across different natural populations and cultured isolates (Bouman et al. 2018). The relationship between photosynthesis and light can be fitted to different mathematical equations and can be described by just two parameters, while a third parameter is needed if photoinhibition is present (also see section 3.5.1.2) (Jassby and Platt 1976; Platt et al. 1980; Sakshaug et al. 1997). The chlorophyll-normalized PE parameters may be applied in the estimation of primary production over large scales by using ocean-color remote-sensing derived maps of chlorophyll *a* (Sathyendranath et al. 1995; Antoine and Morel 1996).

3.3.4.1. Time of sampling

It is recommended that samples are collected before noon, as photosynthetic parameters may vary significantly throughout the day with a maximum at around noon (Babin et al. 1995; Anning et al. 2000; Behrenfeld et al. 2008). Sample collection later during the day is also possible, but care has to be taken in interpretation of results and the use of PE parameters in further analysis as variations in PE parameter estimates could affect the calculation of daily primary productivity (Isada et al. 2013; Kulk et al. 2020).

3.3.4.2. Incubation duration

Short incubations are preferred, with times ranging from 0.5-1 h for high biomass regions and 2-3 h for oligotrophic regions. Photosynthesis versus irradiance incubations should be less than 4 h to prevent the effects of photoacclimation processes (Lewis and Smith 1983).

3.3.4.3. Photosynthesis-irradiance incubator design

Photosynthesis-irradiance incubations are performed in a so-called photosynthetron, in which sea water samples are incubated against a gradient of light. Photosynthetron designs vary to accommodate different incubation bottle volumes, but all have a light source and a recirculating water-bath to control temperature. It is advised to keep temperatures within ±2 ºC of *in situ* temperatures. Different photosynthetron designs are available in Lewis and Smith (1983), Babin et al. (1994) and Kyewalyanga et al. (1997). A common incubator design is one with all black Plexiglas® walls, except for the wall facing the light source (Figure 3.2).

3.3.4.4. Incubator lamp and light gradient

Light sources that provide photosynthetically active radiation (PAR, 400-700 nm) in high intensities (>2,000 µmol photons m^{-2} s^{-1}; which is equivalent to solar irradiance at the sea surface on a bright sunny day; Mobley 1994) and have a spectrum close to solar irradiance are preferred. A range of light sources may be used, including tungsten halogen, halogen, metal halide and fluorescent lamps (brands include Philips, OSRAM and ILT; for an overview see Bouman et al. 2018). Tungsten halogen lamps are the most commonly used, because they can provide high light intensities, but their spectrum is heavily weighted towards the red and infrared and will require spectral correction (see section 3.5.1.1).

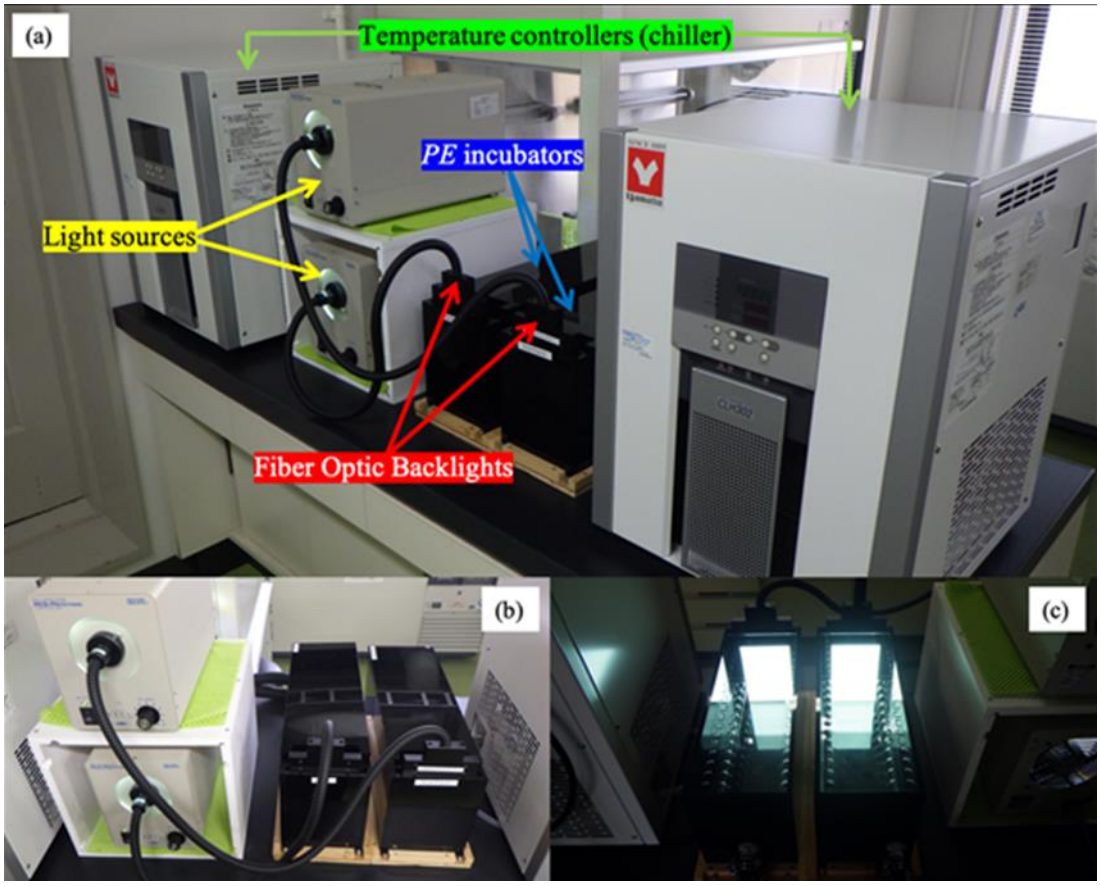

Figure 3.2. An example of photosynthetron used for photosynthesis-irradiance (PE) incubations with two incubators connected to a light source and temperature controller. A) Shows the complete setup, B) shows the front of the PE incubators and C) shows the inside of the PE incubators.

A gradient of light can be created using neutral density filters (i.e., Lee and Rosco filters, metal screen, black cheese cloth), either in the incubator or by covering the incubation bottles. The PAR gradient within the incubators is generally adjusted to range between 1-2,500 µmol photons m^{-2} s^{-1} for surface samples and between 1-500 µmol photons m^{-2} s^{-1} for subsurface chlorophyll maximum samples, also depending on the oceanic region. The light gradient should contain at least 20 different light levels, with sufficient low light levels (1/3 of total) to correctly estimate α^B (section 3.5.1.2). Three additional places should be available for dark incubations. PAR reaching the incubation bottles should be measured and regularly checked using a scalar PAR sensor (for example a QSL-2100 from Biospherical instruments or a US-SQS/L from Walz).

A further refinement in the incubator design is to use one or more types of spectral filters. Similar to on-deck, simulate *in situ* incubations, broad-band blue filters like the Lee and Rosco gel filters are sometimes used to better approximate *in situ* irradiance (e.g., Bouman et al. 2018). Despite their visual appearance, these filters still have high transmission in the red. A more spectrally specific approach is to define different regions of the PAR spectrum with interference filters placed between the lamp and incubation containers, which is most practically done for

small-volume incubations. Lewis et al. (1985) used a photosynthetron with twelve 25 nm bandpass filters to define an action spectrum of photosynthesis for open ocean assemblages. On the other hand, long-pass cut-off filters in combination with a full spectrum light source (e.g., xenon bulb) are used to resolve the spectral dependence of UV inhibition (Cullen et al. 1992; Neale et al. 2014). Long-pass filters better emulate the spectral variation of UV in the ocean, which should always be added to a background of high PAR.

3.3.4.5. Sample incubation

Once samples have been enriched with ^{14}C- or ^{13}C-bicarbonate, the light and dark incubation bottles are placed in the photosynthetron for the chosen incubation time. It is important to turn the photosynthetron on approximately 30-60 minutes prior to the incubation so the appropriate temperature and light settings are reached at the start of the incubation.

3.4. Sample processing and analysis

3.4.1. ^{14}C measurements

3.4.1.1. Filtration and pretreatment of samples for analysis

After *in situ*, on-deck, simulated *in situ* or photosynthesis-irradiance incubations, the ^{14}C enriched samples (including dark samples) are filtered and further processed. Selection of the material, diameters and pore size of the filters depends on the aim of the study and practicalities such as the size of the filtration setup (details in section 3.2.1.5). Options include GF/F, polycarbonate or cellulose filters with 25 and 47 mm being the most used diameter for filtration funnels. Samples can be filtered on standard vacuum filtration rigs (dedicated to radioactive work only) using low vacuum pressure (<50 mm Hg or <0.006 MPa). For measuring total or size-fractionated particulate organic carbon (POC) production, the entire volume of the incubation bottles is filtered. The filtration procedure for the measurement of dissolved organic carbon (DOC) along with POC is detailed in section 3.6.1, with more details in IOCCG (2021).

After filtration, filters are acidified for 24 h to remove excess ^{14}C-bicarbonate and ^{14}C-calcium carbonate. To this end, filters can be placed in open Eppendorf vials on a tray or directly on a tray that is placed in an enclosed container (for example a glass desiccator) with fuming HCl (1-2 mL, 37%) or 100 µL HCl (1 N) can be added to the filters directly in a scintillation vial. If not acidified in a scintillation vial, filters are then placed in a plastic or glass scintillation vial (6 or 20 mL, depending on the filter diameter and scintillation counter) and scintillation cocktail is added. Enough scintillation cocktail should be added to cover the filter (3.5-10 mL). Vials are vigorously shaken and stored in the dark for an additional 24 h before counting.

3.4.1.2. Sample analysis

It is recommended that samples are counted as soon as possible, i.e., at sea or in the field. The activity of ^{14}C is measured using a liquid scintillation counter. Different types of liquid scintillation counters are available that may have preselected programs for counting ^{14}C in Disintegrations Per Minute (DPM). It is recommended that a ^{14}C quenching curve is generated for the specific scintillation vial, scintillation cocktail and filter used in the incubation (for example using the 'Internal Standard Kit for Liquid Scintillation Counting' from Perkin Elmer). Samples should be counted using a dual ending mode based on time (>180 s) or precision (1% threshold error).

3.4.1.3. Storage recommendations

Once scintillation cocktail is added, filtered and acidified samples can be stored for several weeks before activity decreases due to the loss of performance of the scintillation cocktail. Samples can be stored for longer periods of time (1-2 months) if a scintillation cocktail suitable for long storage is used (for example InstaGel Plus, Perking Elmer). Samples should be stored in the dark and preferable at low temperature (4 ºC, check specifications of the scintillation cocktail) to prevent degradation, evaporation and leakage of ^{14}C.

3.4.1.4. Calculation of photosynthetic rates

Measured ^{14}C activity (in DPM) in all samples of the *in situ* and on-deck, simulated *in situ* incubations are converted to daily rates of primary production (P in mg C m^{-3} d^{-1}) following JGOFS protocol (1996):

$$P = \frac{DPM_S \times 1.05 \times DIC \times V_T}{V_S \times t \times DPM_T} \quad (3.1)$$

where DPM_S is the activity in the incubation sample (in DPM), V_S is the volume of the incubation sample (in L), 1.05 is a correction factor for the lower uptake of ^{14}C compared with ^{12}C, DIC is the concentration of dissolved inorganic carbon (in mg C m^{-3}, approximately 25,000 mg C m^{-3} for oceanic regions), V_T is the volume of the total activity (working solution) sample (in L), V_S is the volume of the incubation sample (in L), t is time (in d) and DPM_T is the total activity in the working solution sample. For final primary production rates, triplicate values of P are averaged for each sampling depth and (mean) P values in the dark incubation are subtracted. The separate reporting of daily primary production rates in the light and dark incubations is often a requirement by data repositories (such as SeaBASS, BCO-DMO and PANGAEA; also see section 3.8). If this is not the case, final daily primary production rates at each depth can also be calculated directly using Equation (3.1) by replacing DPM_S by [DPM_S - DPM_{dark}] with DPM_{dark} as the (mean) activity in the dark incubations (in DPM) (Banse 1993). Daily depth-integrated primary production (mg C m^{-2} d^{-1}) can be calculated using the trapezoidal rule (see section 3.5.2).

For photosynthesis-irradiance incubations, measured ^{14}C activity (in DPM) in each incubation bottle are converted to chlorophyll *a* normalized photosynthetic rates (P^B in mg C mg Chl-a^{-1} h^{-1}) following:

$$P^B = \frac{(DPM_S - DPM_D) \times 1.05 \times DIC \times V_T}{V_S \times t \times Chl \times DPM_T} \quad (3.2)$$

where DPM_S is the activity of the incubation sample (in DPM), DPM_D is the (mean) activity of the dark samples (in DPM), 1.05 is a correction factor for the lower uptake of ^{14}C compared with ^{12}C, DIC is the concentration of dissolved inorganic carbon (in mg C m^{-3}, approximately 25,000 mg C m^{-3} for oceanic regions), V_T is the volume of the total activity (working solution) sample (in mL), V_S is the volume of the incubation sample (in mL), t is time of the incubation (in h), Chl is the chlorophyll *a* concentration of the incubation samples (in mg m^{-3}), and DPM_T is the total activity in the working solution sample (in DPM).

3.4.1.5. Calibration, uncertainties, and accuracy

Calibration of ^{14}C measurements is not possible, but they can be compared with results from other methods such as O_2 fluxes. There are a few limits on carbon assimilation based on physiology (Platt and Jassby 1976; Platt et al. 1980; Sakshaug et al. 1997). For example, it has been determined that the assimilation number P^B_m cannot exceed 25 mg C mg Chl-a^{-1} h^{-1} (Falkowski 1981) and higher values should be viewed with suspicion. Another physiological limit is provided by the maximum quantum yield of carbon fixation (Φ_m), which theoretically cannot exceed 0.125 mol C mol quanta^{-1} (Platt and Jassby 1976; Sakshaug et al. 1997). This value is based on the long-standing quantum requirement for the evolution of oxygen, where it takes 8 quanta to evolve 1 molecule of O_2.

Scintillation counters have advanced to the stage where their results can be easily accepted and standard procedures should be followed to convert counts per minute to disintegrations per minute and to correct for quenching (section 3.4.1.2).

3.4.1.6. Advantages, disadvantages, and caveats

The advantage of the ^{14}C method is its extreme sensitivity. There are no ocean environments where the method fails in its usage. The high specific activity of ^{14}C-bicarbonate and the low concentration of unlabeled bicarbonate in seawater (2.2 mM) allows ^{14}C-bicarbonate to be added to seawater samples at true tracer concentrations. The high specific activity also means that ^{14}C incubations can be performed in small-volume samples allowing many samples to be processed and treated at once such as in photosynthesis-irradiance experiments. Moreover, the specific activity of ^{14}C is high enough that single cell experiments can be performed with reasonable signal-to-noise, especially when cells can be sorted with flow cytometers (see section 3.6.2). The ^{14}C method can also be combined with the radioactive isotope of phosphorus (^{33}P) (Duhamel et al. 2006), making it possible to measure the carbon and phosphate uptake by phytoplankton simultaneously. Finally, the ^{14}C method is relatively easy and the activity of ^{14}C used in the incubations is safe.

Yet, ^{14}C is a radioactive isotope and employed at orders of magnitude greater than natural abundances. Therefore, shipboard use requires isolation and care in handling so as not to contaminate the ship for other natural abundance uses such as radiocarbon dating, circulation studies and other geochemical research. The high sensitivity of the ^{14}C technique also translates to more regulations, difficulties and cost in safe handling of radioisotopes in experiments in the natural environment and in management of waste. This is particularly true when shipping radioisotopes and waste across international borders. Research institutes may have a dedicated health and safety department that can assist in training and handling of radioisotopes on expeditions, with established protocols for monitoring contamination. However, some countries have prohibited or restricted the use of radioisotopes, which limits the use of the ^{14}C method in some coastal and oceanic regions.

There is also the question of what the ^{14}C method measures along the scale running from gross primary production to net community production (Marra 2002). The ^{14}C method measures assimilation into particulate matter and depending on how long the phytoplankton population is exposed to the isotope, the ^{14}C method will estimate gross (~minutes), net primary (minutes to

hours) or net community production (24 h). At longer times, and at isotope equilibrium, the ^{14}C method can provide an estimate of carbon biomass.

3.4.2. ^{13}C measurements

3.4.2.1. Filtration and pretreatment of samples for analysis

At the end of the incubation, samples are gently vacuum filtered (< 0.013 MPa) onto pre-combusted (450 ^{o}C for 4 h) GF/F. The filtration cups are carefully rinsed with filtered seawater for collecting all particles in the walls and to rid the sample of excess ^{13}C labelled $NaHCO_3$. The filters are placed in petri dishes or 2 mL cryovials and stored at -80 ^{o}C in a deep freezer or in liquid nitrogen until analysis. The filters are then exposed to fuming HCl in a fume hood for removing unincorporated ^{13}C-bicarbonate or incorporated ^{13}C-calcium carbonate, then transferred into pre-combusted (450 ^{o}C for 4 h) glass Petri dishes. Alternatively, ca.100 µL of 10% or less HCl can directly be added to the filters. Following this process, the filters are dried at least 24 h in a desiccator (Figure 3.3).

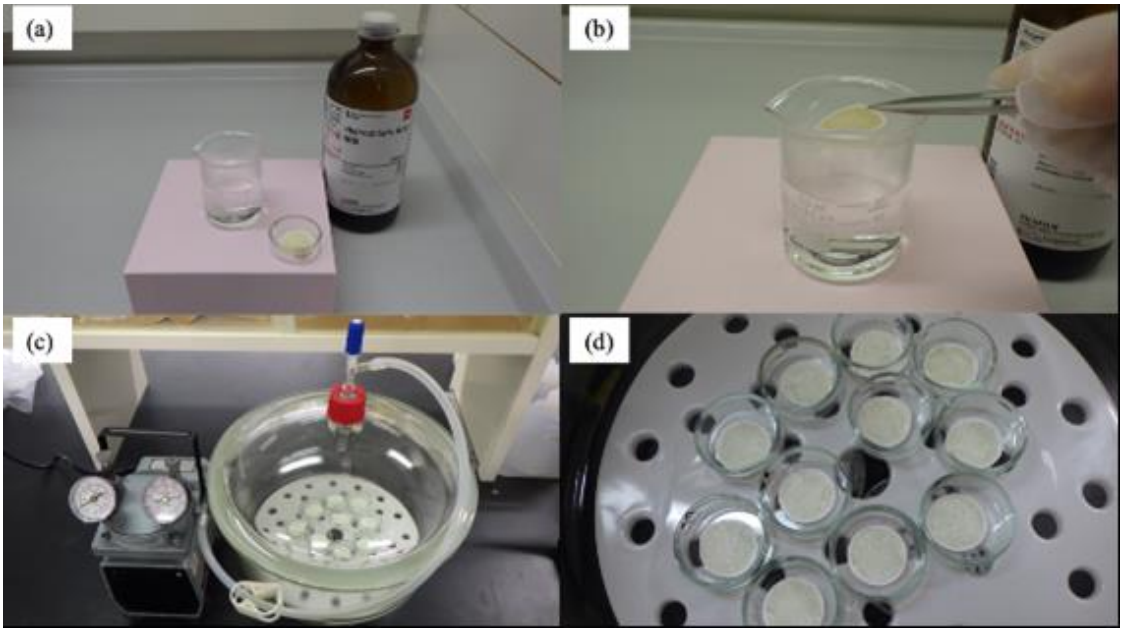

Figure 3.2. Examples of the pre-treatment of ^{13}C samples with (a) the preparation of HCl in a draft chamber, (b) the exposure of filter to HCl fume, (c) the DURAN desiccator with Millipore Vacuum/Pressure Pump for desiccating the filters, and (d) the HCl exposed and dried samples on the pre-combusted glass petri dishes.

Finally, the filters should be pelletized prior to analysis in the mass spectrometer (Figure 3.4). The filter is pelletized in pressed tin capsules (10x10 mm). The final pellet should be as small as possible and cylindrical, and no holes or breakages should be observed in the capsule after pelletizing. As a rule of thumb, if the pellet fits loosely into a 48 wells plate, it is well done.

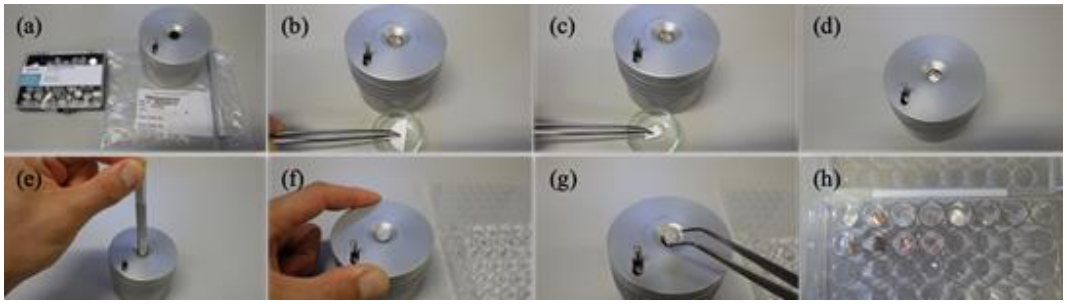

Figure 3.3. An example for pelletizing filters from ^{13}C incubations with the sealing device (Thermo Fisher Scientific, product 25209010).

3.4.2.2. Sample Analysis

Samples can be processed with an elemental analyzer coupled with a stable isotope ratio mass spectrometer (EA-IRMS) or by using laser absorption spectroscopic techniques (Cavity Ring-Down Spectroscopy, CRDS). The measurement of the particulate organic matter and the ^{13}C:^{12}C ratio of the samples can be conducted by both systems, i.e., EA-IRMS or by CRDS. There are several instruments available, including the ANCA-GSL elemental analyzer (Sercon), the Delta V with Flash2000 and the ConFlo IV (Thermo Scientific) and the CM-CRDS (Picarro, Inc.). We recommend measuring the carbon content of pre-combusted GF/F (at least three filters) as a blank.

The CM-CRDS consists of three components: The combustion module (Costech Analytical Technologies Inc., California, USA), the interface, and the Cavity Ring-Down Spectrometer analyzer (CM-CRDS G2201-i, Picarro, Inc., Santa Clara CA, USA). After loading the samples into the auto-sampler attached to the combustion module, it is important to specify the time that each sample will be processed. Although the time must be assessed according to the origin of the samples, 600 s is a good starting point (further details in López-Sandoval et al. 2019).

3.4.2.3. Storage recommendations

After filtration, filters can be placed in petri dishes or 2 mL cryovials and stored at -80 ºC or liquid nitrogen until further analysis.

3.4.2.4. Calculation of photosynthetic rates

Photosynthetic rates based on the ^{13}C tracer technique are determined using the method of Hama et al. (1983). The isotopic balance of ^{13}C and ^{12}C in the enriched sample and the ^{13}C in the sample after incubation are as follows:

$$a_{is} \times POC = a_{ns} \times (POC - \Delta POC) + a_{ic} \times \Delta POC \quad (3.3)$$

where a_{is} is the atom percentage of ^{13}C in the incubated light or dark sample, a_{ns} is the atom percentage of ^{13}C in the natural sample, a_{ic} is the atom percentage of ^{13}C in the total inorganic carbon, *POC* (in mg C m^{-3}) is particulate organic carbon in the incubated sample and ΔPOC (in mg C m^{-3}) is the increase in *POC* during the incubation. The ^{13}C atom percentage of natural POC samples used is 1.1%. The photosynthetic production (ΔPOC) is then calculated by rearranging Equation (3.3) for ΔPOC:

$$\Delta POC = POC \times \frac{(a_{is} - a_{ns})}{(a_{ic} - a_{ns})} \quad (3.4)$$

The photosynthetic rate (P in mg C m^{-3} h^{-L} or mg C m^{-3} d^{-1}) can be obtained following:

$$P = \frac{\Delta POC}{t} \times f \quad (3.5)$$

where t (in h or d) is the incubation time and f is the discrimination factor of ^{13}C, of which the value is a debated point (see section 3.4.2.5). This calculation is made for each incubation bottle and subsequently the triplicate light bottles are averaged. The mean production values in the light bottles are subtracted by the production value of the dark bottle (or mean if multiple dark bottles) for each depth. Depth-integrated primary production within the euphotic layer (mg C m^{-2} d^{-1}) is calculated by the trapezoidal rule (see section 3.5.2).

3.4.2.5. Calibration, uncertainties, and accuracy

Equation (3.5) assumes that the changes in a_{is} by non-algae carbon during the incubation period are minimal. However, bacterial uptake and zooplankton grazing during the incubation period may alter the atom percentage of ^{13}C in the sample, which could affect the calculation of photosynthetic rates measured with either carbon protocols (Karl et al. 1998; Teira et al. 2001; Collos et al. 2014). The adsorption effect becomes negligible as sample sizes increase (>1 L samples) (López-Sandoval et al. 2018). Although the enrichment of ^{13}C within the range from 5-15% of total DIC has little effect on the photosynthetic rate (Hama et al. 1983), the fixed values of discrimination factors (1.02 or 1.025 for the ^{13}C method) could bias the photosynthetic rate estimate, because the carbon isotopic fractionation varies among species and groups of phytoplankton, cell geometry and growth condition (Fry 1996; Popp et al. 1998; Close 2019). In practice, the correction factor is usually not applied (i.e., f = 1), because the correction has little significant effect on the uptake rate compared with ^{14}C methods (Slawyk et al. 1979; Hama et al. 1993).

3.4.2.6. Advantages, disadvantages, and caveats

One of the main advantages of the ^{13}C method is that it does not pose potential radioactive contamination and health safety concerns as opposed to the ^{14}C method. Moreover, the ^{13}C tracer techniques can be combined with other stable isotopes that are typically used for phytoplankton physiological rate measurements, for example with ^{15}N labelled solutions of nitrogenous nutrients or nitrogen gas (NO_3^-, NO_2^-, NH_4^+, Urea and N_2). The dual stable isotope method thus permits measurement of not only carbon, but also nitrogenous nutrients uptake rates. Care has to be taken in the application of the ^{13}C protocol for dual stable isotope measurements as the acidification method might affect the analysis of the stable isotope ratios of nitrogen ($\delta^{15}N$) (Brodie et al. 2011a; b). Finally, the larger bottles used in the ^{13}C method reduce "bottle effect" problems associated with smaller size incubation bottles typically used in the ^{14}C method.

A disadvantage of using ^{13}C tracer techniques lies in the sensitivity of the method. Since mass spectrometric measurements of ^{13}C are less sensitive than scintillation counting of ^{14}C, the stable isotope technique requires larger sample volumes and longer incubation times compared to the latter. It is important to note that this is changing, however, as mass spectrometers are becoming more sensitive. Another disadvantage is that the costs of the consumable supplies for EA-IRMS are expensive and it requires more user training. However, CRDS could overcome these problems (López-Sandoval et al. 2019).

3.5. Post processing

3.5.1. Photosynthesis-irradiance models

3.5.1.1. Spectral correction of incubator light source

The spectral distribution of the incubation light source affects the value of the initial slope of the photosynthesis-irradiance curve (α^B) and a correction for the spectral quality is required to compare results from incubations using different types of light sources (Kyewalyanga et al. 1997; Bouman et al. 2018). A correction factor (X) can be used to calculate α^B under a spectrally neutral ("white") light environment and can be determined by using the following equation:

$$X = \frac{\bar{a}_P}{\bar{a}_L} \tag{3.6}$$

where $\bar{a}_P$ is the unweighted mean absorption coefficient of phytoplankton and $\bar{a}_L$ is mean absorption coefficient weighted by the shape of the emission spectrum of the light source:

$$\bar{a}_P = \frac{\int_{400}^{700} a_P(\lambda) d\lambda}{\int_{400}^{700} d\lambda} \tag{3.7}$$

and

$$\bar{a}_L = \frac{\int_{400}^{700} a_P(\lambda) E_L(\lambda) d\lambda}{\int_{400}^{700} E_L(\lambda) d\lambda} \tag{3.8}$$

where E_L is the normalized lamp irradiance spectrum. To obtain spectrally corrected irradiance levels for each incubation bottle, the irradiance intensity in the photosynthetron is multiplied by the correction factor X. Further spectral corrections may be necessary to estimate in situ photosynthesis at depths for which the ambient light spectrum deviates substantially from white light (Cullen et al. 2012).

3.5.1.2. Estimation of photosynthesis-irradiance parameters

Photosynthesis-irradiance (PE) measurements can be fitted to a variety of mathematical equations in which the PE parameters are estimated (Figure 3.5) (Jassby and Platt 1976; Platt et al. 1980). The three-parameter function of Platt et al. (1980) is the most commonly used equation in the presence of photoinhibition:

$$P^B(E) = P_s^B \left(1 - \exp\left(-\frac{\alpha^B E}{P_s^B}\right)\right) exp\left(-\frac{\beta^B E}{P_s^B}\right) \tag{3.9}$$

where P^B (in mg C mg Chl-a^{-1} h^{-1}) is the chlorophyll *a* normalized photosynthetic rate, E (in µmol photons m^{-2} s^{-1}) is the scalar irradiance, $P^B{}_s$ (in mg C mg Chl-a^{-1} h^{-1}) is the hypothetical maximum photosynthetic rate in the absence of photoinhibition, α^B (in mg C mg Chl-a^{-1} h^{-1} [µmol photons m^{-2} s^{-1}]$^{-1}$) is the initial slope of the PE curve and β^B (in mg C mg Chl-a^{-1} h^{-1} [µmol photons m^{-2} s^{-1}]$^{-1}$) is the photoinhibition parameter describing the decrease in the photosynthetic rate at high irradiance. Values of the maximum photosynthetic rate ($P^B{}_m$ in mg C mg Chl-a^{-1} h^{-1}) can be derived using the following equation:

$$P_m^B = P_s^B \left(\frac{\alpha^B}{\alpha^B + \beta^B}\right)\left(\frac{\beta^B}{\alpha^B + \beta^B}\right)^{\frac{\beta^B}{\alpha^B}} \tag{3.10}$$

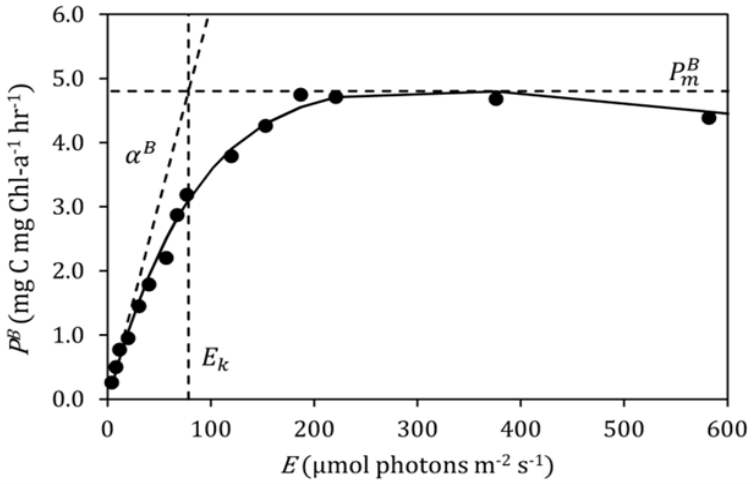

Figure 3.5. Photosynthesis-irradiance (PE) curve showing the two biomass-normalized photo-physiological parameters, the initial slope (α^B) and the assimilation number (P^B_m) of the PE curve.

In the absence of photoinhibition (i.e., $\beta^B = 0$) the maximum photosynthetic rate is equal to P^B_s. Alternatively, a two-parameter hyperbolic tangent function (Figure 3.5) (Jassby and Platt 1976) can be used in the absence of photoinhibition:

$$P^B(E) = P_m^B tanh\left(\frac{\alpha^B E}{P_m^B}\right) \quad (3.11)$$

For both functions, the photoadaptation parameter (E_K in µmol photons m^{-2} s^{-1}) can be calculated as:

$$E_K = \frac{P_m^B}{\alpha^B} \quad (3.12)$$

The maximum quantum yield of carbon fixation (Φ_m), which gives the efficiency of the conversion of light energy into carbon fixation, is derived by dividing α^B by the spectrally weighted mean chlorophyll *a*-specific absorption coefficient of phytoplankton ($\bar{a}^*_{ph}$) (see the IOCCG Protocol Series (2018) for more details on $\bar{a}^*_{ph}$ measurements). Different software packages can be used to perform the curve fit, including curve fitting modules in Python, R and Matlab. The R package Phytotools (Silsbe and Kromkamp 2012; Silsbe and Malkin 2015) is recommended to calculate PE parameters (available via www.rdocumentation.org/packages/phytotools/versions/1.0) (Figure 3.6).

3.5.2. Calculation of daily depth integrated primary production.

Primary production measurements using the *in situ* and on-deck, simulated *in situ* incubation methods can be used to calculate daily depth integrated primary production (P in mg C m^{-2} d^{-1}) by trapezoidal integration (Figure 3.7) (JGOFS 1996). To obtain total production within a depth interval, the measured primary production for each pair of depths is averaged and multiplied by the difference between the two depths. The measurement near the surface is assumed to be constant up to the surface (0 m) and primary production is integrated to the deepest incubation depth used (for example, 175 m in Figure 3.7). The total production within each depth interval is then summed to obtain the integrated primary production for the entire depth range.

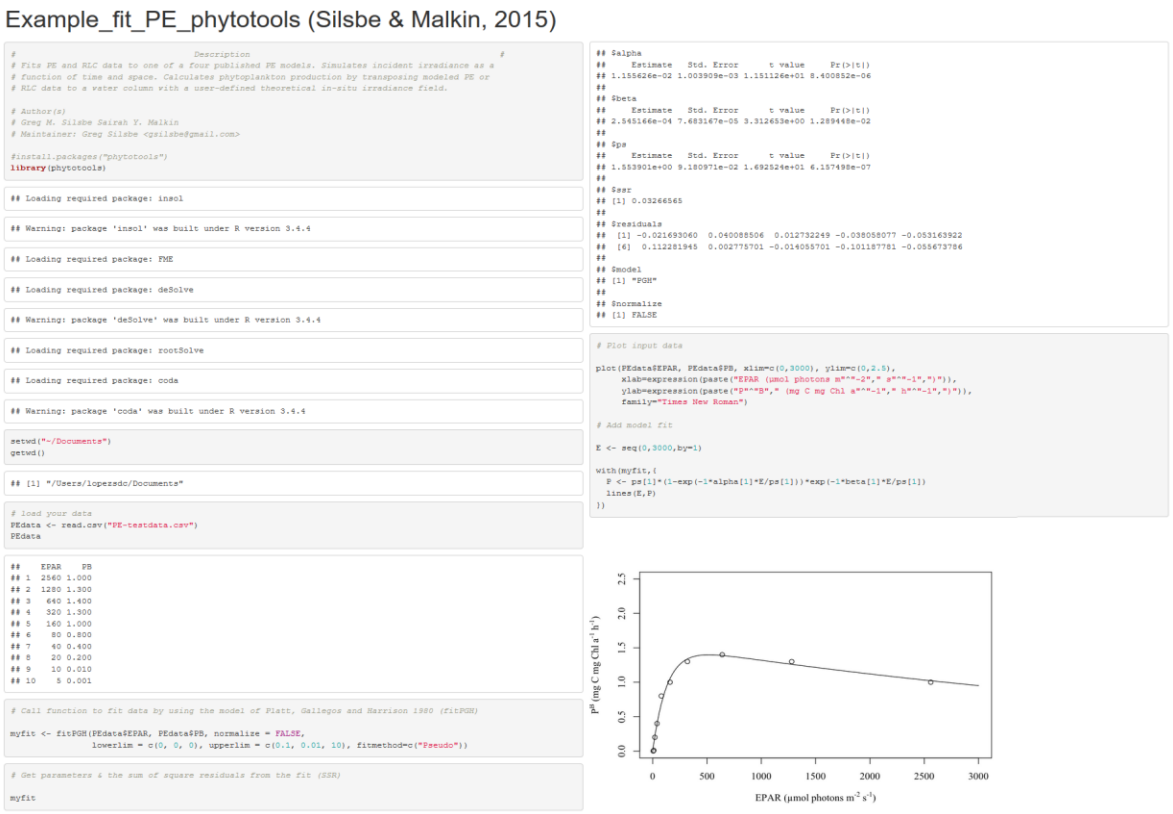

Figure 3.6. Example of curve fitting of photosynthesis-irradiance measurements using the R package Phytotools (Silsbe and Malkin 2015). The package is available at `https://www.rdocumentation.org/packages/phytotools/versions/1.0`

3.6. Additional approaches

3.6.1. Dissolved Organic Carbon production

Dissolved Organic Carbon (DOC) production by phytoplankton can also be measured with ^{14}C. The original technique was developed by Mague et al. (1980) and has been applied to many systems since (Karl et al. 1998; Marañón et al. 2004; Viviani et al. 2015; Balch et al. 2016). Essentially, a subsample of the filtrate from a normal ^{14}C-bicarbonate incubation is further filtered through a 0.2 µm polycarbonate filter and the activity of the ^{14}C-DOC filtrate is measured following the removal of all remaining ^{14}C-dissolved inorganic carbon by acidification to a pH of 2-3 with 1 N H_2SO_4 and venting the samples for 24 h (Mague et al. 1980). What remains is the non-acid-labile ^{14}C-DOC that passed a 0.2 µm filter. This activity is then quantified using liquid scintillation counting. Note, however, that the scintillation cocktail must remain functional with high efficiency following ~50% dilution with acidified seawater. One cocktail that works well for this application is *EcoLume*™ liquid scintillation cocktail (MP Biomedicals). Polycarbonate membrane filters (0.2 µm pore-size) are preferred for this technique due to the low levels of adsorption of DOC to these type of filters during the filtration process as opposed to GF/F that adsorb significant quantities of DOC, subsequently causing underestimates in the DOC production (Maske and Garcia-Mendoza 1994; Karl et al. 1998; Morán et al. 1999).

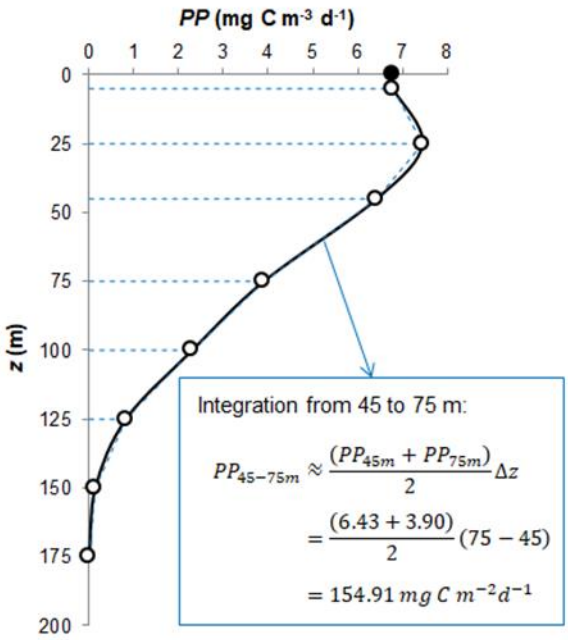

Figure 3.7. Example of the trapezoidal integration for estimating daily depth integrated primary production for in situ or on-deck, simulated in situ incubations. Primary production (PP) is estimated for each depth (*z*) interval, with an example given for 45-75 m, and then summed to obtain primary production for the entire depth range. PP0-175m for this example is 600 mg C m^{-2} d^{-1}. Data from the Hawaii-Ocean Time series (March 1, 2000; hahana.soest.hawaii.edu/hot/).

3.6.2. Cell-specific techniques

The most abundant marine organisms, especially in oceanic gyres and oligotrophic seas, are small phytoplankton cells (<5 µm, but essentially <2 µm): *Prochlorococcus*, *Synechoccocus*, pico- and nanophytoeukaryotes. These phytoplankton groups cannot be accurately separated using membrane filters of different porosities, because their respective size range overlaps. Therefore, the classical size fractionation approach does not allow resolving primary production by the dominant marine phytoplankters.

Chisholm et al. (1988) first estimated primary production by the newly discovered *Prochlorococcus* by "sorting the cells in question after incubation with ^{14}C-labelled bicarbonate, using the cell-sorting capability of the flow cytometer", while Balch and Kilpatrick (1993) used a flow cytometer to sort ^{14}C labeled coccolithophores to measure the rate of coccolith formation (calcification) and coccolith detachment. However, it was not until the pioneering work of Li (1994) that a new avenue opened to resolve primary production by the smallest, but most abundant, groups of marine phytoplankton. Li (1994) used a flow cytometer sorter (FACSort, Becton Dickinson) to separate groups of phytoplankton labeled with ^{14}C by fluorescence-activated cell sorting (FACS). Quantification of high ^{14}C specific activity per sample (1.85 or 3.7 MBq mL-^{1}; Table 3.4) enabled the author to detect radioactivity in sorted cells based on a signal of 50

Table 3.4.

Protocols used to measure cell-specific primary production by fluorescence-activated cell sorting (FACS): Seawater volume and final 14C activity per incubation, sample fixation with paraformaldehyde (PFA, final concentration), cell concentration prior to cell sorting, post-sorting filtration and volume and concentration of hydrochloric acid (HCl) used to remove unincorporated ^{14}C after sorting. Pro = *Prochlorococcus*, Syn = *Synechococcus*, Peuk = picophytoeukaryotes, N.D. = Not Determined, N.A. = Not Available.

Reference	Sample volume,mL	Total activity, MBq mL^{-1}	Final PFA (%)	Cell concentration for Pro and Syn sorting	Cell concentration for Peuk sorting	Post sorting filtration	HCl
Björkman et al. (2015)	15 or 40	0.137	0.24	None. Preserved 2 to 4-mL	N.D.	None	500-µL, 2N
Duhamel et al. (2018)	60	0.122	0.5	30 to 50 mL concentrated onto 0.2-µm to 4-mL	N.D.	None	500-µL, 1N
Duhamel et al. (2019)	70	0.243	2	20-mL concentrated onto 0.2-µm to 2-mL	~47-mL concentrated onto 0.8-µm to 4-mL	None	500-µL, 1N
Grob et al. (2011)	120	0.123	1	N.D.	60-mL concentrated onto 0.8-µm to 1.8-mL	0.8-µm	N.A., 10%
Hartmann et al. (2014)	60	0.246	1	20-mL concentrated onto 0.6-µm	40-mL concentrated onto 0.8-µm	0.2-µm for Pro and Syn, 0.8-µm for Peuk	1-mL, 10%
Jardillier et al. (2010)	7.8	0.95	1	N.D.	None	0.2-µm	1-mL, 1%
Li 1994	20	1.85 or 3.7	None	None. 3-mL	None. 3-mL	Yes	N.A., concentrated
Rii et al. (2016a)	75	0.09	0.24	None. Preserved 5-mL	None. Preserved 5-mL	None	150-µL, 1N
Rii et al. (2016b)	30	0.14	0.24	None. Preserved 5-mL	None. Preserved 5-mL	None	200-µL, 2N

disintegrations per minute (DPM) above background, which they defined as values of the *y*-intercept in regressions slope of DPM vs. number of sorted cells. The author concluded that, "It is a significant step toward an important goal in biological oceanography: Namely, the recovery of the bulk properties of phytoplankton from the details of the properties of the constituents".

Despite the initially successful application of flow cytometric sorting of wild cells labeled with ^{14}C, there has been limited work done since Li (1994) to quantify cell-specific primary production using this technique. This is likely due to the requirement of combining high-end instrumentation (e.g., most benchtop flow cytometers cannot distinguish surface *Prochlorococcus* from the background noise) with the use of radioactive material. Additionally, the method requires

specialized user-training and the use of expensive isotopes, which are needed to incubate under high ^{14}C concentration compared to incubations for bulk or size-fractionated measurements. Nonetheless, recent advances in flow cytometry sorting offer greater detection sensitivity, sort purity and speed (e.g., the BD Influx). Since 2010, the improved instrumentation allowed for new studies to emerge (Jardillier et al. 2010; Grob et al. 2011; Hartmann et al. 2014; Björkman et al. 2015; Rii et al. 2016a; b; Duhamel et al. 2018, 2019) and proved to be a powerful approach to characterize the contribution of specific groups of phytoplankton to primary production as well as to study their growth and metabolism in the wild.

3.6.2.1. Incubation and sample preparation for FACS

This method requires using high ^{14}C concentrations and therefore the incubation volume should be kept as low as possible. However, the choice of volume must also be large enough to account for expected cell abundances and activities. For example, while Li (1994) used 1.85 or 3.7 MBq mL^{-1} per 20 mL incubation, ~3 mL was sufficient to sort enough cells to detect radioactivity above background. Recent studies typically added ^{14}C at a final concentration of ~0.12 to ~0.24 MBq mL^{-1} (Table 3.4). Using a ^{14}C concentration in the higher range is helpful in environments where growth rates are expected to be low because per-cell radioactivity is expected to be lower.

Another way to obtain radioactivity above background in the sorted cells, is to sort a larger number of cells (Table 3.5). Typically, authors sort at least three numbers of cells for a given phytoplankton group per sample (e.g., 50,000, 75,000, and 100,000 *Prochlorococcus*; 5,000, 10,000, and 15,000 *Synechococcus*; and 800, 1600, and 3200 picophytoeukaryotes) and use the regressions slope of DPM vs. number of sorted cells to calculate per cell radioactivity (DPM $cell^{-1}$). It is recommended to select the highest sorting purity mode available on the flow cytometer (e.g., "1.0 drop single" on the BD Influx or

Table 3.3.

Number of cells sorted to measure cell-specific primary production by fluorescence-activated cell sorting. Pro = *Prochlorococcus*, Syn = *Synechococcus*, Peuk = picophytoeukaryotes, N.D. = Not Determined, N.A. = Not Available.

Reference	# sorted Pro	# sorted Syn	# sorted PPE
Björkman et al. (2015)	25,000 to 200,000	N.D.	N.D.
Duhamel et al. (2018)	10,000 to 300,000	10,000 to 300,000	N.D.
Duhamel et al. (2019)	25,000 to 100,000	5,000 to 15,000	400 to 3,200
Grob et al. (2011)	N.D.	N.D.	8,000 to 35,000
Hartmann et al. (2014)	unspecified	N.D.	N.D.
Jardillier et al. (2010)	3,000 to 18,000	1,000 to 6,000	200 to 1,000
Li (1994)	~50,000	~10,000	N.A.
Rii et al. (2016a)	30,000 to 200,000	2,000 to 75,000	2,700 to 20,000
Rii et al. (2016b)	25,000	100 to 10,000	360 to 35,000

"single-cell" sort mode on the BD FACSort). However, using stringent sorting parameters to maintain high sorting performance (Riddell et al. 2015) such as purity (defined as quality of the sorted sample: Are we recovering the targeted cells only?) and recovery (defined as the number of particles sorted relative to the number of original particles to be sorted: Are we recovering the number of cells targeted?) slows down sorting rates. For instance, it is not unusual to spend at least 30 min processing a single sample acquired from an oligotrophic environment. Consequently, a sample volume larger than 3 mL is typically needed to sort at least three number of cells for several phytoplankton groups from one sample. This is especially critical for less abundant groups of phytoplankton such as pico- and nanophytoeukaryotes. Therefore, some authors incubate a larger seawater volume and then concentrate the sample before cell sorting (Table 3.4). Cell concentration is typically carried out by gentle vacuum filtration (<100 mm Hg) or using a syringe pump onto a polycarbonate membrane filter. Filtration is stopped before the filter goes dry and the filter is transferred to a cryovial containing a volume of either pre-filtered (0.2 µm polycarbonate filter) seawater (Fawcett et al. 2011) or the corresponding radiolabeled sample (Duhamel et al. 2018, 2019). Cryovials are vortexed to dislodge cells from the filter before cryopreservation. It is recommended to fix the cells using electron microscopy grade aqueous solution of paraformaldehyde (PFA) or glutaraldehyde (e.g., Electron Microscopy Sciences) before concentrating the samples to preserve cell integrity.

When sorting cells, it is important to monitor the event rate, which is dependent on cell concentration, to insure high sorts purity and recovery (Kormelink et al. 2016). The maximum event rate that a flow cytometer can handle while maintaining high purity and recovery depends on the instrument nozzle size as well as sheath fluid and sample pressure. For example, using the Influx with a 70-µm nozzle, sheath fluid and sample pressure at 30 and 31 Psi, respectively, and the 1.0 drop single sorting mode, an event rate of <5,000 per second works well to sort *Prochlorococcus* and *Synechococcus* (with the sheath fluid <10 events per second) (Bock et al. submitted); though higher event rates can be used to sort less abundant groups, such as picophytoeukaryotes (Fawcett et al. 2011). While correctly setting up a flow cytometer for cell sorting is critical, a detailed description of the processes is beyond the scope of this protocol, but can be found in the literature (Shapiro 2003; Arnold and Lannigan 2010; Cossarizza et al. 2017).

3.6.2.2. Post-sorting sample processing

Sorted cells are either collected onto a polycarbonate membrane through gentle filtration and transferred into a scintillation vial or collected directly into a scintillation vial (Table 3.4). If the sorted cells are collected in a scintillation vial, they will be diluted in sheath fluid, the volume of which varies according to the choice of nozzle size and the number of sorted cells. In any case, the maximum volume in the tube after sorting a population should be kept low, preferably less than a quarter of the tube volume to allow addition of hydrochloric acid (HCl) and scintillation cocktail. Typically, 150 µL to 1 mL HCl 1 N or 2 N are added to the sorted cells to remove unincorporated ^{14}C (Table 3.4). It is recommended to leave the tubes uncapped under the fume hood for 24 to 48 hours before adding the scintillation cocktail.

Considering the relatively low activities expected per sorted cells, it is important to use a scintillation cocktail with very low background levels and high counting efficiency. Moreover, if the sorted cells are not filtered, they will be diluted in sheath fluid plus HCl. Therefore, selecting a scintillation cocktail with high water capacity is critical. One cocktail that works well for this

application is Ultima Gold LLT (Perkin Elmer, up to 54% water capacity). Radio-assaying of samples should be carried out using an ultra-low-level liquid scintillation counter, such as the TriCarb 2910TR or 3110 TR (Perkin Elmer) or the 1220 Quantulus (Wallac).

3.6.2.3. Controls

Killed controls can be prepared to determine unspecific radioactivity. Typically, a sample is fixed with PFA at least 15 min before the addition of the radiotracer and then treated as the other samples. Radioactivity measured in the sorted population is then deduced from radioactivity in the respective sample (Duhamel et al. 2018, 2019). Some authors omit the preparation of killed controls and instead sort calibration beads to estimate unspecific radioactivity. This is especially handy when sorting cells directly into a scintillation vial, to account for radioactivity in the small volume of seawater associated with the sorted cells (Björkman et al. 2015). Fluorescent reference beads (typically 1-µm diameter, Fluoresbrite, Polyscience) are added to each sample before sorting. Two to four sort streams are collected simultaneously, directly into individual scintillation vials to separate the microbial cells selected and the fluorescent reference beads. The radioactivity measured in the sorted beads (DPM $bead^{-1}$) is then subtracted from the radioactivity obtained from the cells (DPM $cell^{-1}$). However, the radioactivity measured in sorted killed controls or beads is typically small and by nature of measuring low DPM per cell or beads, generally leading to an overestimation of unspecific radioactivity. Considering that unincorporated ^{14}C-sodium bicarbonate can be removed by acidification, such control can be omitted for the measurement of cell-specific primary production by FACS (as opposed to the measurement of cell-specific uptake rates of other molecules). However, it is good practice to prepare such controls to verify that unspecific radioactivity is indeed negligible.

A set of samples should be incubated in the dark to estimate the contribution of dark CO_2 fixation. Although the dark-fixation values are typically close to background, values should be subtracted from light mediated fixation rates (Jardillier et al. 2010).

It is recommended to verify sort purity and mean recovery from sorts on a regular basis. Typically, sort purity is calculated as the proportion of sorted events falling into the prescribed gate as a percentage of total event rate, while sort recovery is calculated as the number of target events recovered as a percentage of the number of positive sort decisions recorded by the acquisition software (Fawcett et al. 2011; Duhamel et al. 2018). For example, with their FACS configuration (Influx flow cytometer, 70 µm nozzle, sample and sheath pressure of 28.5 Psi and 27.5 Psi, respectively, event rate <20,000 s^{-1}, coincident event detection of ±1 droplet), Fawcett et al. (2011) obtained sort purity >95% and 98.1±1.1% mean recovery from sorts. Alternatively, sorting recovery has been assessed by filtering subsamples (100, 150, 200, 300, 300 and 450 mL) onto 0.2 µm pore size polycarbonate filters, washed twice with deionized water and radio-assayed by liquid scintillation counting and comparing with the sum of activity in the sorted populations (Jardillier et al. 2010). It is recommended to prepare spare samples to determine sort purity and recovery, but a mixture of calibration beads can also be used. For example, Zubkov and Tarran (2008) used a mixture of two 0.5 µm beads with different yellow–green fluorescence to sort one type of beads and determined that with their FACS configuration, the sorted material was 99.8% enriched with the target beads and the sorted bead recovery was 98.8±0.9% (n = 7).

3.6.2.4. Calculation

The activity per liter for different groups of phytoplankton can be calculated as the mean per cell radioactivity (DPM $cell^{-1}$) multiplied by the total number of cells in the respective group (cell L^{-1}), and converted to fixation rates as nmol C L^{-1} h^{-1} by their respective specific activities (DPM mol^{-1}) (Björkman et al. 2015). The average per cell rate can also be determined (amol C $cell^{-1}$ h^{-1}). Alternatively, the cell-specific fixation rate (nmol C $cell^{-1}$ h^{-1}) can be calculated by dividing the radioactivity per cell (DPM $cell^{-1}$) by the total (bulk >0.2 µm) activity (DPM L^{-1}) measured in the same sample and then multiplied by the total fixation rate at ambient DIC concentration (nmol C L^{-1} h^{-1}) (Duhamel et al. 2018, 2019).

It is important to note that the sum of ^{14}C fixation measured per phytoplankton group separated by FACS does not necessarily equal the total amount of primary production by the entire phytoplankton community. Indeed, phytoplankton larger than 2 to 5 µm would not be accounted for. Moreover, as underlined by Li (1994), only small volumes are analyzed, which would likely not include a proportional representation of the less abundant cells: Typically, larger cells would be underrepresented. Considering the isometric scaling of phytoplankton photosynthesis with cell size, despite being less abundant, larger cells tend to contribute more substantially to primary production on a per cell level, even after normalizing to their biovolume (Duhamel et al. 2019).

3.6.2.5. Alternative using 13C-sodium bicarbonate

In theory, a similar approach can be taken using incubation with ^{13}C-sodium bicarbonate. For example, to study group-specific marine nitrogen cycling, authors have incubated seawater with ^{15}N labeled compounds, separated phytoplankton groups by FACS and analyzed the isotopic composition by mass spectrometry (Casey et al. 2007; Fawcett et al. 2015). Because ^{13}C detection by mass spectrometry is much less sensitive than ^{14}C detection by liquid scintillation counting, a greater isotopic enrichment would be necessary, and a prohibitively large number of cells would need to be sorted (Berthelot et al. 2019). More recently authors have taken advantage of the sensitivity of nano-scale secondary ion mass spectrometers (nanoSIMS) to measure cell-specific incorporation of stable-isotope-labeled substrates (for review see Mayali 2020), including ^{13}C-sodium bicarbonate (Zimmermann et al. 2015; Berthelot et al. 2019). A major drawback remains the cost associated with the NanoSIMS instrument (~$6 million USD, Mayali 2020), which cascades into steep user fees, limiting the number of samples that can be processed within a reasonable budget.

3.6.2.6. Other methods to measure cell-specific primary production

Photopigment radiolabeling has been used to measure carbon-specific growth rates among phytoplankton taxa (Redalje and Laws 1981; Goericke and Welschmeyer 1993). The method relies on coupling the ^{14}C technique to the separation of diagnostic photopigments by High-Performance Liquid Chromatography (HPLC; for review see Paerl 2007). The method is quite tedious and may not be as specific as needed (e.g., co-elution of ^{14}C-labeled colorless compounds with photopigments; Pinckney et al. 1996). Despite advances in column and instrumentation technology, as well as improvements of software applicable to data interpretation and synthesis (Pinckney et al. 2001), this technique has not been broadly applied.

Microautoradiography can also be used to analyze samples that have been incubated with ^{l4}C, to determine photosynthetic capabilities and rates at the single-cell level (Paerl 2007).

Microautoradiography has been used in microbial ecology for many years (Brock and Brock 1966). The technique relies on detection and microscopic visualization of radiation-sensitive silver halide emulsions reacting with radioactive organisms that are subsequently processed by standard photographic techniques. Microautoradiography has been used to quantify primary productivity on a cell-specific basis (Watt 1971; Stull et al. 1973; Douglas 1984). Conveniently, this technique can be combined with fluorescent *in situ* hybridization (FISH), for the identification of target organisms, to link the structural and functional aspects of microbes (Lee et al. 1999; Nielsen and Nielsen 2005). However, microautoradiography is time consuming, requires experience (e.g., detection of false positives), is limited by microscopic resolution and can be prone to interpretational differences among investigators (Paerl 2007).

3.6.3. Phytoplankton calcification rates

Isotope tracers are useful to directly measure calcification rates in phytoplankton. Typically, these methods involve the addition of trace quantities of ^{14}C (as $NaH^{14}CO_3$) or ^{45}Ca (as $^{45}CaCl_2$) in bottle samples that are incubated, and the subsequent incorporation of the isotope into biogenic $CaCO_3$ is then quantified. This approach provides a measure of net calcification over the incubation period, resulting from biomineralization subtracting dissolution. Radioisotope methods are highly sensitive and, if used appropriately, are able to measure extremely low rates of calcification. This allows relatively short incubation times (hours to days), which is a distinct advantage when working at sea.

Coccolithophore calcification rates in cultures, mesocosms, and field populations have been reported using ^{14}C uptake methods in a multitude of studies (Paasche 1963; Paasche and Brubak 1994; Balch and Kilpatrick 1996; Paasche et al. 1996; Balch et al. 2000, 2007; Buitenhuis et al. 2001; Delille et al. 2005; Poulton et al. 2007, 2013, 2014; Charalampopoulou et al. 2016; Daniels et al. 2016; Marañón et al. 2016; White et al. 2018) and less frequently using ^{45}Ca uptake (Van der Wal et al. 1987; van der Wal et al. 1994; Kayano and Shiraiwa 2009; Fukuda et al. 2014). Generally, ^{14}C is easier to use than ^{45}Ca in coccolithophore calcification rate experiments because the unincorporated isotope is more readily rinsed from samples than is ^{45}Ca. A commonly-used (but older) technique is to filter two samples that have been incubated with ^{14}C, carefully rinse both filters, fume one filter with acid (as described earlier in this chapter), and measure the ^{14}C activity of each filter. The fumed filter provides the photosynthetic fixation of ^{14}C, while the difference between the two filters is the acid-labile component of ^{14}C fixation, assumed to be calcification. The problem with this approach, however, is that calcification is calculated as the small difference between two large numbers, each with significant error. Moreover, these errors compound.

3.6.3.1. Microdiffusion method

The microdiffusion method (Paasche and Brubak 1994) is a highly sensitive method that allows the direct measurement of ^{14}C fixation into both particulate organic carbon (POC) as well as coccolith particulate inorganic carbon (PIC; aka calcite) in the same sample. Briefly, this method entails filtration and rinsing of the incubated sample onto a 0.4 μm pore size polycarbonate filter. The filter is placed on the side of a scintillation vial, a small volume of 1% phosphoric acid is pipetted to the bottom of the vial, and a small Glass Fiber Filter (GF/F) containing a CO_2-absorbent (KOH or phenethylamine) is placed on the inside of the cap of the vial. The capped vial is placed on its side and rotated such that the acid covers the polycarbonate filter, dissolving any labeled

particulate inorganic carbon and the resultant $^{14}CO_2$ is absorbed onto the GF/F with CO_2 absorbent. The cap with the glass-fiber filter and CO_2 absorbent is transferred to a new scintillation vial, scintillation cocktail added and the activity in both filters is then counted for ^{14}C activity. Routine checks with filter efficiency tests and total isotope recovery tests (Paasche and Brubak 1994) are critical to ensure proper application of this method. Incubation times of coccolithophore calcification experiments that have used radioisotopes typically range from minutes to a day. The method was adapted further for work on ships by Balch et al. (2000) by fitting scintillation vials with rubber septa with hanging buckets. The filter with CO_2-absorbent is then placed in the bucket, septum mounted on the scintillation vial where the cap would normally be, and the 1% phosphoric acid injected through the rubber septum, past the bucket, onto the sample filter on the bottom of the vial. The resultant ^{14}C-CO_2 emitted from the sample filter is then captured by the absorbent-soaked filter suspended in the bucket.

Blank filter runs are also suggested in calcification experiments using ^{14}C, in order to correct for non-biological adsorption of radiolabel. Buffered-formalin-killed blanks are most commonly used. Paasche (1962) reported that such blanks corresponded to <1% of the calcification in living cells under conditions of maximum photosynthesis. Further, Paasche (1963) found that the non-biological isotope exchange as measured by buffered-formalin-killed samples accounted for 0.5-4% of the coccolith calcification at light-saturated photosynthesis and this blank was consistently higher in artificial medium than in natural seawater. This finding supports the notion that the chemistry of $CaCO_3$ surfaces is complex and that formalin may alter this chemistry at least under some conditions. However, buffered-formalin-killed blanks provide reproducible estimates of passive exchange of ^{14}C onto calcite coccoliths. Under conditions of reduced light, low coccolithophore abundance, or other factors that can result in low values of coccolithophore calcification rates, care must be taken with processing both blank and treatment filters, owing to the reduced ratio of sample-to-background signals. Calcification rates determined with isotopes typically are recorded as mass or moles of C or $CaCO_3$ per cell or individual organism, per unit time (e.g., μmol C $cell^{-1}$ d^{-1}). Isotope-derived calcification rates also have been normalized to chlorophyll in coccolithophore cultures (Balch et al. 2007). The reader is also referred to Fabry and Balch (2010) for more details on measuring carbon fixation through calcification in marine phytoplankton.

3.7. Ancillary measurements

For photosynthesis-irradiance (PE) incubations, the location (latitude, longitude, depth) and time of sampling should be noted as well as *in situ* and incubation temperatures. To calculate photosynthetic rates from PE measurements knowledge of the following variables are required: Chlorophyll *a* concentration, dissolved inorganic carbon concentration (section 3.3.1), Chlorophyll *a* specific absorption spectra and the irradiance spectrum of the light source of the photosynthetron. Additional measurements including PAR, salinity, micro- and macronutrient concentrations and taxonomic composition and size structure of the phytoplankton community could provide valuable information in comparing photosynthetic characteristics of marine phytoplankton across different natural populations.

3.8. SeaBASS standardized fields and units

Most online repositories require the use of standardized field names and associated units for submitting data. The National Aeronautics and Space Administration (NASA) Ocean Biology Processing Group (OBPG) maintains a publicly shared archive of *in situ* oceanographic and atmospheric data in the SeaWiFS Bio-optical Archive and Storage System (SeaBASS). Naming conventions for carbon-based primary production for this repository are available in Table 3.6, and naming conventions for other variables can be found at https://seabass.gsfc.nasa.gov/wiki/stdfields.

Table 3.6.

Standardized field names and associated units for carbon-based primary production data that are currently available in the SeaWiFS Bio-optical Archive and Storage System (SeaBASS). The field names are not case sensitive.

Field name	Units	Description
GPP	mg/m^3/d	Gross Primary Productivity
NPP	mg/m^3/d	Net Primary Productivity
PP	mgC/mgchla/hr	Primary productivity
rate_13C_uptake_bottle	mol/L/d,mol_L^-1_d^-1	Primary productivity determined using ^{13}C. This field should include the experiment time (incubation time) "_###hr".
rate_14C_uptake_bottle	mol/L/d,mol_L^-1_d^-1	Primary productivity determined using ^{14}C. This field should include the experiment time (incubation time) "_###hr".

3.9. References

Anning, T., H. L. MacIntyre, S. M. Pratt, P. J. Sammes, S. Gibb, and R. J. Geider. 2000. Photoacclimation in the marine diatom Skeletonema costatum. Limnol. Oceanogr. **45**: 1807–1817. doi:10.4319/lo.2000.45.8.1807

Antoine, D., and A. Morel. 1996. Oceanic primary production: 1. Adaptation of a spectral light-photosynthesis model in view of application to satellite chlorophyll observations. Global Biogeochem. Cycles **10**: 43–55. doi:10.1029/95GB02831

Arnold, L. W., and J. Lannigan. 2010. Practical Issues in High-Speed Cell Sorting. Curr. Protoc. Cytom. **51**: 1.24.1-1.24.30. doi:10.1002/0471142956.cy0124s51

Babin, M., A. Morel, and R. Gagnon. 1994. An incubator designed for extensive and sensitive measurements of phytoplankton photosynthetic parameters. Limnol. Oceanogr. **39**: 694–702. doi:10.4319/lo.1994.39.3.0694

Babin, M., J. C. Therriault, L. Legendre, B. Nieke, R. Reuter, and A. Condal. 1995. Relationship between the maximum quantum yield of carbon fixation and the minimum quantum yield of chlorophyll a in vivo fluorescence in the Gulf of St. Lawrence. Limnol. Oceanogr. **40**: 956–968. doi:10.4319/lo.1995.40.5.0956

Balch, W. ., and K. Kilpatrick. 1993. Coccolith production and detachment by Emiliania Huxleyi (Prymensiophyceae). J. Phycol. **29**: 566–575.

Balch, W., D. Drapeau, B. Bowler, and E. Booth. 2007. Prediction of pelagic calcification rates using satellite measurements. Deep. Res. Part II Top. Stud. Oceanogr. **54**: 478–495. doi:10.1016/j.dsr2.2006.12.006

Balch, W. M., D. T. Drapeau, and J. J. Fritz. 2000. Monsoonal forcing of calcification in the Arabian Sea. Deep. Res. Part II Top. Stud. Oceanogr. **47**: 1301–1337. doi:10.1016/S0967-0645(99)00145-9

Balch, W. M., T. Huntington, G. Aiken, D. Drapeau, B. Bowler, L. C. Lubelczyk, and K. Butler. 2016. Toward a quantitative and empirical dissolved organic carbon budget for the Gulf of Maine, a semienclosed shelf sea. Global Biogeochem. Cycles **30**: 268–292. doi:10.1002/2015GB005332.Received

Balch, W. M., and K. Kilpatrick. 1996. Calcification rates in the equatorial Pacific along 14O degrees W. Deep Sea Res. Part II Top. Stud. Oceanogr. **43**: 971–993.

Banse, K. 1993. On the dark bottle in the 14C method for measuring marine phytoplankton production., p. 132–140. *In* W.K.W. Li and S.Y. Maestrini [eds.], Measurement of Primary Production from the Molecular to the Global Scale. ICES Marine Science Symposia.

Barber, R. T., and A. K. Hilting. 2002. History of the Study of Plankton Productivity., p. 16–43. *In* P.J.I.B. Williams, D.N. Thomas, and C.S. Reynolds [eds.], Phytoplankton Productivity: Carbon Assimilation in Marine and Freshwater Ecosystems. Wiley.

Behrenfeld, M. J., K. H. Halsey, and A. J. Milligan. 2008. Evolved physiological responses of phytoplankton to their integrated growth environment. Philos. Trans. R. Soc. B Biol. Sci. **363**: 2687–2703. doi:10.1098/rstb.2008.0019

Berthelot, H., S. Duhamel, S. L'Helguen, J. F. Maguer, S. Wang, I. Cetinić, and N. Cassar. 2019. NanoSIMS single cell analyses reveal the contrasting nitrogen sources for small phytoplankton. ISME J. **13**: 651–662. doi:10.1038/s41396-018-0285-8

Björkman, K. M., M. J. Church, J. K. Doggett, and D. M. Karl. 2015. Differential assimilation of inorganic carbon and leucine by prochlorococcus in the oligotrophic north pacific subtropical gyre. Front. Microbiol. **6**: 1–14. doi:10.3389/fmicb.2015.01401

Bock, N. No Title.

Bouman, H. A., T. Platt, M. Doblin, and others. 2018. Photosynthesis-irradiance parameters of marine phytoplankton: Synthesis of a global data set. Earth Syst. Sci. Data **10**: 251–266. doi:10.5194/essd-10-251-2018

Brenna, J. T., T. N. Corso, H. J. Tobias, and R. J. Caimi. 1998. High-percision continuous-flow isotope ratio mass spectrometry. Mass Spectrom. Rev. 227–258.

Brock, T., and M. Brock. 1966. Autoradiography as a Tool in Microbial Ecology. Nature **209**: 734–736. doi:10.1038/209734a0

Brodie, C. R., T. H. E. Heaton, M. J. Leng, C. P. Kendrick, J. S. K. Casford, and J. M. Lloyd. 2011a. Evidence for bias in measured δ15N values of terrestrial and aquatic organic materials due to pre-analysis acid treatment methods. Rapid Commun. Mass Spectrom. **25**: 1089–1099.

Brodie, C. R., M. J. Leng, J. S. L. Casford, C. P. Kendrick, J. M. Lloyd, Z. Yongqiang, and M. I. Bird. 2011b. Evidence for bias in C and N concentrations and δ13C composition of terrestrial and aquatic organic materials due to pre-analysis acid preparation methods. Chem. Geol. **282**: 67–83. doi:10.1016/j.chemgeo.2011.01.007

Buitenhuis, E. T., P. Van Der Wal, and H. J. W. De Baar. 2001. Blooms of Emiliania hyxleyi are sinks of atmospheric carbon dioxide: A field and mesocosm study derived simulations. Global Biogeochem. Cycles **15**: 577–587.

Casey, J. R., M. W. Lomas, J. Mandecki, and D. E. Walker. 2007. Prochlorococcus contributes to new poduction in the Sargasso Sea deep chlorophyll maximum. Geophys. Res. Lett. **34**: 1–5. doi:10.1029/2006GL028725

Charalampopoulou, A., A. J. Poulton, D. C. E. Bakker, M. I. Lucas, M. C. Stinchcombe, and T. Tyrrell. 2016. Environmental drivers of coccolithophore abundance and calcification across Drake Passage (Southern Ocean). Biogeosciences **13**: 5917–5935. doi:10.5194/bg-13-5917-2016

Chisholm, S. W., R. J. Olson, E. Z. Zettler, R. Goericke, J. B. Waterbury, and N. A. Welschmeyer. 1988. A novel free-living prochlorophyte abundant in the oceanic euphotic zone. Nature **334**: 340–343. doi:10.1038/334340a0

Close, H. G. 2019. Compound-Specific Isotope Geochemistry in the Ocean. Ann. Rev. Mar. Sci. **11**: 27–56. doi:10.1146/annurev-marine-121916-063634

Collos, Y., C. Jauzein, and E. Hatey. 2014. Particulate carbon and nitrogen determinations in tracer studies: The neglected variables. Appl. Radiat. Isot. **94**: 14–22. doi:10.1016/j.apradiso.2014.06.015

Collos, Y., and G. Slawyk. 1985. On the compatibility of carbon uptake rates calculated from stable and radioactive isotope data: implications for the design of experimental protocols in aquatic primary productivity. J. Plankton Res. **7**: 595–603. doi:10.1093/plankt/7.5.595

Cossarizza, A., H. D. Chang, A. Radbruch, and others. 2017. Guidelines for the use of flow cytometry and cell sorting in immunological studies. Eur. J. Immunol. **47**: 1584–1797. doi:10.1002/eji.201646632

Cullen, J. J. 2001. Primary Production Methods. Encycl. Ocean Sci. 2277–2284. doi:10.1006/rwos.2001.0203

Cullen, J. J., P. J. Neale, and M. P. Lesser. 1992. Biological weighting function for the inhibition of phytoplankton photosynthesis by ultraviolet radiation. Science (80-.). **258**: 646–650. doi:10.1126/science.258.5082.646

Cullen, J. J., Davis, R. F., & Huot, Y. (2012). Spectral model of depth-integrated water column photosynthesis and its inhibition by ultraviolet radiation. Global biogeochemical cycles, 26(1).

Cutter, G. A., L. Codispoti, P. Croot, W. Geibert, L.-E. Heimbürger, M. Lohan, and H. Planquette. 2010. Sampling and Sample-handling Protocols for GEOTRACES Cruises.

Daniels, C. J., A. J. Poulton, J. R. Young, M. Esposito, M. P. Humphreys, M. Ribas-Ribas, E. Tynan, and T. Tyrrell. 2016. Species-specific calcite production reveals Coccolithus pelagicus as the key calcifier in the Arctic Ocean. Mar. Ecol. Prog. Ser. **555**: 29–47. doi:10.3354/meps11820

Delille, B., J. Harlay, I. Zondervan, and others. 2005. Response of primary production and calcification to changes of pCO2 during experimental blooms of the coccolithophorid Emiliania huxleyi. Global Biogeochem. Cycles **19**: 1–14. doi:10.1029/2004GB002318

Dickson, A. G., C. L. Sabine, and J. R. Christian. 2007. Guide to Best Practices for Ocean CO2 measurements. PICES Special Publication,.

Douglas, D. 1984. Microautoradiography-based enumeration of photosynthetic picoplankton with estimates of carbon-specific growth rates. Mar. Ecol. Prog. Ser. **14**: 223–228. doi:10.3354/meps014223

Duhamel, S., F. Zeman, and T. Moutin. 2006. A dual-labeling method for the simultaneous measurement of dissolved inorganic carbon and phosphate uptake by marine planktonic species. Limnol. Oceanogr. Methods 4: 416–425. doi:10.4319/lom.2006.4.416

Duhamel, S., Moutin, T., Wambeke, F. V., Mooy, B. V., Rimmelin, P., Raimbault, P., & Claustre, H. (2007). Growth and specific P-uptake rates of bacterial and phytoplanktonic communities in the Southeast Pacific (BIOSOPE cruise). Biogeosciences, 4(6), 941-956.

Duhamel, S., F. Van Wambeke, D. Lefevre, M. Benavides, and S. Bonnet. 2018. Mixotrophic metabolism by natural communities of unicellular cyanobacteria in the western tropical South Pacific Ocean. Environ. Microbiol. 20: 2743–2756. doi:10.1111/1462-2920.14111

Duhamel, S., E. Kim, B. Sprung, and O. R. Anderson. 2019. Small pigmented eukaryotes play a major role in carbon cycling in the P-depleted western subtropical North Atlantic, which may be supported by mixotrophy. Limnol. Oceanogr. **64**: 2424–2440. doi:10.1002/lno.11193

Fabry, V. J., and W. M. Balch. 2010. Direct measurements of calcification rates in planktonic organisms, p. 260. *In* U. Riebesell, V.J. Fabry, L. Hansson, and J.-P. Gattuso [eds.], Guide to best practices for ocean acidification research and data reporting. Publications Office of the European Union.

Falkowski, P. G. 1981. Light-shade adaptation and assimilation numbers. J. Plankton Res. **3**: 203–216.

Fawcett, S. E., M. W. Lomas, J. R. Casey, B. B. Ward, and D. M. Sigman. 2011. Assimilation of upwelled nitrate by small eukaryotes in the Sargasso Sea. Nat. Geosci. **4**: 717–722. doi:10.1038/ngeo1265

Fawcett, S. E., B. B. Ward, M. W. Lomas, and D. M. Sigman. 2015. Vertical decoupling of nitrate assimilation and nitrification in the Sargasso Sea. Deep. Res. Part I Oceanogr. Res. Pap. **103**: 64–72. doi:10.1016/j.dsr.2015.05.004

Fitzwater, S. E., G. A. Knauer, and J. H. Martin. 1982. Metal contamination and its effect on primary production measurements. Limnol. Oceanogr. **27**: 544–551. doi:10.4319/lo.1982.27.3.0544

Fry, B. 1996. 13C/12C fractionation by marine diatoms. Mar. Ecol. Prog. Ser. **134**: 283–294. doi:10.3354/meps134283

Fukuda, S. Y., Y. Suzuki, and Y. Shiraiwa. 2014. Difference in physiological responses of growth, photosynthesis and calcification of the coccolithophore Emiliania huxleyi to acidification by acid and CO2 enrichment. Photosynth. Res. **121**: 299–309. doi:10.1007/s11120-014-9976-9

Goericke, R., and N. A. Welschmeyer. 1993. The chlorophyll-labeling method: Measuring specific rates of chlorophyll a synthesis in cultures and in the open ocean. Limnol. Oceanogr. **38**: 80–95. doi:10.4319/lo.1993.38.1.0080

Grob, C., M. Hartmann, M. V. Zubkov, and D. J. Scanlan. 2011. Invariable biomass-specific primary production of taxonomically discrete picoeukaryote groups across the Atlantic Ocean. Environ. Microbiol. **13**: 3266–3274. doi:10.1111/j.1462-2920.2011.02586.x

Hama, T., J. Hama, and N. Handa. 1993. ^{13}C Tracer methodology in microbial ecology with special reference to primary production processes in aquatic environments, p. 39–83. *In* J.G. Jones [ed.], Advances in Microbial Ecology. Plenum Press, New York.

Hama, T., T. Miyazaki, Y. Ogawa, T. Iwakuma, M. Takahashi, A. Otsuki, and S. Ichimura. 1983. Measurement of photo- synthetic production of a marine phytoplankton population using a stable 13C isotope. Mar. Biol. **73**: 31–36.

Hartmann, M., P. Gomez-Pereira, C. Grob, M. Ostrowski, D. J. Scanlan, and M. V. Zubkov. 2014. Efficient CO_2 fixation by surface Prochlorococcus in the Atlantic Ocean. ISME J. **8**: 2280–2289. doi:10.1038/ismej.2014.56

IOCCG Protocol Series. 2018. Inherent optical property measurements and protocols: absorption coefficient, *In* A.R. Neeley and A. Mannino [eds.], IOCCG Ocean optics and biogeochemistry protocols for satellite ocean colour sensor validation. IOCCG.

IOCCG Protocol Series. 2021. Particulate Organic Matter Sampling and Measurement Protocols: Consensus Towards Future Ocean Color Missions. J.E. Chaves, I. Cetinić, G. Dall'Olmo, M. Estapa, W. Gardner, M. Goñi, J. R. Graff, P. Hernes, P. J. Lam, Z. Liu, M. W. Lomas, A. Mannino, M. G. Novak, R. Turnewitsch, P. J. Werdell, T. K. Westberry. IOCCG Ocean Optics and Biogeochemistry Protocols for Satellite Ocean Colour Sensor Validation, Volume 6, In review, IOCCG, Dartmouth, NS, Canada.

Isada, T., T. Iida, H. Liu, S. I. Saitoh, J. Nishioka, T. Nakatsuka, and K. Suzuki. 2013. Influence of Amur River discharge on phytoplankton photophysiology in the Sea of Okhotsk during late summer. J. Geophys. Res. Ocean. **118**: 1995–2013. doi:10.1002/jgrc.20159

Jardillier, L., M. V. Zubkov, J. Pearman, and D. J. Scanlan. 2010. Significant CO2 fixation by small prymnesiophytes in the subtropical and tropical northeast Atlantic Ocean. ISME J. **4**: 1180–1192. doi:10.1038/ismej.2010.36

Jassby, A. D., and T. Platt. 1976. Mathematical formulation of the relationship between photosynthesis and light for phytoplankton. Limnol. Oceanogr. **21**: 540–547. doi:10.4319/lo.1976.21.4.0540

JGOFS. 1992. Joint Global Ocean Flux Study: Implementation Plan. IGBP Report No 23, IGBP Secretariat, Stockholm

JGOFS. 1996. Protocols for the Joint Global Ocean Flux Study (JGOFS) core measurements, p. 170. *In* A. Knap [ed.], Report no. 19 of the Joint Global Ocean Flux Study.

Karl, D. M., D. V. Hebel, K. Björkman, and R. M. Letelier. 1998. The role of dissolved organic matter release in the productivity of the oligotrophic North Pacific Ocean. Limnol. Oceanogr. **43**: 1270–1286. doi:10.4319/lo.1998.43.6.1270

Kayano, K., and Y. Shiraiwa. 2009. Physiological regulation of coccolith polysaccharide production by phosphate availability in the coccolithophorid emiliania huxleyi. Plant Cell Physiol. **50**: 1522–1531. doi:10.1093/pcp/pcp097

Koblentz-Mishke, O. J., V. V. Volkovinsky, and J. G. Kabanova. 1970. Plankton primary production of the world ocean, p. 183–193. *In* W.S. Wooster [ed.], Scientific Exploration of the South Pacific. National Acamdemy of Science.

Kormelink, T. G., G. J. A. Arkesteijn, F. A. Nauwelaers, G. van den Engh, E. N. M. Nolte-'t Hoen, and M. H. M. Wauben. 2016. Prerequisites for the analysis and sorting of extracellular vesicle subpopulations by high-resolution flow cytometry. Cytom. Part A **89**: 135–147. doi:10.1002/cyto.a.22644

Kulk, G., T. Platt, J. Dingle, and others. 2020. Primary production, an index of climate change in the ocean: Satellite-based estimates over two decades. Remote Sens. **12**. doi:10.3390/rs12050826

Kyewalyanga, M. N., T. Platt, and S. Sathyendranath. 1997. Estimation of the photosynthetic action spectrum: Implication for primary production models. Mar. Ecol. Prog. Ser. **146**: 207–223. doi:10.3354/meps146207

Lee, N., P. E. R. H. Nielsen, K. H. Andreasen, S. Juretschko, J. L. Nielsen, K. Schleifer, and M. Wagner. 1999. Combination of Fluorescent *In situ* Hybridization and Microautoradiography—a New Tool for Structure-Function Analyses in Microbial Ecology. Appl. Environ. Microbiol. **65**: 1289–1297.

Lewis, M. R., R. E. Warnock, and T. Platt. 1985. Absorption and photosynthetic action spectra for natural phytoplankton populations: Implications for production in the open ocean. Limnol. Oceanogr. **30**: 794–806. doi:10.4319/lo.1985.30.4.0794

Lewis, M., and J. Smith. 1983. A small volume, short-incubation-time method for measurement of photosynthesis as a function of incident irradiance. Mar. Ecol. Prog. Ser. **13**: 99–102. doi:10.3354/meps013099

Li, W. K. W. 1994. Primary production of prochlorophytes, cyanobacteria, and eucaryotic ultraphytoplankton: Measurements from flow cytometric sorting. Limnol. Oceanogr. **39**: 169–175. doi:10.4319/lo.1994.39.1.0169

López-Sandoval, D. C., A. Delgado-Huertas, and S. Agustí. 2018. The 13 C method as a robust alternative to 14 C-based measurements of primary productivity in the Mediterranean Sea. J. Plankton Res. **40**: 544–554. doi:10.1093/plankt/fby031

López-Sandoval, D. C., A. Delgado-Huertas, P. Carrillo-de-Albornoz, C. M. Duarte, and S. Agustí. 2019. Use of cavity ring-down spectrometry to quantify 13 C-primary productivity in oligotrophic waters. Limnol. Oceanogr. Methods **17**: 137–144. doi:10.1002/lom3.10305

Mague, T. H., E. Friberg, D. J. Hughes, and I. Morris. 1980. Extracellular release of carbon by marine phytoplankton; a physiological approach. Limnol. Oceanogr. **25**: 262–279. doi:10.4319/lo.1980.25.2.0262

Marañón, E., W. M. Balch, P. Cermeño, and others. 2016. Coccolithophore calcification is independent of carbonate chemistry in the tropical ocean. Limnol. Oceanogr. **61**: 1345–1357. doi:10.1002/lno.10295

Marañón, E., P. Cermeño, E. Fernández, J. Rodríguez, and L. Zabala. 2004. Significance and mechanisms of photosynthetic production of dissolved organic carbon in a coastal eutrophic ecosystem. Limnol. Oceanogr. **49**: 1652–1666. doi:10.4319/lo.2004.49.5.1652

Marañón, E., P. Cermeño, and V. Pérez. 2005. Continuity in the photosynthetic production of dissolved organic carbon from eutrophic to oligotrophic waters. Mar. Ecol. Prog. Ser. **299**: 7–17. doi:10.3354/meps299007

Marra, J. 2002. Approaches to the measurement of plankton production, p. 78–108. *In* P.J. L. B. Williams, D.N. Thomas, and C.S. Reynolds [eds.], Phytoplankton Productivity: Carbon Assimilation in Marine and Freshwater Ecosystems. Blackwell Science Ltd.

Marra, J. 2009. Net and gross productivity: Weighing in with 14C. Aquat. Microb. Ecol. **56**: 123–131. doi:10.3354/ame01306

Marra, J., and R. T. Barber. 2004. Phytoplankton and heterotrophic respiration in the surface layer of the ocean. Geophys. Res. Lett. **31**: 12–15. doi:10.1029/2004GL019664

Maske, H., and E. Garcia-Mendoza. 1994. Adsorption of dissolved organic matter to the inorganic filter substrate and its implications for 14C uptake measurements. Appl. Environ. Microbiol. **60**: 3887–3889. doi:10.1128/aem.60.10.3887-3889.1994

Matsumoto, K., T. Fujiki, M. C. Honda, M. Wakita, H. Kawakami, M. Kitamura, and T. Saino. 2012. Inhibition of primary production by nitrile rubber O-rings in Niskin sampler.

Mayali, X. 2020. NanoSIMS: Microscale Quantification of Biogeochemical Activity with Large-Scale Impacts. Ann. Rev. Mar. Sci. **12**: 449–467. doi:10.1146/annurev-marine-010419-010714

Mobley, C. D. 1994. Light and Water : Radiative Transfer in Natural Waters, C.D. Mobley [ed.]. Academic Press.

Morán, X. A. G., J. M. Gasol, L. Arin, and M. Estrada. 1999. A comparison between glass fiber and membrane filters for the estimation of phytoplankton POC and DOC production. Mar. Ecol. Prog. Ser. **187**: 31–41.

Mousseau, L., S. Dauchez, L. Legendre, and L. Fortier. 1995. Photosynthetic carbon uptake by marine phytoplankton: comparison of the stable (13C) and radioactive (14C) isotope methods. J. Plankton Res. **17**: 1449–1460.

Moutin, T., Raimbault, P., & Poggiale, J. C. (1999). Production primaire dans les eaux de surface de la Mediterranee occidentale. Calcul de la production journaliere. Comptes Rendus de l'Académie des Sciences-Series III-Sciences de la Vie, 322(8), 651-655.

Neale, P. J., A. L. Pritchard, and R. Ihnacik. 2014. UV effects on the primary productivity of picophytoplankton: Biological weighting functions and exposure response curves of Synechococcus. Biogeosciences **11**: 2883–2895. doi:10.5194/bg-11-2883-2014

Nielsen, J. N., and P. H. Nielsen. 2005. Advances in Microscopy: Microautoradiography of Single Cells, Methods in Enzymology. Methods Enzymol. **397**: 237–256.

Paasche, E. 1962. Coccolith formation. Nature **193**: 1094–1095.

Paasche, E. 1963. The Adaptation of the Carbon-14 Method for the Measurement of Coccolith Production in Coccolithus huxleyi. Physiol. Plant. **16**: 186–200. doi:10.1111/j.1399-3054.1963.tb08302.x

Paasche, E., and S. Brubak. 1994. Enhanced calcification in the coccolithophorid Emiliania huxleyi (Haptophyceae) under phosphorus limitation. Phycologia **33**: 324–330.

Paasche, E., S. Brubak, S. Skattebol, J. R. Young, and J. C. Green. 1996. Growth and calcification in the coccolithophorid Emiliania huxleyi (Haptophyceae) at low salinities. Phycologia **35**: 394–403.

Paerl, H. 2007. Primary Productivity and Producers, *In* C. Hurst, R. Crawford, J. Garland, M. Lipson, A. Mills, and L. Stezenbach [eds.], Manual of Environmental Microbiology. ASM Press.

Peterson, B. J. 1980. Aquatic primary productivity and the 14C-CO2 method: a history of the productivity problem., p. 359–386. *In* R.F. Johnston, P.W. Frank, and C.D. Michener [eds.], Annual review of ecology and systematics.

Pinckney, J. L., T. L. Richardson, D. F. Millie, and H. W. Paerl. 2001. Application of photopigment biomarkers for quantifying microalgal community composition and *in situ* growth rates. Org. Geochem. **32**: 585–595. doi:10.1016/S0146-6380(00)00196-0

Platt, T., C. L. Gallegos, and W. G. Harrison. 1980. Photoinhibition of photosynthesis in natural assemblages of marine phytoplankton. J. Mar. Res. **38**: 103–111.

Platt, T., and A. D. Jassby. 1976. The relationship between photosynthesis and light for natural assemblages of coastal marine phytoplankton. J. Phycol. **12**: 421–430.

Popp, B. N., E. A. Laws, R. R. Bidigare, J. E. Dore, K. L. Hanson, and S. G. Wakeham. 1998. Effect of phytoplankton cell geometry on carbon isotopic fractionation. Geochim. Cosmochim. Acta **62**: 69–77. doi:10.1016/S0016-7037(97)00333-5

Poulton, A. J., T. R. Adey, W. M. Balch, and P. M. Holligan. 2007. Relating coccolithophore calcification rates to phytoplankton community dynamics: Regional differences and implications for carbon export. Deep. Res. Part II Top. Stud. Oceanogr. **54**: 538–557. doi:10.1016/j.dsr2.2006.12.003

Poulton, A. J., S. C. Painter, J. R. Young, N. R. Bates, B. Bowler, D. Drapeau, E. Lyczsckowski, and W. M. Balch. 2013. The 2008 Emiliania huxleyi bloom along the Patagonian Shelf: Ecology, biogeochemistry, and cellular calcification. Global Biogeochem. Cycles **27**: 1023–1033. doi:10.1002/2013GB004641

Poulton, A. J., M. C. Stinchcombe, E. P. Achterberg, and others. 2014. Coccolithophores on the north-west European shelf: Calcification rates and environmental controls. Biogeosciences **11**: 3919–3940. doi:10.5194/bg-11-3919-2014

Price, N., P. Harrison, M. Landry, F. Azam, and K. Hall. 1986. Toxic effects of latex and Tygon tubing on marine phytoplankton, zooplankton and bacteria. Mar. Ecol. Prog. Ser. **34**: 41–49. doi:10.3354/meps034041

Redalje, D. G., and E. A. Laws. 1981. A New Method for Estimating Phytoplankton Growth Rates and Carbon Biomass. Mar. Biol. **62**: 73–79.

Regaudie-de-Gioux, A., S. Lasternas, S. Agustí, and C. M. Duarte. 2014. Comparing marine primary production estimates through different methods and development of conversion equations. Front. Mar. Sci. **1**: 1–14. doi:10.3389/fmars.2014.00019

Riddell, A., R. Gardner, A. Perez-Gonzalez, T. Lopes, and L. Martinez. 2015. Rmax: A systematic approach to evaluate instrument sort performance using center stream catch. Methods **82**: 64–73. doi:10.1016/j.ymeth.2015.02.017

Rii, Y. M., S. Duhamel, R. R. Bidigare, D. M. Karl, D. J. Repeta, and M. J. Church. 2016a. Diversity and productivity of photosynthetic picoeukaryotes in biogeochemically distinct regions of the South East Pacific Ocean. Limnol. Oceanogr. **61**: 806–824. doi:10.1002/lno.10255

Rii, Y. M., D. M. Karl, and M. J. Church. 2016b. Temporal and vertical variability in picophytoplankton primary productivity in the North Pacific Subtropical Gyre. Mar. Ecol. Prog. Ser. **562**: 1–18. doi:10.3354/meps11954

Sakamoto, M., M. M. Tilzer, R. Gächter, and others. 1984. Joint field experiments for comparisons of measuring methods of photosynthetic production. J. Plankton Res. **6**: 365–383. doi:10.1093/plankt/6.2.365

Sakshaug, E., A. Bricaud, Y. Dandonneau, and others. 1997. Parameters of photosynthesis: Definitions, theory and interpretation of results. J. Plankton Res. **19**: 1637–1670. doi:10.1093/plankt/19.11.1637

Sathyendranath, S., A. Longhurst, C. M. Caverhill, and T. Platt. 1995. Regionally and seasonally differentiated primary production in the North Atlantic. Deep. Res. Part I **42**: 1773–1802. doi:10.1016/0967-0637(95)00059-F

Shapiro, H. M. 2003. Flow Sorting, p. 736. *In* H.M. Shapiro [ed.], Practical Flow Cytometry. John Wiley & Sons.

Silsbe, G. M., and J. C. Kromkamp. 2012. Modeling the irradiance dependency of the quantum efficiency of photosynthesis. Limnol. Oceanogr. Methods **10**: 645–652. doi:10.4319/lom.2012.10.645

Silsbe, G. M., and Y. Malkin. 2015. Phytotools: Phytoplankton production tools. R package Version 1.0. https://CRAN.R-project.org/package=phytotools.

Slawyk, G., Y. Collos, and C. Auclair. 1979. Reply to comment by Fisher et al. Limnol. Oceanogr. **24**: 595–597. doi:10.4319/lo.1979.24.3.0595

Slawyk, G., Y. Collos, and J. -C Auclair. 1977. The use of the 13C and 15N isotopes for the simultaneous measurement of carbon and nitrogen turnover rates in marine phytoplankton. Limnol. Oceanogr. **22**: 925–932. doi:10.4319/lo.1977.22.5.0925

Slawyk, G., M. Minas, Y. Collos, L. Legendre, and S. Roy. 1984. Comparison of radioactive and stable isotope tracer techniques for measuring photosynthesis: 13C and 14C uptake by marine phytoplankton. J. Plankton Res. **6**: 249–257.

Steemann Nielsen, E. 1952. The use of radioactive carbon (14C) for measuring production in the sea. J. du Cons. Perm. Int. pour L'Exploration la Mer **18**: 117–140.

Stull, E. A., E. De Amezaga, and C. R. Goldman. 1973. The Contribution of Individual Species of Algae to Primary Productivity of Castle Lake, California. SIL Proc. 1922-2010 **3**: 1776–1783.

Teira, E., M. J. Pazó, P. Serret, and E. Fernández. 2001. Dissolved organic carbon production by microbial populations in the Atlantic Ocean. Limnol. Oceanogr. **46**: 1370–1377. doi:10.4319/lo.2001.46.6.1370

Viviani, D. A., D. M. Karl, and M. J. Church. 2015. Variability in photosynthetic production of dissolved and particulate organic carbon in the North Pacific Subtropical Gyre. Front. Mar. Sci. **2**: 73. doi:10.3389/fmars.2015.00073

van der Wal, P., J. D. L. van Bleijswijk, and J. K. Egge. 1994. Primary productivity and calcification rate in blooms of the coccolithophorid emiliania huxleyi (lohmann) hay et mohler developing in mesocosms. Sarsia **79**: 401–408. doi:10.1080/00364827.1994.10413571

Van der Wal, P., J. P. M. de Vrind, E. W. de Vrind-de Jong, and A. H. Borman. 1987. Incompleteness of the coccosphere as a possible stimulus for coccolith formation in Pleurochrysis carterae (Prymnesiophyceae). J. Phycol. **23**: 218–221.

Watt, W. D. 1971. Measuring the primary production rates of individual phytoplankton species in natural mixed populations. Deep. Res. Oceanogr. Abstr. **18**: 329–339. doi:10.1016/0011-7471(71)90038-6

White, A. E., K. S. Watkins-Brandt, and M. J. Church. 2018. Temporal variability of Trichodesmium spp. and diatom-diazotroph assemblages in the North Pacific Subtropical Gyre. Front. Mar. Sci. **5**: 1–12. doi:10.3389/fmars.2018.00027

Williams, P. J. L. B., and J. I. Robertson. 1989. A serious inhibition problem from a Niskin sampler during plankton productivity studies. Limnol. Oceanogr. **34**: 1300–1305. doi:10.4319/lo.1989.34.7.1300

Williams, P. J. L. B., D. N. Thomas, and C. S. Reynolds. 2002. Phytoplankton Productivity: Carbon Assimilation in Marine and Freshwater Ecosystems, P.J. L. B. Williams, D.N. Thomas, and C.S. Reynolds [eds.]. Blackwell Science Ltd.

Zimmermann, M., S. Escrig, T. Hübschmann, and others. 2015. Phenotypic heterogeneity in metabolic traits among single cells of a rare bacterial species in its natural environment quantified with a combination of flow cell sorting and NanoSIMS. Front. Microbiol. **6**: 1–11. doi:10.3389/fmicb.2015.00243

Zubkov, M. V., and G. A. Tarran. 2008. High bacterivory by the smallest phytoplankton in the North Atlantic Ocean. Nature **455**: 224–226. doi:10.1038/nature07236

4. The $H_2{}^{18}O$ incubation method for the determination of gross oxygen production

Sara Ferrón[1], Lauren W. Juranek[2]

[1]*Department of Oceanography, University of Hawaii at Manoa, Hawaii, USA*
[2]*College of Earth, Ocean, and Atmospheric Sciences, Oregon State University, Oregon, USA*

4.1. Overview and history of the $H_2{}^{18}O$ incubation method

The $H_2{}^{18}O$ incubation method consists of spiking a discrete water sample with ^{18}O-labeled water and measuring the amount of $^{18}O^{16}O$ that evolves from the splitting of water through photosynthesis, after the sample is incubated in the light (Bender et al., 1987). This method provides a direct measurement of gross O_2 production (GOP) that, in the open ocean, is not affected by respiratory losses or incubation duration, assuming that the O_2 produced by photosynthesis is well mixed with the dissolved O_2 pool. This is because the dissolved O_2 pool is large compared to O_2 respiration rates. By conducting parallel measurements of net O_2 exchange (e.g., as the net change in O_2 to Ar molar ratios), it is possible to also calculate, by difference, respiration rates (Bender et al., 1987, 1999; Grande et al., 1989). GOP (mmol O_2 m^{-3} d^{-1}) using the $H_2{}^{18}O$ incubation method (^{18}O-GOP) is determined from the change in the isotope ratio of dissolved O_2 over the incubation period (Bender et al., 1987; Kiddon et al., 1995):

$$GOP = \left[\frac{^{18}R(O_2)_{final} - {}^{18}R(O_2)_{initial}}{^{18}R(H_2O) - {}^{18}R(O_2)_{initial}}\right] \times [O_2]_{initial} \quad (4.1)$$

where $^{18}R(O_2)_{initial}$ and $^{18}R(O_2)_{final}$ are the initial and final isotope ratios ($^{18}O/^{16}O$) for dissolved O_2, $[O_2]_{initial}$ is the initial dissolved O_2 concentration, and $^{18}R(H_2O)$ is the isotope ratio of the incubation water.

If O_2 to Ar molar ratios are also measured, the net O_2 change (NOC) during the incubation can be simultaneously determined (Bender et al., 1999):

$$NOC = \left[\frac{(O_2/Ar)_{final}}{(O_2/Ar)_{initial}} - 1\right] \times [O_2]_{initial} \quad (4.2)$$

where $(O_2/Ar)_{initial}$ and $(O_2/Ar)_{final}$ are the initial and final O_2/Ar ratios. Respiration can be calculated as the difference between GOP and NOC, assuming that photosynthesis and respiration are the only two processes affecting changes in O_2/Ar in the incubation bottle (Ferrón et al., 2016).

The $H_2{}^{18}O$ incubation method was first introduced in the 1980s by K. Grande, M. Bender, and colleagues (Grande et al., 1982; Bender et al., 1987). It is important to distinguish the $H_2{}^{18}O$ method from a different O_2 isotopic tracer method introduced earlier by Brown and colleagues (Brown, 1953) in which the O_2 pool, instead of the water, is labeled with ^{18}O. The ^{18}O-O_2 labeling approach allows one to simultaneously determine photosynthesis and respiration in the light in phytoplankton cultures and plant leaf samples, with the rate of photosynthesis determined from

the rate of increase in $^{16}O^{16}O$, and the rate of respiration calculated from the decrease in $^{18}O^{16}O$. The introduction of the $H_2{}^{18}O$ incubation method allowed a more sensitive and easier implementation of the isotope tracer approach to the study of GOP in natural oceanic waters. However, by the time this method was developed, the ^{14}C assimilation method (Steemann Nielsen, 1952, see Chapter 3) had already become widely used as the standard primary production method for the oceanographic community. Perhaps because of this, the $H_2{}^{18}O$ incubation method has not been used frequently for studies of oceanic primary production, and GOP measurements derived from this method account for a small fraction of all oceanic primary production measurements (e.g., Regaudie-de-Gioux et al., 2014). However, studies comparing ^{18}O-GOP and ^{14}C assimilation rates (^{14}C-PP) have proven very valuable in helping interpret what ^{14}C assimilation rates really measure (Bender et al., 1999; Bender & Grande, 1987; González et al., 2008; Grande et al., 1989; Juranek & Quay, 2005; Kiddon et al., 1995; Laws et al., 2000; Quay et al., 2010). A number of these comparisons were part of major collaborative programs, such as the Plankton Rate Processes in Oligotrophic OceanS (PRPOOS) and the Joint Global Ocean Flux Study (JGOFS), aimed at comparing and establishing methodological protocols for measuring primary production in the ocean (e.g., Bender et al., 1999; Dickson et al., 2001; Grande et al., 1989; Laws et al., 2000, see Chapter 3). These studies have shown that ^{14}C-PP in 12- to 24-hour incubations typically yield a value between net community and gross C production (Marra, 2009), but where exactly ^{14}C-PP lie in relation to net community and gross C production depends, among other things, on phytoplankton community structure (Pei & Laws, 2013), net growth rate (Halsey et al., 2011; Pei & Laws, 2014), incubation time (Halsey et al., 2011), and dissolved organic C production (typically not measured) (Karl et al., 1998).

One of the advantages of the $H_2{}^{18}O$ incubation method compared to the ^{14}C method is that it unambiguously measures the gross O_2 production from the photosynthetic splitting of water. In addition, the labeled product remains in a well defined pool (dissolved O_2) and the measurement is relatively insensitive to recycling. However, as with other in vitro approaches, this technique is susceptible to artifacts associated with incubating seawater in a confined bottle, such as grazer exclusion and perturbations of the natural environmental conditions (Robinson & Williams, 2005). Another potential caveat of this method is the need to know the photosynthetic quotient in order to convert to gross C production. In addition, the $H_2{}^{18}O$ incubation method measures gross O_2 production regardless of the fate of this O_2 and whether it is linked to the fixation of organic C. A fraction of newly produced O_2 may be consumed by light-dependent reactions (e.g., Mehler reaction, photorespiration), which could result in an overestimation of gross C fixation determined from the $H_2{}^{18}O$ incubation method if these processes are ignored (Bender et al., 1999; Bender et al., 2000).

Some potential drawbacks that might limit the widespread application of the $H_2{}^{18}O$ technique to studies of marine primary production are: 1) the need for a specialized isotope ratio mass spectrometer (IRMS), and 2) the handling and analysis of samples for $^{18}O/^{16}O$ are technically difficult and require highly trained personnel. As stated by Falkowski and Raven (2007) in their book Aquatic Photosynthesis: “This technique allows a relatively precise measurement of gross photosynthesis; however, the method is tedious, requires a (bulky and expensive) mass spectrometer, and hence has not been widely used in studies of aquatic photosynthesis in nature.” Recently, Ferrón et al. (2016) demonstrated that GOP can be precisely measured with the $H_2{}^{18}O$ incubation method using membrane inlet mass spectrometry (MIMS), potentially making this

method easier to implement and more accessible to the broader oceanographic community. This novel approach has the advantage of only requiring a relatively inexpensive quadrupole mass spectrometer (~$30-50K USD), which are small, easy to operate, and can be taken to sea. In addition, the handling and analysis of samples are technically easy, as the gases are directly diffused from the water sample into the mass spectrometer, without the need for a gas extraction step, which would be more prone to contamination.

4.2. Sample collection

4.2.1. General precautions

Seawater samples for incubations should be collected to the extent possible using clean techniques (Fitzwater et al., 1982; JGOFS 1996). Gas-tight glass bottles, typically with ground-glass stoppers, are used for incubation. Silica-glass can potentially release significant amount of trace metals during an incubation, even after being thoroughly cleaned (Fitzwater et al., 1982), and therefore, quartz-glass bottles are preferable, as they should not release trace metals if properly cleaned (e.g., quartz filters are suitable for most trace metal analyses https://www.geotraces.org/methods-cookbook/). In addition, quartz-glass bottles are more transparent to the full spectrum of environmental light.

In general, powderless polyethylene gloves are the preferred choice when collecting samples for primary production. However, because their loose fit in the hands they can make the sample collection and preparation cumbersome, in which case powder free latex gloves are sufficient. Nitrile gloves should be avoided as they might contaminate nitrate.

4.2.2. Pre-cruise sample bottle preparation

The preferred cleaning protocol for the incubation bottles is the same as for ^{14}C and ^{13}C incubations (see Chapter 3): 1) washing with a dilute solution of trace metal clean detergent, 2) thorough rinsing with deionized water, 3) soaking in 5-10% HCl solution for over 24 hours, and 4) thorough rinsing with Milli Q water.

4.2.3. Water sampling

Determining GOP using equation (1) requires knowing four terms: the initial and final isotopic ratio ($^{18}O/^{16}O$) of dissolved O_2, the initial isotopic ratio of water (after the spike), and the initial concentration of dissolved O_2. The initial isotopic ratio of water is determined from the amount of labeled water added and the calibrated volume of the incubation bottles. It is necessary to collect initial samples in addition to the incubation bottles for initial and final measurements of the isotopic ratio for dissolved O_2. The initial concentration of dissolved O_2 can be determined by the Winkler method (Carpenter, 1965) in a separate sample, from the *in situ* dissolved O_2 concentration measured by the CTD O_2 sensor, or measured concurrently with the initial isotopic ratio for dissolved O_2 if using MIMS (Ferrón et al., 2016). The samples are typically subsampled from a larger container, such as Niskin-type bottles attached to a CTD rosette (see Chapter 3).

4.2.3.1. Incubation samples

The incubation samples are collected by attaching an acid-washed silicone tubing to the spigot of the Niskin-type bottle and inserting it to the bottom of the glass bottle. Once the water starts flowing, the bottle is rinsed with the seawater sample, and then filled from bottom to top making

sure no bubbles are trapped in the tubing or bottle, overflowing at least once the volume of the bottle. The incubation samples are spiked with $H_2{}^{18}O$ before being closed with the stoppers, which are also rinsed with the seawater sample.

Once the incubation samples are collected, these are spiked with ^{18}O-labeled water (e.g., Medical Isotopes, >97% ^{18}O). It is important to make sure not to introduce contaminants (e.g., trace metals, macronutrients, etc) to the incubation bottle with the spike. This can be done by measuring the concentrations of metals and macronutrients in the stock solution to be sure that they are below background levels, triple distilling the ^{18}O-labeled water with a sub-boiling Teflon still (Juranek & Quay, 2005), or conducting experiments to make sure the addition of the spike does not significantly alter the production rates (Ferrón et al., 2016).

The final target enrichment of the water depends on the expected productivity and should be calculated during the planning stages of field work. An enrichment of 5-10 ‰ in the dissolved O_2 pool after the incubation is ideal, although for very low photosynthetic rates (such as at the base of the euphotic zone), the enrichment may be lower. Care should be taken to not overdose the incubation samples with ^{18}O-spike, particularly if analysis is by IRMS, since labs that measure natural abundance oxygen isotopes will be wary of analyzing heavily enriched samples. The isotopic enrichment of the incubated sample relative to the initial sample is calculated as:

$$\delta^{18}O(O_2) = \left[\frac{{}^{18}R(O_2)_{final}}{{}^{18}R(O_2)_{initial}} - 1\right] \times 1000 \quad (4.3)$$

Because the isotopic ratio of the water after the spike is typically not measured but calculated based on the amount of labeled water added and the calibrated volume of the incubation bottle, it is important to accurately know the volume of the flask and the volume of added ^{18}O-labeled water. The fractional abundance ($^{18}O/^{16}O+^{18}O$) of the water after the spike ($^{18}F_{water}$) is calculated as follows:

$${}^{18}F_{water} = \frac{V_{spike}\,{}^{18}F_{spike} + V_{sample}\,{}^{18}F_{SMOW}}{V_{sample} + V_{spike}} \quad (4.4)$$

where V_{spike} and V_{sample} are the volumes of the spike and sample, respectively, $^{18}F_{spike}$ and $^{18}F_{water}$ are the fractional abundances of the spike and the Standard Mean Ocean Water (SMOW), respectively. The isotopic ratio of the water ($^{18}R_{water}$) can be then calculated as $^{18}F_{water}/1\text{-}^{18}F_{water}$.

A pipette with sterile pipette tips is recommended for spiking the sample. The ^{18}O-labeled water is denser than seawater and will sink to the bottom of the bottle, so it is important to make sure the pipette tip is placed below the neck of the bottle when spiking the sample, so that no labeled water is expelled when the bottle is capped with the ground-glass stopper. After the spike, the samples are gently mixed and kept in the dark until the incubation starts. A new pipette tip is used for every sample. The handling of the samples is conducted under low light conditions.

4.2.3.2. Initial samples

The collection procedure for the initial (Time-zero) samples depends on whether the analysis is to be done by IRMS or MIMS. For the latter, the samples are collected in the same way as the

incubation sample and poisoned with saturated mercuric chloride solution at the start of the incubation to inhibit microbial activity (see section 4). Samples for IRMS analysis are typically collected in pre-evacuated glass flasks containing mercuric chloride. The neck of the flasks, which are typically 200-250 mL in volume, is equipped with a Louwers Hanique^{TM} valve (with single or double o-ring). The preparation of the flasks is similar to that described for O_2 /Ar and triple oxygen isotope gas sampling (see Chapters 7,8 for detailed overview), and includes: 1) dosing flasks with 100 µL of saturated mercuric chloride solution and drying at 70°C, 2) evacuating them using a vacuum pump to <1E^{-2} mtorr, and 3) filling the neck of the flasks with CO_2 (Emerson et al., 1999) or distilled water and capping them, to avoid contamination with atmospheric gas through the o-rings during storage before sampling. Extreme care is needed during sampling to avoid contamination with atmospheric gas bubbles. When possible, the neck of the flask is flushed with CO_2 before sampling to dislodge ambient air. While flushing with CO_2, a ~1/8" Nylon tube connected to the spigot of the Niskin-type bottle is inserted into the neck of the flask. When the sample valve from the Niskin-type bottle is open, a water lock is established with a small volume of seawater, making sure all bubbles in the neck are removed by tapping the glass valve. Then the glass valve is opened and, while maintaining the water lock, the flask is filled with a small volume of seawater sample (~50-100 mL). After the valve is closed the neck of the flask is either filled with CO_2 or distilled water and capped, to avoid air contamination during storage until analysis.

4.3. Incubation

Typically the samples are collected before sunrise and incubated from pre-dawn to dusk, or for 24 hours. In contrast to ^{14}C- and ^{13}C-derived primary production, ^{18}O-GOP is independent on whether the duration of the incubation is from dawn to dusk or 24 hours, as there is no splitting of water in the dark and the measurement is not affected by recycling. Once the samples have been spiked, they are incubated keeping to the extent possible the *in situ* environmental conditions. This can be achieved by incubating the samples *in situ* or simulating the *in situ* conditions (e.g., using on deck incubators). For a review of incubation methods refer to Chapter 3. At each station, samples are collected at different depths within the euphotic zone (8 depths are typically recommended; JGOFS, 1996). For *in situ* incubations, replicate bottles (at least 3 recommended) from the same depth are attached to a custom-made rack and deployed at the appropriate depth of a free-floating mooring array. It is important to keep the samples in the dark until deployment and after recovery. Therefore, it is recommended that the deployment and recovery of the array is conducted before sunrise and after sunset, respectively. Alternatively, the samples can be incubated in on-deck incubators that simulate the *in situ* conditions. In this case, information is needed prior to the start of the incubation regarding the temperature and light conditions through the water column (Chapter 3).

4.3.1. Termination of the incubation and sample storage

The incubation can be terminated by transferring a subsample from the incubation bottle into a different gas-tight container, and then inhibiting biological activity using saturated mercuric chloride solution. Due to its toxicity, it is important to use gloves when dealing with mercuric chloride. Transferring of a subsample from the incubation bottle to a different container is done by siphoning from the bottom of the container, making sure no air bubbles are trapped in the line. The procedure for the collection of the subsample depends on whether these are going to be analyzed by IRMS or MIMS.

For IRMS, subsamples are transferred into evacuated pre-poisoned flasks with Louwers Hanique^{TM} valves, as described in section 4.2 and Chapters 7 and 8. Samples are stored in the dark until analysis. Maximum recommended storage time for gas samples is <2 months.

When using MIMS, subsamples can be transferred into any gas-tight bottle, for example borosilicate crimped-sealed serum bottles (Ferrón et al., 2016) or screw cap vials with rubber septa (e.g., 12 mL Labco Exetainer®). The subsample is transferred by siphoning, filling the serum bottle at low flow from bottom to top, allowing it to overflow. Subsequently, saturated mercuric chloride solution can be added using a pipette, inserting the pipette tip below the neck of the bottle. As the mercuric chloride solution is denser than seawater, it will sink to the bottle, and will not be expelled when the bottle or vial is closed. Alternatively, the mercuric chloride spike can be added after closing the bottle or vial using a 1-mL syringe (connected to a needle) loaded with mercuric chloride solution. In this case, a short needle that will act as a vent is first inserted through the septum or rubber stopper, subsequently a longer needle connected to the syringe is inserted and the right amount of mercuric chloride solution is added to the vial or bottle before removing both needles. Care must be taken not to inadvertently inject an air bubble while fixing the sample. Using a pipette is recommended as it avoids the risk of working with needles while handling toxic mercuric chloride solution. Once the sample is fixed with mercuric chloride, it should be gently mixed and stored in the dark until analysis. It is recommended that water samples for MIMS analysis are measured as soon as possible, as O_2 is a chemically active gas in seawater, ideally within a week of collection.

Alternatively, if using MIMS, the sample can be terminated directly in the incubation bottle by fixing with mercuric chloride saturated solution. To be able to re-close the bottle with no bubbles, a glass-ground stopper that displaces more water than the one used for incubation is needed. In this case, it is important to keep the stopper in place (e.g., using tape) and store the samples immersed in water (to keep the glass-ground joint gas tight by keeping it wet). This can be achieved by storing the samples upside down inside a compartmentalized rack with beakers filled with water.

4.4. Isotopic analysis

The isotopic ratio ($^{18}O/^{16}O$) of dissolved O_2 can be measured by IRMS or MIMS. Both approaches can also measure O_2 to Ar molar ratios.

4.4.1. IRMS

Samples collected into gas-tight flasks are returned to a shore-side laboratory where the sample is left to equilibrate with the headspace by continuous agitation for 8-10 hours, which allows 97-98% of the dissolved gases to exsolve (Emerson et al., 1999). The water flask is then inverted, and sample water is removed from the flask using a vacuum pump, leaving less than 1 mL of sample water to maintain the exsolved gases in the headspace. The sidearm of the flask is then rinsed with distilled water, capped and stored until analysis.

Samples are processed using a high-vacuum gas line that allows samples to be transferred from sample flask through several cryotraps to remove water vapor and CO_2 from the sample, similar to O_2 /Ar analysis described in Chapter 8. Samples are then admitted to the IRMS and the mass/charge (m/z) ratio of $^{18}O^{16}O$ (m/z 34) relative to $^{16}O^{16}O$ (m/z 32) is determined for the sample

versus an internal working standard. Typically, an average of 6 measurements are used to constrain the $^{18}O/^{16}O$ value. The $^{18}O/^{16}O$ should be corrected for the O_2 /Ar of the sample, as gas matrix effects will affect the ionization efficiencies of oxygen isotopologues differently (see Chapter 7.

4.4.2. MIMS

A MIMS analyzer consists of a membrane inlet system (Ferrón et al., 2016; Kana et al., 1994) connected to a quadrupole mass spectrometer (e.g Pfeiffer HiQuad™ QMG 700, Pfeiffer PrismaPlus® QMG 220). It is recommended to use a secondary electron multiplier when measuring m/z 34 ($^{18}O^{16}O$). When using MIMS, a fraction of the gases is transferred directly from the water sample to the mass spectrometer, so no prep steps are needed. It is recommended to remove water vapor and CO_2 from the gas stream (e.g., using a cryotrap) as these gases can affect the ionization, and to maintain the membrane inlet at a constant temperature (as diffusing across the membrane is temperature-dependent). Calibration can be done by air equilibrating seawater of known salinity at a given temperature (± 0.01°) (Ferrón et al., 2016). To calculate the concentrations of dissolved O_2 and Ar in the standard we recommend using the solubility equations of García & Gordon (1992) and Hamme & Emerson (2004), respectively. The isotopic composition of dissolved O_2 in the standard can be determined using the solubility fractionation reported by Kroopnick & Craig (1972). It is recommended to run a standard periodically while measuring the samples (every ~20-30 min) to account for drift in the signals (Kana et al., 1994, 2006). Further details can be found in Ferrón et al. (2016).

4.5. Accuracy and uncertainty

As with any other method for measuring primary production, there are no available standards against which to calibrate ^{18}O-GOP, so it is not possible to calculate the accuracy. Instead, comparison of primary production measured by different approaches, as well as making sure that measured rates are physiologically plausible are two common approaches to validate primary production results (see Chapter 3).

The analytical uncertainty in ^{18}O-GOP can be estimated by propagating the errors in the different terms of Equation (3.1), which are typically assumed to be the standard deviation of replicate samples. The isotopic ratio of the water after the spike is typically not measured, but when measured, predicted values agreed with measured ones within 5% (Juranek & Quay, 2005). The reproducibility of dissolved O_2 measurements by the Winkler method, measured as the coefficient of variation of replicate samples, is typically between ±0.1-0.2%. The precision for the isotopic ratio of O_2 is typically ~ ±0.002% (0.02 per mil) when using IRMS and ~ ±0.05% when using MIMS (Ferrón et al., 2016). The analytical ^{18}O-GOP error (typically between ± 1-5%) is typically considerably smaller than the coefficient of variation from triplicate incubated samples (~10-20%) (Ferrón et al., 2016; Juranek & Quay, 2005).

4.6. References

Bender, M. L., Grande, K., Johnson, K., Marra, J., Williams, P. J. L. B., Sieburth, J., et al. (1987). A comparison of four methods for determining planktonic community production. *Limnology and Oceanography*, *32*, 1085–1098. https://doi.org/10.4319/lo.1987.32.5.1085

Bender, M. L., Orchardo, J., Dickson, M.-L., Barber, R., & Lindley, S. (1999). In vitro O_2 fluxes

compared with ^{14}C production and other rate terms during the JGOFS Equatorial Pacific experiment. *Deep-Sea Research Part I*, *46*, 637–654.

Bender, M. L., Dickson, M., & Orchardo, J. (2000). Net and gross production in the Ross Sea as determined by incubation experiments and dissolved O_2 studies, *Deep-Sea Research Part II*, *47*, 3141–3158. https://doi.org/10.1016/S0967-0645(00)00062-X

Brown, A. H. (1953). The effects of light on respiration using isotopically enriched oxygen. *American Journal of Botany*, *40*, 719–729. https://doi.org/10.2307/2439688

Carpenter, J. H. (1965). The accuracy of the Winkler method for dissolved oxygen analysis. *Limnology and Oceanography*, *10*, 135–140. https://doi.org/10.4319/lo.1965.10.1.0135

Dickson, M. L., Orchardo, J., Barber, R. T., Marra, J., McCarthy, J. J., & Sambrotto, R. N. (2001). Production and respiration rates in the Arabian Sea during the 1995 Northeast and Southwest Monsoons. *Deep-Sea Research Part II*, 48: 1199-1230. https://doi.org/10.1016/S0967-0645(00)00136-3

Emerson, S., Stump, C., Wilbur, D., & Quay, P. D. (1999). Accurate measurement of O_2, N_2, and Ar gases in water and the solubility of N_2. *Marine Chemistry*, *64*, 337–347. https://doi.org/10.1016/S0304-4203(98)00090-5

Ferrón, S., del Valle, D. A., Björkman, K. M., Quay, P. D., Church, M. J., & Karl, D. M. (2016). Application of membrane inlet mass spectrometry to measure aquatic gross primary production by the ^{18}O in vitro method. *Limnology and Oceanography: Methods*, *14*, 610–622. https://doi.org/10.1002/lom3.10116

Fitzwater, S. E., Knauer, G. A., & Martin, J. H. (1982). Metal contamination and its effect on primary production measurements. *Limnology and Oceanography*, *27*, 544–551. https://doi.org/10.4319/lo.1982.27.3.0544

García, H. E., & Gordon, L. I. (1992). Oxygen solubility in seawater: Better fitting equations. *Limnology and Oceanography*, *37*(6), 1307–1312.

González, N., Gattuso, J. P., & Middelburg, J. J. (2008). Oxygen production and carbon fixation in oligotrophic coastal bays and the relationship with gross and net primary production. *Aquatic Microbial Ecology*, *52*, 119–130. https://doi.org/10.3354/ame01208

Grande, K. D., Kroopnick, P., Burns, D., & Bender, M. L. (1982). ^{18}O as a tracer for measuring gross primary productivity in bottle cxpcriments. (Abstr.) *Eos*, 63: 107.

Grande, K. D., Williams, P. J. L. B., Marra, J., Purdie, D. A., Heinemann, K., Eppley, R. W., & Bender, M. L. (1989). Primary production in the North Pacific gyre : a comparison of rates determined by the ^{14}C, O_2 concentration and ^{18}O methods. *Deep Sea Research*, *36*, 1621–1634.

Halsey, K. H., Milligan, A. J., & Behrenfeld, M. J. (2011). Linking time-dependent carbon-fixation efficiencies in Dunaliella Tertiolecta (Chlorophyceae) to underlying metabolic pathways. *Journal of Phycology*, *47*, 66–76. https://doi.org/10.1111/j.1529-8817.2010.00945.x

Hamme, R. C., & Emerson, S. (2004). The solubility of neon, nitrogen and argon in distilled water and seawater. *Deep-Sea Research Part I: Oceanographic Research Papers*, *51*, 1517–1528.

https://doi.org/10.1016/j.dsr.2004.06.009

JGOFS. 1996. Protocols for the Joint Global Ocean Flux Study (JGOFS) core measurements, p. 170. In A. Knap (ed.), Report no. 19 of the Joint Global Ocean Flux Study.

Juranek, L. W., & Quay, P. D. (2005). In vitro and *in situ* gross primary and net community production in the North Pacific Subtropical Gyre using labeled and natural abundance isotopes of dissolved O_2. *Global Biogeochemical Cycles*, *19*, 1–15. https://doi.org/10.1029/2004GB002384

Kana, T. M., Darkangelo, C., Hunt, M. D., Oldham, J. B., Bennett, G. E., & Cornwell, J. C. (1994). Membrane inlet mass spectrometer for rapid high-precision determination of N_2, O_2, and Ar in Environmental Water Samples. *Analytical Chemistry*, *66*, 4166–4170.

Kana, T. M., Cornwell, J. C., & Zhong, L. (2006). Determination of denitrification in the Chesapeake Bay from measurements of N2 accumulation in bottom water. *Estuaries and Coasts*, *29*, 222–231. https://doi.org/10.1007/BF02781991

Karl, D. M., Hebel, D. V., Björkman, K., & Letelier. (1998). The role of dissolved organic matter release in the productivity of the oligotrophic North Pacific Ocean. *Limnology and Oceanography*, *43*, 1270–1286. https://doi.org/10.4319/lo.1998.43.6.1270

Kiddon, J., Bender, M. L., & Marra, J. (1995). Production and respiration in the 1989 North Atlantic spring bloom: an analysis of irradiance-dependent changes. *Deep-Sea Research Part I*, *42*, 553–576. https://doi.org/10.1016/0967-0637(95)00008-T

Kroopnick, P., & Craig, H. (1972). Atmospheric oxygen: Isotopic composition and solubility fractionation. *Science*, *175*, 54–55. https://doi.org/10.1126/science.175.4017.54

Laws, E. A., Landry, M. R., Barber, R. T., Campbell, L., Dickson, M. L., & Marra, J. (2000). Carbon cycling in primary production bottle incubations: Inferences from grazing experiments and photosynthetic studies using ^{14}C and ^{18}O in the Arabian Sea. *Deep-Sea Research Part II: Topical Studies in Oceanography*, *47*, 1339–1352. https://doi.org/10.1016/S0967-0645(99)00146-0

Marra, J. (2009). Net and gross productivity: Weighing in with ^{14}C. *Aquatic Microbial Ecology*, *56*, 123–131. https://doi.org/10.3354/ame01306

Pei, S., & Laws, E. A. (2013). Does the ^{14}C method estimate net photosynthesis? Implications from batch and continuous culture studies of marine phytoplankton. *Deep-Sea Research Part I: Oceanographic Research Papers*, *82*, 1–9. https://doi.org/10.1016/j.dsr.2013.07.011

Pei, S., & Laws, E. A. (2014). Does the ^{14}C method estimate net photosynthesis? II. Implications from cyclostat studies of marine phytoplankton. *Deep-Sea Research Part I: Oceanographic Research Papers*, *91*, 94–100. https://doi.org/10.1016/j.dsr.2014.05.015

Quay, P. D., Peacock, C., Björkman, K., & Karl, D. M. (2010). Measuring primary production rates in the ocean : Enigmatic results between incubation and non - incubation methods at Station ALOHA. *Global Biogeochemical Cycles*, *24*(GB3014). https://doi.org/10.1029/2009GB003665

Regaudie-de-Gioux, A., Lasternas, S., Agustí, S., & Duarte, C. M. (2014). Comparing marine

primary production estimates through different methods and development of conversion equations. *Frontiers in Marine Science*, *1–14*, 135–140. https://doi.org/10.3389/fmars.2014.00019

Robinson, C., & Williams, P. J. L. B. (2005). Respiration and its measurement in surface marine waters. In P. A. del Giorgio & P. J. L. B. Williams (Eds.), *Respiration in Aquatic Ecosystems* (pp. 147–180). New York: Oxford University Press. https://doi.org/10.1093/acprof:oso/9780198527084.003.0009

Steemann Nielsen, E. (1952). The use of radio-active carbon (C^{14}) for measuring organic production in the sea. *ICES Journal of Marine Science*, *18*, 117–140. https://doi.org/10.1093/icesjms/18.2.117

5. Light and dark dissolved oxygen rate measurements using the Winkler method.

Chris Langdon[1], E. Elena García-Martín[2]

[1]*Rosenstiel School of Marine and Atmospheric Science, University of Miami, Florida, USA*
[2]*National Oceanography Centre, Southampton, UK*

5.1. Introduction

Changes in oxygen concentration are directly linked to biological processes. Photosynthesis produces oxygen whereas aerobic respiration consumes oxygen and forms carbon dioxide. Therefore, the quantification of the dissolved oxygen concentration provides us with very useful information about the balance of the metabolic processes in aquatic systems. Ludwig Winkler, at the end of the XIX century, developed a technique to determine indirectly the concentration of dissolved oxygen in water using a series of multi-steps chemical reactions (Winkler 1888). Four years later, Natterer applied the technique for the first time to seawater samples (Natterer 1892). However, it was not until 1927 when Gaarder and Gran (1927) used it to measure biological oxygen fluxes. Combining light and dark bottles, Gaarder and Gran measured the production and consumption of the oxygen dissolved in an enclosed seawater sample with respect to an initial oxygen concentration. The original method was subject to several limitations during the manipulation and analysis of the samples which introduced errors that affected the precision and replicability between samples. These limitations were resolved by the introduction of whole bottle titrations (Carritt and Carpenter 1966; Carpenter 1965) and with the development of automated titration using potentiometric, amperometric or photometric end-point detection (Oudot 1988; Culberson and Huang 1987; Williams and Jenkinson 1982).

The method proposed by Winkler is a multi-step process, based on the oxidation of Mn(II) to Mn(III) by oxygen in an alkaline solution (made up of sodium iodide and sodium hydroxide), ultimately releasing free diatomic iodine (I_2) into the solution. These reactions are visualized by the formation of a brown-colored precipitate. The I_2 molecules are directly proportional to the molecules of oxygen. Therefore, in order to know the molecules of dissolved oxygen in water, the I_2 is titrated with thiosulphate. The stoichiometric equations for the reactions are:

$Mn^{+2} + 2OH^- \rightarrow Mn(OH)_2$	
$2Mn(OH)_2 + ½\ O_2 + H_2O \rightarrow 2MnO(OH)_3$	oxidation of Mn(II) to Mn(III)
$2MnO(OH)_3 + 2I^- + 6H+ \rightarrow\ 2Mn^{+2} + I_2 + 6H_2O$	oxidation of iodide to iodine
$I_2 + I \rightarrow +I_3^-$	oxidation of thiosulphate to tetrathionate and
$I_3^- + 2\ S_2O_3^{-2} \rightarrow 3I^- + S_4O_6^{2-}$	reduction of iodine complex to iodide ions

Parallel to the development of the light/dark bottle dissolved oxygen method, the use of radiolabeled ^{14}C method was introduced to estimate photosynthesis (Chapter 3). The popularity of the ^{14}C incorporation method can be observed in the vast amount of photosynthesis measurements collected in a few years, which allowed the construction of detailed maps of photosynthetic activities in the ocean (Koblentz-Mishke, 1967). Despite the current popularity of the ^{14}C incorporation method, its use is limited to the estimation of gross and net primary production, as plankton community respiration cannot be quantified directly. Therefore, estimations of plankton community respiration and net community production can only be made by measuring changes in the dissolved oxygen concentrations of a water sample.

It is important to understand the difference between net primary production and net community production, as well as their ecological implications, to decide on the method to use. Net primary production refers to the gross primary production minus the respiration of the autotrophs, and therefore represents the rate at which phytoplankton produces biomass. Whilst, net community production is the difference between the gross primary production minus the total community respiration (autotrophic and heterotrophic respiration). Knowledge of net community production is necessary to quantify the carbon that a system can potentially export. Thus, on an annual basis, net community production corresponds to the organic carbon biologically produced in the euphotic layer that can be exported to the deep ocean, a process known as the "biological carbon pump" (Emerson 2014).

In this section, we describe the light/dark bottle dissolved oxygen method for measurement of primary production rates using *in situ* or on-deck incubations. The method has been employed to determine the primary production rates of natural phytoplankton communities in a wide range of environments, including some of the most oligotrophic open ocean waters (Williams et al 1983, Grande et al 1989). The method can also be used to get rates of community respiration below the photic zone (Robinson et al 2002a, 2002b).

Here we describe how the pre-cruise preparation of chemical solutions needed for the determination of oxygen concentration of the samples, the options for ship-board automated titration analysis of the samples, and the set up for *in situ* and on-deck incubations. Finally, we give the precision of the rates that can be expected under typical conditions.

5.2. Best Practices of On-Deck/ *in situ* Incubations

5.2.1. Chemical reagents

Five different reagents are required for the sampling and analysis of the dissolved oxygen concentration in seawater. All chemicals should be stored in amber glass bottles once prepared. Wear nitrile gloves and safety glasses during the preparation of the reagent solutions and do them in a fume hood cupboard.

- Manganous chloride solution ($MnCl_2 \cdot 4H_2O$, 3 M). Dissolve 600 g of manganous chloride tetrahydrate ($MnCl_2 \cdot 4H_2O$) in a graduated volumetric flask containing 500-700 mL of Milli-Q water. Stir until all the crystals have dissolved. The solution may cool during preparation. Allow it to get into room temperature before making the solution up to a final volume of 1 litre. Manganous sulphate ($MnSO_4 \cdot 4H_2O$, 3M) may be used instead of the manganous chloride solution. Dissolve 450 g of manganous sulphate tetrahydrate

($MnSO_4 \cdot 4H_2O$) in a graduated volumetric flask containing 500-700 mL of Milli-Q water. Stir until all the crystals have dissolved. The solution may cool during preparation. Allow it to get into room temperature before making the solution up to a final volume of 1 litre.

- Solution of sodium iodide (NaI, 4M) and sodium hydroxide (NaOH, 8M). Dissolve 320 g of NaOH in a graduated volumetric flask containing 500 mL of MilliQ water. This is an exothermic reaction, so it is recommended to cool down the solution stirring the volumetric flask inside an ice bath. Once all the compound is dissolved, add slowly 600 g of NaI and stir until it completely dissolves. It can take several hours. Make the solution up to a final volume of 1 litre. If the solution is not transparent (there are some tracers of reagents that have not dissolved), filter the solution through a coarse glass fiber filter to remove the non-dissolved material. If the solution presents a yellowish-brownish color, discard it and prepare it again with fresh reagents
- Sulphuric acid (H_2SO_4, 5M): Slowly add 280 mL of H_2SO_4, into 650 mL of Milli-Q water. This is an exothermic reaction and will generate a lot of heat as well as corrosive gasses. Do it inside a fume hood cupboard and preferably submerge the volumetric flask inside an ice bath, to cool it down. Once the solution reaches room temperature, make it up to 1 litre.
- Sodium thiosulphate pentahydrate ($Na_2S_2O_3 \cdot 5H_2O$). The concentration of the thiosulphate will depend on the volume of the burette of your titration system. The concentration should be one which allows your titration system to dispense around 80-90 % of the burette volume. For example, for a titration system with 1 mL burette and oxygen bottles of 125 mL, the common concentration is 0.2 M. Dissolve 24.821 g of $Na_2S_2O_3 \cdot 5H_2O$ into 900 mL of Milli-Q water. Make the solution up to 1 litre.
- Potassium iodate (KIO_3, 0.0100 N). It is very important to be very accurate measuring this compound as it will be used as a primary standard to standardize the thiosulphate concentration. It could be bought already as a solution, or be prepared in the laboratory. Weight 0.5 g of KIO_3 and dry it in an oven at 120 °C for several hours. Weigh out, to the closest decimal, 0.3567 g of the dried KIO_3 and dissolve it in 1L of Milli-Q water in a volumetric glass. Use a pipette to add drops at the end to properly level the meniscus to the line of the volumetric glass.

5.2.2. Sampling and incubation bottles

The most common and generally accepted containers for collecting water samples for the determination of dissolved oxygen concentration are 100 mL borosilicate glass bottles. Other volumes (i.e from 50 to 500 mL) can be used, but smaller volumes could undersample part of the plankton population, and larger bottles will need more water to be collected, larger incubator systems and the use of a larger volume of reagents. Borosilicate glass bottles are non “trace-metal clean” and remove part of the UV radiation, which could affect the primary production rates (Regaudie de-Gioux et al., 2014; Garcia-Corral et al., 2016). Quartz bottles can be used instead. However, quartz bottles are extremely expensive and very easy to break during the incubation. In addition, the incubation occurs under polycarbonate blue and neutral density filters, which block the penetration of wavelengths below 400 nm. Therefore, the 100 mL borosilicate bottles are the preferred option. Bottles should be numbered (engraved numbers or with a water-resistant label) as well as their corresponding ground joint stoppers. All bottles must be calibrated and the volume of each bottle known to ±0.06 ml. As a standard procedure, borosilicate bottles are calibrated at

20 °C. The volume of the bottles (V_{bottle}) experiment changes with temperature. Therefore, during the analysis of the sample, it is important to correct for the temperature effect on the volume applying the equation:

$$V_{bottle} = V_{bottle} [1 - \alpha(t - 20)], \quad (5.1)$$

where α is the volumetric coefficient of expansion of the glass (3.2×10^{-6} K^{-1} for borosilicate glass) and t is the temperature of the seawater sample.

We recommend at least 15 bottles per depth. Five bottles will be fixed before the incubation ("initial"), five bottles will be incubated in dark ("dark") and the remaining five will be incubated under *in situ* simulated light conditions.

Prior to sampling, it is a good practice to confirm that all the material needed is in place (bottles, chemical reagents inside their dispenser bottles, a digital thermometer, the sampling sheet with the numbers of the bottles written down and a pencil).

5.3. Shipboard Sampling Procedure

At each station, sea water samples will be collected from different depths using water samplers (Niskin bottles) mounted on a rosette system. It is recommended to sample a minimum of 6 depths, preferable 8, through the entire euphotic zone (depth at which the incident irradiance is 1% of surface irradiance). The sampling depths should include the surface depth, the euphotic depth, the depth of maximum chlorophyll, the depth at the top of the chlorophyll gradient and the depth at the bottom of the chlorophyll gradient, to properly determine the variability of the primary production rates (Figure 5.1). The sampling should be carried out before sunrise.

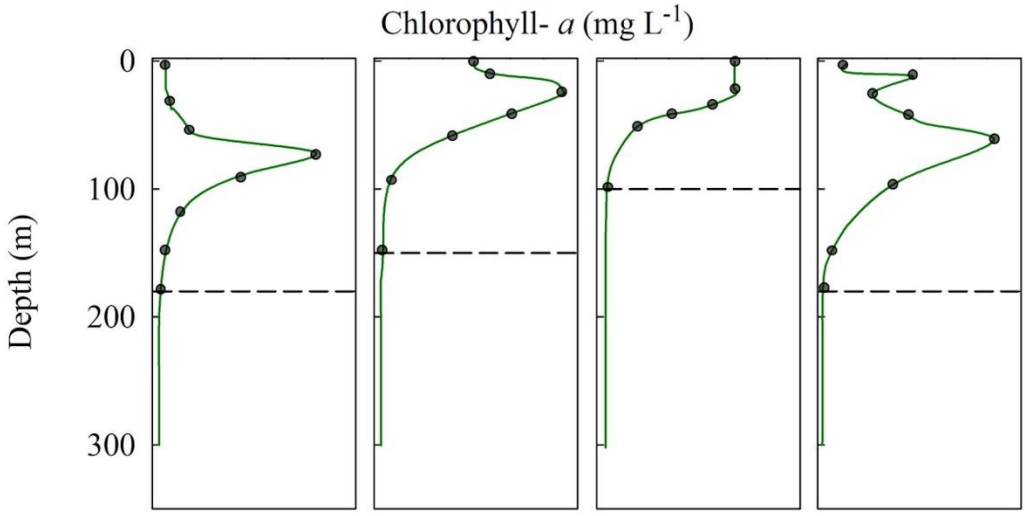

Figure 5.1. Conceptual diagram showing vertical profiles of chlorophyll-a fluorescence. In these examples, the grey dots represent the recommended sampling depths and the dotted line indicates the position of the euphotic depth.

Acid-clean HDPE carboys will be needed to transfer the seawater from the Niskin bottles. The carboys should be wrapped in black plastic bags to shield the samples from the boat lights. The transfer of 10 litres of seawater from each Niskin to their corresponding acid-clean HDPE carboys is done by a Tygon or silicon tubing, rinsing the carboys at least three times prior to filling. The order for the sampling from the carboys into the dissolved oxygen bottles should be from the deepest depth to the most surface one. This considers that the water sample from the deepest depth is colder and has lower oxygen concentration than surface waters.

Seawater is gently transferred from each carboy into the dissolved oxygen bottles using a sampling tubing, checking that bubbles are not formed and stuck into the tube. Ideally bottles should be rinsed by filling them and letting the water overflow for three times the volume of the bottle. In order to not entrap bubbles inside the bottle, the filling should be up to the top of the bottle neck. Stoppers need to be rinsed and will be carefully placed to their corresponding bottle once that all the bottles from the same depth are filled.

When all the carboys are sampled, it is time to fix the "initial" bottles. First, the temperature is measured from each bottle. Then, 1 mL of the $MnCl_2$ solution followed by 1 ml of the NaI/NaOH solution are added to each bottle and the stoppers are replaced carefully without capturing any bubbles. The bottles are shaken vigorously by inverting the bottles around 30 times. A second round is done to ensure that the reagents have reacted with all the oxygen. It is recommended to hold the stopper as well as the base of the bottle when shaking the bottles, as the stopper could pop up. The "initial" bottles are stored under water, whereas the "dark" and "light" bottles are taken to their incubators. As the "dark" and the "light" bottles are incubated in the same incubators, it is important that the "dark" bottles are covered to avoid any light inside the bottles. There are several options to darken them, including taping the bottle with electrical tape, wrapping in aluminium foil and using an opaque cloth. We do not recommend to tape the bottles as it might be difficult to check the appearance of bubbles inside the bottles during the incubation. Aluminium foil can be easily broken and then the light could bounce inside the bottle. Hence, the preferred option is to use an opaque cloth/plastic bag.

5.4. Sample incubation and incubation time

The incubation duration for the estimation of primary production (gross and net) with the dissolved oxygen incubation is 24 h, and therefore considered a daily rate. The sampling is performed pre-dawn and the incubation is set to start during the sunrise to contain the light and dark hours of a day. The oxygen consumption measured in the "dark" bottles represents the respiration over 24 h and it has the inherent assumption that the oxygen consumption in the light is equivalent to the oxygen consumption in the dark. This assumption was tested with 18O enrichment of dissolved O_2 and oxygen microelectrodes and it was found that oxygen consumption in the light could be greater than in the dark and therefore gross primary production could be underestimated applying this methodology (Grande et al. 1989, Luz et al. 2002, Pringault et al. 2007, Robinson et al. 2009).

Incubation lasting 24 hours could introduce some biases associated with "bottle effects" that include changes in the mixing conditions, greater bacterial growth, increase of grazing, among others (Robinson and Williams 2005, Vernet and Smith 2007). These biases could have an effect

on the respiration rates and therefore on the net community production. Yet, despite the potential changes in the community structure of the sample, several studies have shown linear decrease in oxygen concentration (Biddanda et al. 1994, Smith and Kemp 2001, García-Martín et al. 2011).

5.4.1. In situ incubation

In situ incubations allow to perfectly match the light intensity and spectral quality as well as the temperature during the incubation. The incubation system is usually formed by a buoy or a floating device, weights attached to the bottom and trays with hooks in which to secure the bottles (Figure 5.2). Trays should be floating at the depths from which the seawater samples were collected. It is important that the hooks are designed to hold the bottle stopper in position, so the bottles cannot be accidentally opened during the incubation. It is recommended to lay light bottles on their side, so the stoppers do not block the light.

This incubation implies the necessity to be close to the buoy during the 24 h that the incubation lasts, and therefore, it is not very practical for cruises that cover a long sampling area, but are ideal for coastal areas and experiments in a small research area.

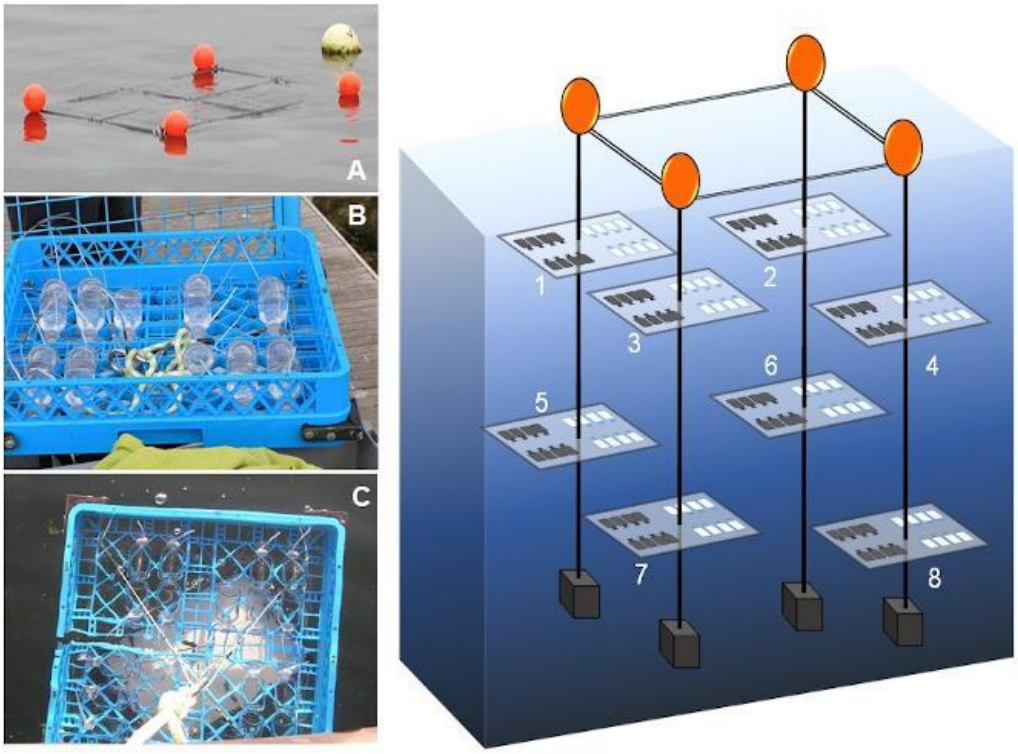

Figure 5.2. Pictures of in situ incubations showing the different parts of the incubation system. (A) Floating buoys, (B-C) Incubation trays with light bottles, (D) schematic diagram of the whole system with 8 trays (numbers indicate 8 different incubation depths)

5.4.2. On-deck incubations

The alternative to in situ incubations are on-deck incubations (Figure 5.3). This incubation requires information about in situ variables, such as light intensity and temperature, in order to simulate the *in situ* conditions. As the sampling is performed prior to the sunrise, there is no information of the *in situ* light conditions from the sampling day. Generally, the PAR profile from the previous day is adopted.

Incubators can have different designs, but overall, the system consists of plexiglass containers with two connectors, one to pump water into the incubator and the other one to let the water out. The *in situ* light intensities are adjusted with blue and neutral density filters. There should be as many incubators as depths sampled, so all the bottles are incubated approximately at their *in situ* light conditions. Temperature is controlled by running surface water into the system to the incubators containing the bottles from the surface depth or from those depths within the thermocline. For incubators containing bottles from deeper depths, usually at colder temperatures, chilled water is re-circulated from a chiller system. During night hours, it is recommended to cover the incubators with an opaque plastic or cloth, as the lights from the ship could disturb the metabolic processes.

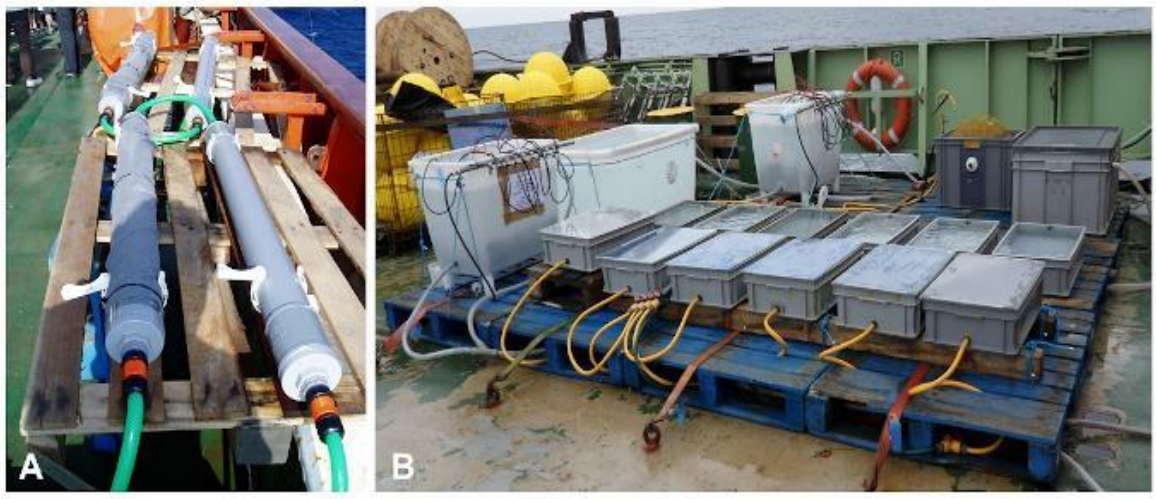

Figure 5.3. Examples of different on deck incubators (A) cylindrical and (B) plastic boxes with plexiglass lids. Incubators are connected to water baths that supply water at in situ temperature.

5.5. Sample Processing and analysis

After the in situ or on deck incubations, all bottles ("light" and "dark") are removed from the incubators covered with dark plastic bags and taken to the laboratory. It is important to check for bubbles inside the bottles, as they can introduce biases to the measurements. Fixation is carried out following the same procedure as for the "initial" bottles described above (section 2.3), recording the temperature just prior to the addition of the reagents. Once that all bottles are shaken, and the solution is uniform, they should be kept underwater in darkness, until the precipitate settles (usually 1 – 2 h). Once the precipitate is settled in the bottom, the bottles are ready for analysis. It

is convenient to proceed with the analysis straight after the settling period. Some guidelines indicate that the bottles can be stored in darkness and underwater for up to a month (HELCOM guidelines). However, as it is important to avoid temperature changes, we recommend minimizing the time they are stored.

5.5.1. Titration method

There are three titration methods to determine the dissolved oxygen concentration of a water sample: a photometric titration, a potentiometric titration and an amperometric titration.

5.5.1.1. Photoometric titration

The photometric endpoint detection method involves putting the sample bottle in the path of a beam of light and measuring the change in absorbance at 360 nm as I_2 is converted to a colorless form by the addition of thiosulfate. An automated version suitable for shipboard primary productivity use has been described by Williams and Jenkinson (1982). A typical precision of 0.03-0.1% was claimed.

5.5.1.2. Potentiometric titration

The potentiometric method involves measuring the potential measured across a dual platinum electrode. The endpoint is detected as a maximum in the change in potential per unit addition of thiosulfate. An automated version suitable for shipboard primary productivity use has been described by Oudot et al. (1988). A typical precision of 0.1% was claimed.

5.5.1.3. Amperometric titration

The amperometric method involves applying a potential of 100 mV to a dual platinum electrode placed into the sample bottle. The endpoint is detected as the point at which the current goes to zero. The amperometric method is also known as the 'dead-stop' method. An automated version suitable for shipboard primary productivity and routine hydrographic work has been described by Langdon (2010). A typical precision of 0.06% was claimed.

5.5.2. Blank determination

Reagents can contain impurities that may interfere with the reduction-oxidation reactions involved in the dissolved oxygen analysis. Therefore, it is important to perform a reagent blank to quantify the contribution to the changes in oxygen concentration by the reagents. An empty bottle is filled with 100 ml of Milli-Q water and a stir bar. The reagent components are added in inverse order to the sampling procedure, mixing in between the additions. First 1 ml of the H_2SO_4 is added, then 1 ml of the NaI-NaOH solution, followed by 1 mL of the $MnCl_2$ solution and 1 ml of the KIO_3 standard at the end. Titration of the sample is carried out until the endpoint is reached. Then, another 1 ml of the KIO_3 standard is added and titrated again to find a second end point. The volume of the blank is calculated as V1 -V2, where V1 is the volume of thiosulfate used to titrate the first KIO_3 aliquot, and V2 is the volume of thiosulfate used in the titration of the second KIO_3 aliquot. The blank sampling is repeated with ~5 replicates, and the blank value (V_{blk}) is the average of the five independent replicates.

5.5.3. Standardization of the thiosulfate

The thiosulphate concentration can change its molarity as a result of changes in temperature. Therefore, it is recommended to standardize it frequently, at least once per day of analysis.

Six empty bottles are filled with 100 mL of Milli-Q water and a stir bar. The reagent components are added in inverse order to the sampling procedure, mixing in between the additions. First 1 mL of the H_2SO_4 is added, then 1 mL of the NaI-NaOH solution, followed by 1 mL of the $MnCl_2$ solution and 10 mL of the KIO_3 standard at the end. The sample with reagents is titrated and the endpoint recorded.

The molarity of the thiosulphate solution is calculated as follows:

$$M_{thio} = V_{KIO3} * N_{KIO3} /(V_{std} – V_{blk}) \quad (5.2)$$

where V_{KIO3} is the volume of KIO_3 standard added (mL), N_{KIO3} is the molarity of standard KIO_3 (mol/L), V_{std} is the volume of thiosulfate (mL) and V_{blk} is the volume of the blank as measured in the previous section (mL).

The molarity of the thiosulfate solution is determined as the average of the six replicates, and the standard deviation of the replicates should be lower than 1 $x10^{-6}$ (L). If the standard deviation is higher, additional samples should be considered.

5.5.4. Analysis of the samples

The analysis of the sample can start once that the precipitate has settled. It is recommended to analyze the "initial", "dark" and "light" bottles from the same depth in the same batch. In addition, the precipitate is light sensitive, so it is a good practice to remove only one or two bottles at a time for analysis. Any possible remaining water is wiped, the stopper removed and a stir bar added into the bottle taking care that the precipitate is not resuspended. The precipitate is dissolved by adding 1 mL of H_2SO_4 into the bottle and gently mixed. The sample in the bottle is titrated and the added volume of thiosulfate at the endpoint is recorded. The oxygen concentration of the sample is then calculated by the following equation:

$$[O2] (\mu mol/L) = [(¼) * 10^6 * (V_{sam} - V_{blk}) * M_{thio} - 7.6x10^{-8}] / (V_{bot} - V_{reg}) \quad (5.3)$$

where (¼) converts moles of thiosulfate to moles of O_2, 10^6 converts from moles O_2 to micro moles O_2, V_{sam} is the volume of the thiosulphate used during the titration of the sample (L), V_{blk} is the volume of the blank as measured in the previous section (L), M_{thio} is the molarity of thiosulphate calculated during the standardization of the thiosulfate (mol/L), V_{bot} is the volume of sample bottle (L), V_{reg} is the volume of the reagents used during the fixation of the sample (0.002 L), and $7.6x10^{-8}$ is the absolute moles of oxygen added with the reagents (Murray et al. 1968).

If V_{KIO3}=0.010 L, N_{KIO3}=0.010 Equiv/L, V_{std}=0.000700, V_{blk}=0.000001, M_{thio}=0.14306, V_{sam}=0.000800, V_{bot}=0.143, V_{reg}=0.002, O_2=202.67 µmol/L.

Titrated samples should be discarded following the regulation of the country. The bottles, once empty, are rinsed with deionized water.

5.6. Calculation of Photosynthetic Rates of Phytoplankton

Measuring changes in dissolved oxygen concentration incubated over 24 hours provide us with two different primary production rates: gross primary production (GPP) and net community production (NCP).

Net community production is estimated as the difference in oxygen concentration between the average of the replicate "light" measurements and the average of the replicate "initial" measurements. Community respiration is estimated as the difference in oxygen concentration between the average of the replicate "dark" measurements and the average of the replicate "initial" measurements. Gross primary production is calculated as the difference between average of the replicate "light" measurements and the average of the replicate "dark" measurements.

$$NCP = \text{average } [O_2]_{light} - \text{average } [O_2]_{initial} \quad (5.4)$$

$$CR = \text{average } [O_2]_{dark} - \text{average } [O_2]_{initial} \quad (5.5)$$

$$GPP = NCP + CR \quad (5.6)$$

5.7. Uncertainties/Accuracy

The precision of the oxygen method is estimated to be ±10-17 mmol C m^{-2} d^{-1} based on averaging the standard error of the means (SEM) obtained in the studies of Williams et al. 1983, Grande et al. 1989 and Robinson et al. 2009 assuming n=8-10 bottles at each depth. In other units, the average SEM was ±1.4 µg C L^{-1} $(12\ h)^{-1}$ and ±16 µg C (µg Chla)$^{-1}$ $(12\ h)^{-1}$. Assessing the accuracy of the oxygen method would involve delving into the pathways of light respiration and is beyond the scope of this review.

5.8. Cleaning Procedures

Silicone tubing and glass bottles should be cleaned with a 5 – 10 % hydrochloric acid solution before the start of the cruise. Glass bottles could be also cleaned with a dilute solution of non-phosphate detergent (i.e Decon 90) followed by a vigorous rinse with Milli-Q water. Throughout the cruise, it is important that the silicone tubing is rinsed with 5 – 10 % hydrochloric acid plus Milli-Q water every day after using it. However, Milli-Q water could be used to rinse the glass bottles after the titration if they are going to be used the following day. The regular use of the bottles can lead to the appearance of yellowish/brownish stains in the inside part of the neck of the bottle and in the stopper. This is caused by the accumulation of tracers of reagents in the grounded areas of the bottle. It is better to remove the stains as soon as they are noticed and not let them dry or accumulate for long periods of time, as the removal could be more difficult. If stains start to appear in the neck of the bottle, we recommend to add a small volume of concentrated thiosulphate and leave it for a couple of minutes up to hours. If the stain appears on the stopper, a small volume of thiosulphate can be added on top of it, or the stopper can be left inside a vase covered with thiosulphate. Once that the stain disappears, the bottle or/and stopper are rinsed with Milli-Q to remove any possible rest of thiosulphate which could bias the measurements.

5.9. Advantages, Disadvantages and Caveats

All methodologies have strengths and limitations, so it is important to know them and their potential errors in order to choose the best one depending on the research interest and the study area. The Winkler-based light/dark incubation is a very accessible, cheap and precise method to estimate net community primary production, gross primary production and community respiration

rates. In order to achieve high precision, it is important to be meticulous and have high numbers of "light", "dark" and "initial" replicates. The large number of bottles needed implies collection of large volume of seawater and long analytical time, which in some circumstances (i.e. research cruises with a small rosette, high water demands or low human capability) could be considered as a drawback. The equipment required is easily portable and could be mounted in land-based laboratories or research vessels. Furthermore, the reagents needed are not radioactive, and therefore the method can be applied in all laboratories and research vessels and does not require the presence of a certified radioactive responsible person.

The main limitation of the Winkler-based light/dark incubation method is that rates are calculated from two single points measured over 24 hours. As commented in section 5.2.4, the method assumes linear oxygen consumption in the dark bottles between the two incubation times. However, if the oxygen consumption is not linear (Gattuso et al. 2002, Pomeroy et al. 1994), it could underestimate or overestimate the calculation of GPP.

There are several limitations that are common to other methodologies. Similar to any *in vitro* incubation, the Winkler-based light/dark incubation method cannot accurately mimic the *in situ* environmental condition. In addition, enclosing a water sample inside bottles could have a potential effect on the plankton community structure, which may affect the metabolic rates. This is a common drawback for all methods that confine seawater samples in bottles (i.e oxygen microelectrodes or optodes, ^{14}C tracer method and ^{13}C tracer method) and are not exclusive to this technique. However, the longer incubation time required for the Winkler-based light/dark incubation method (24 h) compared to other methods (12 h for the ^{14}C tracer method) may amplify the potential biases.

Despite being an easy and straightforward technique, it is important to be meticulous in the procedures as there are several potential sources of error. We will comment on the most common ones.

- All bottles should be careful calibrated with their respective stoppers. Stoppers may get chipped with use, which could cause changes in the bottle volume. If noticed, bottles should be marked and calibrated again.

- Before starting the titration, it is important to properly shake the bottle containing the thiosulphate and to flush the burette and the connecting tubes to remove any possible remains of thiosulphate left from the previous day of analysis. Thiosulphate left from the previous day could have a different concentration to the thiosulphate inside the dispenser bottle, and therefore the first samples titrated could be subjected to errors.

- During the flushing process, it is recommended to check for air bubbles in the burette or in the connecting tubes. The presence of an air bubble during the titration procedure will affect the precision of the measurement, as the volume of air will be registered as a volume of thiosulphate. This implies that the volume of thiosulphate dispensed by the titrator will not be the amount calculated by the software. There are several ways to remove air bubbles. If the air bubble is in the tip or in the connecting tubes, the easiest approach to

remove it will be to gently tap the burette tip and connecting tubes at the same time that the thiosulphate is flushing. An alternative method will be more appropriate if the air bubble is in the burette and flows forward and backwards through the connecting tubes while flushing and filling the burette. In this case, it will be necessary to untighten the upper valve of the burette very quickly while the air bubble gets flushed out of the burette through the connecting tubes. It is recommended to do it while wrapping the valve with hand towel paper, so the thiosulphate drips into the hand towel paper instead of onto the electrical equipment. If the air bubble is not easily removed, for example it gets formed on the inside surface of the burette, then the easiest approach will be to untighten the burette from the upper valve and remove the burette from the dispenser unit. After discarding the thiosulphate from inside the burette, it should be filled with thiosulphate manually using a clean glass syringe/pipette. Once filled, it will be connected back to the dispenser unit. In theory, a stuck air bubble which does not get flushed, should not bias the readings. However, it is recommended to remove it, as it could be released during the titration process and it may go unnoticed.

- During the analysis of the samples we do not recommend acidifying more than 2 bottles at once as the iodine concentration may decrease due to evaporation and light degradation while waiting to be analysed. If two bottles are acidified at the same time, the bottle waiting should be covered and kept away from the light. In addition, it is important to keep the room temperature as stable as possible, as changes in temperature may facilitate the evaporation of the iodine while being titrated.

5.10. Ancillary Data Collection

Several environmental data, such as temperature, salinity, light attenuation and fluorescence, are fundamental to the application and interpretation of the results for *in situ* and on deck incubations, as explained in Gundersen and Vandermeulen (Chapter 6). Firstly, this information is needed to decide the sampling depths. Secondly, temperature and light irradiance information is essential for the on-deck incubations in order to decide on the neutral filters and to regulate the temperature of the water-bath system. In addition, oxygen saturation can be calculated as a function of temperature and salinity (García and Gordon 1992). Changes in the oxygen saturation in the initial bottles compared to the *in situ* oxygen saturation may affect the microbial community and interfere with the estimations of the metabolic rates, especially in the undersaturated deep sampling depths.

5.11. References

Biddanda, B., S. Opshal, and R. Benner. 1994. Plankton respiration and carbon flux through bacterioplankton on the Louisiana shelf. Limnology and Oceanography 39:1259-1275.

Carpenter, J. H. (1965). The accuracy of the Winkler method for dissolved oxygen analysis. Limnology and Oceanography 10: 135–140. doi: 10.4319/lo.1965.10.1.0135

Carrit, D. E., and Carpenter, J. H. (1966). Comparison and evaluation of currently employed modifications of the Winkler method for determining dissolved oxygen in sea-water. Journal of Marine Research 24: 286–318.

Culberson, C.H. and S. Huang. 1987. Automated amperometric oxygen titration. Deep-Sea Research, 34, 875-880

Emerson, S. (2014), Annual net community production and the biological carbon flux in the ocean. Global Biogeochemical Cycles 28: 14– 28, doi:10.1002/2013GB004680.

Gaarder, T. and Gran, H. H. 1927. Investigations of the production of plankton in the Oslo Fjord. Rapports et proces-verbaux des reunions. Conseil International pour 1'Exploration de la Mer 42:1-48.

García, H. E. and L. I. Gordon. 1992. Oxygen solubility in seawater: Better fitting equations. Limnology and Oceanography, 37, 1307-1312.

Garcia-Corral, L. S., J. M. Holding, P. Carrillo-de-Albornoz, A. Steckbauer, M. Pérez-Lorenzo, N. Navarro, P. Serret, C. M. Duarte, and S. Agusti. 2016. Effects of UVB radiation on net community production in the upper global ocean. Global Ecology and Biogeography 26:54-64.

García-Martín, E. E., P. Serret, and M. Pérez-Lorenzo. 2011. Testing potential bias in marine plankton respiration rates by dark bottle incubations in the NW Iberian shelf: incubation time and bottle volume. Continental Shelf Research 31:496-506.

Gattuso, J. P., S. Peduzzi, M. D. Pizay, and M. Tonolla. 2002. Changes in freshwater bacterial community composition during measurements of microbial and community respiration Journal of Plankton Research 24:1197-1206.

Grande, K. D., J. Marra, C. Langdon, K. Heinemann and M. L. Bender. 1989. Rates of respiration in the light measured in marine-phytoplankton using an O-18 isotope-labeling technique. Journal of Experimental Marine Biology and Ecology 129(2): 95-120.

Koblentz-Mishke, O. J.: Primary production. [Russ.] In: The Pacific Ocean; biology of the Pacific Ocean, I. Plankton, pp 86–97. Ed. by V. G. Bogorov. Moscow, Moskva Izdat Nauk 1967.

Langdon, C. 2010. Determination of dissolved oxygen in seawater by Winkler titration using the amperometric technique. In BM Sloyan and C. Sabine, editors. GO-SHIP repeat hydrography manual: a collection of expert reports and guidelines. IOC/IOCCP, Paris.

Luz, B., E. Barkan, and Y. Sagi. 2002. Evaluation of community respiratory mechanism with oxygen isotopes: A case study in Lale Kinneret. Limnology and Oceanography 47: 33-42.

Murray, C. N., J. P. Riley, and T. R. S. Wilson. 1968. The solubility of oxygen in Winkler reagents used for the determination of dissolved oxygen. Deep Sea Research and Oceanographic Abstracts 15:237-238.

Natterer K. 1892. Chemische untersuchungen in östlichen Mittelmeer. Denkschr. Akad. Wiss., Wien, 59, 83-92

Oudot, C., R. Gerard, P. Morin and I. Gningue. 1988. Precise shipboard determination of dissolved oxygen (Winkler procedure) for productivity studies with a commercial system1. Limnology and Oceanography 33(1): 146-150.

Pomeroy, L. R., J. E. Sheldon, and W. M. Sheldon. 1994. Changes in bacterial numbers and Leucine assimilation during estimations of microbial respiratory rates in seawater by the precision Winkler method. Applied & Environmental Microbiology 60:328-332.

Pringault, O., V. Tassas, and E. Rochelle-Newall. 2007. Consequences of respiration in the light on the determination of production in pelagic systems. Biogeosciences 4: 105-114.

Regaudie-de-Gioux, A., S. Agustí, and C. M. Duarte. 2014. UV sensitivity of planktonic net community production in ocean surface waters. Journal of Geophysical Research: Biogeosciences 119:929-936.

Robinson, C., P. Serret, G. Tilstone, E. Teira, M. V. Zubkov, A. P. Rees, and E. M. S. Woodward. 2002a. Plankton respiration in the eastern atlantic ocean. Deep Sea Research Part I: Oceanographic Research Papers 49:787-813.

Robinson, C., C. E. Widdicombe, M. V. Zubkov, G. A. Tarran, A. E. J. Miller, and A. P. Rees. 2002b. Plankton community respiration during a coccolithophore bloom. Deep Sea Research Part II: Topical Studies in Oceanography 49:2929-2950.

Robinson, C., G. H. Tilstone, A. P. Rees, T. J. Smyth, J. R. Fishwick, G. A. Tarran, B. Luz, E. Barkan, and E. David. 2009. Comparison of in vitro and in situ plankton production determinations. Aquatic Microbial Ecology 54:13-34.

Robinson, C., and P. J. l. B. Williams. 2005. Respiration and its measurements in surface marine waters. Pages 147-180 in P. Del Giorgio and P. J. l. B. Williams, editors. Respiration in aquatic ecosystems. Oxford University Press, Oxford.

Smith, E. M., and W. M. Kemp. 2001. Size structure and the production/respiration balance in a coastal plankton community. Limnology and Oceanography 3:473-485.

Vernet, M., and R. C. Smith. 2007. Measuring and modeling primary production in marine pelagic ecosystems. Pages 142-174 in T. J. Fahey and A. K. Knapp, editors. Principles and standards for measuring primary production. Oxford University Press, Oxford.

Williams, P., and N. Jenkinson. 1982. A transportable microprocessor-controlled precise Winkler titration suitable for field station and shipboard use1. Limnology and Oceanography 27(3):576-584.

Williams, P. J. L. B., K. R. Heinemann, J. Marra, and D. A. Purdie. 1983. Comparison of ^{14}C and O_2 measurements of phytoplankton production in oligotrophic waters. Nature, 305, 49-50.

Winkler, L. W. 1888. Die bestimmung des im wasser gelösten sauerstoffes. Berichte der deutschen chemischen Gesellschaft 21:2843-2854.

6. Calculating Net Community Production and Respiration from Continuous Optode Measurements

Kjell Gundersen[1] and Ryan Vandermeulen[2]

[1]*Plankton Research Group, Institute of Marine Research, Bergen, Norway*
[2]*Ocean Ecology Laboratory, NASA Goddard Space Flight Center, Maryland, U.S.A.*

6.1. Introduction

In this section, we describe the best practices for estimating gross and net community production (GPP and NCP) and community respiration (CR) rates derived from optode sensors that continuously measure dynamic luminescence quenching of dissolved oxygen (DO) within a controlled volume. Incubation bottles retrofitted with an optode sensor can be deployed *in-situ* or used *in-vitro* in laboratory experiments or in deck board incubations. The optode technology is relatively new to aquatic sciences and has only recently been used in CR studies (Warkentin et al. 2007, Wikner et al. 2013, Lehner et al. 2015) and in combined measurements of NCP and CR (Vandermeulen 2012, Collins et al. 2018).

Early optode technology in aquatic biology (Klimant et al. 1995) was not commercially available and was primarily aimed at replacing the use of microelectrodes (Revsbech et al. 1980) in benthic sediments. The "microoptrode" (Klimant et al. 1995), later renamed "micro-optode" (Glud et al. 1999a), was essentially a foil matrix attached to the tapered tip of an optical glass fiber cable. The micro-optode was first used to follow oxygen developments in microbial mats and benthic sediments in shallow waters, and to create micro-depth-profiles of oxygen in deep water sediments (Glud et al. 1999a, 1999b). So far, the optode sensor foil is only supplied by one manufacturer (*PreSens GmbH*, Germany). In more recent years, the same optode foil has been built into commercially available oxygen sensors, such as "sensor spots" or "planar optodes" from the same manufacturer (Tengberg et al. 2006, Warkentin et al. 2007).

Some of the greatest advantages to the optode technology, are that it does not utilize oxygen molecules (e.g., like the Clark electrode) and that it measures DO continuously. The DO optode sensor consists of a unique hydrophobic silicone foil embedded with a platinum porphyrin compound that illuminates (red fluorescence) when excited by a blue or green LED light. The DO molecules interfere with the fluorescence characteristics of the foil membrane (dynamic luminescence quenching) in proportion to its concentration (as well as temperature) in water (Tengberg et al. 2006). Thus, DO concentration can be measured non-invasively through internal monitoring of the luminescence in the sensor foil. The foil is sensitive to direct sunlight and is therefore stabilized in an analyte-permeable matrix to shield it from UV-light. This is however, posing a challenge to gas diffusion and response times since a more effective coating necessarily means less permeability. A lot of effort in recent years has been put into improving the response time in optodes (initially estimated at 15-30 s) by improving permeability of the protective coating. Macro-sensors with optode technology today (Table 6.1) have similar response times to conventional DO sensors (e.g., the Clark electrode).

Table 6.1

Reported DO-optode macro-sensors showing type of sensors, precision, accuracy, and response time. Type of sensor calibration and applications are also listed.

Reference	Sensor	Precision (µM)	Accuracy (±µM)	Response time (s)	Calibration	Application
Tengberg et al. 2006	AADI 3830, 3930	0.5-1	<5 & <2	45	2-point & n=30	*In-situ* measurements
Uchida et al. 2008	AADI 3830	12	10	21	2-point	*In-situ* measurements
Vandermeulen 2012	AADI 3830	0.6	NA	<30	2-point	*In-situ* NCP, CR incubations
Wikner et al. 2013	AADI 3830	0.3	4.2	25	2-point	*In-vitro* CR incubations
Collins et al. 2018	AADI 4531D	<1	8	<30	2-point	*In-situ* NCP, CR incubations
Vikström et al. 2019	AADI 4330	0.2	5.8	NA	N=12	*In-vitro* CR incubations

AADI = Aanderaa Data Instruments; NA = not available

In this chapter we present an overview of commercially available, stand-alone, optode sensors (Table 6.2), where only a subset can be reasonably retrofitted to incubation containers. Wikner et al. (2013) and later Vikstrøm et al. (2019) used Aanderaa Data Instruments (AADI) optodes and measured CR in 1 L glass bottles in the dark (Figure 6.1A). The original micro-optode (see above) has also been retrofitted (Figure 6.1B) and can now measure CR in the nanomolar range in natural seawater (Lehner et al. 2015). The first light-dark *insitu* incubations were reported by Collins et al. (2018) using AADI optodes retrofitted to large volume polycarbonate chambers (2.6 and 5.7 L), that were lowered and closed at depth (Figure 6.1C). Vandermeulen (2012) mounted an AADI optode inside a 1 L polycarbonate bottle for *in situ* surface deployments (Figure 6.1D). Below we discuss the use of two *in situ* optode incubators: One automated system for *in situ* sampling and direct NCP and CR measurements (Collins et al. 2018), and one manually sampled incubator used in daylight surface waters in a turbid estuary in the northern Gulf of Mexico (Vandermeulen 2012).

Table 6.2

List of commercial vendors (alphabetical order) that offer optode technology.

Vendor	Product
Aanderaa Data Instruments, Norway	Oxygen Optode (3830, 3930, 3975, 4330, 4835, 4831)
Alec Electronics Co., Japan	RINKO series, RINKO-profiler, AAQ-RINKO
Franatech GmbH, Germany	Model D-Opto
HACH, USA	Luminescent Dissolved Oxygen (LDO) sensor
Ocean Optics, USA	FOXY Fiber Optic Oxygen Sensor
Precision Measurement Engineering Inc., USA	miniDOT Logger, miniDOT Clear Logger
PyroScience GmbH, Germany	FireSting O2 Optical Oxygen Meter
Sea & Sun Technology GmbH, Germany	Fast SST-DO oxygen sensor
SeaBird Scientific, USA	SBE 63 Optical Dissolved Oxygen Sensor
Unisense A/S, Denmark	O_2 Microoptode
YSI-Xylem, USA	YSI 6150 Reliable Oxygen Sensor (ROX)

There are several benefits to optode sensor incubations, such as ease of use, near continuous, non-intrusive, readings of oxygen levels, and the fact that water samples can be subsampled from the incubation bottle (e.g., for microscope counts or biogeochemical parameters) upon termination of the incubation period. Fast repetitive oxygen sensors, such as the DO-optode, are also ideal for kinetic measurements (e.g., light response curves) on a time scale that cannot be reached with other conventional batch incubation methods for NCP and CR measurements (i.e the light/dark bottle method). Continuous oxygen measurements in natural seawater incubations *in-situ*, clearly demonstrate that DO-optodes are highly responsive to fast environmental changes such as photosynthetic active radiation (PAR, Figure 6.2)

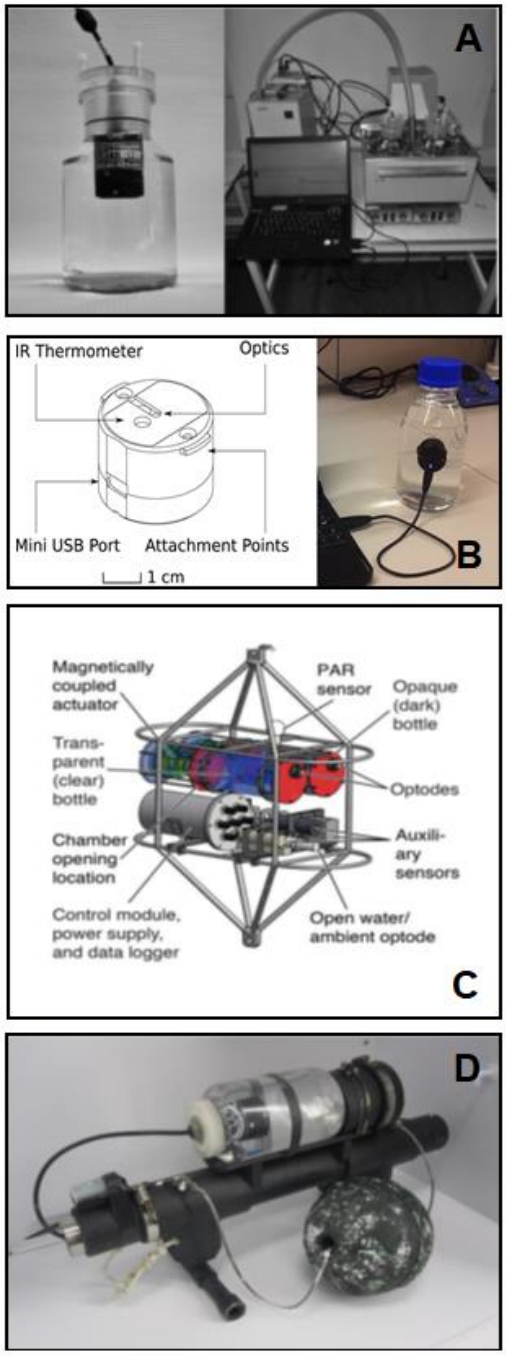

Figure 6.1. Examples of DO-optodes used in-vitro and in field incubations. Wikner et al. (2013) measured CR in-vitro using an Aanderaa Data Instruments (AADI) 3833 oxygen optode (A); Lehner et al. (2015) created a Luminescence Measuring Oxygen Sensor (LUMOS) for in-vitro CR measurements in the nanomolar range (B); Collins et al. (2018) retrofitted water samplers with AADI 4531 DO-optodes for in-situ sampling and NCP and CR measurements (C); and Vandermeulen (2012) retrofitted an AADI 3835 optode to an incubation bottle for in-situ NCP and CR measurements (D). All images are reprinted in accordance with authors and publisher's terms of use.

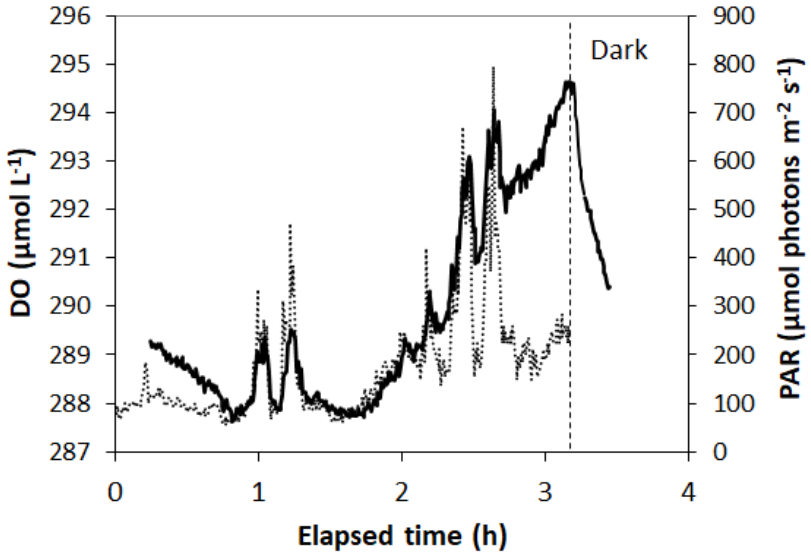

Figure 6.2. Changes in DO concentration (whole line) and subsurface photosynthetic active radiance (PAR, dotted line) measured in the Mississippi Sound on July 21st, 2011 (Vandermeulen & Gundersen, unpubl.). Zooplankton >200 um was gently removed from a surface water sample and incubated in a polycarbonate bottle retrofitted with an AADI 3835 DO-optode and a gimballed magnet stirrer (see Figure 6.3 for details). The DO incubation bottle and data logger was mounted on a PVC frame (Figure 6.1D) and fitted with a Hobo Pendant® sensor (UA-002-08, Onset Computers) that recorded incident PAR at 0.25 m depth during the incubation.

6.2. Best Practices

6.2.1. Sensor accuracy and precision –

Most DO-optodes are calibrated from the manufacturer (multiple-point calibrations) but we recommend that the foil membrane sensitivity is re-calibrated regularly by the user. The DO-optode is most commonly calibrated by exposing the sensor to oxygen-free (anoxic) and completely gas-saturated (100 %) conditions in a 2-point calibration. Zero DO concentration can be obtained by adding sodium sulfite (5 % w/v conc. with trace amounts of cobalt (II) chloride as a catalyst) or sodium dithionite to tap water (e.g., Warkentin et al. 2007, Staudinger et al. 2018). Air-saturated water can be obtained by shaking a bottle of water vigorously (Staudinger et al. 2018), but we prefer to bubble air through the tap water using an aquarium pump, for about 1 hour. The tap water is by then oversaturated and will have to sit for an equal amount of time to equilibrate. Most commercial software used with DO optodes have a 2-point calibration, but some studies (e.g., Tengberg et al. 2006, Vikström et al. 2019) have opted for multiple-point calibrations (n=30 and n=12 respectively) in order to improve accuracy (Table 1). Tengberg et al. (2006) used a 30-point calibration curve of their DO-optode and managed to improve accuracy from <5 µmol O_2 L^{-1} to <2 µmol O_2 L^{-1} deviation. They concluded however, that most *in-situ* applications (e.g., productive coastal waters) show DO gradients on a much larger scale and hence, a 2-point batch calibration should be sufficient (Tengberg et al. 2006). In general, low accuracy is not a detriment to DO-optode incubations as we often follow short-term time-course developments of oxygen (relative change over time) in a closed container. Precision of a DO-optode however (Table 6.2), as we will demonstrate below, is inherently crucial to short-term NCP and CR determinations. Historically, NCP and CR measurements in low production environments have been a challenge

Table 6.3

A guide to estimate required incubation time to resolve metabolic rates (NCP, CR) based on optode sensor precision. Table shows estimated minimum incubation length needed to gain sufficient signal to noise, at different precision levels with the DO-optode.

		Precision (±µmol O_2 $L^{-1}h^{-1}$)			
		0.2	0.5	1	2
	NCP, CR (µmol O_2 $L^{-1}h^{-1}$)	Minimum incubation length (h)			
Oligotrophic waters	0.1	4	10	20	40
Shelf areas	1	0.4	1	2	4
Coastal waters	5	0.08	0.2	0.4	0.8
Eutrophic waters	10	0.04	0.1	0.2	0.4

to conventional oxygen sensors. A significant signal-to-noise ratio would require a large plankton biomass, as is most often the case in highly productive waters (Table 6.3). In open ocean oligotrophic waters, rate extrapolations from long-term incubations are often necessary, in order to get significant NCP or CR rates. Precision of the DO optode sensor (e.g., the AADI optode at ±0.2 µmol O_2 L^{-1}; Tengberg & Hovdenes 2014) is in the same order as the precision of widely accepted Winkler titrations (± 0.06 - 0.12 µmol O_2 L^{-1}; see Langdon & García-Martín chapter), with the added benefit of continuous measurements. The latter range was estimated by assuming 0.03 % precision for photometric titrations, 0.06 % precision for amperometric titrations, and a generic DO concentration level of 200 µmol O_2 L^{-1}. In this chapter we argue that a 2-point batch calibration of the DO optode (and an accuracy of < 5 µmol O_2 L^{-1}) is sufficient to estimate GPP, NCP and CR rates in a closed incubator,

DO-optodes appear to be stable (months to years) but after only 2-3 days of continuous deployment, optode signal may drift due to the appearance of biofouling (Tengberg et al. 2006). Stirring (e.g., by a magnet stirrer in an incubation bottle) has no effect on the optode sensor itself (Klimant et al. 1995) but, DO-optode used on a profiling platform shows pressure hysteresis (approximately 4 % per 100 m) that is fully recoverable at surface (Tengberg et al. 2006). Temperature and conductivity have an effect on the gas solubility of the foil membrane and hence, on measured *in situ* DO concentrations, but this is accounted for in calculations and the expression of results (Uchida et al. 2008). All DO-optodes are therefore dependent on ambient temperature, conductivity and depth readings for accurate results. Accuracy of the DO-optode (Table 6.1) is by now well documented (Tengberg et al. 2006, Uchida et al. 2008, Wikner et al. 2013, Vikström et al. 2019) and comparable to determinations by the Winkler titration method (Winkler 1888, Carpenter 1965, Strickland & Parson 1972). Since DO-optodes provide stable readings over long periods of time (months to years), we consider inaccurate recalibrations and biofouling the two most significant sources of error for these sensors in field applications.

6.2.2. Response time

The optode's ability to respond to abrupt changes in DO concentrations (usually calculated as the time it takes to go from zero oxygen to 65 % or 90 % of DO saturation) is defined as the response time (t_{65}, t_{90}). Manufacturers are usually reporting the response time in pure oxygen gas solutions and at optimal temperatures (20 – 25 ºC) in order to claim optimal response for their product (from fractions to 10-15 s), and these are rarely achieved *in situ* at suboptimal temperatures. Response times reported in the literature (Table 6.1) are therefore often found to be

longer since they are estimated in a liquid solution and at lower temperatures. Due to a relatively slower response time than e.g., the Clark-electrode in water (2 – 10 s), the DO-optode initially appeared less suited for profiling applications. However, the DO-optode has frequently been applied in fixed and moveable buoy platforms where the response time is less critical as DO-concentrations are measured continuously on longer time scales. Since the response time is dependent on oxygen dissolution over a permeable foil membrane, the protective layer of black silicone used as protection against ambient light and optical interference from the surrounding water (Klimant et al. 1995) may slow down the response time. A thinner layer would give a faster response time but comes with the risk of making the sensor unstable. Improvements to the oxygen gas diffusion of the silicone coating and, in some cases combined with the use of a water pump in a closed space void of ambient light, imply that optodes are comparable to other conventional DO-sensors in profiling applications.

6.2.3. The incubation bottle

The choice of an incubation chamber is an important consideration when measuring changes of dissolved oxygen concentrations in a controlled volume. Polymer materials are advantageous because they are more robust than e.g., glass to stand up to dynamic sea conditions and deployments. However, the majority of available polymers are not transparent and the ones that are (e.g., acrylic and polycarbonate) may have PAR attenuation issues (see below). Air-dry polymers are also permeable to gas and, if not preconditioned, they can leak (desorb) dissolved oxygen into the water sample and compromise metabolic rate measurements (Wikner et al. 2013). It is also possible that oxygen may get absorbed by the polymers used inside incubators (e.g stoppers or the acetal casing of some optode sensors) if the sample is not preconditioned, which may compromise the measurements by artificially removing oxygen from the water sample. Stevens (1992) measured desorption of polymer materials and found that nylon, acetal and polyvinylchloride (PVC) released the least amount of oxygen. Acrylic and high-density polyethylene (HDPE) were more permeable, while polycarbonate and Teflon bottles showed the highest gas permeability. Incubator bottles made of polymers should therefore be "preconditioned" by soaking in water at similar DO-concentration and temperature to *in-situ* conditions (min 24 h), in order to expel air-saturated oxygen from the dry material. However, the use of these polymers inside incubation bottles should be minimized or completely avoided when assessing extremely low biological rates (e.g., in hypoxic environments or oligotrophic waters). It is also recommended that a test is performed, using sterilized (autoclaved) tap water in order to check for non-biological drift of the DO-optode (i.e., gas absorption or desorption of dissolved oxygen), over a time-course similar to the one intended for the actual incubation. Glass bottles are less robust but have no gas permeability issues and, for NCP measurements, only quartz glass show minimal attenuation over the entire spectrum of visible light.

Beyond permeability, incubation bottles can also impact the quality of light in optode incubations. Most polymers, as well as borosilicate glass (e.g., Pyrex), are opaque to UV-B radiation and may underestimate the impact of UV stress/photoinhibition on metabolic rates (Gala and Giesy 1991, Regaudie-de-Gioux et al. 2014). Quartz bottles are most transparent to UV radiation, but this may not be so important if neutral density (or blue) filters are used to cause UV attenuation in deck-board incubations (e.g., Robinson et al. 2009). If photoinhibition processes are the focus of your study, quartz bottles should be used without UV-attenuating filters. Otherwise, it may be more practical to use polymer containers (e.g., PVC or polycarbonate bottles) for *in situ* and deck-board incubations.

Note that the incubation bottle containing the optode must also be impermeable to gas/water exchange at the time of incubation. When creating a seal between removeable parts, avoid using nitrile O-rings or any organic leaching material (e.g., rubber stoppers or rubber cords in Niskin bottles) that can adversely impact biological rates (Williams and Robertson 1989, Matsumoto et al. 2012). We recommend the use of Viton O-rings and non-toxic stoppers (never silicon stoppers) for incubation bottles. Prior to use, the incubation bottles as well as the sealing material should be washed with a dilute solution of trace metal-free, non-ionic detergent, followed by thorough rinsing with purified (Milli-Q) water that has been sterilized. Both sensors and bottles should be left soaking in sterile Milli-Q water to desorb for at least 24 hours prior to use.

6.2.4. Sample water collections

Sample water should be collected immediately before the incubation takes place, and great care should be taken to avoid introducing air bubbles when filling the incubation bottle. Collins et al (2018) collected water directly *in-situ* using a timer to close the PHORCYS incubator (Figure 6.1C). The benefits of direct sampling *in-situ*, immediately followed by an *in-situ* incubation in the same bottle, is that the body of water is left undisturbed. However, there is no way of prescreening the incubation water in order to remove larger zooplankton (see details below).

The most common way of collecting sample water, is by using a Niskin-type of water samplers that can be fired at discrete depths. Non-toxic o-rings should also here be used in the sealed water samplers (e.g., the original Niskin bottle with stainless steel spring or the relatively new Niskin-X), or other similar equipment used for collection of Winkler-titration samples. The benefits of using water samplers are that the sample water can be size fractionated, but there are challenges to collecting water at depth that is subsequently processed at surface (e.g., the sudden change in temperature, pressure and dissolved oxygen concentration) that may inadvertently change the physical characteristics of the water.

The third option is to only collect surface water, in order to avoid the sudden change in temperature, pressure and dissolved oxygen concentrations, by using a large volume bucket (Vandermeulen 2012) or a Niskin-type of water sampler. If a large volume bucket is used (10 – 20 L), the incubation water can be prescreened directly by reverse filtration (Vandermeulen 2012) and the incubation bottle filled by lowering the entire bottle directly into the sample water (use long sleeved gloves!). For diurnal (sunrise to sunset) or 24 h diel incubations, sample water should be collected prior to first light (ideally 1 h before sunrise). For daily NCP and CR estimates, the incubator bottle should be deployed before sunrise and retrieved after sunset. If this is not possible, great care should be taken to avoid abrupt changes in temperature (work fast!) and the water sample should not be exposed to direct sunlight prior to *in-situ* deployment (use a tent or canopy for dim light conditions).

6.2.5. Sample volume and prescreening

Size of the incubation bottle has in principle, no limit for DO-optode incubations. Wikner et al. (2013) opted for no prescreening of their samples, as the literature suggests that the majority of all respiration (99-100 %) can be accounted for by cells < 200 µm (Robinson & Williams 2005, and references therein). However, in coastal waters in spring, when there is a high abundance of mesozooplankton (>10 individuals L^{-1}), there is also a good chance that larger zooplankton can be included in the incubation chamber (Wikner et al. 2013). Therefore, if the aim of the study is to also include mesozooplankton, or even macrozooplankton, we recommend that you use natural

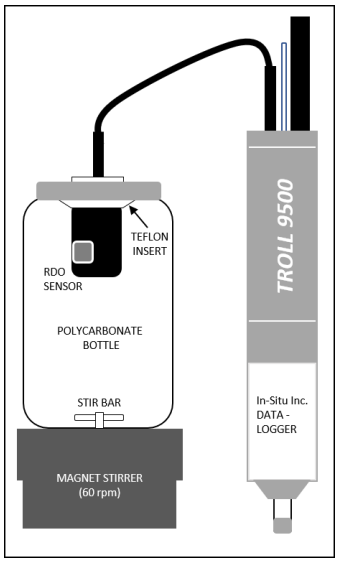

Figure 6.3. DO-incubator retrofitted with an AADI 3835 oxygen optode mounted inside the lid of a 1L polycarbonate centrifuge bottle. The optode was attached to an In-Situ Instruments Troll 9500 data logger. To avoid heterogeneity in the bottle during incubations, a magnet stir bar was mounted in a gimble suspension attached to the bottom of the PC bottle. The stir bar was rotated by a magnet stirrer (70 rpm) positioned immediately outside the bottom of the incubation bottle. In order to avoid contamination from oxygen trapped in the Teflon insert and the PC bottle itself, the unit was left soaking in tap water near in-situ temperature for a minimum of 48 h prior to incubation. From Gundersen & Vandermeulen (unpubl.)

seawater in a large incubation bottle (>> 2 L) and no prescreening of the sample. On the other hand, if you are looking at small-scale processes including the most abundant micro and nano-plankton, we suggest a smaller incubation bottle (e.g., 1 L) where individuals >200 µm (predominantly meso- and macrozooplankton) has been separated by gentle, reverse filtration (see Vandermeulen 2012 for details).

6.2.6. In-situ incubations

Most DO-optodes are stand-alone units designed for long and short-term *in situ* deployments in the water column or short-term monitoring of benthic DO profiles in sediments (Table 2). Therefore, most of the units are not specifically designed for an incubation chamber that require gas-tight conditions. The AADI optode is a relatively small unit with a bulk-head mount for the sensor platforms used by the company and, so far, is the one design used in *insitu* incubations (Figures 6.1C and 6.1D).

An *in-situ* DO-incubator may be retrofitted with an optode mounted inside the incubation chamber lid or another point in the chamber that can be sealed (e.g., Figure 6.3). Collins et al. (2018) opted for a complete *in situ* system (Figure 6.1C) with polycarbonate incubation bottles (5.7 L usable volume) fitted with DO-optodes. The PHORCYS incubation bottles automatically open and close at designated time-intervals. This solution allows for undisturbed *insitu* incubations of whole sea water samples, where CR (dark bottle) and NCP (clear bottle) are measured simultaneously. The PHORCYS is also equipped with an array of other sensors keeping track of environmental parameters that may influence measured NCP and CR (CTD, external DO-optode, 2pi PAR sensor, beam transmissometer, chlorophyll fluorometer). Vandermeulen (2012) retrofitted a DO-optode in a polycarbonate bottle (Figure 6.3) that was mounted on a surface float

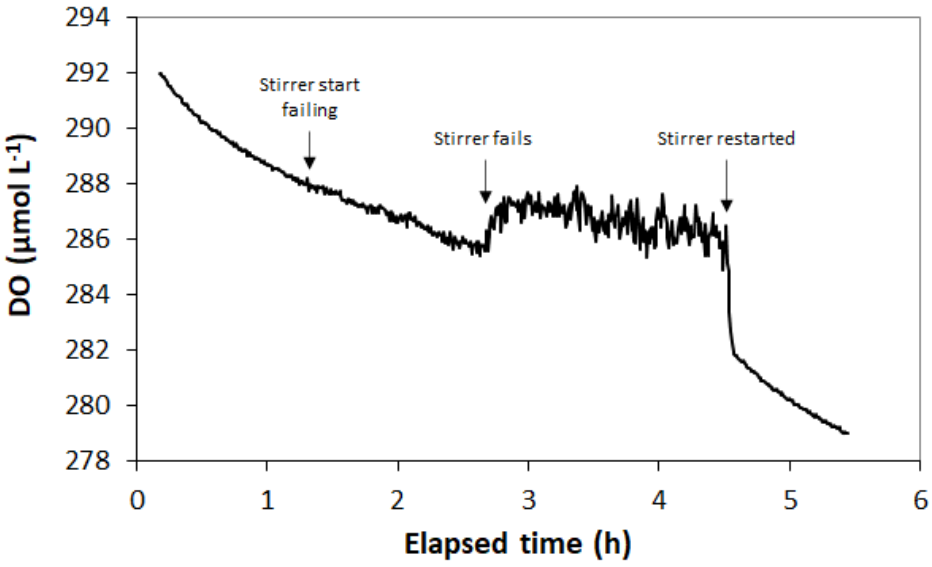

Figure 6.4. Changes in DO concentration in a PC incubation bottle (see Figure 6.3 for details) where the magnet stirrer (70 rpm) stopped working. The incubator (Figure 6.1D) was quickly retrieved, batteries replaced, and the unit was covered in double layers of heavy-duty aluminum foil for the dark incubation (CR) as the stirrer was restarted. From Vandermeulen & Gundersen (unpubl.).

(Figure 6.1D). Early *in situ* incubations revealed that more stable, homogenous readings were achieved by a slowly rotating magnet stirrer (Figure 6.4). In order to avoid desorption (Stevens 1992), the unit was left soaking in tap water at room temperature for a minimum of 48 h prior to each incubation. The surface float, equipped with a Hobo sensor (temperature and PAR), was deployed manually at sunrise (Vandermeulen 2012).

DO-optodes are prohibitively expensive compared to BOD bottles and Winkler titrations. Since we are still in an exploratory phase of *in-situ* incubations with DO-optodes, we have no data on replicate *in-situ* optode incubations. The variability between replicate incubation bottles may exceed optode accuracy and precision faster, especially in highly productive waters with high biological activity. Therefore, replicate incubation volumes > 1 L that are not prescreened for larger swimmers (mesozooplankton), may have an even greater potential to develop differently and express differing NCP or CR rates, than < 200 µm incubations.

6.2.7. Time-course incubations

Collins et al. (2018) measured NCP and CR rates simultaneously in sub-Arctic open ocean waters, using the PHORCYS incubator (Figure 6.1C) over a wide range of incubation times (10 – 94 h). Similarly, Gundersen & Vandermeulen (unpubl.) determined NCP from *in-situ* light incubations (2 – 4 h), immediately followed by a short dark incubation to determine instantaneous CR (0.2 – 0.3 h), in a strongly eutrophic estuary in the northern Gulf of Mexico (Figure 5). The continuous recordings of DO in both these incubations, showed that rates of NCP are typically not linear during the course of a day (Figure 6.5, Collins et al. 2018).

These changes could be a result of changes in incident irradiance or *in-situ* temperature. DO-optode readings (which are temperature sensitive) can be slightly off with abrupt changes in *in-situ* temperature. Also, abrupt response in community photosynthesis to changes in incident

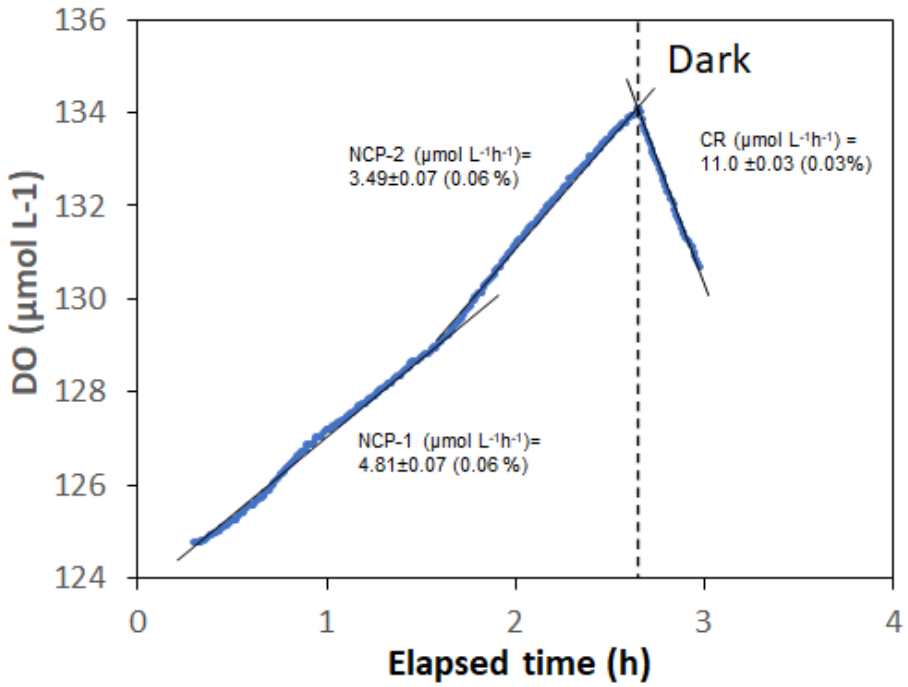

Figure 6.5. Measured NCP and CR in in the Mississippi Sound on September 13th, 2010. Surface sea water was collected at sunrise using a 20 L bucket and zooplankton >200 µm was gently removed by gently lowering another bucket with a 200 µm Nytex screen in the bottom. The <200 µm incubation water was collected in a PC bottle retrofitted with an AADI 3835 optode and a gimballed magnet stirrer (see Figure 6.3 for details). The DO incubation bottle was mounted on a PVC frame (Figure 6.1D) for approximately 2.5 hours at 0.25 m depth (NCP). The unit was quickly retrieved, wrapped with double layers of heavy-duty aluminum foil and redeployed for a 15 min dark incubation (CR). Sensor sampling frequency was 0.03 Hz (blue markers) and two significantly different periods of production were identified (NCP-1, NCP-2) and one rate of dark respiration (CR) was calculated. In a separate test, an incubator was filled with sterilized water (DO blank) but showed no uniform sensor drift (±0.3 µmol L^{-1}).

irradiance (PAR) is well documented in the literature and previously in this chapter (Figure 6.2). Therefore, differences in the rate of DO may change rates of NCP and CR during the course of a day and hence, should be taken into account when calculating daily metabolic budgets. Gross primary production (GPP) is calculated from NCP and CR (GPP = NCP + CR). During periods of low photosynthesis (e.g., at low incident irradiance) DO concentrations in the light incubated bottles may show no net changes when GPP equals CR (NCP = 0). Collins et al. (2018) and Figure 6.4 shows that in some cases the optode signal in the light incubated bottle may show a decrease in DO concentrations with time (NCP < 0) but, as DO consumption in the dark incubated bottle will be equal or greater than in the light bottle, the calculated GPP rate will still be zero or positive. These observations only emphasize the importance of accurate CR (dark bottle) estimates in daily GPP determinations.

6.2.8. Incubation length

Contrary to BOD incubations and Winkler DO-titrations, optodes are able to measure short-term changes in the DO concentration in the order of minutes to hours (e.g., Figure 6.5). This is partially a function of a high sampling rate (n) of continuous measurements, which clusters values

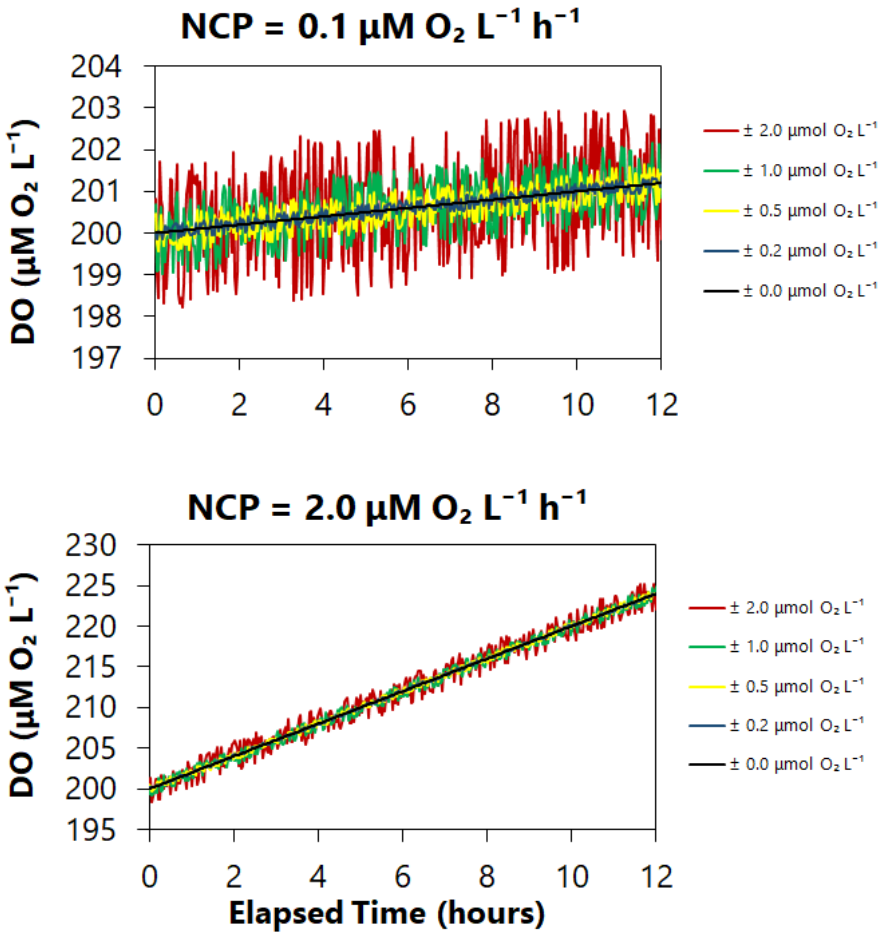

Figure 6.6. Demonstration of changes in DO concentration, in a time-course at varying levels of optode sensor precision (±µmol L^{-1} conc. on right hand side). The simulated time-course is shown for (A) low rates of NCP typically encountered in oligotrophic waters, and (B) moderate rates commonly found in coastal/shelf environments.

more around the true population mean compared to incremental values, reducing the standard deviation, and thus enabling an increased capability to resolve subtle rate changes. However, this enhanced utility is highly dependent on the level of ambient biological rates. For example, oligotrophic waters where GPP often is balanced by daytime CR, longer incubation times may be required in order to overcome the sensor sensitivity. To illustrate the impacts of this sensitivity, we modeled two constant linear rates of oxygen evolution (0.1 and 2.0 µmol O_2 L^{-1} h^{-1}) and introduced controlled random Gaussian noise bounded by various manufacturer precision levels of 0.2 – 2.0 µmol O_2 L^{-1} (Figures 6.6). At low rates of oxygen evolution (Figure 6.6A) that are indicative of extremely oligotrophic waters (Williams et al. 2004), only the highest precision measurements (< 0.5 µmol O_2 L^{-1}) are capable of resolving linear rates over a 12-hour period. More moderate rates of oxygen evolution (Figure 6.6B) exhibit more flexibility with regards to overcoming the signal-to-noise ratio at all precision levels, however, higher precision sensors offer the ability to make shorter term rate assessments. This analysis can be extended more quantitatively to determine the length of time it takes for a given rate of oxygen evolution to exceed

the magnitude of random noise by a factor of two, thus guiding recommendations for minimum incubation duration for various sensor precision levels (Table 6.3). Finally, incubation bottles retrofitted with a slow-moving magnet stirrer (Figure 6.3) may also improve the precision of your DO-readings, and this is clearly demonstrated in Figure 6.4. We also note that the linear extrapolated rates of NCP and CR in the northern Gulf of Mexico (Figure 6.5), using a slow-moving stirrer, had very good precision (0.03 – 0.07 µmol O_2 L^{-1}).

6.3. Calculations and expressions of results

6.3.1. Expression of results –

If ambient pressure and temperature readings are available (see *Ancillary Data* below), you will have several options of available units for your DO readings (mL L^{-1}, mg L^{-1}, µmol L^{-1}). At standard temperature and pressure (STP) it follows that O_2 L^{-1} can be expressed as;

$$1\ \mu mol = 44.6596\ mL = 31.2512\ mg$$

Early reports on DO determinations, such as the descriptions of the Winkler titration method, were in mg-at L^{-1} or mL L^{-1} (Strickland & Parsons 1972). The v/v unit has been used up until recent times and can still be seen in long-term monitoring data archives going back multiple decades. As of today, the most common denomination for DO is µmol O_2 L^{-1} in oceanography. Accurate DO-optode profile measurements today are commonly compensated for temperature, conductivity and pressure changes as a function of depth (Uchida et al. 2008).

Rates of net community production (NCP) and community respiration (CR) can be calculated directly from linear regressions (e.g., Figure 6.5). Gross primary production (GPP) is calculated as the rate of NCP corrected for community respiratory losses (GPP=NCP+CR). NCP and CR rates can also be expressed in carbon units (see PQ and RQ conversion below). Also, NCP is often normalized to autotroph biomass (measured as Chlorophyll-*a*) since this, despite its flaws (Ramaraj et al. 2013) is one of the most common biomass-estimates of the phototroph community. Detecting dissolved oxygen changes in light and dark bottle incubations is a function of metabolic rates (NCP and CR), sensor precision and the length of the incubation (Table 6.3). In low productive regions, changes in the dissolved oxygen concentration, as a function of time, may become increasingly difficult to differentiate isolated segments of NCP and CR within a day, as signal-to-noise ratio is low (Figure 6.6). For an overall long-term estimate, this can to some extent be remedied by extending the incubations period (Table 6.3) in extreme environments. To detect changes in dissolved oxygen concentrations in oligotrophic oceans, i.e., to get an estimate within the confines of a day, we recommend an optode precision < 0.2 µmol O_2 L^{-1} (Table 6.3). Likewise, in all other regions (coastal and shelf areas) you can still get significant daily rates with an optode precision in the 2-5 µmol O_2 L^{-1} range (Table 6.3), but this level of precision may not aid you in determining varying NCP and CR rates during the course of the day.

6.4. PQ & RQ conversion

The photosynthetic quotient (PQ) is the molar ratio of oxygen development to carbon biomass by primary productivity. Autotroph cellular carbohydrate synthesis, and protein synthesis utilizing ammonia as an N-source, have both a PQ approximating 1, while other common cellular products (proteins synthesized from nitrate as an N-source and lipids) are in the range of 1.4-1.6 (Valiela 1984, and references therein). Robinson & Williams (1999) demonstrated the huge variability in PQ from field studies and associated the estimated lower range (PQ=1.03) with cell synthesis using

ammonium as the N-source, while the upper boundary matched theoretical cell synthesis based on nitrate (PQ=1.4). Recommended choice of PQ will depend on *in-situ* concentrations of ammonium and nitrate. However, many current PQ estimates are from dawn-to-dusk incubations of BOD-bottles (light-and-dark bottles) and CO_2 assimilation by the ^{14}C-bicarbonate method. There are inherent differences in these two approaches, since Winkler BOD is a less sensitive method than ^{14}C-incubations and hence, in extreme environments (e.g., at depth, at low light and with minimal photosynthesis) these ratios may become highly variable and inaccurate. The wide range in respiration quotients (RQ) reported by Robinson & Williams (1999) can also be ascribed to uncertainty with the methods (Winkler BOD and DIC analysis) in addition to variable substrate compositions. "Typical" plankton material would have a theoretical RQ=0.89 (Williams & Robertson 1991, Hedges et al. 2002) based on stoichiometry alone (see details in the main introduction to this report). We also note that since NCP is a balance between GPP and CR (GPP=NCP+CR), PQ cannot be applied directly to calculate a carbon-based NCP. Rather, selected PQ and RQ should be applied to GPP and CR, respectively, and NCP is calculated as the difference between the two (NCP=GPP-CR).

6.5. Ancillary data collection

The changing regime of physical parameters with depth, such as ambient temperature, salinity, and light attenuation, are essential in order to interpret the results from *in situ* incubations. In addition to community composition of auto- and heterotrophs inside the incubation bottle, temperature and incident light are perhaps the two parameters with most profound impact on NCP and CR rates. A number of light irradiance sensors are set up to measure PAR (400-700 nm), but UV-A and UV-B inhibition (radiation in the 280-400 nm range) is not accounted for in these measurements. Therefore, if light inhibition is an important focus of your study, you may want to consider a full spectral light sensor in addition to PAR determinations. We strongly recommend that, as a bare minimum, *in-situ* PAR, temperature and the Chl-*a* biomass are measured during the DO-optode incubations.

Optode incubation chambers are in the unique position that they can be sampled for ancillary data both before and after deployment. Therefore, remaining sample water that were not used in the incubator can be analyzed at start and, due to its non-invasive nature, the sample water inside the incubator can also be sampled after deployment. Of special interest are parameters describing the community composition (abundance estimates of auto- and heterotrophic plankton) and its potential development during the incubation period. A broader characterization of the photoautotrophs (than just Chlorophyll-*a* estimates) may also be of interest, and a more comprehensive characterization of the multitude of pigments can be obtained from HPLC and the use of *CHEMTAX* (e.g., Mackay et al. 1996 and others). More advanced instrumentation, such as flowcytometry for bacteria and imaging techniques such as *ZooSCAN* (e.g., Grosjean et al. 2004) and *FlowCAM* (e.g., Le Bourg et al. 2015) for phyto- and zooplankton cell abundance and volume, are now also available. Alternatively, low-cost solutions to microscope imaging (e.g., the PlanktonScope) are now also showing promising results (DOI: 10.1101/2020.04.23.056978). The latter techniques will perhaps with time replace more conventional cellular abundance detection by microscope.

Inside the DO-optode incubator, it may also be of interest to monitor environmental parameters that change during the course of the incubation. These are first and foremost the macronutrients (dissolved inorganic, dissolved organic, and particulate derivatives) which, together with ambient

light, are essential for all biological activity inside the incubator. Dissolved inorganic nutrients (nitrate, nitrite, phosphate, silicate and ammonium) are measured with conventional techniques (e.g., Strickland & Parsons 1972) and may become depleted during longer time-course incubations. Available nutrients are also paramount in your choice of photosynthetic and respiratory quotients (see section on *PQ & RQ conversion* above) for your expression of results.

6.6. Summary

6.6.1. Advantages

The main advantage of DO-optodes over Winkler is the capacity to measure continuous changes in the oxygen concentration over time. With careful maintenance and calibrations, the optode is an accurate and precise sensor for oxygen measurements with a reasonable response time that cover changes in DO concentrations for most NCP and CR processes in an incubation bottle. For these reasons, DO-optodes can also be used to calculate NCP and CR rates on shorter time-scales and with greater precision than what is possible in a Winkler BOD incubation. Since optodes provide near-continuous measurements of DO in an incubator bottle (with time-resolution as low as 30 s), it is possible in regions with high primary productivity, it is possible to conduct short-term manipulations (e.g., light-dark treatments) to elucidate short-term NCP and CR rates.

In order to account for the metabolic rates (NCP and CR) associated with the majority of organisms, the volume of the incubator ought to be > 1 L, and this has been a challenge in Winkler BOD incubations. The volume in optode incubations can in theory be of infinite size. However, it is a logistical challenge to handle large volume containers as well as keeping the incubation volume homogenous. Abundance estimates indicate that plankton organisms < 200 µm account for 99 % of CR and are adequately represented in a 1 L incubator.

6.6.2. Caveats

Compared to expenses associate with Winkler BOD incubations, the cost of an optode is considerably more expensive and this may limit the number of available sensors for an investigator. Expression of results from DO-optodes are highly dependent on concurrent temperature readings. DO gas dissolution is also depending on ambient conductivity and pressure, but in an incubator bottle this will not change (contrary to temperature) provided that the incubation depth remains constant. On a short-term temporal scale, the optode is also sensitive to diffusion issues and microscale biological activities during the course of an incubation, that may appear as noise in the DO-readings. However, if the goal is to measure whole community rates in a given volume of seawater, microscale production and respiration can be avoided by using a slow-moving magnet stirrer (50-70 rpm) mounted in a gimble.

The optode foil membrane may also experience interference from hydrogen peroxide, gaseous sulphur dioxide and chlorine (cross-sensitivity), but this is usually not an issue in most natural environments. Incubations at deeper depths will lead to membrane hysteresis and inaccurate DO readings but, if the incubator is kept at the same depth for the longevity of the incubation and precision is maintained, this may not have any significant implications on NCP and CR rate calculations.

6.7. Acknowledgements

This work was in part supported by the Northern Gulf Institute research grant (09-NGI-13) to Kjell Gundersen. The authors would also like to thank Elena García-Martín for comments to an early version of this chapter.

6.8. References

Collins, J. R., Fucile, P. D., McDonald, G., Ossolinski, J. E., Keil, R. G., Valdes, J. R., ... & Van Mooy, B. A. (2018). An autonomous, *in situ* light-dark bottle device for determining community respiration and net community production. Limnology & Oceanography: Methods, 16(6), 323-338.

Gala, W. R., & Giesy, J. P. (1991). Effects of ultraviolet radiation on the primary production of natural phytoplankton assemblages in Lake Michigan. Ecotoxicology and Environmental Safety, 22(3), 345-361.

Glud, R. N., Klimant, I., Holst, G., Kohls, O., Meyer, V., Kühl, M., & Gundersen, J. K. (1999a). Adaptation, test and *in situ* measurements with O2 microopt (r) odes on benthic landers. Deep-Sea Research Part I: Oceanographic Research Papers, 46(1), 171-183.

Glud, R. N., Kühl, M., Kohls, O., & Ramsing, N. B. (1999b). Heterogeneity of oxygen production and consumption in a photosynthetic microbial mat as studied by planar optodes. Journal of Phycology, 35(2), 270-279.

Grosjean, P., Picheral, M., Warembourg, C., & Gorsky, G. (2004). Enumeration, measurement, and identification of net zooplankton samples using the ZOOSCAN digital imaging system. ICES Journal of Marine Science, 61(4), 518-525.

Holtappels, M., Tiano, L., Kalvelage, T., Lavik, G., Revsbech, N. P., & Kuypers, M. M. (2014). Aquatic respiration rate measurements at low oxygen concentrations. PLoS One, 9(2), e89369.

Hedges, J. I., Baldock, J. A., Gélinas, Y., Lee, C., Peterson, M. L., & Wakeham, S. G. (2002). The biochemical and elemental compositions of marine plankton: A NMR perspective. Marine Chemistry, 78(1), 47-63.

Klimant, I., Meyer, V., & Kühl, M. (1995). Fiber-optic oxygen microsensors, a new tool in aquatic biology. Limnology & Oceanography, 40(6), 1159-1165.

Le Bourg, B., Cornet-Barthaux, V., Pagano, M., & Blanchot, J. (2015). FlowCAM as a tool for studying small (80–1000 µm) metazooplankton communities. Journal of Plankton Research, 37(4), 666-670.

Lehner, P., Larndorfer, C., Garcia-Robledo, E., Larsen, M., Borisov, S. M., Revsbech, N. P., ... & Klimant, I. (2015). LUMOS-A sensitive and reliable optode system for measuring dissolved oxygen in the nanomolar range. PLoS One, 10(6), e0128125.

Mackey, M. D., Mackey, D. J., Higgins, H. W., & Wright, S. W. (1996). CHEMTAX-a program for estimating class abundances from chemical markers: application to HPLC measurements of phytoplankton. Marine Ecology Progress Series, 144, 265-283.

Matsumoto, K., T. Fujiki, M. C. Honda, M. Wakita, H. Kawakami, M. Kitamura, & T. Saino. 2012. Inhibition of primary production by nitrile rubber O-rings in Niskin sampler. AMSTEC Report of Research and Development, 14, 17-25.

Pollina et al. (2020) The PlanktonScope (DOI: 10.1101/2020.04.23.056978)

Ramaraj, R., Tsai, D. D., & Chen, P. H. (2013). Chlorophyll is not accurate measurement for algal biomass. Chiang Mai J. Sci, 40(4), 547-55.

Regaudie-de-Gioux, A., Lasternas, S., Agustí, S., & Duarte, C. M. (2014). Comparing marine primary production estimates through different methods and development of conversion equations. Frontiers in Marine Science, 1, 19.

Robinson, C., & Williams, P. J. le B. (1999). Plankton net community production and dark respiration in the Arabian Sea during September 1994. Deep-Sea Research Part II: Topical Studies in Oceanography, 46(3-4), 745-765.

Robinson, C., & Williams, P. L. B. (2005). Respiration and its measurement in surface marine waters, pp 147-180. In: del Giorgio, P.A. & Williams, P.J. le B., Respiration in aquatic ecosystems, Oxford University Press.

Robinson, C., Tilstone, G. H., Rees, A. P., Smyth, T. J., Fishwick, J. R., Tarran, G. A., ... & David, E. (2009). Comparison of in vitro and *in situ* plankton production determinations. Aquatic Microbial Ecology, 54(1), 13-34.

Staudinger, C., Strobl, M., Fischer, J. P., Thar, R., Mayr, T., Aigner, D., ... & Fritzsche, E. (2018). A versatile optode system for oxygen, carbon dioxide, and pH measurements in seawater with integrated battery and logger. Limnology and Oceanography: Methods, 16(7), 459-473.

Stevens, E. D. (1992). Use of plastic materials in oxygen-measuring systems. Journal of Applied Physiology, 72(2), 801-804.

Strickland, J.D.H. & Parsons, T.R. (1972) A practical handbook of seawater analysis. Fisheries Research Board of Canada, Bulletin 167, pp 310.

Tengberg, A., Hovdenes, J., Andersson, H. J., Brocandel, O., Diaz, R., Hebert, D., ... & Rey, F. (2006). Evaluation of a lifetime-based optode to measure oxygen in aquatic systems. Limnology & Oceanography: Methods, 4(2), 7-17.

Tengberg, A., & Hovdenes, J. (2014). Information on long-term stability and accuracy of Aanderaa oxygen optodes; information about multipoint calibration system and sensor option overview. Aanderaa Data Instruments AS Tech. Note.

Uchida, H., Kawano, T., Kaneko, I., & Fukasawa, M. (2008). *In situ* calibration of optode-based oxygen sensors. Journal of Atmospheric and Oceanic Technology, 25(12), 2271-2281.

Valiela, I. (1984). Producers and processes involved in primary production. In Marine ecological processes (pp. 3-37). Springer, New York, NY.

Vandermeulen, R.A. (2012) Factors influencing the spatial and temporal distribution of primary productivity and community respiration in the Mississippi coastal Estuarine region. The University of Southern Mississippi, MS-thesis, pp 152

Vikström, K., Tengberg, A., Wikner, J. (2019) Improved accuracy of optode-based oxygen consumption measurements by removal of system drift and non-linear derivations. Limnology & Oceanography: Methods 17:179-189.

Warkentin, M., Freese, H. M., Karsten, U., & Schumann, R. (2007). New and fast method to quantify respiration rates of bacterial and plankton communities in freshwater ecosystems by using optical oxygen sensor spots. Applied and Environmental Microbiology, 73(21), 6722-6729.

Wikner, J., Panigrahi, S., Nydahl, A., Lundberg, E., Båmstedt, U., & Tengberg, A. (2013). Precise continuous measurements of pelagic respiration in coastal waters with oxygen optodes. Limnology & Oceanography: Methods, 11(1), 1-15.

Williams, P. L., & Robertson, J. I. (1989). A serious inhibition problem from a Niskin sampler during plankton productivity studies. Limnology and Oceanography, 34(7), 1300-1305.

Williams, P. I., & Robertson, J. E. (1991). Overall planktonic oxygen and carbon dioxide metabolisms: the problem of reconciling observations and calculations of photosynthetic quotients. Journal of Plankton Research, 13(supp1), 153-169.

Williams, P. J. L. B., Morris, P. J., & Karl, D. M. (2004). Net community production and metabolic balance at the oligotrophic ocean site, station ALOHA. Deep-Sea Research Part I: Oceanographic Research Papers, 51(11), 1563-1578.

7. *In Situ* Gross Primary Production from Triple Oxygen Isotopes

Rachel H. R. Stanley[1], Laurie W. Juranek[2], and David P. Nicholson[3]

[1]*Department of Chemistry, Wellesley College, Massachusetts, USA*
[2]*College of Earth, Ocean, and Atmospheric Sciences, Oregon State University, Oregon USA*
[3]*Marine Chemistry and Geochemistry Department, Woods Hole Oceanographic Institution, Massachusetts, USA*

7.1. Introduction

Rates of gross primary production (GPP) and net community production (NCP) yield important mechanistic information about the marine carbon cycle. Triple oxygen isotopes (TOI) of dissolved oxygen and the closely related O_2/Ar ratios (see Chapter 8) are gas tracers than can quantify GPP and NCP *in situ*. GPP, the total photosynthetic flux, represents the total amount of carbon processed in a biological system. It reflects the amount of energy coming from the sun and thus the maximal possible photosynthesis. Net primary production (NPP), which is often assessed by ^{14}C or ^{13}C incubations, represents GPP minus autotrophic respiration. NCP represents GPP minus autotrophic and heterotrophic respiration and represents the net amount of carbon that can be exported. Triple oxygen isotopes have been used to quantify GPP in the Atlantic (Howard et al., 2017; Luz and Barkan, 2000; 2009), Pacific (Haskell et al., 2016; Hendricks et al., 2005; Juranek and Quay, 2005; Juranek and Quay, 2010; Juranek et al., 2012; Palevsky et al., 2016; Quay et al., 2010; Stanley et al., 2010), Southern (Cassar et al., 2007; Goldman et al., 2015; Hamme et al., 2012; Hendricks et al., 2004; Reuer et al., 2007), and Arctic Oceans (Ji et al., 2019; Stanley et al., 2015), as well as in coastal environments (Haskell et al., 2017; Manning et al., 2019; Manning et al., 2017b; Munro et al., 2013), and salt marshes (Howard et al., 2020; Stanley and Howard, 2013).

Why care about GPP vs. the more commonly measured NPP? GPP is useful because it reflects the energy at the true base of the ecosystem and thus might be more directly related to environmental variables such as sunlight and chlorophyll than is NPP. Hence it might be easier to develop parameterizations of GPP as a function of easily measured variables, either *in situ* variables or remotely sensed ones. Furthermore, including GPP directly in models allows for mechanistic cell allocation models (Nicholson et al., 2018). The most powerful approach is to measure all three types of production concurrently: GPP, NPP, and NCP. When all three types of production are measured together, it is possible to construct energy flow diagrams (Halsey et al., 2010; Manning et al., 2017b) that show the total amount of biological energy/carbon in the system and how it is distributed between different pools (Figure 7.1).

7.1.1. Interpreting triple oxygen isotope derived rates of photosynthetic production

Because the isotopic signature of oxygen produced from photosynthesis is different than the isotopic signature of oxygen derived from air-sea gas exchange, and because respiration does not impact the triple oxygen isotope signature, TOI allows one to quantify rates of photosynthesis only – no assumptions about respiration need to be made. In contrast, oxygen concentrations, as measured on floats (e.g., Riser and Johnson, 2008), gliders (e.g., Nicholson et al., 2015), or bottles

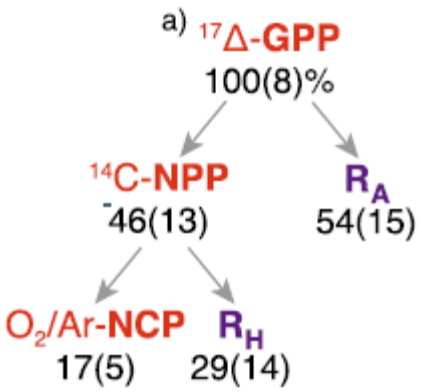

Figure 7.1. Energy flow diagram from Monterey Bay before an upwelling event. Numbers outside the parentheses represent the percent of energy in each of the productivity pools; numbers inside the parentheses represent the uncertainty associated with the percentage. R_A represents autotrophic respiration and R_H heterotrophic respiration. Figure from Manning et al. (2017b).

(e.g., Collins et al., 2018) -- see Chapters 6 and 10 for more information on such methods -- are very valuable but constrain the net effect of photosynthesis and respiration and thus assumptions about respiration are needed (i.e., equivalence of dark and light respiration) to isolate the photosynthetic signature if GPP is calculated.

Triple oxygen isotopes directly constrain gross oxygen production (GOP), a measure of the oxygen produced during photosynthesis (Juranek and Quay, 2013; Luz and Barkan, 2000). GOP can then be converted to GPP through use of a photosynthetic quotient to convert from oxygen to carbon units. Typically, the photosynthetic quotient for marine organisms is considered to be 1.4 if nitrate is the dominant nitrogen source and 1.1 if ammonium is the dominant nitrogen source (Laws, 1991). In addition, photorespiration and the Mehler reaction are two processes that result in oxygen production in the photosystem but not direct fixation of carbon. Thus, when converting from GOP to GPP, the combined effect of those two processes must be estimated; typically, they are considered to be 15% to 20% of the total GOP (Bender et al., 1999; Halsey et al., 2010; Halsey et al., 2013; Kana, 1992).

Gross primary production determined from triple oxygen isotopes typically reflects photosynthetic production integrated over the mixed layer over the previous days to several weeks, depending on the depth of the mixed layer and the gas transfer velocity – shallower mixed layers and larger gas transfer velocities lead to shorter residence times of oxygen and thus a shorter time-scale. Spatially, the gases represent processes that occurred as a given water mass traveled during that time period, and thus can represent production integrated over tens to hundreds of kilometers. However, GPP from triple oxygen isotopes reflects the patchiness of the water it was sampled from - water in the surface ocean is often patchy, with different water masses in close proximity (Klein and Lapeyre, 2009); each of these water masses has its own spatial trajectory and biological activity and will therefore show distinctive GPP. Thus GPP reveals spatial variability in biological production (Juranek and Quay, 2010; Palevsky et al., 2016; Stanley et al., 2017) in spite of the time integration.

7.1.2. Advantages and Disadvantages of triple oxygen isotopes

Like all methods for assessing production, triple oxygen isotopes have advantages and disadvantages. Probably the largest advantage is that triple oxygen isotopes yield *in situ* estimates of GPP – the water does not have to be manipulated and thus potential biases due to bottle effects are avoided. Samples are poisoned as they are drawn into sample bottles and thus the data reflects the community photosynthesis in its natural environment. Furthermore, no assumptions about light and dark respiration have to be made (as is typical in other oxygen studies) removing a large source of uncertainty. Additionally, since the rates are based on oxygen, and the residence time of oxygen in the upper ocean is typically a few days to two weeks, TOI-derived GPP rates give a weighted average of production over the previous few residence times, even when the system is not in steady-state (Teeter et al., 2018). This can be an advantage since the data reflects a longer production history than the limited temporal and spatial footprint of snap-shot approaches such as incubations, and thus may yield a truer picture of productivity in that region. However, it also can be a disadvantage when attempts are made to compare TOI-derived rates to other instantaneous measures of production or environmental variables (such as chlorophyll distributions, temperature, etc.) or during times of rapid change when estimates with shorter time-scales would more accurately reflect current conditions.

TOI measurements require specialized, high vacuum sample processing lines that must be custom-built by a laboratory (i.e., no commercial options exist). Samples are negatively impacted by atmospheric contamination and by failure to incompletely separate dissolved nitrogen gas from samples as it negatively impacts isotopic analysis. After preparation, samples must be analyzed on an isotope ratio mass spectrometer with appropriate cup configuration for amplifying the rare $^{17}O^{16}O$ isotopologue, to enable very high precision (5 to 7 per meg) in order to yield oceanographically relevant results. All of these factors dictate a significant investment in time, cost, and expertise-- setting up a lab for measurement of triple oxygen isotopes can easily take a year or more. One option for working around this significant time and financial investment is for investigators to collect triple oxygen isotope samples themselves and then send them off for analysis at one of the labs that measures triple oxygen isotopes routinely. Once a laboratory invests in the required instruments to measure TOI (or collaborates with a laboratory where such measurements are being made), it is relatively easy to collect large sample numbers. On a single cruise, 200 to 300 samples can be taken with relative ease, while achieving this high of a sampling rate for incubations on a cruise would not be feasible. Finally, triple oxygen isotopes can be paired easily with O_2/Ar samples (see chapter 8) since O_2/Ar data is obtained from the same analyses, yielding information on NCP and ratios of NCP/GOP at the same time for no additional effort. The NCP/GOP ratio is particularly valuable at estimating carbon cycle efficiency (akin to the f-ratio).

Other disadvantages are related to the model-based assumptions required to convert TOI observations into GPP rates. TOI provide estimates of GPP in the mixed layer only, unless a time-series is possible where depths below the mixed layer can be sampled in the same water mass at subsequent times. Mixed layer production is often the bulk of production but in some locations, significant production can occur below the mixed layer and would be missed by the triple oxygen isotope method. There can also be large uncertainty in the rates of GPP estimated from TOI if physical transport – vertical mixing, entrainment, lateral advection, etc. – is not properly accounted for (Nicholson et al., 2014) and in some regions, the transport is not simply known well enough to

allow precise corrections to the triple oxygen isotope data to be made. These corrections have varying effects depending on time of year and location and thus depending on the study design, can be of minor to major significance.

7.2. Theoretical Underpinnings

For a full description of the theoretical underpinnings of the triple oxygen isotope method, see Juranek and Quay (2013) or the seminal papers by Luz (Luz and Barkan, 2000; 2005; Luz et al., 1999). Here, a short description is furnished so interested readers can learn the basic rationale of the method. On the surface of the earth, isotopes undergo mass dependent fractionation. Because ^{18}O (natural abundance 0.20%) has a two atomic mass unit difference from ^{16}O (natural abundance 99.76%), whereas ^{17}O (natural abundance 0.04%) has a one atomic mass unit difference from ^{16}O, most surface earth processes fractionate ^{18}O approximately twice as much as ^{16}O. Thus, for example, during respiration, oxygen that is removed is depleted in ^{18}O by twice as much as ^{17}O is depleted. Similarly, the remaining O_2 dissolved in the water will be twice as enriched in ^{18}O relative to ^{17}O. In contrast, in the stratosphere, mass independent processes, such as ultraviolet induced interactions between O_2, O_3, and CO_2, lead to mass independent fractionation (Lammerzahl et al., 2002; Thiemens et al., 1995). The notation $^{17}\Delta$ is used to quantify the triple oxygen isotope signature of dissolved oxygen in a sample:

$$^{17}\Delta = 10^6 \times \left(\ln\left(\frac{\delta^{17}O}{1000}+1\right) - \lambda \ln\left(\frac{\delta^{18}O}{1000}+1\right)\right) \quad (7.1)$$

where $\delta^X O$ represents standard isotopic notation: ($^X O/^{16}O$-1) x 1000 with ^{X} = 17 or 18, and λ represents the slope of mass-dependent respiration, which equals 0.5179 (Luz and Barkan, 2005; 2009). When defined in this way, $^{17}\Delta$ is insensitive to respiration, since respiration is a mass dependent process that removes oxygen.

Photosynthetic activity adds oxygen with a $^{17}\Delta$ signature based on the isotopic composition of seawater to the dissolved oxygen "pool". For example, if seawater has the isotopic composition of VSMOW (standard mean ocean water), then $^{17}\Delta$ of dissolved oxygen due to photosynthesis is 249 per meg (Luz and Barkan, 2000). Air-sea exchange adds oxygen with an isotopic composition of 8 per meg (Reuer et al., 2007) – the $^{17}\Delta$ of tropospheric air (0 per meg) combined with the solubility effect of dissolving the air in water. Hence, any sample of oxygen dissolved in seawater represents a mixture of air and photosynthetic oxygen and thus lies on an isotopic mixing line between those two extremes (Figure 7.2). The $^{17}\Delta$ thus can be used to calculate the fraction of dissolved oxygen in the sample that is derived from photosynthesis.

In order to obtain a rate of photosynthesis and thus of GPP, the $^{17}\Delta$ signature is combined with an estimate of gas exchange. A mass balance of oxygen isotopes shows that $^{17}\Delta$ is increased by photosynthesis and eroded by gas exchange. Commonly steady-state is assumed, and thus gas exchange balances photosynthesis and provides a "clock" for calculating the rate. In practice, calculations are done with $\delta^{17}O$ and $\delta^{18}O$ (see Calculations, Section 7.3) for more accurate estimation of GPP (Prokopenko et al., 2011). Additionally, steady state does not have to be assumed- including a time rate of change term (if data exists to constrain this term) can improve estimates of GPP in the surface ocean (Manning et al., 2017b) and is essential for constraining

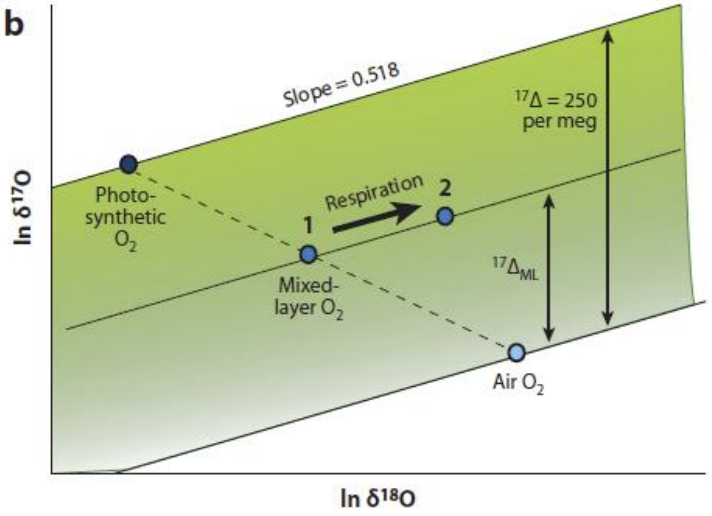

Figure 7.2. Photosynthetic O_2 represents one end-member with a $^{17}\Delta$ of approximately 250 per meg. Air O_2 represents another, with a $^{17}\Delta$ of 0 per meg. A sample falls within the middle of these two and the $^{17}\Delta$ of that sample reflects the fraction of dissolved O_2 in that sample stemming from photosynthesis vs. air-sea exchange. Respiration changes the $\delta^{17}O$ and $\delta^{18}O$ but does not change the $^{17}\Delta$. Figure from Juranek and Quay (2013).

GPP below the mixed layer (Quay et al., 2010). Furthermore, corrections have to be made if the seawater does not have SMOW isotopic composition, as is typical in Arctic or some coastal/inland waters (Manning et al., 2017a).

7.3. Calculations

7.3.1. Equations

Typically, triple oxygen isotopes are used to calculate GOP integrated over the mixed layer, neglecting horizontal and vertical advection and assuming steady state. In that case, GOP is calculated using Equation 7 in Prokopenko et al. (2011):

$$\frac{G}{kO_{eq}} = \frac{\frac{X_{dis}^{17} - X_{eq}^{17}}{X_{dis}^{17}} - \lambda \frac{X_{dis}^{18} - X_{eq}^{18}}{X_{dis}^{18}}}{\frac{X_P^{17} - X_{dis}^{17}}{X_{dis}^{17}} - \lambda \frac{X_P^{18} - X_{dis}^{18}}{X_{dis}^{18}}} \quad (7.2)$$

where G is GOP rate in units of mmol m^{-2} d^{-1}, *k* is the gas transfer velocity in units of m d^{-1}, O_{eq} is the solubility value of oxygen in units of mmol O_2 m^{-3}, X^{17} is the ratio of $^{17}O^{16}O/^{16}O^{16}O$ of the sample ($X^{17}{}_{dis}$), equilibrated water ($X^{17}{}_{eq}$) or photosynthetic end member ($X^{17}{}_{P}$) and the same for X^{18} but it is the ratio of $^{18}O^{16}O/^{16}O^{16}O$ in those substances. λ =0.5179 and is a constant for mass dependent fractionation between ^{17}O and ^{18}O during respiration (Luz and Barkan, 2005; 2009). In δ notation, Eq 7.2 equals

$$\frac{G}{kO_{eq}} = \frac{\left(1 - \frac{10^{-3}\delta^{17}O_{eq} + 1}{10^{-3}\delta^{17}O_{dis} + 1}\right) - \lambda\left(1 - \frac{10^{-3}\delta^{18}O_{eq} + 1}{10^{-3}\delta^{18}O_{dis} + 1}\right)}{\left(\frac{10^{-3}\delta^{17}O_{P} + 1}{10^{-3}\delta^{17}O_{dis} + 1} - 1\right) - \lambda\left(\frac{10^{-3}\delta^{18}O_{P} + 1}{10^{-3}\delta^{18}O_{dis} + 1} - 1\right)} \quad (7.3)$$

.

where $\delta^{17}O_{eq}$ is the $\delta^{17}O$ value of equilibrated water, $\delta^{17}O_{dis}$ is the $\delta^{17}O$ value measured in the sample, and $\delta^{17}O_P$ is the $\delta^{17}O$ value of photosynthetic end member, with similar meaning for the $\delta^{18}O$ values.

The non-steady state version of this equation (Eq S8 in Propenko et al, 2011) can be used if the time rate of change is known. It is similar to Eq 7.2 and 7.3, but includes a term $\partial^{17}\Delta/dt$, which represents the change in $^{17}\Delta$ with time:

$$G = kO_{eq}\left(\frac{\frac{X_{dis}^{17} - X_{eq}^{17}}{X_{dis}^{17}} - \lambda\frac{X_{dis}^{18} - X_{eq}^{18}}{X_{dis}^{18}}}{\frac{X_P^{17} - X_{dis}^{17}}{X_{dis}^{17}} - \lambda\frac{X_P^{18} - X_{dis}^{18}}{X_{dis}^{18}}}\right) + \frac{hO_{dis}\frac{\partial^{17}\Delta}{\partial t}}{\frac{X_P^{17} - X_{dis}^{17}}{X_{dis}^{17}} - \lambda\frac{X_P^{18} - X_{dis}^{18}}{X_{dis}^{18}}} \quad (7.4)$$

and could also be expressed in δ notation if desired. Software for calculating GOP using these equations is available on Github http://github.com/caramanning/calcGOP (Manning and Nicholson, 2017).

If information is known below the mixed layer and the area is one with active entrainment or vertical diffusion, then equations that take into account vertical mixing and entrainment can be used. See the supplemental information of Howard et al. (2017) for the relevant equations.

7.3.2. Isotopic End Members: : $\delta^x O_{eq}$ and $\delta^x O_P$

In order to use these equations, values must be known for the isotopic ratios of equilibrated water and photosynthetic end members. The equilibrated end members can be determined by measuring the isotopic value of water equilibrated with air (see section 7.6.2).

The photosynthetic endmembers are more difficult to ascertain since they depend both on the organisms conducting photosynthesis (Luz and Barkan, 2011) and on the isotopic composition of seawater itself (Manning et al., 2017a). The isotopic composition of photosynthetic oxygen is slightly different for diatoms ($\delta^{18}O_P$= -19.001 vs cyanobacteria $\delta^{18}O_P$ = -22.868) for example. Complete lists of the isotopic values for different community groups as well as a seawater average that can be used when community composition is not known can be found in Luz and Barkan (2011). The values above are based on assuming seawater has VSMOW isotopic composition and indeed most studies assume the seawater isotopic composition is equal to VSMOW. However, certain environments, especially those that contain large amounts of meteoric water such as waters affected by ice melt in the Arctic or inland/very near coastal environments, have $\delta^{18}O$-H_2O that differ from VSMOW by 6 per mil or greater. Ignoring the isotopic composition of seawater can

lead to errors of up to 60%. The Github calculation software described above (http://github.com/caramanning/calcGOP) also contains modules for calculating photosynthetic end member based on the measured isotopic composition of seawater at the sample location.

Because the choice of end-member values affects the GOP calculation, and such choices may be revised in the future, when data is reported it should include the end-members used in the calculation.

7.3.3. Calculating gas transfer velocity k

Another term in the GOP equations (Eq. 7.2-7.4) that has to be carefully considered is *k*, the gas transfer velocity. Numerous parameterizations exist for calculating *k* in open, ice-free marine waters (e.g., Ho et al., 2006; Nightingale et al., 2000; Wanninkhof, 2014) and any of these equations could be used for calculating *k*. Bubbles are not expected to influence triple oxygen isotopes but can be included if desired (Kaiser, 2011). It is important to carefully choose a wind product and an appropriate weighting scheme when calculating *k*. The gas tracers integrate mixed layer productivity over several previous residence times of oxygen in the mixed layer – with the residence time being typically days to weeks. Thus, it would not be appropriate to use the instantaneous wind speed (such as measured on a ship) when calculating *k*. Instead, it is best to use a record of wind speed over the preceding month or two months, such as those from the NCEP/NCAR reanalysis (Kalnay et al., 1996), winds from a buoy within the study region, or from remote sensing data based on scatterometry (i.e., QuikSCAT, ASCAT, or future sensors). Wind data for 30-60 days preceding sample collection should be used to calculate k, using the weighting scheme by Reuer et al. (2007) (updated by Teeter et al. (2018) to work for shorter weighing times) which calculates the fraction of oxygen ventilated at time point back in time and uses that fraction to calculate a weighted effective gas transfer velocity, can be used to calculate a weighted gas transfer velocity appropriate for each sample.

In ice-covered waters, such as in the Arctic or Southern Ocean, calculating *k* is more difficult since there is a lot of uncertainty with regards to how ice cover effects gas exchange. The most straightforward approach is to scale the gas transfer velocity by the fraction of free water (Butterworth and Miller, 2016; Prytherch et al., 2017). Other parameterizations that take into account open water are also being developed (Loose et al., 2014; Loose et al., 2017) and could be used. With partially-covered water, it is important to have an ice history, such as from remote sensing, so the weighting scheme can be applied on both the ice and the winds.

7.3.4. Relative Sizes of Uncertainties in the Calculations

The relative amount of uncertainty stemming from the various terms in the equations for GOP depends on the condition – in general, the errors associated with measurement of $\delta^{17}O$ and $\delta^{18}O$ contribute the largest fraction of error, leading to 10% to 30% uncertainties depending on how productive the region is and how well a particular mass spectrometric system is working (Juranek and Quay, 2013 and references therein). However, in regions of higher productivity, uncertainties in $\delta^{17}O$ and $\delta^{18}O$ matter less than in regions of lower productivity (since it is a difference between $\delta^{17}O_{dis}$ and $\delta^{17}O_{eq}$ that is used in the equations). The next largest source of error is from the gas transfer velocity – in the ice-free open ocean, errors associated with *k* are probably around 10% (Wanninkhof et al., 2009). In ice-covered regions or regions with high winds or limited fetch,

errors associated with gas transfer are likely higher. Other uncertainties stem from the end members – these uncertainties can be lowered if the isotopic composition of seawater is known and if the community composition is measured so informed choices of photosynthetic end members can be made.

7.4. Study Design Considerations

Several factors must be considered when setting up a sampling plan for triple oxygen isotope samples in order to quantify GPP. Typically, samples are collected from the underway water on a ship or from Niskin bottles on a CTD rosette triggered within the mixed layer in order to assess mixed layer GPP. As described above, the most common method is to assume steady-state – this is because samples are typically only available from a particular water mass at one point of time. However, if it is possible to collect multiple samples from the same water mass at different times (i.e., sampling at multiple time points in a Lagrangian cruise), then the time rate of change term can be calculated which will increase accuracy of GPP (Manning et al., 2017b), and in particular will allow "instantaneous rates" to be calculated, rather than rates that integrate over several residence times of the tracer (as done by Hamme et al. (2012) for O_2/Ar). Note that sampling at the same location (latitude/longitude) a few hours to days later does not mean the same water mass is being sampled. Interpreting TOI observations within a time rate-of-change framework requires Lagrangian tracking approaches.

In general, TOI samples can be collected from a ship's underway system or from Niskin bottles on the CTD Rosette. Sampling from the underway system can enable a much higher sampling density than sampling solely from the CTD on many cruises. However, since discrepancies between underway and surface water can be observed either due to respiration in the lines (Juranek et al., 2010) or perhaps because bubbles in the underway line or gas contamination during the process of pumping underway water, it is always important to collect a number of comparison samples between underway water and surface CTD bottles by comparing samples collected from the underway system at the same time that the surface CTD is fired.

Additionally, depending on the amount of vertical mixing expected, a recommended best practice is to collect TOI samples below the mixed layer at some locations during the cruise, (this necessitates collection from Niskins). A sample 5 or 10 m below the mixed layer can be used to calculate the effect of vertical diffusion across the base of the mixed layer (Howard et al., 2017; Nicholson et al., 2014). Deeper samples can be used to estimate the effect of sudden changes in mixed layer depth and thus can be used in corrections for entrainment.

Lateral advection and diffusion are usually neglected in the calculations. However, if the sampling area is one with large advection, it should be possible to correct for lateral advection by collecting samples upstream of the main sampling area and estimating the horizontal velocities.

It may not be possible to fully correct for all physical effects and thus care should be taken when designing a study – it is best to not try to use triple oxygen isotopes during a time of a lot of entrainment – such as during the fall in the northern subtropical gyres when mixed layers are deepening, or in a region of very strong advection, such as in the gulf stream or other western boundary currents. Back of the envelope calculations or OSSEs can be used to determine if corrections can be made in a particular environment. Additionally, Nicholson et al. (2014) contains maps with expected sizes of various corrections, as estimated by incorporating triple oxygen

isotopes in a 3D model. Such a map can be used to guide study design and the feasibility of using triple oxygen isotopes in a given time and location.

7.5. Sample Collection

7.5.1. Triple Oxygen Isotope Sample Collection

Triple oxygen isotope samples are collected in pre-evacuated, custom-made sample bottles (Emerson et al., 1991) (Figure 7.3). The bottles are typically made by a glassblower from 500 mL bottles that are attached to Louwers Hanique (formerly called Louwers Houpert) valves (part number H10402009). Each bottle should be prepared by first having added to it 100 μg of saturated mercuric chloride solution that is then dried in a 70 °C oven – the relatively low temperature of the oven helps the mercuric chloride stay at the bottom of the bottle; when the oven temperature is 100 °C, the solution spreads and mercuric chloride may get inside the neck of the bottle where it could interfere with the seal. The "stem" of the bottle (the glass part with the o-rings) should never go in the oven. O-rings on the valves of the bottles should be inspected carefully before each cruise and should be greased lightly with Torrlube or apiezon. Some informal reports suggest apiezon may interfere with mass spectrometry at the later stages of analysis so Torrlube is preferred. The bottles should then be evacuated on a vacuum manifold to pressures smaller than $1x10^{-4}$ torr and sealed under vacuum. These pre-evacuated, poisoned bottles can then be used for samples.

Figure 7.3. A custom-made triple oxygen isotope sample bottle contained a seawater sample. Note the water in the neck that is used as a diffusion barrier.

Since gases can diffuse in or out of Niskins after they are opened, triple oxygen isotope samples are usually among the first sampled from a Niskin – sampled after CFC's or helium but before DIC, nutrients, salts, etc. Water from the underway system or from a Niskin should be gravity fed via silicone tubing into the valve neck with a strong enough flow so that the water overflows. Usually two different sizes of tubing are joined with a nylon adaptor – for example 1/4" ID tubing to fit around the nipple of a Niskin is joined with 3/16" ID thin-walled tubing that will fit inside the valve neck. The valve on the sample bottle is slowly opened, allowing some water to enter the sample flask and the rest of the water to overflow the whole time – the water in the valve neck forms a barrier that prevents atmospheric air from entering and contaminating the sample. It is imperative to make sure the water in the tubing and neck of the bottle is bubble-free – to ensure that, it often is necessary to tap the neck before you open the valve in order to dislodge bubbles. When the sample flask is roughly half-full, the valve should be closed. The neck should be rinsed and then refilled with freshwater and capped to form a diffusion barrier – keeping water in the neck of the flask enables samples to stay gas-tight for 3 months as opposed to for only days to weeks (Reuer et al., 2007). For detailed instructions on sampling procedures, see Appendix A.

7.5.2. Ancillary Data Collection:

Temperature and salinity data are required for the calculations that convert triple oxygen isotope signatures into rates of GPP since the solubility of oxygen is a function of temperature and salinity (Garcia and Gordon, 1992). Additionally, wind speed information is needed from external databases based on either buoy data, reanalysis fields (e.g., NCEP/NCAR, (Kalnay et al., 1996) or remote sensing products (see section 7.3.3). Since a wind history is needed, rather than instantaneous wind speed, wind products from particular cruises are usually not helpful. Nonetheless, when designing a study, make sure wind data will be available (which can be more of a challenge in very near-shore or very remote environments). Other ancillary data that is not required for sample calculations but can aid interpretation of the data, and thus is recommended if possible, are O_2/Ar ratios (which can be measured on the same samples), fluorescence data, and information on community composition. It is important to keep in mind when collecting ancillary data – and when ultimately comparing GPP to this ancillary data – that GPP rates from triple oxygen isotopes have a longer temporal and spatial footprint then many other kinds of data (see section 7.1.1).

7.6. Sample Analysis

7.6.1. Processing Line and Isotope Ratio Mass Spectrometry

Before being attached to the processing line, samples have to be drained of most of their water. First, the samples should be shaken for at least 6 hours in order to equilibrate gases between the headspace and the water in the samples - unless it is deemed they have been shaken enough in transport. The samples should then be attached to a vacuum drainage system, inverted, and water drained into an evacuated filter flask, being sure to leave a "plug" of ~1 cm^3 of water in the neck so that the sample gas itself is not pumped away. The samples – that now contain all the gas but only a small amount of water – are ready for analysis.

Triple oxygen isotope samples are analyzed by first processing the sample on a specialized processing line (Barkan and Luz, 2003) to remove CO_2, water vapor and N_2 gas, and then analyzing the remaining gas on an isotope ratio mass spectrometer (IRMS) for ^{16}O, ^{17}O, ^{18}O, and Ar. Typically a ThermoFisher 253 MAT or Delta XP IRMS is used. Different labs have variations of the processing line (Juranek and Quay, 2005; Stanley et al., 2015) but all contain the same essential elements: a water trap that removes water vapor from the system (typically at temperatures < -65 °C), two molsieve traps that can be either at liquid nitrogen temperatures or heated in order to trap and release gases both before and after gas chromatography, a gas chromatography column that is used to separate the O_2 and Ar from other gases (primarily nitrogen but also CO_2, Methane, etc.), and a cryogenic trap (Lott, 2001) or a tube at liquid helium samples that is used to trap the final gas before release into the IRMS. GC columns range in length from 2 to 5 m (Barkan and Luz, 2003; Stanley et al., 2015) and are held at different temperatures – such as -5 °C or 50 °C. Each lab determines based on column length and temperature what timing gives good separation of the gases. Such separation should be checked occasionally since the separation timing differs with sample size and may drift over time.

Some labs have tried to omit the final cryogenic trap since liquid helium is hard to obtain and cryogenic traps are expensive. However, an intercalibration assessment between 5 labs that measured triple oxygen isotopes on the same air and water samples showed that the final cryogenic trap (or liquid helium) was necessary in order to obtain accurate $\delta^{17}O$ and $\delta^{18}O$ measurements (Stanley, unpublished). If samples are from salt marshes or other high methane environments, an additional cold trap may be required to trap out methane before sample analysis (Howard et al., 2020).

Some systems have the processing line attached directly to an IRMS, allowing a sample to be processed and then analyzed on the IRMS immediately with no connections needing to be changed (Stanley et al., 2015) (Figure 7.4) and allowing for 24 hour a day operation. Other systems operate by processing a suite of samples (e.g., 6-8) on a dedicated processing line and then collecting on a sample manifold. This manifold is then moved to the IRMS the subsequent day for analysis (Reuer et al., 2007). When operating properly, the TOI processing line and associated mass spectrometer should yield uncertainties of 4 to 7 per meg in $^{17}\Delta$, 0.01 to 0.02 per mil for $\delta^{17}O$ and $\delta^{18}O$. Constant vigilance is required to maintain these high level of precision – and in particular to make sure there are no leaks in any part of the system, degradation of the water traps or GC column, impurities in the helium gas stream, problems with the cryogenics, etc.

7.6.2. Standardization

Standardization of triple oxygen isotope samples occurs on multiple levels. First, samples are directly run on the IRMS in conjunction with a running standard, typically a custom-made gas that has O_2 and Ar in similar proportions to seawater (such as 95% O_2, 5% Ar). It is important this running standard is not regular air, since air contains large amounts of nitrogen which interferes with the triple oxygen isotopic measurements. Since triple oxygen isotope data needs to be reported compared to real air (rather than to the running standard), air standards need to be run on the line as well. Thus approximately every day, a sample of atmospheric air should be measured and the difference between the air and the running standard can be used to calculate the difference between seawater samples and air. Atmospheric air is typically collected from a “clean air” location such

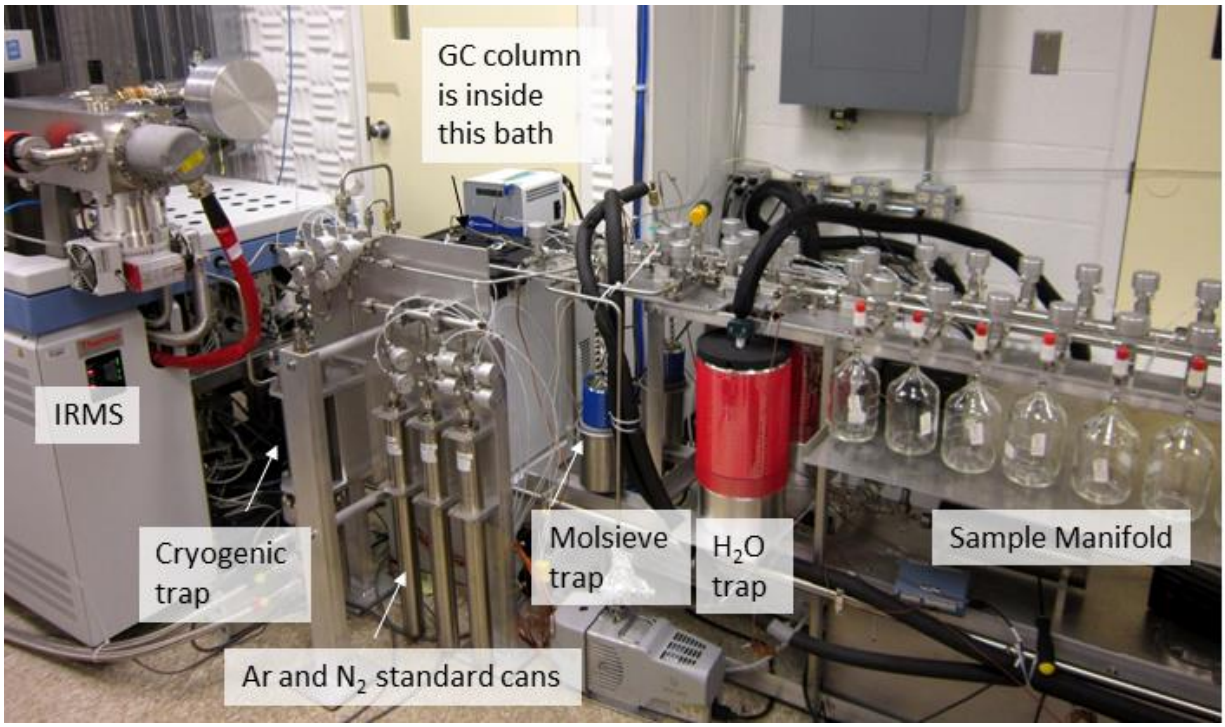

Figure 7.4. Photograph of a triple oxygen isotope sampling line and the attached Isotope Ratio Mass Spectrometer (IRMS). Samples are attached to a sample manifold so that multiple samples can be analyzed in quick succession. One sample at a time is opened and the gas contained in that sample is expanded through an H_2O trap, caught by a molsieve trap, and passes through a gas chromatography (GC) column held in a constant temperature bath (-5 °C for this line but temperatures can vary) to separate the oxygen and argon from other gases. The oxygen and argon are caught in a liquid nitrogen cooled molsieve trap and then on a cryogenic trap held at 12 K. The cryogenic trap is warmed and the sample is released into the IRMS where it is analyzed for $^{16}O^{16}O$, $^{17}O^{16}O$, and $^{18}O^{16}O$. Often the sample is analyzed for Ar as well in order to quantify NCP as well as GPP.

as from a beach with wind blowing off the ocean or from a mountain top. It is assumed that tropospheric air around the globe does not have significant natural variations in TOI, i.e., the variations are small enough to be undetectable given current measurement capabilities.

Additionally, to confirm that the line is working well and to furnish data required for the calculations, samples of equilibrated water should be measured frequently (daily to weekly depending on the lab). Dissolved oxygen in water equilibrated with the atmosphere has a known $^{17}\Delta$ value of 8 per meg (Stanley et al., 2010). Originally, the equilibrated water $^{17}\Delta$ value was reported as 8 per meg on larger samples (Reuer et al., 2007) vs. 16 per meg on smaller samples (Juranek and Quay, 2005; Luz and Barkan, 2000) or as being temperature dependent (Luz and Barkan, 2009) but after corrections for the size of the sample were taken into account, labs converged on a value of 8 per meg regardless of size or temperature (Stanley et al., 2010). Equilibrated water can be made by stirring distilled water (not too vigorously – bubbles should not be entrained) that has been previously poisoned with mercuric chloride, in a partially covered beaker for several days. Sample from this equilibrated water can then be collected as described in the sample collection section.

7.6.3. Required Corrections

Given the required high levels of precision, each sample is typically measured for approximately two hours in the IRMS. The IRMS then directly outputs values for $\delta^{17}O$ and $\delta^{18}O$ for each sample. $^{17}\Delta$ can be calculated based on Eq. 7.1. However, a number of corrections need to be made to the data before it can be used in calculations. First, the presence of Ar in the mass spectrometer changes the $\delta^{17}O$ and $\delta^{18}O$ via matrix effects. Some labs remove all Ar in the gas chromatography step to avoid this problem (Yeung et al., 2018) but other labs want to measure O_2/Ar to obtain rates of NCP from the same samples and thus cannot remove Ar. They therefore correct for the presence of Ar. Argon corrections can be made by creating a suite of standards that have the same oxygen content and isotopic composition but variable amounts of Ar. These standards can be run regularly (every few weeks), and the response of $\delta^{17}O$, $\delta^{18}O$, and $^{17}\Delta$ to the presence of Ar can be determined and then used to correct natural samples where the $\delta^{17}O$ and $\delta^{18}O$ is not already known. The Ar correction can take the form of plotting $^{17}\Delta$, $\delta^{17}O$, or $\delta^{17}O$ vs $\delta Ar/O_2$ for all the standards (Figure. 7.5a) and then using the resulting slope to correct the seawater samples based on the sample $\delta Ar/O_2$.

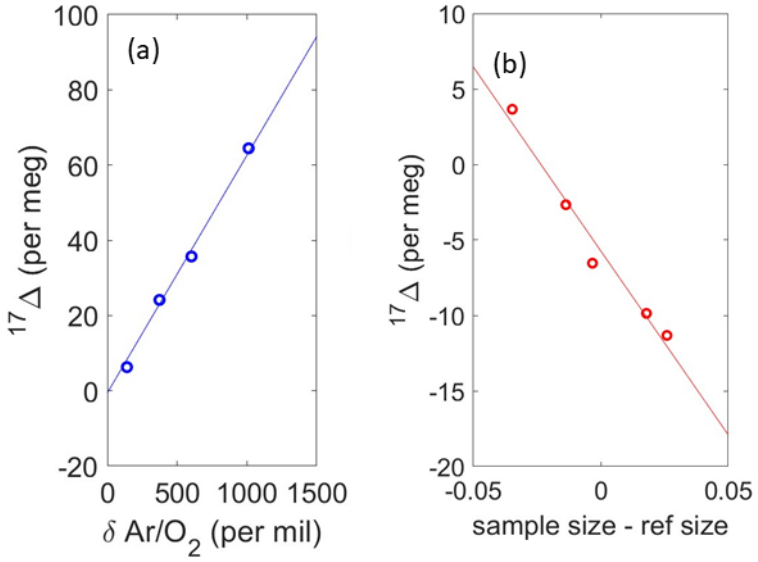

Figure 7.5. (a) The presence of Ar in the mass spectrometer interferes with the $^{17}\Delta$ measurement so $^{17}\Delta$, $\delta^{17}O$, and $\delta^{18}O$ are all corrected for Ar by running a calibration curve of the same oxygen standard but with varying amounts of Ar. Only the calibration curve for $^{17}\Delta$ is shown here. $\delta\frac{Ar}{O_2} = \left(\frac{\left(\frac{Ar}{O_2}\right)_{std}}{\left(\frac{Ar}{O_2}\right)_{ref}} - 1\right) \times 1000$, where std refers to the given Ar standard and ref refers to the reference gas in the IRMS. (b) The difference in sizes of the sample in the standard and reference bellows affects the $^{17}\Delta$, $\delta^{17}O$ and $\delta^{18}O$ measurements so calibrations are also run where the reference gas is in both standard and reference bellows but at different relative sizes. "Sample size – reference size" refers to $\frac{O_{2\ int\ smpl} - O_{2\ end\ smpl}}{O_{2\ int\ smpl}} - \frac{O_{2\ int\ ref} - O_{2\ end\ ref}}{O_{2\ int\ ref}}$, where $O_{2\ int\ smpl}$ is the integrated ^{32}O in millivolts reported by the IRMS for the sample side bellows, $O_{2\ end\ smpl}$ is the jump to mass 32 measured in millivolts at the end of the block for the sample side bellows, $O_{2\ int\ ref}$ is the integrated ^{32}O in millivolts reported by the IRMS for the reference side bellows, and $O_{2\ end\ ref}$ is the jump to mass 32 in millivolts measured at the end of the block for the reference side bellows.

Second, the effect of differing sizes of samples within the sample and the reference bellows needs to be corrected for (Stanley et al., 2010). The differing sizes may cause problems because larger samples lead to slower changes of pressure within the bellows during the sample block – the bellows are pressure adjusted at the beginning of the block but not during the block itself. The size corrections can be obtained by analyzing "zeros" of differing sizes – reference gas in both standard and reference bellows but with the bellows initially at different volumes (such as 100% standard and 50% reference vs 50% standard size and 100% reference side). Thus, the gas should have a 0 offset since it is the same gas in each side but because of the size effect, the offset will be nonzero. The size of the calculated $\delta^{17}O$, $\delta^{18}O$, and $^{17}\Delta$ can be used to calculate a calibration curve (Figure 7.5b) that is then applied to all samples. This size correction also inherently corrects for any effects due to pressure imbalance and thus it precludes the necessity for separate pressure imbalance corrections.

The presence of nitrogen in the IRMS interferes with the proper determination of triple oxygen isotope signatures. Typically, the separation with the GC column is good enough that there is practically no nitrogen within the IRMS and correcting for this very small amount of nitrogen is not necessary. However, standard curves can be run in much the same way as for Ar (an artificial standard created with same O_2 content as regular air standard but differing amount of nitrogen) and the resulting calibration curve applied to all standards. For typical levels of nitrogen found after a properly working GC column, however, the corrections due to nitrogen are on the order of 0.1 per meg and thus are not required.

7.7. Databases

When reporting triple oxygen isotope data and GOP rates derived from triple oxygen isotopes to a database, it is important to report both the direct oxygen isotopic data as well as the ancillary data and other values used that are required for the calculations. For example, data on $\delta^{17}O$, $\delta^{18}O$, and $^{17}\Delta$ should be reported ($^{17}\Delta$ should be reported separately from $\delta^{17}O$ and $\delta^{18}O$ because even though $^{17}\Delta$ can be calculated from $\delta^{17}O$ and $\delta^{18}O$, mass spectrometric calibrations can be directly done on $^{17}\Delta$ giving more accurate values – see section 7.6.3). Additionally, if measured, O_2/Ar data from the samples should be reported. If isotopic samples were collected of seawater itself-i.e., if $\delta^{17}O$ -H_2O and $\delta^{18}O$ -H_2O were made, those should be reported too.

Metadata that needs to be included are depth of sample, temperature, salinity, latitude and longitude, and time samples were collected. It would be useful to include a value of the weighted gas transfer velocity and the weighted square of the wind speed for each data point, where the weightings are made using the scheme of Reuer et al. (2007) to take into account fraction ventilated (see section 7.3.3). It also could be useful to include mixed layer depth, along with an explanation of which criterion was used to calculate mixed layer depth. Mixed layer depth is important for anyone wishing to convert the areal productivity rates to volumetric ones, which enables easier comparison with ^{14}C-derived primary productivity.

It is important in the documentation to explain how GOP was calculated, what assumptions were made (e.g., assumed steady state, neglecting lateral advection, etc.), which equations were used, and which values were used of the photosynthetic and equilibrium end-members.

7.8. Appendix A - Detailed instructions on how to collect a triple oxygen isotope sample

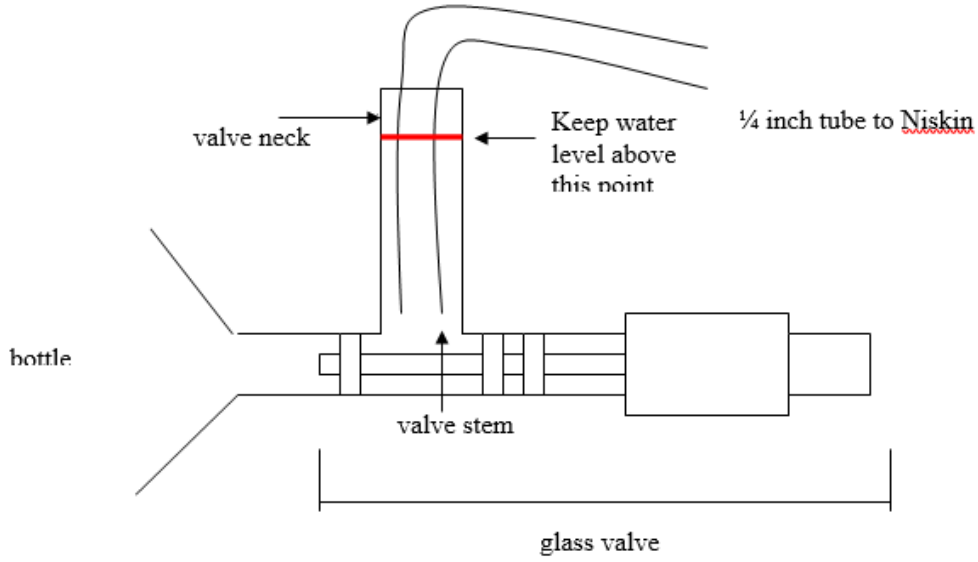

1. Attach larger diameter tubing (~3/8 in) to Niskin bottle nipple. If using a continuous seawater system, attach tubing to seawater supply
2. Remove black rubber cap, and drain deionized water from neck of triple oxygen isotope bottle. If cap sticks you might need to wet it with water from the Niskin or from a squirt bottle.
3. Place small diameter tubing inside the bottle neck to almost touching the valve stem.
4. Open the Niskin bottle.
5. Open plastic flow controller and adjust seawater flow to establish a strong stream (I've found that 3 "clicks" works well). Hold tubing in a gentle curve, making sure tubing isn't kinked.
6. Allow sample seawater to flow for several seconds or until the neck of the valve has flushed 3-4 times and until the water in the neck is bubble free (you can tap on glass gently or mash tubing around to get rid of bubbles).
7. **Slowly open the glass valve, while ensuring that flow is sufficient to keep the bottle neck flush with sample. This is very important**. If the water level drops below the Louwer's valve stem, the vacuum in the bottle will pull in atmospheric gases and contaminate the sample. A good rule is to not let the water level in the neck to drop below the half way mark and to always try to keep the water level at the top.
8. **Fill bottle to 1/2 to 2/3rds full**, always keeping an eye on the water level in the valve
9. Close glass valve
10. Refill valve neck with sample water, making sure the water is bubble free. Fill black cap with sample water.
11. Recap valve neck with black rubber cap

7.9. References

Barkan, E., and B. Luz (2003), High-precision measurements of O-17/O-16 and O-18/O-16 of O-2 and O-2/Ar ratio in air, *Rapid Communications in Mass Spectrometry*, *17*(24), 2809-2814. doi:

Bender, M., J. Orchardo, M. L. Dickson, R. Barber, and S. Lindley (1999), In vitro O-2 fluxes compared with C-14 production and other rate terms during the JGOFS Equatorial Pacific experiment, *Deep-Sea Res. Part I-Oceanogr. Res. Pap.*, *46*(4), 637-654. doi:

Butterworth, B. J., and S. D. Miller (2016), Air-sea exchange of carbon dioxide in the Southern Ocean and Antarctic marginal ice zone, *Geophysical Research Letters*, *43*(13), 7223-7230. doi: 10.1002/2016gl069581

Cassar, N., M. L. Bender, B. A. Barnett, S. Fan, W. J. Moxim, H. Levy, and B. Tilbrook (2007), The Southern Ocean biological response to Aeolian iron deposition, *Science*, *317*(5841), 1067-1070. doi:

Collins, J. R., P. D. Fucile, G. McDonald, J. E. Ossolinski, R. G. Keil, J. R. Valdes, S. C. Doney, and B. A. S. Van Mooy (2018), An autonomous, *in situ* light-dark bottle device for determining community respiration and net community production, *Limnol. Oceanogr. Meth.*, *16*(6), 323-338. doi: 10.1002/lom3.10247

Emerson, S., P. Quay, C. Stump, D. Wilbur, and M. Knox (1991), O2, Ar, N2, and 222Rn in surface waters of the subarctic ocean: Net biological O2 Production, *Global Biogeochemical Cycles*, *5*, 49-69. doi:

Garcia, H. E., and L. I. Gordon (1992), Oxygen solubility in water: better fitting equations, *Limnology and Oceanography*, *37*(6), 1307-1312. doi:

Goldman, J. A. L., S. A. Kranz, J. N. Young, P. D. Tortell, R. H. R. Stanley, M. L. Bender, and F. M. M. Morel (2015), Gross and net production during the spring bloom along the Western Antarctic Peninsula, *New Phytol.*, *205*(1), 182-191. doi: 10.1111/nph.13125

Halsey, K. H., A. J. Milligan, and M. J. Behrenfeld (2010), Physiological optimization underlies growth rate-independent chlorophyll-specific gross and net primary production, *Photosynth. Res.*, *103*(2), 125-137. doi: 10.1007/s11120-009-9526-z

Halsey, K. H., R. T. O'Malley, J. R. Graff, A. J. Milligan, and M. J. Behrenfeld (2013), A common partitioning strategy for photosynthetic products in evolutionarily distinct phytoplankton species, *New Phytol.*, *198*(4), 1030-1038. doi: 10.1111/nph.12209

Hamme, R. C., N. Cassar, V. P. Lance, R. D. Vaillancourt, M. L. Bender, P. G. Strutton, T. S. Moore, M. D. DeGrandpre, C. L. Sabine, D. T. Ho, and B. R. Hargreaves (2012), Dissolved O2/Ar and other methods reveal rapid changes in productivity during a Lagrangian experiment in the Southern Ocean, *J. Geophys. Res.-Oceans*, *117*, C00F12. doi: 10.1029/2011JC007046,

Haskell, W. Z., M. G. Prokopenko, R. H. R. Stanley, and A. N. Knapp (2016), Estimates of vertical turbulent mixing used to determine a vertical gradient in net and gross oxygen production in the oligotrophic South Pacific Gyre, *Geophysical Research Letters*, *in press*. doi:

Haskell, W. Z., M. G. Prokopenko, D. E. Hammond, R. H. R. Stanley, and Z. O. Sandwith (2017), Annual cyclicity in export efficiency in the inner Southern California Bight, *Global Biogeochemical Cycles*, *31*(2), 357-376. doi: 10.1002/2016gb005561

Hendricks, M. B., M. L. Bender, and B. A. Barnett (2004), Net and gross O-2 production in the Southern Ocean from measurements of biological O-2 saturation and its triple isotope composition, *Deep-Sea Res. Part I-Oceanogr. Res. Pap.*, *51*(11), 1541-1561. doi:

Hendricks, M. B., M. L. Bender, B. A. Barnett, P. Strutton, and F. P. Chavez (2005), Triple oxygen isotope composition of dissolved O-2 in the equatorial Pacific: A tracer of mixing, production, and respiration, *J. Geophys. Res.-Oceans*, *110*(C12), doi:10.1029/2004JC002735. doi:

Ho, D. T., C. S. Law, M. J. Smith, P. Schlosser, M. Harvey, and P. Hill (2006), Measurements of air-sea gas exchange at high wind speeds in the Southern Ocean: Implications for global parameterizations, *Geophysical Research Letters*, *33*(16). doi:

Howard, E. M., C. Durkin, G. M. M. Hennonw, F. Ribalet, E. V. Armbrust, and R. H. R. Stanley (2017), Biological production and export across 8000 km: Basin scale homogeniety and mesoscale variabillity, *Global Biogeochemical Cycles*, *31*, 1066-1088. doi: 10.1002/2016GB005488

Howard, E. M., A. C. Spivak, J. S. Karolewski, K. M. Gosselin, Z. O. Sandwith, C. C. Manning, and R. H. R. Stanley (2020), Oxygen and Triple Oxygen Isotope Measurements Provide Different Insights into Gross Oxygen Production in a Shallow Salt Marsh Pond, *Estuaries and Coasts*. doi: doi.org/10.1007/s12237-020-00757-6

Ji, B. Y., Z. O. Sandwith, W. J. Williams, O. Diaconescu, R. Ji, Y. Li, E. Van Scoy, M. Yamamoto-Kawai, S. Zimmerann, and R. H. R. Stanley (2019), Variations in Rates of Biological Production in the Beaufort Gyre as the Arctic Changes: Rates from 2011 to 2016, *Journal of Geophysical Research Oceans*, *124*(6). doi: 10.1029/2018JC014805

Juranek, L. W., and P. D. Quay (2005), In vitro and *in situ* gross primary and net community production in the North Pacific Subtropical Gyre using labeled and natural abundance isotopes of dissolved O-2, *Global Biogeochemical Cycles*, *19*(3), doi:10.1029/2004GB002384. doi:

Juranek, L. W., and P. D. Quay (2010), Basin-wide photosynthetic production rates in the subtropical and tropical Pacific Ocean determined from dissolved oxygen isotope ratio measurements, *Global Biogeochem. Cycles*, *24*(GB2006). doi: 10.1029/2009GB003492

Juranek, L. W., and P. D. Quay (2013), Using Triple Isotopes of Dissolved Oxygen to Evaluate Global Marine Productivity, in *Annual Review of Marine Science, Vol 5*, edited by C. A. Carlson and S. J. Giovannoni, pp. 503-524, Annual Reviews, Palo Alto.

Juranek, L. W., R. C. Hamme, J. Kaiser, R. Wanninkhof, and P. D. Quay (2010), Evidence of O-2 consumption in underway seawater lines: Implications for air-sea O-2 and CO2 fluxes, *Geophysical Research Letters*, *37*, doi:10.1029/2009GL040423. doi:

Juranek, L. W., P. D. Quay, R. A. Feely, D. Lockwood, D. M. Karl, and M. J. Church (2012), Biological production in the NE Pacific and its influence on air-sea CO2 flux: Evidence from dissolved oxygen isotopes and O2/Ar, *J. Geophys. Res.-Oceans*(117). doi: 10.1029/2011JC007450

Kaiser, J. (2011), Technical note: Consistent calculation of aquatic gross production from oxygen triple isotope measurements, *Biogeosciences*, *8*(7), 1793-1811. doi: 10.5194/bg-8-1793-2011

Kalnay, E., M. Kanamitsu, R. Kistler, W. Collins, D. Deaven, L. Gandin, M. Iredell, S. Saha, G. White, J. Woollen, Y. Zhu, M. Chelliah, W. Ebisuzaki, W. Higgins, J. Janowiak, K. C. Mo, C. Ropelewski, J. Wang, A. Leetmaa, R. Reynolds, R. Jenne, and D. Joseph (1996), The NCEP/NCAR 40-year reanalysis project, *Bulletin of the American Meteorological Society*, *77*(3), 437-471. doi: 10.1175/1520-0477(1996)077<0437:TNYRP>2.0.CO;2

Kana, T. M. (1992), Relationship Between Photosynthetic Oxygen Cycling and Carbon Assimilation in Synechococcus Wh7803 (cyanophyta), *J. Phycol.*, *28*, 304-308. doi: doi:10.1111/j.0022-3646.1992.00304.x.

Klein, P., and G. Lapeyre (2009), The Oceanic Vertical Pump Induced by Mesoscale and Submesoscale Turbulence, *Annu. Rev. Mar. Sci.*, *1*, 351-375. doi:

Lammerzahl, P., T. Rockmann, C. A. M. Brenninkmeijer, D. Krankowsky, and K. Mauersberger (2002), Oxygen isotope composition of stratospheric carbon dioxide, *Geophysical Research Letters*, *29*(12), 10.1029/2001GL014343. doi:

Laws, E. A. (1991), Photosynthetic quotients, new production and net community production in the open ocean, *Deep-Sea Research Part a-Oceanographic Research Papers*, *38*(1), 143-167. doi:

Loose, B., W. R. McGillis, D. Perovich, C. J. Zappa, and P. Schlosser (2014), A parameter model of gas exchange for the seasonal sea ice zone, *Ocean Sci.*, *10*(1), 17-28. doi: 10.5194/os-10-17-2014

Loose, B., R. P. Kelly, A. Bigdeli, W. Williams, R. Krishfield, M. R. van der Loeff, and S. B. Moran (2017), How well does wind speed predict air-sea gas transfer in the sea ice zone? A synthesis of radon deficit profiles in the upper water column of the Arctic Ocean, *J. Geophys. Res.-Oceans*, *122*(5), 3696-3714. doi: 10.1002/2016jc012460

Lott, D. E. (2001), Improvements in noble gas separation methodology: a nude cryogenic trap, *Geochemistry, Geophysics, Geosystems*, *2*, 10.129/2001GC000202. doi:

Luz, B., and E. Barkan (2000), Assessment of oceanic productivity with the triple-isotope composition of dissolved oxygen, *Science*, *288*(5473), 2028-2031. doi:

Luz, B., and E. Barkan (2005), The isotopic ratios O-17/O-16 and O-18/O-16 in molecular oxygen and their significance in biogeochemistry, *Geochimica Et Cosmochimica Acta*, *69*(5), 1099-1110. doi:

Luz, B., and E. Barkan (2009), Net and gross oxygen production from O-2/Ar, O-17/O-16 and O-18/O-16 ratios, *Aquatic Microbial Ecology*, *56*(2-3), 133-145. doi:

Luz, B., and E. Barkan (2011), Proper estimation of marine gross O(2) production with (17)O/(16)O and (18)O/(16)O ratios of dissolved O(2), *Geophysical Research Letters*, *38*. doi: L1960610.1029/2011gl049138

Luz, B., E. Barkan, M. L. Bender, M. H. Thiemens, and K. A. Boering (1999), Triple-isotope composition of atmospheric oxygen as a tracer of biosphere productivity, *Nature*, *400*(6744), 547-550. doi:

Manning, C. C., and D. P. Nicholson (2017), http://github.com/caramanning/calcGOP, in *calcGOP: Functions for calculating gross oxygen production from measurements of the triple oxygen isotopic composition of dissolved O2*, edited.

Manning, C. C., E. M. Howard, D. P. Nicholson, B. Y. Ji, Z. O. Sandwith, and R. H. R. Stanley (2017a), Revising estimates of aquatic gross oxygen production by the triple oxygen isotope method to incorporate the local isotopic composition of water., *Geophysical Research Letters*, *44*. doi: 10.1002/2017GL074375

Manning, C. C., R. H. R. Stanley, D. P. Nicholson, B. Loose, A. Lovely, P. Schlosser, and B. G. Hatcher (2019), Changes in gross oxygen production, net oxygen production, and air-water gas exchange during seasonal ice melt in Whycocomagh Bay, a Canadian estuary in the Bras d'Or Lake system, *Biogeosciences*, *16*(17), 3351-3376. doi: doi.org/10.5194/bg-16-3351-2019

Manning, C. C., R. H. R. Stanley, D. P. Nicholson, J. M. Smith, J. T. Pennington, M. R. Fewings, M. E. Squibb, and F. P. Chavez (2017b), Impact of recently upwelled water on productvity investigated using *in situ* and incubation-based methods in Monterey Bay, *J. Geophys. Res.-Oceans*, *122*, 1901-1926. doi: 10.1002/2016JC012306.

Munro, D. R., P. D. Quay, L. W. Juranek, and R. Goericke (2013), Biological production rates off the Southern California coast estimated from triple O2 isotopes and O2:Ar gas ratios, *Limnology and Oceanography*, *58*(3), 1312-1328. doi:

Nicholson, D. P., R. H. R. Stanley, and S. C. Doney (2014), The triple oxygen isotope tracer of primary productivity in a dynamic ocean, *Global Biogeochem. Cycles*. doi: 10.1002/2013GB004704

Nicholson, D. P., R. H. R. Stanley, and S. C. Doney (2018), A Phytoplankton Model for the Allocation of Gross Photosynthetic Energy Including the Trade-Offs of Diazotrophy, *Journal of Geophysical Research Biogeosciences*, *132*(6), 1796-1816. doi: doi.org/10.1029/2017JG004263

Nicholson, D. P., S. T. Wilson, S. C. Doney, and D. M. Karl (2015), Quantifying subtropical North Pacific gyre mixed layer primary productivity from Seaglider observations of diel oxygen cycles, *Geophysical Research Letters*, *42*(10), 4032-4039. doi: 10.1002/2015gl063065

Nightingale, P. D., G. Malin, C. S. Law, A. Watson, P. S. Liss, M. I. Liddicoat, J. Boutin, and R. Upstill-Goddard (2000), *In situ* evaluation of air-sea gas exchange parameterizations using novel conservative and volatile tracers, *Global Biogeochemical Cycles*, *14*(1), 373-387. doi:

Palevsky, H. I., P. D. Quay, D. E. Lockwood, and D. P. Nicholson (2016), The annual cycle of gross primary product ion, net community production, and export efficiency across the North Pacific Ocean, *Global Biogeochem. Cycles*, *30*, 361-380. doi: 10.1002/2015GB005318

Prokopenko, M. G., O. M. Pauluis, J. Granger, and L. Y. Yeung (2011), Exact evaluation of gross photosynthetic production from the oxygen triple-isotope composition of O(2): Implications for the net-to-gross primary production ratios, *Geophysical Research Letters*, *38*. doi: L1460310.1029/2011gl047652

Prytherch, J., I. M. Brooks, P. M. Crill, B. F. Thornton, D. J. Salisbury, M. Tjernstrom, L. G. Anderson, M. C. Geibel, and C. Humborg (2017), Direct determination of the air-sea CO2

gas transfer velocity in Arctic sea ice regions, *Geophysical Research Letters*, *44*(8), 3770-3778. doi: 10.1002/2017gl073593

Quay, P. D., C. Peacock, K. Bjorkman, and D. M. Karl (2010), Measuring primary production rates in the ocean: Enigmatic results between incubation and non-incubation methods at Station ALOHA, *Global Biogeochemical Cycles*, *24*(3), doi:10.1029/2009GB003665. doi:

Reuer, M. K., B. A. Barnett, M. L. Bender, P. G. Falkowski, and M. B. Hendricks (2007), New estimates of Southern Ocean biological production rates from O-2/Ar ratios and the triple isotope composition of O-2, *Deep-Sea Res. Part I-Oceanogr. Res. Pap.*, *54*(6), 951-974. doi:

Riser, S. C., and K. S. Johnson (2008), Net production of oxygen in the subtropical ocean, *Nature*, *451*(7176), 323-U325. doi:

Stanley, R. H. R., and E. M. Howard (2013), Quantifying photosynthetic rates of microphytobenthos using the triple isotope composition of dissolved oxygen, *Limnol. Oceanogr. Meth.*, *11*, 360-373. doi: 10.4319/lom.2013.11.360

Stanley, R. H. R., Z. O. Sandwith, and W. J. Williams (2015), Rates of summertime biological productivity in the Beaufort Gyre: A comparison between the low and record-low ice conditions of August 2011 and 2012, *Journal of Marine Systems*, *147*, 29-44. doi:

Stanley, R. H. R., D. J. McGillicuddy, Z. O. Sandwith, and H. M. Pleskow (2017), Submesoscale hotspots of productivity and respiration: Insights from highresolution oxygen and fluorescence sections, *Deep Sea Resarch Part I, 130*, 1-11. doi:

Stanley, R. H. R., J. B. Kirkpatrick, B. Barnett, N. Cassar, and M. L. Bender (2010), Net community production and gross production rates in the Western Equatorial Pacific, *Global Biogeochemical Cycles*, *24*, GB4001, doi:4010.1029/2009GB003651. doi:

Teeter, L., R. C. Hamme, D. Ianson, and L. Bianucci (2018), Accurate estimation of net community production from O2/Ar measurements, *Global Biogeochem. Cycles*, *32*. doi: 10.1029/2017GB005874

Thiemens, M. H., T. Jackson, E. C. Zipf, P. W. Erdman, and C. Vanegmond (1995), Carbon-Dioxide and Oxygen-Isotope Anomalies in the Mesosphere and Stratosphere, *Science*, *270*(5238), 969-972. doi:

Wanninkhof, R. (2014), Relationship between wind speed and gas exchange over the ocean revisited, *Limnol. Oceanogr. Meth.*, *12*, 351-362. doi: 10.4319/lom.2014.12.351

Wanninkhof, R., W. E. Asher, D. T. Ho, C. Sweeney, and W. R. McGillis (2009), Advances in quantifying air-sea gas exchange and environmental forcing, *Annu. Rev. Mar. Sci.*, *1*, 213-244. doi:

Yeung, L. Y., J. A. Hayles, H. Hu, J. L. Ash, and T. Sun (2018), Scale distortion from pressure baselines as a source of inaccuracy in triple-isotope measurements, *Rapid Communications in Mass Spectrometry*, *32*(20), 1811-1821. doi: 10.1002/rcm.8247

8. *In situ* Net Community Production with dissolved O_2/Ar

L.W. Juranek[1], R.H. Stanley[2], D.P. Nicholson[3]

[1]*College of Earth, Ocean, and Atmospheric Sciences, Oregon State University, Oregon USA*
[2]*Department of Chemistry, Wellesley College, Massachusetts, USA*
[3]*Marine Chemistry and Geochemistry Department, Woods Hole Oceanographic Institution, Massachusetts, USA*

8.1. Introduction:

This chapter describes methods pertaining to the use of the dissolved ratio of oxygen to argon (O_2/Ar) to constrain net biological oxygen production *in situ*. Net biological oxygen production can be used to evaluate ocean metabolic balance (i.e., autotrophy vs heterotrophy) and to calculate net community production (NCP) rates at the community level without the need for incubation and associated bottle containment effects. O_2/Ar observations can constrain NCP rates over timescales of days to weeks, and spatial scales of a few hundreds of meters to hundreds of kilometers, depending on how the data are collected and interpreted.

8.2. Method Background

8.2.1 Theoretical underpinnings

Net biological oxygen production, the quantity directly tracked by O_2/Ar observations, is stoichiometrically linked to the net community production of organic carbon and when averaged over appropriate space and time scales, equal to carbon export from the biological pump. The premise is based on the simple stoichiometric relationship between O_2 generation and organic carbon production in the photosynthesis/respiration equation (summarized in shorthand version as follows):

$$CO_2 + H_2O \leftrightarrow CH_2O + O_2 \quad (8.1)$$

The generation of dissolved O_2 is proportional to the organic carbon (CH_2O) produced by photosynthesis. Any subsequent respiration of organic carbon would also require consumption of O_2, hence the net biological O_2 production tracks organic carbon residing in the system and available for export. Importantly, net O_2 tracks the organic carbon export potential of both particulate and dissolved organic carbon phases, and thus in theory should be the sum of vertical sinking flux and physical subduction of dissolved organic carbon contained within water masses. Recent work has shown that the net community production of organic matter inferred from net biological oxygen correlates well to export production over spatial scales on order of tens of kilometers, although these terms can be decoupled at sub-mesoscales, (Estapa et al. 2015). To the extent that respiration of organic matter consumed by vertically migrating zooplankton is not co-located with the region of O_2 generation, (i.e., the surface mixed layer) the approach would also capture this mode of vertical transport. Most commonly, dissolved gas observations are used to constrain NCP in the surface mixed layer; however, with information on the time evolution of O_2/Ar at depth the approach can be extended throughout the photic zone (e.g., Quay et al., 2010).

Dissolved O_2 concentrations in the surface ocean are set primarily by solubility, which is a function of temperature and salinity (Garcia and Gordon, 1992), with warm and salty waters typically containing less O_2 than cold and less saline water masses. Absent any biological or

physical perturbation, surface ocean O_2 would be in equilibrium with the atmosphere for the given temperature and salinity (i.e., at its solubility value). However, both biotic and abiotic processes perturb O_2 concentrations slightly from equilibrium. Because these deviations are small relative to the absolute O_2 concentration range, an insightful metric is the deviation from expected equilibrium, i.e., the gas saturation:

$$\Delta O_2 = 100 \times \left(\frac{C_{meas}}{C_{equil}} - 1\right), \tag{8.2}$$

where C_{meas} and C_{equil} refer to the measured and equilibrium concentration of O_2, respectively, and a negative/positive value would imply less/more O_2 is present relative to that expected. The C_{equil} is calculated using the equations of Garcia and Gordon (1992). Deviations from solubility equilibrium are driven by both biological and non-biological sources: for example, an excess of photosynthesis over respiration would cause ΔO_2 to become positive (supersaturated), but a recent warming of the water mass (without sufficient time for the water to re-equilibrate at the new temperature) would result in a lower C_{equil}, and thus could also result in positive ΔO_2. Air injection by breaking/collapsing bubbles and gas rejection during sea ice formation also lead to a supersaturation of dissolved gases (Hamme and Emerson, 2006; Hamme et al., 2019; Stanley et al., 2009). Cooling, an excess of community respiration over photosynthesis, or significant contribution of ice melt (because gases are excluded from the ice matrix as it forms) can contribute to negative ΔO_2. Regardless of biological or physical origin, the surface ocean will always be restored toward a solubility equilibrium by air-sea gas exchange; the characteristic timescale associated with this process depends on a number of factors including the gas-transfer rate (*k*, usually parameterized as a function of wind-speed, Wanninkhof, 2014), the mixed layer depth, and the magnitude of the deviation of gas saturation from equilibrium. For most of the ocean, the timescale of re-equilibration is on the order of a few weeks.

The tracer gas argon (Ar) is employed because it has very similar solubility and diffusivity characteristics to O_2 but no known biological sources or sinks (Benson and Krause, 1984; Craig and Hayward, 1987; Hamme et al., 2019; Spitzer and Jenkins, 1989). Thus, Ar responds in the same way as O_2 to physical processes but not to biological ones. This allows a user to isolate the physical processes affecting gas saturations (e.g., recent warming or cooling) from those that are driven by net biological processes. The O_2 /Ar gas saturation is defined similarly to ΔO_2:

$$\Delta O_2/Ar = 100 \times \left(\frac{R_{meas}}{R_{equil}} - 1\right) \tag{8.3}$$

(where R_{meas} and R_{equil} refer to the measured and equilibrium O_2/Ar, respectively. To compute O_2/Ar solubility, O_2 solubility is calculated from given temperature and salinity using Garcia and Gordon (1992) as before, and Ar solubility is calculated using either Hamme and Emerson (2004) or Jenkins et al. (2019). As described by Kaiser et al., (2005), $\Delta O_2/Ar$ is equivalent to net biological oxygen saturation. A small, proportional error is induced when Ar concentrations deviate from equilibrium. To use $\Delta O_2/Ar$ to derive NCP rates, some further assumptions (described in section 8.4) must be made.

8.2.2 Historical Application and Method evolution

The O_2 /Ar approach has been applied widely throughout the global oceans. Some of the earliest work focused on time-series measurements in the subtropical Atlantic and Pacific Oceans to evaluate the biological contribution toward a subsurface oxygen saturation maximum that occurs seasonally in these regions (e.g., Craig and Hayward, 1987; Schulenberger and Reid, 1981; Spitzer and Jenkins, 1989). Over the last several decades a number of studies have used repeated, seasonally-resolved observations of O_2 /Ar in the surface ocean at time-series sites (HOT, BATS, Stn P, CalCOFI) to evaluate NCP (e.g., Emerson et al., 1991; Emerson et al., 1997; Luz and Barkan, 2009; Munro et al. 2013, Quay et al., 2010). Importantly, these annually-resolved data have indicated that the annual NCP (ANCP), i.e., NCP integrated over a full annual cycle, implies that oligotrophic oceans export 2-3 mol C m^{-2} $yr^{-}1$ from the surface ocean (Emerson, 2014); this stands in contrast to results of incubation-based approaches for constraining NCP (O_2 light/dark approach, see chapter xxxx) which have tended to imply the oligotrophic oceans are heterotrophic and require import of organic carbon (see Williams et al., 2013 for further discussion).

Another salient point that has emerged from constraint of ANCP with O_2 budgets at time-series sites is the recognition that in many open ocean systems, a fraction of the summer NCP is associated with shallow carbon export. Respiration of this shallow carbon export results in O_2 loss (and CO_2 accumulation) that is later mixed in to the surface layer via entrainment in fall or winter and re-equilibrated with the atmosphere (e.g., Emerson, 2014; Palevsky and Nicholson, 2018). From a carbon budgeting perspective, this temporary carbon export does not contribute to ocean biological pump uptake and storage; however, many field studies are not designed to sample in fall and winter months to capture this process. Therefore, it is important to be mindful of the timescales implied from observational data and to distinguish between shorter-term, seasonal and longer-term, annual storage implied from gas-based approaches.

The O_2 /Ar approach has also been used on ship transits to evaluate regional and basin-scale trends in NCP. Initial studies utilized discrete sampling from either the surface seawater pumped from a bow intake of a research or commercial cargo vessel (colloquially known as “surface underway”) or from traditional CTD casts spanning zonal or meridional gradients (e.g., Hendricks et al., 2004; Hendricks et al., 2005; Howard et al., 2010; Juranek et al., 2012; Reuer et al., 2007). However, in some cases biases were observed when sampling dissolved gases from the surface underway due to microbial growth in the plumbing of these systems (Juranek et al., 2010). Therefore, studies that utilize surface underway for dissolved gas sampling should make efforts to cross-calibrate with samples collected from CTD-based water samplers, if possible.

More recently, the use of sea-going mass spectrometers to measure O_2/Ar with higher spatial- or temporal resolution has become more commonplace (Kaiser et al., 2005; Cassar et al., 2009; Tortell and Long, 2009; Stanley et al., 2010). An advantage of these high-resolution studies is that it allows sufficient data quantity to compare with other easily obtainable sensor-based and discrete observations (temperature, salinity, fluorescence, Fv/Fm, particle size distributions, nutrients, community composition, optical properties) to help diagnose underlying physical and biological drivers (e.g., Eveleth et al., 2014; Hamme et al., 2012; Juranek et al., 2019; Stanley et al., 2010)

8.3. O_2/Ar data acquisition and quality control

8.3.1 Bottle-based sampling

A discrete sampling approach can be used to obtain O_2/Ar data. This discrete-sampling approach is the one most commonly used for obtaining depth profiles of O_2/Ar, which are useful in diagnosing potential mixing biases to surface values (as discussed in section 8.4), but can also be used for sampling in the surface ocean.

8.3.1.1 Preparation of high-vacuum gas sampling bottles

Most commonly, the sampling is achieved using a custom glass bottle with a volume of 200-600 mL, equipped with a Louwers-Hanique high vacuum stopcock. The sampling bottle specifications are identical to those for triple oxygen isotope sampling and in fact the same bottle sample can be used to obtain both measurements (see Chapter xxxx for further description and pictures). Bottles are prepared by dosing with 100 µL of saturated mercuric chloride and drying at 70°C (higher temperatures lead to volatilization of Hg). Bottles must be sealed with high vacuum grease (Apiezon or TorrLube) and evacuated to less than 1E-2 mtorr. When time and resources allow, "leak checks" of bottles should be performed one week post-evacuation to help identify any problems. Both the evacuation and leak check of bottles require access to a high vacuum line equipped with vacuum pumps, a pressure gauge, and leak-tight seals for attaching sampling bottles (e.g., Swagelok Ultratorr fittings).

8.3.1.2 Collecting a water sample using high-vacuum sampling bottles

The approach for obtaining a high-quality dissolved gas sample is similar to that described in the triple oxygen isotope sampling protocol (see chapter xxxx) and has also been described by Emerson et al. (1999). Primary concerns are to preserve the unique gas signature dissolved in seawater and to not contaminate a sample by atmospheric contact. This is achieved by creating and maintaining a water "lock" of several inches between the point where a sample is being admitted to the sample bottle and ambient air. To create and maintain the water lock, a thinner diameter tubing containing flow from the sample source (whether a Niskin bottle or underway seawater supply) is inserted into a larger diameter outer tubing attached to the side arm of the bottle. Care must be taken to completely dislodge and eliminate any bubbles in the tubing prior to sampling. After eliminating bubbles and throughly flushing tubing with sample water, the Louwers-Hanique valve is slowly opened to admit the sample, until the sample bottle is roughly half full. The Louwers-Hanique valve is then re-seated to close, and the space above the valve is flushed with de-ionized water for storage. The sidearm of the valve is then sealed with a flexible plastic cap. This step helps to ensure salt crystals do not form on the valve o-rings, forms a diffusion barrier which greatly reduces the inflow of atmospheric air while the sample is being transported and stored, and reduces the potential for leaks (Reuer et al., 2007).

8.3.1.3 Analysis of bottle samples

Upon return to a shoreside lab, the bottle sample is equilibrated with the headspace by gently shaking for several hours. The sample bottle is inverted and the sample water contained therein is gently pumped by vacuum suction until only approximately 1 mL of water remains in the neck, isolating the gases that remain in the bottle headspace. After closing the Louwers-Hanique valve the sidearm of the bottle is again flushed with DI water and capped for storage until analysis.

Samples are prepared for analysis by first passing through a cryogenic trap to remove water vapor, and are collected into a temporary holding vessel using a cryotrap or liquid helium (Emerson et al., 1999). Samples are then admitted into an isotope ratio mass spectrometer for analysis of O_2 /Ar gas ratio. The O_2 /Ar is determined by peak jumping and measurement of mass/charge (m/z) peaks for O_2 (32) and Ar (40). When a sample is also being analyzed for triple oxygen isotopes (see section xxxx) the measurement of O_2 /Ar is typically obtained at the end of the first block of ~25 measurements for oxygen isotopes. The measured O_2 /Ar value is corrected using O_2 /Ar from air standards (O_2 /Ar = 22.4261241970) as well as the value of an internal reference standard that is typically custom-mixed to have an O_2 /Ar similar to the value of most surface ocean samples (e.g., O_2 /Ar ≈20). As with the triple oxygen isotope analysis, equilibrated water samples are also used as an external check, since the solubility of O_2 and Ar for a given temperature are well known (e.g., equilibrium O_2 /Ar = 20.37 at 25°C). See the triple isotope method section xxx for further details on how the equilibrated water standards are made and sampled.

Similar to the case with $\delta^{17}O$, $\delta^{18}O$, and $^{17}\Delta$ analysis for the triple oxygen isotope method, the effect of differing sample and standard sizes and their impact on O_2 /Ar determination must be evaluated. To diagnose these effects, the same reference gas is admitted to both sample and standard sides with sample bellows expanded to varying capacities. This results in differing volumes of the same gas at the same pressure. Because natural samples will contain differing amounts of gas and the size effect can change in slope as an IRMS ionization source ages, the effect should be evaluated semi-frequently (i.e., once each month or for each sample "batch"). Figure 8.1 shows an example of the size effect for a reference gas analyzed against itself at different sample volumes on a ThermoFisher 253 mass spectrometer housed at Oregon State University.

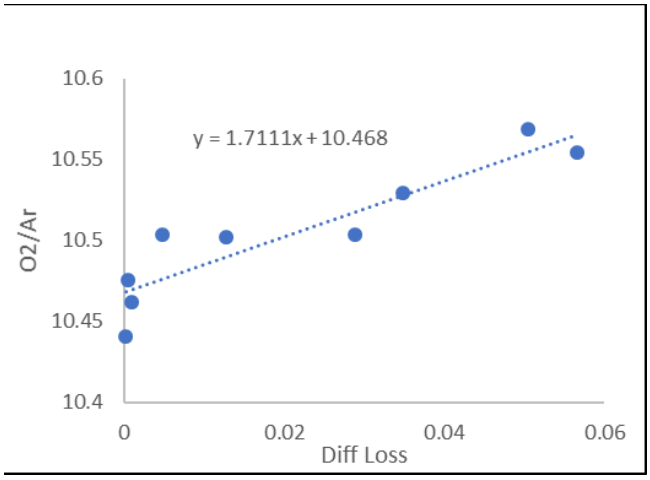

Figure 8.1. Illustration of the size effect on determination of raw 32/40 ratio measured by a Thermo-Fisher IRMS housed at Oregon State University. The "diff loss" is a measure of relative sample size, and is quantified as suggested by Stanley et al. (2010): Diff loss = "Sample size – reference size" or more specifically, $\frac{O_{2\,int\,smpl}-O_{2\,end\ smpl}}{O_{2\,int\,smpl}} - \frac{O_{2\,int\,ref}-O_{2\,end\,ref}}{O_{2\,int\,ref}}$ where $O_{2\ int\ smpl}$ is the integrated ^{32}O in millivolts reported by the IRMS for the sample side bellows, $O_{2\ end\ smpl}$ is the jump to mass 32 measured in millivolts at the end of the block for the sample side bellows, $O_{2\ int\ ref}$ is the integrated ^{32}O in millivolts reported by the IRMS for the reference side bellows, and $O_{2\ end\ ref}$ is the jump to mass 32 in millivolts measured at the end of the block for the reference side bellows. The O_2 /Ar correction is larger for small volume samples.

8.3.1.4 Alternative sampling approaches

Some alternative approaches have also been used to collect discrete samples for O_2 /Ar. These typically include admission of a small volume sample to a glass vial that is either crimp-sealed or otherwise closed in an air-tight fashion without headspace. Plastic containers are gas-permeable and should not be used for dissolved gas sampling. These approaches tend to be more suitable for temporary storage of samples that will be analyzed within a few days of collection, but longer-term storage using these approaches has also been reported (Charoenpong et al., 2014; Ferrón et al., 2015). Similar principles of reducing the possibility of atmospheric contamination with through flushing of the sample vessel and dislodging of bubbles are followed when these sampling approaches are used.

8.3.2 Continuous sampling

In the last several decades, methods to determine O_2 /Ar in a continuous or quasi-continuous mode at sea have become more widely used (Cassar et al., 2009; Kaiser et al., 2005; Tortell, 2005). This allows robust estimates of O_2 /Ar and NCP every few minutes, equivalent to ~1km- scale sampling while a vessel is transiting at normal speed. These methods, known as membrane inlet mass spectrometry (MIMS) or equilibrated inlet mass spectrometry (EIMS) share many core respects, but have important differences that imbue distinct advantages/disadvantages in certain settings. Both approaches use quadrupole mass spectrometers (QMS) as analyzers; these QMS are relatively compact, cost effective (~$30-50K USD), suitable in precision, and have stable performance while at sea. Because QMS analyzers measure samples in a gas phase, dissolved gases must be extracted from seawater prior to analysis, and this critical step is where MIMS and EIMS approaches diverge. In a MIMS, a gas-permeable membrane held at constant temperature allows gases to diffuse into a vacuum chamber attached to the QMS. In an EIMS, a high surface-area contactor membrane allows gases to equilibrate in a head space which is subsampled by a capillary connected to the QMS. For comprehensive details on either approach we direct the reader to the method references given above. However, we will comment briefly on distinct advantages and disadvantages of both approaches for potential users to consider. The equilibration approach used in an EIMS cause these systems to have an inherently slower time-response to a change in O_2/Ar than a MIMS will. Cassar et al. (2009) calculated a 7-minute response time for their system based on theoretical principles, and this is broadly consistent with response lags calculated in the field (e.g., Juranek et al., 2020), although the response time can be reduced to 2-3 minutes if counter air flow is added to the equilibrator cartridge (Manning et al. 2016). This dynamic response lag is typically not a hindrance to use in continuous flow-through applications given normal ship transit speeds and spatial scales over which biogeochemical gradients are observed. A disadvantage to use of a MIMS is that gas separation is sharply affected by temperature of the sample, and therefore a water-bath is required to maintain stable temperature control. MIMS are more flexible in terms of easily adapting to measure a diverse array of gas analytes (including N_2O, dimethylsulfide, and CO_2) whereas EIMS tend to be configured specifically for O_2 /Ar.

The ease of calibration of QMS data also varies between methods – EIMS data can be adjusted in near-real time using periodic admission of uncontaminated air (e.g., from an atmospheric air-intake line) to the QMS using a switching valve controlled by software. MIMS data are typically manually calibrated using a suite of equilibrated water standards.

8.3.3 Additional observations required for calculation of NCP

In addition to the O_2/Ar value obtained from bottle samples, EIMS, or MIMS data, some additional fields are necessary to interpret observations and to compute NCP rates. The most critical observations are *in situ* temperature and salinity of the water sample at the time of collection. Absolute O_2 concentration is also useful for diagnosing differences between biologically-driven and physically-driven gas saturations – i.e., the total gas saturation (ΔO_2) is the sum of net biological ($\Delta O_2/Ar$) and physical gas saturation (determined by difference). However, in order for O_2 concentration data to be useful toward this purpose, they must be well-calibrated -- O_2 sensor data need to be calibrated via comparison to Winkler bottle data frequently as accuracy biases on the order of a few % arising from drift or storage are common.

Wind speed measurements are also necessary to constrain the air-sea gas transfer rate (k), a necessary term in calculation of NCP, as described in section 8.4. The relevant timescale for these observations is the month or two preceding the time of sampling, since dissolved gas concentrations will reflect a weighted average over several previous residence times in the mixed layer (Reuer et al., 2007; Teeter et al., 2018). Therefore, ship-based instantaneous wind-speed observations are not appropriate for estimating gas transfer for purposes of calculating NCP. Reanalysis fields (i.e., NCEP, NARR, ERA) or nearby buoy winds are appropriate choices. A number of parameterizations that relate wind speed to air-sea gas transfer exist (as recently reviewed by Wanninkhof, 2014). A procedure for computing weighted k for O_2 mass balance studies based on wind-speed history is described by Reuer et al. (2007) with an update by Teeter et al. (2018). As bubble-mediated exchange processes are assumed to have similar impact for O_2 and Ar, exchange parameterizations that explicitly include bubble dynamics are often not used for calculating NCP.

8.4. Calculation of O_2 /Ar saturation and NCP

The approach for calculating NCP rates from O_2 /Ar observations should consider the physical setting as well as the spatial and temporal resolution of O_2/Ar data. For example, studies that resolve the diel pattern in O_2 /Ar in a given location can use this information to evaluate the net daily O_2 inventory change and estimate community respiration rates from nighttime O_2 /Ar change (e.g., Hamme et al., 2012; Ferrón et al. 2015). Lacking this temporal resolution, single-point measurements in a given location (as in sampling during transit) are often interpreted in a steady-state framework where net biological production is balanced by air-sea gas transfer of O_2, which allows NCP to be calculated as follows:

$$NCP = kC_{equil}(\Delta O_2/Ar)/100 \quad (8.4)$$

This approach assumes the first order terms determining surface O_2 inventory are production and gas exchange, which, for open ocean regions is often, but not always, appropriate. Though autonomous and high-resolution observations have revealed that the ocean is often not in steady-state, modeling and observational work suggests that even under these circumstances $\Delta O_2/Ar$ tracks a weighted average NCP over the several week equilibration timescale of O_2 (Ferron et al., 2015; Teeter et al., 2018). However, when processes other than gas exchange and biological production influence surface O_2 balance, a steady-state mass balance may not be appropriate (c.f., Manning et al., 2017). For example, during seasonal periods of substantial vertical mixing or

entrainment of subsurface waters into the mixed layer it will be necessary to resolve depth gradients in O_2 /Ar and to model these physical mixing terms (Cassar et al., 2014; Haskell and Felming, 2018; Hamme and Emerson, 2006; Izett et al., 2018; Manning et al., 2017; Munro et al., 2013; Quay et al., 2010). The appropriate way to model these terms will depend on the unique environment, and we direct the reader to the references cited above which contain examples of modified approaches in both dynamic coastal and open ocean settings.

When calculating NCP from O_2 /Ar observations, it is important to keep in mind that in all cases the physical/hydrographic setting should dictate the approach for calculating NCP, and not the resolution of available data. In other words, just because one *can* calculate NCP, doesn't mean one *should*. In cases where significant physical transports influence the O_2 budget, and these effects are not quantified, NCP should either not be reported, or NCP rates should be reported with clear statements regarding the higher uncertainty of estimates and the way they are likely to be influenced by known physical biases.

8.5. Reporting O_2 /Ar and NCP data

O_2 /Ar data should be reported as either a calibrated measured ratio or $\Delta O_2/Ar$ along with time (UTC), location (Latitude, Longitude), *in situ* temperature and salinity, and if measured, dissolved O_2 concentration. Metadata should include a description on method for data acquisition and data quality control for O_2 /Ar and O_2 concentration data (if reported). NCP rates should be reported with the weighted gas transfer coefficient k and a description of how this rate was determined. If terms for vertical mixing or advection are employed in the calculation of NCP, these values should also be reported with the data. It is also helpful to report mixed layer depth and local time offset for UTC (e.g., to evaluate potential day/night effects).

Other variables that may be helpful in interpretation of O_2 /Ar and NCP data and that should be reported if possible include: fluorescence, backscatter, nutrient concentrations, HPLC pigment data and gross O_2 production from triple oxygen isotopes.

8.5.1 Estimating and reporting uncertainties

It is best practice to report an estimate of uncertainty alongside NCP rate information. This uncertainty should include relative uncertainty in O_2 /Ar, the uncertainty in the gas transfer coefficient k (typically taken as ±10% to ±15%), as well as best estimate of uncertainty in any other modeled terms. Generally speaking, this error will increase as signal to noise ratio decreases (as O_2 /Ar observations get closer to equilibrium). The uncertainty can be calculated using standard error propagation techniques, or, in the case of more complex expressions involving physical O_2 flux, can be calculated using a Monte Carlo analysis. The latter approach involves calculating NCP many times with input fields varied in Gaussian random distribution with standard deviation equivalent to uncertainty estimates. The standard deviation of resulting NCP is then taken as a robust estimate of total uncertainty.

8.6. References:

Benson, B.B. and Krause, D. (1984), The concentration and isotopic fractionation of oxygen dissolved in freshwater and seawater in equilibrium with the atmosphere, *Limnol. Oceanogr.*, *29*(3), 620-632.

Cassar, N., Barnett, B. A., Bender, M. L., Kaiser, J., Hamme, R. C., & Tilbrook, B. (2009). Continuous high-frequency dissolved O_2/Ar measurements by equilibrator inlet mass spectrometry. *Analytical Chemistry*, 81(5), 1855–1864. https://doi.org/10.1021/ac802300u

Cassar, N., C. D. Nevison, and M. Manizza (2014), Correcting oceanic O2/Ar-net community production estimates for vertical mixing using N2 O observations,
doi:10.1002/2014GL062040.

Cassar, N., C. D. Nevison, and M. Manizza (2014), Correcting oceanic O2/Ar-net community production estimates for vertical mixing using N2O observations, Geophys. Res. Lett., 41, 8961–8970, doi:10.1002/2014GL062040.

Charoenpong, C. N., Bristow, L. A., & Altabet, M. A. (2014). A continuous flow isotope ratio mass spectrometry method for high precision determination of dissolved gas ratios and isotopic composition: Gas and isotope ratio analysis by CF-IRMS. *Limnology and Oceanography: Methods*, *12*(5), 323–337. https://doi.org/10.4319/lom.2014.12.323

Craig, H., and Hayward, T.L. (1987), Oxygen supersaturation in the ocean: biological vs. physical contributions, *Science*, *235*, 199-202, https://doi.org/10.1126/science.235.4785.199

Emerson, S. (2014). Annual net community production and the biological carbon flux in the ocean. *Global Biogeochemical Cycles*, *28*(1), 14–28. https://doi.org/10.1002/2013GB004680.

Emerson, S., P. Quay, C. Stump, D. Wilbur, and M. Knox (1991), O_2, Ar, N_2, and ^{222}Rn in surface waters of the subarctic ocean: Net biological O_2 production, *Global Biogeochem. Cycles*, *5*, 49-69.

Emerson, S., P. Quay, D. Karl, C. Winn, L. Tupas, and M. Landry (1997), Experimental determination of the organic carbon flux from open-ocean surface waters, *Nature*, *389*, 951-954.

Emerson, S., C. Stump, D. Wilbur, and P. Quay (1999), Accurate measurement of O2, N2, and Ar gases in water and the solubility of N2, *Mar. Chem.*, *64*, 337-347.

Estapa, M. L., D. A. Siegel, K. O. Buesseler, R. H. R. Stanley, M. W. Lomas, and N. B. Nelson (2015), Decoupling of net community and export production on submesoscales in the Sargasso Sea, Global Biogeochem. Cycles, 29, 1266–1282, doi:10.1002/2014GB004913.

Eveleth, R., Timmermans, M.-L., & Cassar, N. (2014). Physical and biological controls on oxygen saturation variability in the upper Arctic Ocean. *Journal of Geophysical Research: Oceans*, 119, 7420–7432. https://doi.org/10.1002/2014JC009816.

Ferrón, S., S. T. Wilson, S. Martínez-García, P. D. Quay, and D. M. Karl (2015), Metabolic balance in the mixed layer of the oligotrophic North Pacific Ocean from diel changes in O2/Ar saturation ratios, Geophys. Res. Lett., 42, 3421–3430, doi:10.1002/2015GL063555.

Garcia, H.E., and L.I. Gordon (1992), Oxygen solubility in seawater: better fitting equations, *Limnol. Oceanogr.*, *37*, 1307-1312, https://doi.org/10.4319/lo.1992.37.6.1307.

Hamme, R. C., Cassar, N., Lance, V. P., Vaillancourt, R. D., Bender, M. L., Strutton, P. G., et al. (2012). Dissolved O2/Ar and other methods reveal rapid changes in productivity during a Lagrangian experiment in the Southern Ocean. *Journal of Geophysical Research*, 117, C00F12. https://doi.org/10.1029/2011JC007046

Hamme, R., and S.E. Emerson (2004), The solubility of neon, nitrogen and argon in distilled water and seawater, *Deep Sea Res., Part I*, *51*, 1517-1528.

Hamme, R., and S.E. Emerson (2006), Constraining bubble dynamics and mixing with dissolved gases: Implications for productivity measurements by oxygen mass balance, *J. Mar. Res.*, *64*(1), p. 73-95.

Hamme, R. C., Nicholson, D. P., Jenkins, W. J., & Emerson, S. R. (2019). Using Noble Gases to Assess the Ocean's Carbon Pumps. *Annual Review of Marine Science*, *11*(1), 75–103. https://doi.org/10.1146/annurev-marine-121916-063604

Haskell, W.Z., J. C. Fleming, (2018), Concurrent estimates of carbon export reveal physical biases in ΔO 2 /Ar-based net community production estimates in the Southern California Bight, Journal of Marine Systems, 10.1016/j.jmarsys.2018.03.008, **183**, (23-31).

Hendricks, M.B., M.L. Bender, and B.A. Barnett (2004). Net and gross O2 production in the southern ocean from measurements of biological O2 saturation and its triple isotope composition. *Deep Sea Res., Part I*, *51*, 1541-1561.

Hendricks, M.B., M.L. Bender, B.A. Barnett, P. Strutton, and F.P. Chavez (2005), Triple oxygen isotope composition of dissolved O2 in the equatorial Pacific: A tracer of mixing, production, and respiration, *J. Geophys. Res.*, *100*, C12021, doi:10.1029/2004JC002735.

Howard, E., S. Emerson, S. Bushinsky, and C. Stump (2010), The role of net community production in air-sea carbon fluxes at the North Pacific subarctic-subtropical boundary region, Limnol. Oceanogr., 55(6), 2585–2596, doi:10.4319/lo.2010.55.6.2585.

Izett, R. W., Manning, C. C., Hamme, R. C., & Tortell, P. D. (2018). Refined Estimates of Net Community Production in the Subarctic Northeast Pacific Derived From ΔO $_2$ /Ar Measurements With N $_2$ O-Based Corrections for Vertical Mixing. *Global Biogeochemical Cycles*, *32*(3), 326–350. https://doi.org/10.1002/2017GB005792

Jenkins, W.J., and J.C. Goldman (1985), Seasonal oxygen cycling and primary production in the Sargasso Sea, *J. Mar. Res.*, *43*, 465-491.

Jenkins, W. J., Lott, D. E., & Cahill, K. L. (2019). A determination of atmospheric helium, neon, argon, krypton, and xenon solubility concentrations in water and seawater. *Marine Chemistry*, *211*, 94–107. https://doi.org/10.1016/j.marchem.2019.03.007.

Juranek, L. W., Hamme, R. C., Kaiser, J., Wanninkhof, R., and Quay, P. D. (2010), Evidence of O_2 consumption in underway seawater lines: Implications for air-sea O_2 and CO_2 fluxes, *Geophys. Res. Lett.*, 37, L01601, doi:10.1029/2009GL040423.

Juranek, L. W., Quay, P. D., Feely, R. A., Lockwood, D., Karl, D. M., & Church, M. J. (2012). Biological production in the NE Pacific and its influence on air-sea CO2 flux: Evidence

from dissolved oxygen isotopes and O2/Ar. *Journal of Geophysical Research*, 117, C05022. https://doi.org/10.1029/2011JC007450

Kaiser, J., M.K. Reuer, B. Barnett, and M.L. Bender (2005), Marine productivity estimates from continuous O2/Ar ratio measurements by membrane inlet mass spectrometry, *Geophys. Res. Lett.*, *32*, L19605, doi:10.1029/2005GL023459.

Luz B, Barkan E (2009) Net and gross oxygen production from O_2/Ar, $^{17}O/^{16}O$ and $^{18}O/^{16}O$ ratios. Aquat Microb Ecol 56:133-145. https://doi.org/10.3354/ame01296.

Manning, C., R. H. R. Stanley, and D. E. Lott III (2016), Continuous Measurements of Dissolved Ne, Ar, Kr, and Xe Ratios with a Field-deployable Gas Equilibration Mass Spectrometer, *Analytical Chemistry*, *88*, 3040-3048. doi: doi: 10.1021/acs.analchem.5b03102.

Manning, C. C., R. H. R. Stanley, D. P. Nicholson, J. M. Smith, J. T. Pennington, M. R. Fewings, M. E. Squibb, and F. P. Chavez (2017), Impact of recently upwelled water on productvity investigated using *in situ* and incubation-based methods in Monterey Bay, *J. Geophys. Res.-Oceans*, *122*, 1901-1926. doi: 10.1002/2016JC012306.

Munro, D.R., Quay, P.D., Juranek, L.W., Goericke, R., (2013), Biological production rates off the Southern California coast estimated from triple O_2 isotopes and O_2 : Ar gas ratios, *Limnology and Oceanography*, 58, doi: 10.4319/lo.2013.58.4.1312.

Palevsky, H.I., and D.P. Nicholson. 2018. The North Atlantic biological pump: Insights from the Ocean Observatories Initiative Irminger Sea Array. Oceanography 31(1):42–49, https://doi.org/10.5670/oceanog.2018.108.

Quay, P. D., Peacock, C., Björkman, K., & Karl, D. M. (2010). Measuring primary production rates in the ocean: Enigmatic results between incubation and non-incubation methods at Station ALOHA. *Global Biogeochemical Cycles*, 24, GB3014. https://doi.org/10.1029/2009GB003665

Reuer, M.K., B.A. Barnett, M.L. Bender, P.G. Falkowski, and M.B. Hendricks (2007), New estimates of Southern Ocean biological production rates from O2/Ar ratios and the triple isotope composition of O2, *Deep-Sea Res., Part I*, *54*, 951-974.

Schulenberger, E., and J.L. Reid (1981), The Pacific shallow oxygen maximum, deep chlorophyll maximum, and primary productivity, reconsidered, *Deep Sea Res.*, *28A*(9), 901-919.

Spitzer, W.S., and W.J. Jenkins (1989), Rates of vertical mixing, gas exchange, and new production: Estimates from seasonal gas cycles in the upper ocean near Bermuda, *J. Mar. Res.*, *47*, 169-196.

Stanley, R. H. R., Jenkins, W. J., Lott, D. E., & Doney, S. C. (2009). Noble gas constraints on air-sea gas exchange and bubble fluxes. *Journal of Geophysical Research*, 114, C11020. https://doi.org/10.1029/2009JC005396.

Stanley, R.H.R., Kirkpatrick, J.B., Cassar, N., Barnett, B.A., Bender, M.L., 2010. Net community production and gross primary production rates in the western equatorial Pacific. Glob. Biogeochem. Cycles 24 . http://dxdoi.org/10.1029/ 2009gb003651.

Teeter, L., Hamme, R. C., Ianson, D., & Bianucci, L. (2018). Accurate estimation of net community production from O2/Ar measurements. *Global Biogeochemical Cycles*, 32, 1163–1181. https://doi.org/10.1029/2017GB005874.

Tortell, P. D. (2005a), Dissolved gas measurements in oceanic waters made
24 – 37

Tortell, P. D. (2005), Dissolved gas measurements in oceanic waters made by membrane inlet mass spectrometry, Limnol. Oceanogr. Methods, 3, 24– 37.

Tortell, P.D., Long, M.C., 2009. Spatial and temporal variability of biogenic gases during the Southern Ocean spring bloom. Geophys. Res. Lett., 36. http://dx.doi. org/10.1029/2008gl035819.

Wanninkhof, R. (2014). Relationship between wind speed and gas exchange over the ocean revisited: Gas exchange and wind speed over the ocean. *Limnology and Oceanography: Methods*, 12(6), 351–362. https://doi.org/10.4319/lom.2014.12.351.

Williams, P. J. le B., Quay, P. D., Westberry, T. K., & Behrenfeld, M. J. (2013). The Oligotrophic Ocean Is Autotrophic. *Annual Review of Marine Science*, *5*(1), 535–549. https://doi.org/10.1146/annurev-marine-121211-172335

9. The use of variable fluorescence for assessment of phytoplankton photophysiology and rates of primary production

Maxim Y. Gorbunov[1], Helga do Rosario Gomes[2]; Joaquim Goes[2], Greg Silsbe[3], Zachary K. Erickson[4]

[1]*Department of Marine and Coastal Sciences, Rutgers University, New Jersey, USA*
[2]*Lamont Doherty Earth Observatory at Columbia University, New York, USA*
[3]*University of Maryland Center for Environmental Science, Maryland, USA*
[4]*Universities Space Research Association, Maryland, USA*

9.1. Introduction

Over the past decade, variable chlorophyll a fluorescence techniques have increasingly been used to estimate biomass and physiological status of phytoplankton and benthic organisms in marine ecosystems. Assessment of the photosynthetic efficiency in organisms relies on the measurement and analysis of chlorophyll-a "variable fluorescence", a property unique to the photosynthetic machinery (Falkowski et al, 2004 for review). Variable fluorescence signals are recorded using Fast Repetition Rate (FRR) Fluorometry (Kolber et al., 1998; Gorbunov et al., 2000) or its technological successor, Fluorescence Induction and Relaxation (FIRe) technique (Gorbunov and Falkowski, 2005; Gorbunov et al., 2020). These optical measurements are sensitive, fast, non-destructive, and can be done in real time and *in situ*.

Variable chlorophyll fluorescence is the most sensitive, non-destructive signal detectable in the upper ocean that reflects instantaneous phytoplankton photophysiology (Falkowski and Kolber, 1995; Kolber et al., 1998). This technique relies on the relationship between chlorophyll fluorescence and the efficiency of photosynthetic processes, and it provides a comprehensive suite of photophysiological characteristics of energy transfer in light-harvesting complexes, photochemical reactions in PSII reaction centers, and photosynthetic electron transport down to carbon fixation (Kolber et al., 1998; Falkowski et al., 2004). These characteristic provide quantitative information about photosynthetic rate and the effects of environmental factors, such as nutrient stress and photoacclimation.

9.2. The use of variable florescence to infer phytoplankton photophysiology - Methodology and Terminology.

At room temperature, chlorophyll *a* fluorescence mainly arises from Photosystem II (PSII). When the PSII reaction centers are in the open state (with Q_a oxidized), the fluorescence yield is minimal, F_o. When the Q_a is reduced (e.g, by exposure to strong light), the reaction centers are closed and the fluorescence yield increases to its maximum level, F_m. To retrieve F_o and F_m, the FIRe technique records, with microsecond resolution, the induction of fluorescence yields induced by a strong saturating flash of light (~ 100 μs long, called a Single Turnover Flash, STF) (Phase 1 in Figure 9.1). The rate of fluorescence induction is proportional to the functional absorption cross section of PSII, σ_{PSII}, whereas the relative magnitude of fluorescence rise, F_v/F_m, is defined by the

quantum efficiency of photochemistry in PSII. The shape of fluorescence induction is controlled by the excitonic energy transfer between individual photosynthetic units and is defined by a "connectivity factor", *p* (Kolber et al. 1998). Thereby, the fluorescence induction is exponential in the absence of energy transfer ($p = 0$) and becomes sigmoidal when *p* increases to the maximum values of ~ 0.5 to 0.7 (Kolber et al. 1998).

The induction of fluorescence yield during a saturating single-turnover flash (Phase 1 in Figure 9.1) is driven by accumulation of closed reaction centers C(t) over time and the resulting increase in fluorescence yield F(t) from its minimum (F_o) to maximum (F_m) values. The rate of increase in C(t) and dynamics of fluorescence yield under a saturating STF flash can be described as follows (adapted from Kolber et al., 1998):

$$dC(t)/dt = \sigma_{PSII} I (1-C(t)) / (1-pC(t)) \quad (9.1)$$

$$F(t) = F_o + F_v C(t) (1-C(t)) / (1-pC(t)) \quad (9.2)$$

Here $F_v = F_m - F_o$ is the variable fluorescence yield. These equations assume that the rate of photochemistry in PSII induced by the saturating single turnover flash is much faster than the rate of Q_a^- reoxidation and the latter can be ignored. In the general case (e.g., when the rate of fluorescence induction is comparable to the rate of Q_a^- reoxidation), the Q_a^- reoxidation kinetics can be taken into account, at the expense of more complex mathematical formalism (Kolber et al., 1998; Gorbunov and Falkowski 2020). The kinetics of electron transport on the acceptor side of PSII (i.e., Q_a re-oxidation) is assessed from analysis of the fluorescence relaxation kinetics after the STF (Phase 2 in Fig. 9.1). The fluorescence kinetics consists of several components, because the rate of Q_a re-oxidation depends on the state of the second quinone acceptor, Q_b, which is a mobile two-electron acceptor (Crofts and Wraight, 1983):

$$Q_a^- Q_b \rightarrow Q_a Q_b^- \ (150 - 200\ \mu s) \quad (9.3)$$

$$Q_a^- Q_b^- \rightarrow Q_a Q_b^= \ (600 - 800\ \mu s) \quad (9.4)$$

$$Q_a^- \_ \rightarrow Q_a^- Q_b \rightarrow Q_a Q_b^- \ (\sim 2000\ ms) \quad (9.5)$$

The reaction (eq. 9.5) corresponds to the conditions when the Q_b is initially out of its binding site on the D1 protein. Also, a fraction of inactive reaction centers with damaged electron transport may contribute to the slowest component in the relaxation kinetics. Description of the Q_a^- relaxation kinetics, with sufficient accuracy, in natural phytoplankton populations requires the use of 3-component model (Gorbunov and Falkowski 2020). Thereby, the average time constant (τ_{Qa}) for the two fastest components (τ_1 and τ_2) reflects the rate of Q_a re-oxidation in active reaction centers (Gorbunov and Falkowski 2020):

$$\tau_{Qa} = (\alpha_1\tau_1 + \alpha_2\tau_2) / (\alpha_1 + \alpha_2) \quad (9.6)$$

The use of three-component kinetic analysis is critical. Two components are not sufficient to describe the complexity of the experimental kinetics (Gorbunov and Falkowski 2020). On the other hand, an increase in the number of components (e.g., up to four) would require much better

signal-to-noise ratio in the measured signals, which is difficult or hardly possible in natural phytoplankton communities, especially in the open ocean.

Analysis of the relaxation kinetics under ambient irradiance offers a way for kinetic-based measurements of photosynthetic electron transport rates (ETR; see below) and such kinetic measurements improve dramatically the accuracy of ETR measurements and fluorescence-based estimates of primary production, as compared to classic amplitude-based ETR measurements. The time constant $\tau_{PSII\text{-}PSI}$ for the electron transport between PSII and PSI can be estimated from analysis of the fluorescence relaxation kinetics following the Multiple Turnover Flash (MTF, Phase 3 and 4 in Figure 9.1). Under most physiological conditions, this time constant is determined by the rate of plastoquinone (PQ) pool re-oxidation and is an order of magnitude slower compared to τ_{Qa}.

Measurement of FIRe fluorescence parameters over a range of ambient irradiances (Figure 9.2) permits one to reconstruct the rates of photosynthetic electron transport, ETR, as a function of irradiance (called light curves or photosynthesis-versus-irradiance curves) (Kolber and Falkowski, 1993). ETR is proportional to the product of irradiance and the quantum yield of photochemistry measured under ambient light ($\Delta F'/F_m'$) (section 9.4.0 below). Analysis of these photosynthesis-versus-irradiance curves provides the maximum rate of photosynthetic electron transport (P_{max}) and the light-saturating parameter (E_k).

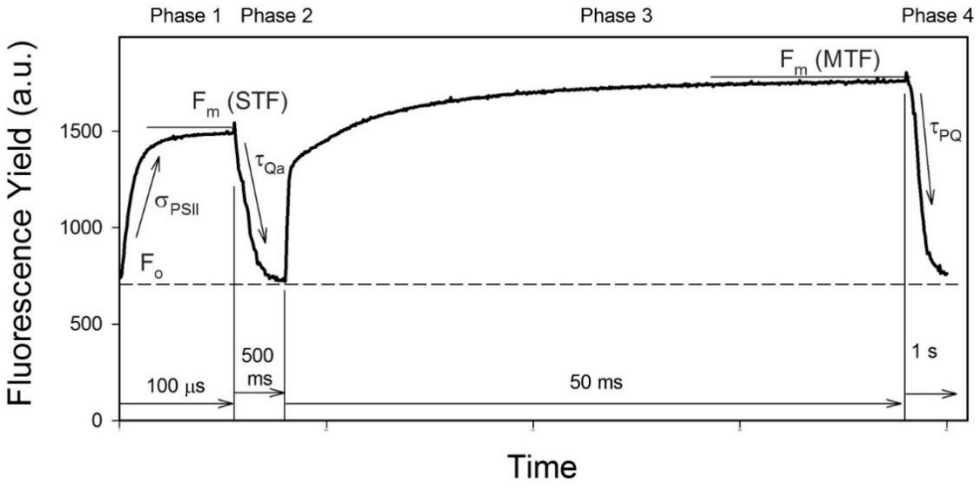

Figure 9.1. An example of the FIRe/FRR fluorescence transient. Kinetics of fluorescence yields is recorded with microsecond time resolution and includes four phases: (Phase 1, 100 µs long) a strong short flash, called a Single Turnover Flash (STF), is applied to cumulatively saturate PSII and to measure the fluorescence induction from F_o to F_m; (Phase 2, 500 ms) weak modulated light is used to measure the relaxation kinetics of fluorescence yield on micro- and millisecond time scales; (Phase 3, 50-100 ms) a strong long pulse of ca. 50-100 ms duration, called a Multiple Turnover Flash (MTF), is applied to saturate PSII and the plastoquinone pool; (Phase 4) weak modulated light is applied to measure the kinetics of the electron transport between Photosystem II and Photosystem I, i.e., the plastoquinone pool re-oxidation. The time axis is non-linear, as sampling frequency changes between phases to reflect the changing temporal resolution required to understand the dynamics of each process.

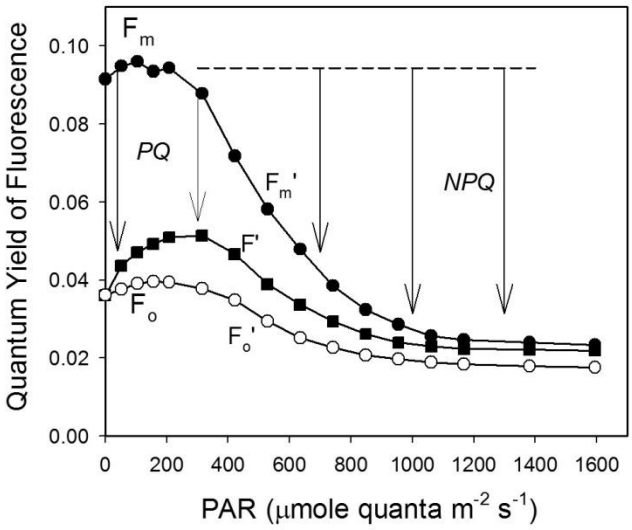

Figure 9.2. The irradiance dependence of the quantum yields of chlorophyll fluorescence in a marine diatom, retrieved from lifetime measurements (Gorbunov, unpublished). F_o and F_m are the minimum (open reaction centers) and maximum (closed centers) yields measured in dark-adapted cells. F_o' and F_m' are the minimum (fully open centers) and maximum (closed centers) fluorescence yields measured in a light adapted state. F' is the actual quantum yield measured under ambient light that corresponds to the yield of SIF recorded remotely from a satellite platform. PQ and NPQ are photochemical quenching and non-photochemical quenching, respectively. The magnitude of non-photochemical quenching is calculated from the light-induced decrease in the maximum fluorescence yield and is characterized by the "NPQ parameter" NPQ = (Fm - Fm')/ Fm' (Bilger and Björkman 1990). Measurements of variable fluorescence as a function of irradiance is the first step in reconstruction of the irradiance dependence of photosynthetic electron transport rates (ETRs) and the fluorescence-based rates of primary production.

9.3. Rationale for using variable fluorescence to derive instantaneous rates of primary production.

Photosynthesis starts with absorption of sunlight by photosynthetic pigments, followed by migration of the absorbed light energy from light-harvesting pigment-protein complexes to photosynthetic reaction centers, where photochemical charge separation occurs. This photochemical process leads to short-term storage of absorbed light energy within the reaction centers. The electrons produced as a result of charge separation then move down the electron transport chain and the energy of absorbed solar light is ultimately used to fix CO2 in the Calvin cycle (Falkowski and Raven, 2007).

Variable fluorescence techniques (such as FRR or FIRe) provide a fast and sensitive tool to quantify the light-driven electron flux with Photosystem II (PSII), commonly called photosynthetic electron transport rates (ETR). ETR is a function of irradiance and is calculated from measurements of variable fluorescence over a range of PAR levels (Figure 9.2). Several models and modifications have been developed to model ETR rates from variable fluorescence (e.g., Kolber and Falkowski 1993; Oxborough et al. 2012; Hughes et al. 2018a; Gorbunov and Falkowski 2020). There are two main approaches to model ETR rates – amplitude-based and kinetic (Gorbunov and Falkowski, 2020; below 9.4.1 and 9.4.2).

Table 9.1

Notations and Terminology	
PSII	Photosystem II
ETR	Electron Transport Rate(s)
ETR_{Fv}	ETR retrieved from amplitude-based Fv measurements
ETR_{τ}	ETR retrieved from kinetic fluorescence analysis
σ_{PSII}^{opt}	Optical absorption cross section of PSII ($Å^2$)
σ_{PSII}	Functional absorption cross section of PSII ($Å^2$) in a dark-adapted state
σ_{PSII}'	Functional absorption cross section of PSII in a light-adapted state (the prime character indicates the measurements are made under ambient light)
F_o, F_m	Minimum and maximum yields of chlorophyll-a fluorescence measured in a dark-adapted state (arbitrary units)
F_v	Variable fluorescence (= F_m - F_o)
F_v/F_m	Maximum quantum yield of photochemistry in PSII, measured in a dark-adapted state (dimensionless)
p	"Connectivity factor", defining the probability of the exciton energy transfer between individual photosynthetic units (dimensionless)
F_o', F', F_m'	Minimum, steady-state, and maximum yields of chlorophyll-a fluorescence measured under ambient light (arbitrary units). F_o' can be measured after a brief (~ 1s) period of darkness to promote opening of all reaction centers
$\Delta F'$	Change in the fluorescence yield measured under ambient light (= F_m' - F')
F_v'	Maximum variable fluorescence measured under ambient light (= F_m' - F_o'). Here F_o' and F_m' corresponds to fully open and closed reaction centers, respectively.
$\Delta F'/ F_v'$	Coefficient of photochemical quenching (= q_p), which is a fraction of open reaction centers in a light-adapted state.
$\Delta F'/F_m'$	Quantum yield of photochemistry in PSII, measured under ambient light (Φ_{PSII} =(F_m'-F')/F_m') (dimensionless)
F_v'/F_m'	Quantum efficiency of photochemistry in open reaction centers of PSII, measured in a light-adapted state (=(F_m'-F_o')/F_m') (dimensionless)
n_{PSII}	The ratio of PSII to the number of Chl-a molecules in the cell (this ratio is called the size of PSII unit)
1/k	The quantum yield of O_2 evolution (i.e., the ratio of O_2 evolved to the number of electrons produced in PSII). 1/k can be assumed to be equal 0.25 (i.e., 4 e- is need to evolve one O_2)
PQ	Photosynthetic quotient, which is the ratio of O_2/CO_2 evolved/fixed in the process of photosynthesis
$\phi_{e,C}$	Electron requirement for carbon fixation (the number of electrons required to fix one CO_2). $\phi_{e,C}$ = (1/k PQ)$^{-1}$
Φ_{NPc}	The electron yield of net primary production, i.e., the ratio of accumulated C per electrons produced in PSII photochemical reactions. Φ_{NPc} is the reciprocal of the electron requirement for net carbon fixation.

Measurement of absolute ETR per PSII reaction center is the starting point in retrieving the photosynthetic rates and rates of primary production. One measure of primary production is the chl-specific rate of CO_2 assimilation (i.e., CO_2 assimilation per mol Chl-a),

$$P^{chl} = ETR\ n_{PSII}\ 0.25/PQ, \tag{9.7}$$

where n_{PSII} is the ratio of PSII to Chl-a molecules, 0.25 is the quantum yield of O_2 evolution (i.e., 4 e^- is needed to evolve one O_2), and PQ is the ratio O_2/CO_2, called the photosynthetic quotient (see Chapter xxx). n_{PSII} cannot be measured directly using variable fluorescence alone (Kolber & Falkowski 1993). Because n_{PSII} is, at first approximation, proportional to the physical size of PSII unit, n_{PSII} can be estimated from the functional absorption cross section of PSII (σ_{PSII}) (Oxborough et al, 2012). However, variations in the pigment packaging effect and the ratio of Chl-a to accessory pigment introduce errors to the relationship between n_{PSII} and σ_{PSII}. Although n_{PSII} may range from 0.001 to 0.007 mol RC / mol Chl-a, the FRR model assumes n_{PSII} = 0.002, a typical average value for eukaryotic algae (Kolber and Falkowski 1993). Because meso-scale variations in σ_{PSII} in the ocean are relatively small, as compared to the above range of laboratory value of n_{PSII} (0.001 to 0.007 mol RC / mol Chl-a), uncertainties in n_{PSII} appear to be a minor source of errors of variable fluorescence estimates of primary production in the ocean (see below on the sources of errors in ETR and primary production measurements). The equation (9.7) can also be rewritten as

$$P^{chl} = ETR\ n_{PSII}\ (\phi_{e,C})^{-1} \tag{9.8}$$

Here $\phi_{e,C}$ is the electron requirement for carbon fixation (i.e., the number of electrons required to fix one CO_2).

The chl-specific rate of CO_2 assimilation P^{chl} in Eq. 9.7 and 9.8 has the dimension of mol CO_2 s^{-1} (mol Chl-a)$^{-1}$. To convert this rate to biomass-specific rate (i.e., CO_2 assimilation rate per g Chl-a), P^{chl} must be divided by the molecular weight of Chl-a ($M_{chl\text{-}a}$ = 803 g/mol):

$$P^B = ETR\ n_{PSII}\ (\phi_{e,C})^{-1}\ (M_{chl\text{-}a})^{-1} \tag{9.9}$$

The bulk rate of CO2 fixation (in mol CO_2 per s per unit volume) is calculated by multiplying Eq. (9.9) by chlorophyll concentration, [Chl-a] (g/m^{-3}):

$$P^{CO2} = ETR\ n_{PSII}\ (\phi_{e,C})^{-1}\ (M_{chl\text{-}a})^{-1}\ [Chl\text{-}a] \tag{9.10}$$

[Chl-a] can be deduced from FRR/FIRe measurements of F_m fluorescence yields calibrated against standard measurements of [Chl-a] in extracts or HPLC.

PQ and $\phi_{e,C}$ cannot be measured directly using amplitude-based fluorescent techniques, but can be estimated from kinetic fluorescence analysis (Figure 9.3). Uncertainties in $\phi_{e,C}$ are the main source of errors in fluorescence-based estimates of primary production. For nutrient replete conditions, PQ is ca. 1.4 (Laws, 1991 and Chapter xxx) and increases with severe N limitation (Lawrenz et al., 2013; Gorbunov and Falkowski, 2020). Comparisons of amplitude-based variable

fluorescence and 14C measurements of primary production in diverse biogeochemical regions of the ocean revealed that the electron requirements (and electron yields) for carbon fixation are influenced by the extent of nutrient limitation and also may vary with taxonomy and other factors (Lawrenz et al. 2013; Hughes et al. 2018b; Zhu et al. 2017; Melrose et al. 2006; Moore et al. 2006; Schubak et al. 2017; Zhu et al. 2016, 2017). Closer examination of environmental factors that may control the electron requirements suggests that nutrient and, more specifically, nitrogen limitation imposes a major control (Hughes et al. 2018b; Ko et al. 2019; Gorbunov and Falkowski 2020).

The reciprocal of the electron requirement, by definition, defines the electron yield of carbon fixation. The electron yield for net carbon fixation Φ_{NPc}, or the ratio of the number of accumulated cellular C to the number of electrons produced by photochemistry in PSII, is maximal under nitrogen-replete conditions and decreases down to near-zero under severe nitrogen starvation (Gorbunov and Falkowski 2020). The application of fluorescence kinetic analysis offers a simple fluorescence-based indicator to predict the electron yields of carbon fixation for the conditions of nitrogen limited growth (Fig. 3; Gorbunov and Falkowski 2020).

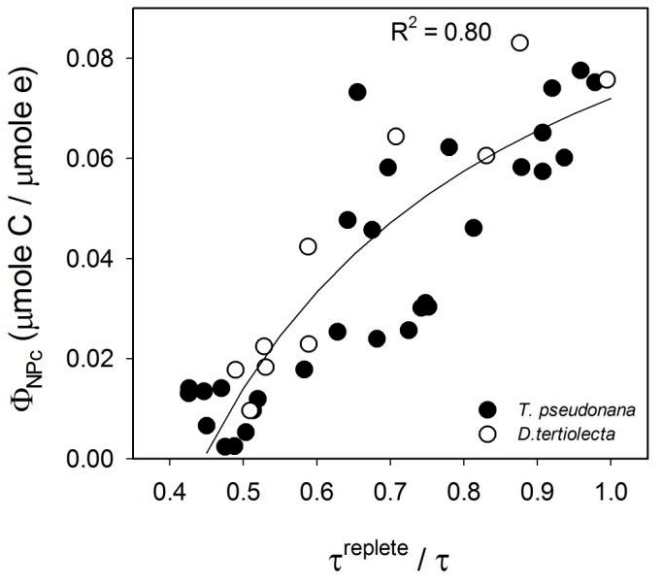

Figure 9.3. Effect of nitrogen limitation on the electron yield of net primary production (Φ_{NPc}), in relation to photosynthetic turnover rates ($1/\tau$). The plot combines data for two model phytoplankton species, including the diatom, *T. pseudonana*, and the green alga, *D.tertiolecta*. The turnover rates were calculated from the analysis of FIRe relaxation kinetics under saturating irradiance. τ and $\tau^{replete}$ are turnover times recorded in nitrogen limited and nitrogen replete samples, respectively. The ratio of $\tau^{replete}/\tau$ characterizes the relative decrease in photosynthetic turnover rates under nitrogen limitation. Data from (Gorbunov and Falkowski 2020).

The photosynthetic turnover time and rates - The photosynthetic turnover time (τ) is defined as the time required for the products of primary photochemical reactions (i.e., electrons produced as a result of charge separation in reaction centers) to complete the whole cycle of transfer from reaction centers to ribulose-1,5-bisphosphate carboxylase/oxygenase (RUBISCO) and CO_2

fixation (Herron and Mauzerall 1971; Myers and Graham 1971). The reciprocal of the turnover time (1/t) is the turnover rate, which determines the maximum rate of this process (P^{max}).

Measurements of photosynthetic turnover rates are fundamentally important for understanding variability of primary production in the ocean, as these rates determine maximum rates of photosynthesis (P^{max}). In turn, P^{max} (and P_b^{opt}) is the key variable that determines the water column integrated primary production in the global ocean (e.g., Behrenfeld and Falkowski 1997).

9.4. Modeling electron transport rates

There are two main approaches to model ETR rates from fluorescence measurements – amplitude-based and kinetic (Gorbunov and Falkowski, 2020). Below we describe and discuss, in turn, these two basic methods.

9.4.1. Amplitude-based fluorescence measurements of ETR

Absolute ETR per open PSII reaction center is calculated from the product of light intensity (E), the optical absorption cross-section of PSII (i.e., how much light is absorbed by a PSII unit), and the quantum yield of photochemistry in PSII, Φ_{PSII} (i.e., the portion of absorbed photons that produce electron flow in PSII). This product must be further multiplied by a fraction of dynamically open centers to reflect the fact that a fraction of reaction centers become dynamically closed under ambient light and only remaining open centers contribute to photosynthetic energy utilization. The fraction of open reaction centers (also called the coefficient of photochemical quenching) can be measured by variable fluorescence technique as a ratio of variable fluorescence under a given irradiance ($\Delta F'$) to the maximum variable fluorescence (F_v') for this irradiance level. F_v' can be measured after a brief (~ 1s) period of darkness to promote opening of all reaction centers that were closed by ambient light. Therefore, ETR as a function of irradiance is expressed as follows:

$$ETR = E\ \sigma_{PSII}^{opt}\ \Phi_{PSII}\ (\Delta F'/F_v') \tag{9.11}$$

The product of the optical absorption cross-section and the quantum yield of photochemistry in PSII is defined as the functional absorption cross section of PSII ($\sigma_{PSII} = \sigma_{PSII}^{opt}\ \Phi_{PSII}$) and this parameter is directly measured using the FRR/FIRe technique. Therefore, the equation (9.11) can be modified as follows (Gorbunov et al. 2000, 2001):

$$ETR = E\ \sigma_{PSII}'\ (\Delta F'/F_v') \tag{9.12}$$

Here, σ_{PSII}' is the functional absorption cross section of PSII and $\Delta F'/F_v'$ is the coefficient of photochemical quenching, recorded at a given level of ambient irradiance (E). $\Delta F'/F_v' = (F_m' - F') / (F_m' - F_o')$ is the fraction of dynamically open reaction centers at a given level of irradiance. By definition, $\Delta F'/F_v' = 1$ in dark and decreases with irradiance as more reaction centers become dynamically closed by ambient light and F' approaches F_m' under high PAR levels (Figure 9.2). The prime character indicates the measurements under ambient irradiance (E). Both σ_{PSII}' and $\Delta F'/F_v'$ are a function of irradiance.

When non-photochemical quenching is caused by thermal dissipation in the light-harvesting antennae, $\sigma_{PSII}/\sigma'_{PSII}=(F_v/F_m)/(F'_v/F'_m)$ (Gorbunov et al., 2001; Suggett et al. 2010) and the equation (11) can be reduced to the following (Gorbunov et al. 2001):

$$ETR = E\ \sigma_{PSII}\ [(\Delta F'/F_m') / (F_v/F_m)] \quad (9.13)$$

where $\Delta F'/F_m'$ (which is sometimes denoted as F_q'/F_m' in oceanographic literature) is the actual quantum yield of photochemistry in PSII at a given irradiance level. Not that $\Delta F'/F_m'$ is the only irradiance-dependent variable in Eq. (9.13) and this parameter is directly measured by FRR/FIRe techniques. Use of Eq. (9.12) requires measurements under both ambient light and after a brief period of darkness (e.g., in both open and dark chambers of the *in situ* FRR fluorometer). For instance, $F_v' = F_m' - F_o'$ can be only recorded after a brief (~ 1s) period of darkness, which is required for all reaction centers to open and for fluorescence yield to reach F_o' level. In contrast, Eq. (9.13) includes parameters recorded only under ambient light, thus eliminating the need to make measurements in darkness.

9.4.2. Kinetic-based fluorescence measurements of ETR

A more direct measurement of ETR relies on the kinetics of the re-oxidation of Q_a following STF (Phase 2 of Figure 9.1). Kinetic analysis is an analytical method for quantitative time-resolved observation of how the concentrations of the reactants in a chemical reaction change over time. Kinetic analysis is the basal approach in chemical kinetics and photochemistry for most accurate measurements of the rate (or rates, if multiple processes are involved) of chemical reactions. This type of analysis can be applied to measure the rates of photosynthetic electron transport by monitoring the kinetics of Q_a re-oxidation in PSII (i.e., transition Q_a^- -> Q_a, where Q_a is the first quinone acceptor of PSII) (Crofts and Wraight 1983; Kolber et al. 1998). Because the redox state of this Q_a acceptor affects the optical properties of PSII (such as the quantum yield of fluorescence), the kinetics of Q_a re-oxidation can be directly derived from the relaxation kinetics of Chl-*a* fluorescence yield after a saturating flash of light, which fully reduces Q_a (Gorbunov and Falkowski 2020). Kinetic fluorescence analysis provides a direct and more accurate way to measure ETR and photosynthetic rates (Gorbunov and Falkowski 2020).

Kinetic measurements of the absolute ETR rely on the rate of photosynthetic turnover ($1/\tau$), which defines maximum ETR achieved under saturating irradiance (Gorbunov and Falkowski 2020). The shape of ETR(E) in relative units is reconstructed from the dependence of the quantum yield of photochemistry in PSII ($\Delta F'/F_m'$ as a function of E):

$$ETR_\tau = 1/\tau\ (E\ \Delta F'/F_m') / (E_{max}\ \Delta F'/F_m'(E_{max})) \quad (9.14)$$

Here, the relative ETR(E) = E $\Delta F'/F_m'$ is normalized to unity by division to its maximum value $E_{max}\ \Delta F'/F_m'(E_{max})$, which is recorded at saturating irradiance (E_{max}). The optimal level of E_{max} is selected at E_{max} ~ 3 x E_k, where E_k is the light saturating parameter of the P versus E curve (Falkowski and Raven 2014), to achieve the maximum precision of ETR_τ measurements. Multiplication of the relative ETR by the photosynthetic turnover rate ($1/\tau$) provides the absolute ETR_τ per PSII unit. $1/\tau$ is calculated directly from the FIRe determined relaxation at saturating

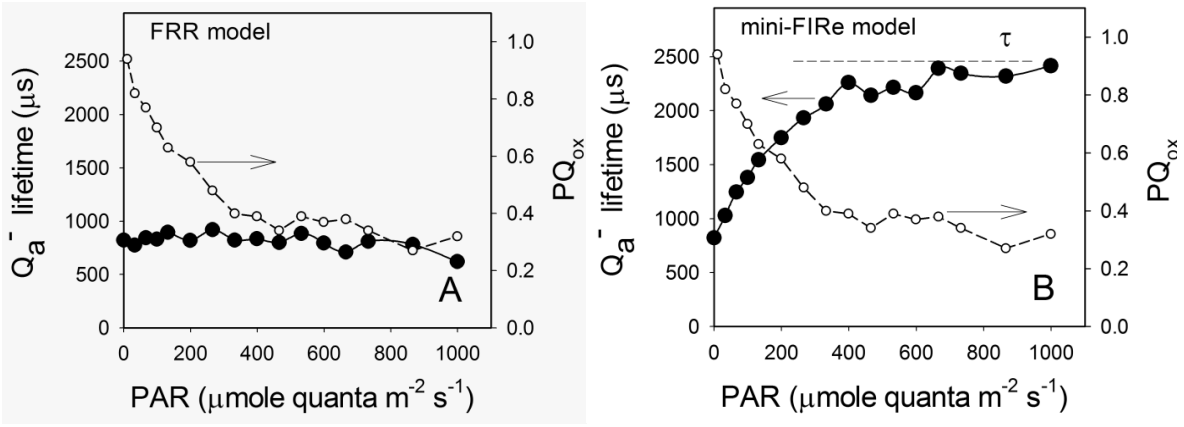

Figure 9.4. The effect of ambient photosynthetically available radiation (PAR) on the time of Q_a reoxidation (solid dots), in relation to PAR-driven alterations in the redox state of the PQ pool (PQ_{ox}, open dots). These time constants were retrieved from the kinetics of fluorescence relaxation in the diatom, *T.pseudonana*, following a saturating single turnover flash by using two different mathematical models, the FRR model (panel **A**) and the new mini-FIRe model (panel **B**). As PAR increases and the PQ pool becomes reduced, the actual rate of electron flow would slow down and the rates of fluorescence relaxation kinetics decrease (panel **B**). Nevertheless, the FRR retrieved relaxation rates remain virtually unchanged with an increase in PAR (panel **A**) and thus do not reflect the actual photosynthetic rates under ambient PAR. In contrast, the mini-FIRe analysis reveals that, as PAR increases and the PQ pool becomes more reduced, τ_{Qa} increases, reflecting a decrease in the actual speed of electron flow (panel **B**). At saturating irradiance, τ_{Qa} plateaus, closely approaching the photosynthetic turnover time (τ) (panel **B**). (Data from Gorbunov and Falkowski, 2020).

irradiance, using the kinetic analysis (see Figure 9.4). The algorithm and operational protocol for kinetic measurements of ETR has been implemented in mini-FIRe instruments developed and manufactured at Rutgers University (Gorbunov and Falkowski 2020).

9.4.3. Comparison between the two methods of calculating ETR

Amplitude-based variable fluorescence techniques became a workhorse in plant physiology and oceanography to derive ETR in phytoplankton and terrestrial plants (Genty et al. 1998; Kolber and Falkowski 1993; Hughes et al. 2018a). Obviously, these techniques do not measure ETR directly; instead ETR are derived from biophysical models. Several models and modifications have been developed (Kolber and Falkowski 1993; Gorbunov et al. 2001; Oxborough et al. 2012; Hughes et al. 2018a). All these models rely on the use of multiple parameters, such as quantum yield of photochemistry in PSII, effective absorption cross-section of PSII or absorption properties, the amount of open and active reaction centers, spectral incident irradiance including its penetration and attenuation within algal cells or leaves. As a consequence, errors in all parameters add up and inevitably increase the overall error of ETR calculations. Also, some of the model parameters, such as absorption cross-sections and light intensities, critically depend on the accuracy of the instrument calibration. Finally, as amplitude-based ETR rates are not measured directly, the overall accuracy of ETR estimates is further reduced by the model assumptions.

In contrast to amplitude-based fluorescence models for ETR, the kinetic analysis offers a direct way to measure the rates of photochemical reactions in PSII and that of electron transport, thus alleviating caveats of amplitude-based methods (Gorbunov and Falkowski 2020). The dramatic improvement in the accuracy of ETR measurements by the kinetic analysis is clearly evident from better correlation between ETR and growth rates (Figure 9.5). The accuracy of the kinetic-based ETR method is essentially determined by uncertainties of a single variable - the photosynthetic

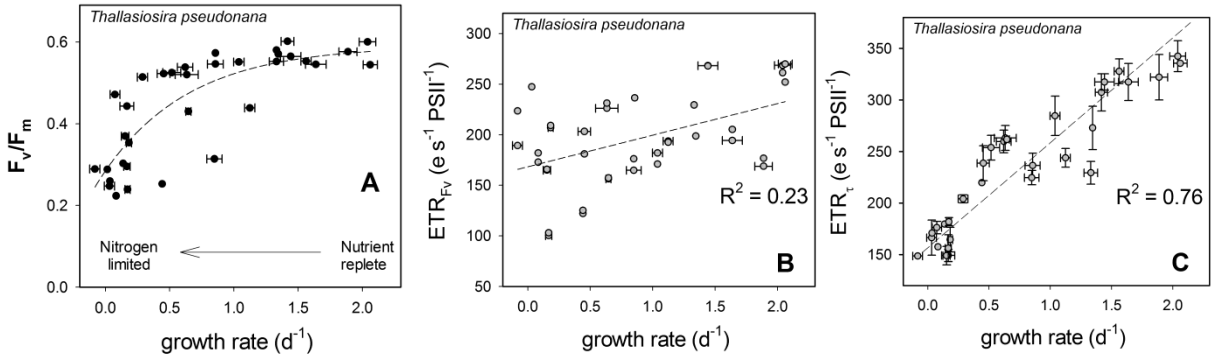

Figure 9.5. Improving ETR measurements using the fluorescence kinetic approach. Relationships between photosynthetic efficiency, ETR and growth rates in the diatom, *Thallasiosira pseudonana* under conditions of nitrogen-limited growth. (**A**) The quantum yield of photochemistry in PSII, F_v/F_m; (**B**) electron transport rates deduced from amplitude-based variable fluorescence; (**C**) electron transport rates deduced from kinetic fluorescence analysis. Kinetic analysis offers a dramatic improvement in the accuracy of ETR measurements, which is clearly evident from better correlation between ETR and growth rates (Fig 9.5C versus 9.5B). Data from (Gorbunov and Falkowski 2020).

turnover rate (see 9.4.2. above), which markedly improves the accuracy of ETR measurements. The extremely high sensitivity of the developed mini-FIRe instruments allows for this kinetic parameter to be measured at high precision (<10%) even in oligotrophic waters of the open ocean.

9.5. Phytoplankton physiology from space – Validation and calibration of solar-induced chlorophyll fluorescence yields

Variable fluorescence signals cannot be recorded from space without high-power lasers or some other source of light – which is not practical, let alone potentially dangerous. An alternative approach to infer phytoplankton physiology and photosynthetic rates is based on measurements of the absolute quantum yields of chlorophyll fluorescence (Lin et al. 2016; Falkowski et al. 2017). With the launch of the MOderate Resoluation Imaging Spectroradiometer (MODIS) and MEdium Resolution Imaging Spectrometer (MERIS) satellites, which possess the capability of detecting solar induced chlorophyll fluorescence signals from the global ocean, it became theoretically possible to calculate the quantum yield of chlorophyll fluorescence from space (Abbott and Letelier 1999; Behrenfeld et al. 2009; Huot et al. 2013). The MODIS/MERIS analytical algorithms retrieve the quantum yields of chlorophyll fluorescence from the ratio of two independent variables, namely the magnitude of solar-induced fluorescence and the number of quanta absorbed by phytoplankton. Solar induced fluorescence (SIF, also called passive fluorescence) from chlorophyll a is detected as a red peak (centered at ca. 683 nm) in spectra of water-leaving radiance (Neville and Gower 1977; Gordon et al. 1988; Gower et al. 1999). Although the presence of phytoplankton in natural waters alters the entire visible spectrum of water-leaving radiance (Gordon et al. 1988; Gower et al. 1999; Morel and Prieur 1977; Gordon and Morel 1983; Esais et al. 1998), SIF is the only signal emitted from the ocean and detectable from space that can be unambiguously ascribed to phytoplankton.

The natural variations of fluorescence yields are the sources of both errors and useful information. SIF yield is highly variable in nature (Cullen et al. 1997; Letelier et al. 1997; Abbott

and Letelier 1998; Maritorena et al. 2000; Morrison 2003; Huot et al. 2005). While the apparently huge variability of chlorophyll fluorescence yield in the ocean (ca. 10 fold) is often correlated with environmental forcing (Letelier et al. 1997; Behrenfeld et al. 2009; Huot et al. 2005; Lin et al. 2016), the mechanisms and interpretation of this relationship remain to be elucidated.

The development of remote sensing algorithms for interpretation of the quantum yields of solar-induced fluorescence crucially depends on comparison with accurate *in situ* measurements of the quantum yields. The quantum yields cannot be measured by using variable fluorescence instruments, but can be measured by using another fluorescence technique, namely picosecond fluorescence kinetics (Lin et al. 2026). Sea-going Picosecond Lifetime Fluorometer (PicoLIF) provides a unique operational tool for ground-truthing of satellite-based retrievals of the quantum yields of solar-induced chlorophyll fluorescence (Lin et al. 2016).

9.5.1. Theoretical basis of fluorescence quantum yields and lifetimes

The quantum yield of fluorescence (ϕ_f) is defined as the ratio of the photons reradiated to those absorbed. The biophysical basis of fluorescence measurements derives from the three possible fates of solar energy absorbed by any photosynthetic organism (Butler 1978). Absorbed photons can (1) generate photochemical reactions (with the rate k_p), (2) be dissipated as heat (k_t), or (3) be emitted back to the environment as fluorescence (k_f). The rate k_p is at first order proportional to the fraction of open or active reaction centers. The rate k_t is the sum of dark component (k_D) and light-dependent component (k_{NPQ}), driven by non-photochemical quenching (Falkowski et al. 2017).

In a dark-adapted state or under low irradiance (when k_{NPQ} is nil and k_t is constant), the quantum yield of chlorophyll fluorescence, ϕ_f ($= k_f/(k_p+k_t+k_f)$), is inversely related to the quantum yield of photochemistry in PSII, $\phi_p = k_p/(k_p+k_t+k_f) = F_v/F_m$:

$$\phi_f = \phi_{fm} (1-F_v/F_m) \tag{9.15}$$

where ϕ_{fm} ($= k_f/(k_t+k_f)$) is the maximum fluorescence yield obtained when the quantum yield of photochemistry is nil (e.g., at saturating background light).

This biophysical model predicts an inverse linear relationship between the quantum yield of photochemistry and that of chlorophyll fluorescence. However, by the early 1980's it was realized that exposure to high irradiance can generate a suite of thermal dissipation mechanisms, collectively called non-photochemical quenching (NPQ). This photoprotective response markedly decreases the quantum yield of chlorophyll fluorescence at high background light. Hence, the relationship between fluorescence yield and photochemistry becomes highly non-linear as NPQ phenomena play an increasingly larger role in energy dissipation (Falkowski et al. 2017).

Fluorescence is a delayed light emission process, which is described by one or more exponential decay functions that can be parameterized by the lifetime, which is the e-folding time of the decay function. The fluorescence lifetime can be quantitatively related to the absolute quantum yield of fluorescence (Lakowicz 2006):

$$\phi_f = \tau/\tau_n \tag{9.16}$$

where τ is the observed lifetime and τ_n is the intrinsic (or "natural") lifetime constant for the molecule. Thus, the longer the lifetime, the higher the quantum yield of fluorescence. Note that the fluorescence lifetime (τ) is deduced from picoseconds kinetic analysis, which is a different technique than the FRR/FIRe analysis of micro- and millisecond relaxation kinetics of Q_a re-oxidation described in 9.4.0.

The "natural" lifetime (τ_n) is that which would be observed if fluorescence emission would be the only path of dissipation of excited state energy; this number cannot be measured directly. The calculated value of τ_n (which is a constant for a specific molecule) for chlorophyll a is 15 ns (Brody and Rabinowitch 1957). In a population of molecules, the actual measured lifetimes are inevitably shorter than the "natural" lifetime due to intra-molecular conversion (i.e., energy dissipation as heat) and triplet state formation. The actual measured lifetimes of isolated chlorophyll a molecules range from ca. 3.0 to 5.1 ns, depending on the solvent polarity. These measured lifetimes correspond to quantum yields ranging from 20 to 32%. Fluorescence lifetimes in living cells are even shorter (ca. 0.3 to ~1.5 ns), as a significant fraction of the absorbed energy is used in photochemical reactions, and reflect the physiological state of the cells (Lin et al. 2016; Falkowski et al 2017).

9.6. Practical Recommendations

9.6.1. Blank (baseline) Correction

Determination of an analytical blank, i.e., the signal associated with the absence of the property being studied, is an important issue in oceanographic measurements, particularly in clear, open ocean waters. The uncertainties in the blank values may become a significant problem when they are comparable with the property (e.g., chlorophyll fluorescence) signal, thus constraining the lower limit of sensitivity (Bibby et al, 2008).

A blank measurement is most accurate when measured on filtered seawater (or media in which you are working). A 0.2 um filter is recommended to remove particles, including algal cells. Using a new, clean filter is important for accurate blank readings. Because filtration procedure often creates micro-bubbles in water, it is recommended to wait for 10-15 minutes after filtration to let these bubbles to disappear. Due to strong elastic scattering of excitation light, micro-bubbles make the measured blank higher that it should normally be. For this reason, it not recommended to use freshly filtered seawater for blank.

In instruments with good optical design, the major portion of blank signal is due to background fluorescence from dissolved organic matter (CDOM) and dissolved degradation products (as pheophytin, etc.) in water. The amount of these degradation products usually increases at depth (below Deep Chlorophyll Max), and it is important to measure at least two blanks (for near-surface and deep layers) for accurate blank correction of vertical profiles.

In some instruments, "instrumental blank" may add to the "natural" DOM blank signal, which should be taken into account. This "instrumental blank" originates from background luminescence from optical parts (lenses, filters, and optical windows) induced by direct or elastically scattered excitation light. Although the instrumental blank can be virtually eliminated or, at least, significantly reduced by improving the optical design (e.g., Gorbunov et al. 2020), each instrument should be evaluated for the magnitude of instrumental blank. The presence and the magnitude of the instrumental blank can be easily estimated by measuring the signal from DI water. For accurate

sapling of phytoplankton variable fluorescence in the open ocean, the instrumental blank from DI water must be negligibly low (< 5% of the Chl-a fluorescence signal in oligotrophic waters and < 1% of the Chl-a fluorescence signal in mesotrophic and eutrophic waters) (Gorbunov et al., 2020; Gorbunov and Falkowski 2020). High instrumental blanks might be difficult to correct. Because the amount of scattered excitation light inevitably varies among samples and, e.g., will dramatically increase when highly-scattering cells (e.g., hyptophytes or some diatoms) are present in the sample, the real instrumental blank will inevitably vary among samples. These variations in the instrumental blank are impossible to take into account by measuring blank signal from filtered seawater. For this reason, it is virtually impossible to accurately measure the instrumental blank and to correct for it in the instruments with high instrumental blank.

9.6.2. Desktop versus in situ deployment

Irradiance dependences of variable fluorescence signals (Fig. 9.2) provide a conceptual framework for retrieving instantaneous photosynthetic rates and modeling the rates of primary production. The light curves ETR(E) can be recorded *in situ*, using submersible FRR fluorometers, or on samples, using benchtop instruments with actinic light source (ALS). In the first case, a range of PAR levels for ETR(E) can be achieved from a vertical profile of *in situ* irradiance in the water column (Kolber and Falkowski 1993), while in the second case – from variations of ALS intensity. Using benchtop mini-FIRe instruments, the light curves ETR(E) can be recorded, in a fully automatic mode, on discrete samples or during underway continuous sampling at sea in a stop-flow regime (Gorbunov and Falkowski 2020; Sherman et al., 2020, Appendix A). Such continuous ETR(E) measurements are helpful for reconstruction of diurnal patterns of photosynthetic rates and modeling daily-integrated primary production.

The *in situ* measurements of photosynthetic rates using submersible instruments are subject to certain limitations. First, because the spectral quality of light varies with depth, the spectral correction is needed for accurate retrievals of absolute ETR rates. Second, reconstruction of ETR(E) from the vertical profiles of *in situ* variable fluorescence relies on the assumption that the physiological status of phytoplankton remains the same over the range of depth. Finally, existing submersible FRR fluorometers are not suitable for kinetic analysis of ETR, which greatly reduces the accuracy of ETR measurements and primary production estimates.

9.6.3. Choosing optimal sampling protocols

Precautions while sample collection and treatment – Photosynthetic rates usually exhibit diel variations, with inactivation of the photosynthetic machinery and a strong decline in the rates at night. To avoid this potential artifact, measurements of photosynthetic rates (e.g., P-versus-E curves), using variable fluorescence, ^{14}C or any other technique should be conducted during daytime.

When samples are collected from the upper layers (0 to ~20 m) during daytime, especially around noon time, they should be pre-acclimated at low light (but not in darkness) to promote recovery from photoinhibition and non-photochemical quenching. Because dark acclimation prevents recovery from photoinhibition and deactivates photosynthetic electron transport, dark acclimation must be avoided. The optimal low light for this pre-acclimation is 50-100 □mole quanta m^{-2} s^{-1}, which is typically about 20-50% of the Ek value.

Importance of ***Slow Light Curves*** – Because the photosynthetic response to a change in light level takes time, the use of so-called “slow light curves” is crucial for reconstruction true ETR(E)

and primary production rates. While programming the ETR(E) protocol, the user should set an acclimation interval (ca. 30s) between PAR steps. This interval is usually sufficient for phytoplankton cells to acclimate to a new PAR level, yet short enough to avoid development of photoinhibition at the highest PAR levels.

Fig. 9.6 shows a light curve ETR(E) recorded in a high light acclimated diatom. Accurate analysis of light curves requires the user to choose an optimal range of PAR levels. First, the maximum PAR level should be selected in such a way that ETR(PAR_{max}) reaches its maximum value. Second, the number of data points must be sufficient (n = 10 or so) to accurately resolve parameters of the ETR(E) curve, such as the initial slope, P_{max}, and E_k. Choosing the optimal PAR_{max} level is most critical. The optimal PAR_{max} is usually about 1000–1500 □mole quanta m^{-2} s^{-1} for near-surface phytoplankton in warm (> 10°C) oceans and decreases under nitrogen limiting conditions, low-light acclimation (e.g., phytoplankton at depth) and in cold waters (polar regions) due to a decrease in E_k.

Practical tip for selecting PAR_{max}: PAR_{max} is optimal when variable fluorescence ratio $\Delta F'/F_m'$ decrease ca. 5x of compared to its maximum at dark (Fig. 9.6B). For example, if $\Delta F'/F_m' = 0.5$ at PAR=0, $\Delta F'/F_m' = 0.1$ at the optimal PAR_{max} (Fig. 9.6B).

Fitting Light Curves ETR(E): There are several mathematic models to fit the light curves (ETR(E) or P-versus-E). The most commonly used model uses a hyperbolic tangent function (Jassby and Platt 1976):

$$ETR = ETR^{max} \tanh(E/E_k) \qquad (9.17)$$

where ETR^{max} is the maximum ETR rate and E_K is the light saturation parameter. Because different models would produce different values for E_k, it is reccomended to use the same model for all data sets for consistency.

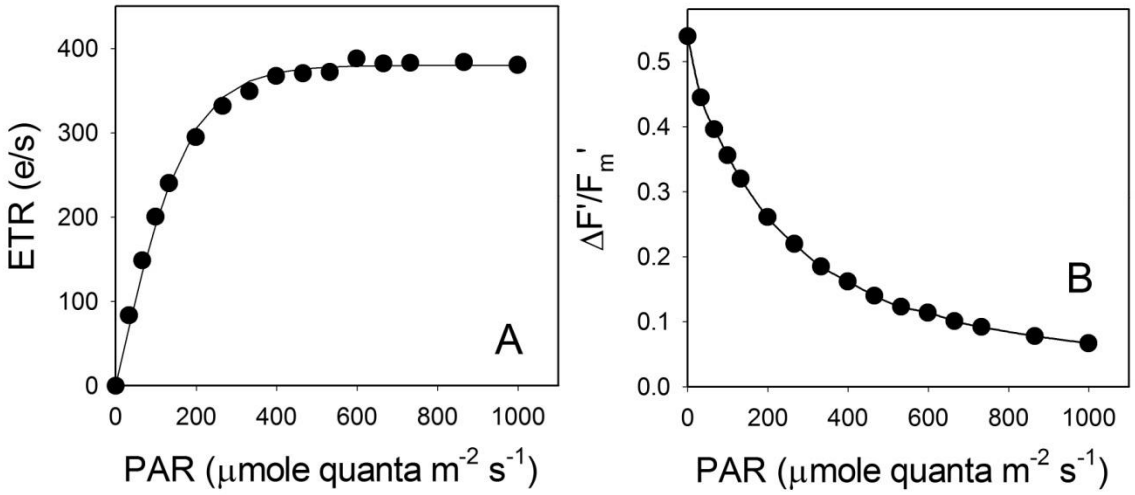

Figure 9.6. (A) Light curve ETR(E) recorded on a high light acclimated diatom. The data points were fitted with a hyperbolic tangent function ETR = ETRmax tanh(E/Ek). (B) Light dependence of the quantum yield of photochemistry, ΔF'/Fm'. The curves were recorded using a mini-FIRe fluorometer with an incorporated Actinic Light Source.

9.6.4. Recommendations for reporting data in a public data repository

The levels of data reporting can be structured as follows:

Level 0: Each instrument generates raw data (relatively large data files). The raw data format may vary among instruments and sampling protocols used. These data files have no value to a general user without access to instrument characterization records. The raw data files are usually stored, with a backup, at user's memory resources (for potential re-processing if needed).

Level 1: Processed data, which includes fluorescence and physiological parameters obtained from fitting the raw fluorescence profiles with a biophysical model (Fo, Fm, Fv, Fv/Fm, Sigma-PSII, relaxation kinetic parameters), together with environmental data, such as PAR, temperature, date/time and GPS data. This data must be generally-readable text files. These processed data must be corrected for blank and instrument detector gain. These data sets provide a backbone for calculating photosynthetic rates, such as ETR). These data files may include the ETR calculated from the biophysical model. The irradiance dependence ETR(E) provides the starting point for fluorescence-based modeling of the rates of primary production.

These processed data files should be accompanied with a README file, which includes information about which instrument, algorithm, protocols, and model were used.

Ancillary data (environmental variables, standard Chl-a measurements, etc.) should be added when available. Diel cycle of *in situ* irradiance is needed to reconstruct the daily integrated primary production from fluorescence-based measurements of instantaneous photosynthetic rates, ETR(E).

9.6.5. Summary – Advantages/Disadvantages/Caveats

Variable fluorescence offers a highly-sensitive and fast measurement of instantaneous photosynthetic rates, as well as a diagnostics of environmental factors, such as nutrient (iron, nitrogen, or phosphorus) limitation and photoacclimation. Fluorescence-based methods for primary production rely on measurements of electron transport rates in PSII and conversion of these rates to carbon fixation by using the electron requirements of carbon fixation (Kolber and Falkowski 1993; Lawrenz et al. 2013).

Amplitude-based variable fluorescence techniques became a workhorse in plant physiology and biological oceanography to derive ETR in phytoplankton and terrestrial plants (Genty et al, 1998; Kolber and Falkowski 1993; Hughes et al. 2018a). Obviously, these techniques do not measure ETR directly; instead ETR are derived from biophysical models (Kolber and Falkowski 1993; Gorbunov et al. 2001; Oxborough et al, 2012; Hughes et al. 2018a). All these models rely on the use of multiple parameters (see **4.1**), such as quantum yield of photochemistry in PSII, effective absorption cross-section of PSII or absorption properties, the amount of open and active reaction centers, spectral incident irradiance including its penetration and attenuation within algal cells. As a consequence, errors in all parameters add up and inevitably increase the overall error of ETR calculations. Also, some of the model parameters, such as absorption cross-sections and light intensities, critically depend on the accuracy of the instrument calibration. Finally, as amplitude-based ETR rates are not measured directly, the overall accuracy of ETR estimates is further reduced by the model assumptions.

Kinetic fluorescence analysis (Section 9.4.2) offers a direct way to measure ETR, thus alleviating caveats of amplitude-based models. The dramatic improvement in the accuracy of ETR measurements by the kinetic analysis is clearly evident from better correlation between ETR and

growth rates (Figure 9.5 and Section 9.4.3). The accuracy of the kinetic-based method is essentially determined by uncertainties of a single variable - the photosynthetic turnover rate (Eq. 9.14 in Section 9.4.2).

Comparisons of amplitude-based variable fluorescence and ^{14}C measurements of primary production in diverse biogeochemical regions of the ocean revealed that the electron requirements for carbon fixation are influenced by the extent of nutrient limitation and also may vary with taxonomy and other factors (Lawrenz et al. 2013; Hughes et al. 2018b; Zhu et al. 2017). Closer examination of environmental factors that may control the electron requirements suggests that nutrient and, more specifically, nitrogen limitation imposes a major control (Hughes et al. 2018b; Ko et al. 2019; Gorbunov and Falkowski 2020). As the variability in the electron requirements of carbon fixation reflects changes in photosynthetic quotients, PQ (Eq. 9.7 and 9.8), this result suggests that PQ in natural phytoplankton communities is strongly affected by nitrogen stress. Fluorescence kinetic analysis offers a simple fluorescence-based indicator to predict the electron yields of carbon fixation for the conditions of nitrogen limited growth (Figure 9.3).

The rate of net primary production is defined by the product of carbon biomass (C) and growth rate (μ):

$$NP_C = dC/dt = C\,\mu \qquad (9.18)$$

As cell growth drives the rates of net primary production, the relationship between kinetic-based ETR measurements and growth rates (e.g., Figure 9.5) offers a path toward modeling the rates of net primary production from fluorescence kinetics.

Conversion of ETR rates to the rates of carbon fixation relies on the electron yield of carbon fixation (Φ_{NPc}, which is the ratio of the number of accumulated C to the number of electrons produced by photochemistry in PSII). Φ_{NPc} is strongly affected by nitrogen limitation (Figure 9.3) and can be inferred from kinetic analysis of photosynthetic turnover rates (Gorbunov and Falkowski 2020). This relationship has been established for nitrogen limiting growth and thus has implications for photosynthesis in the upper, well-lit water column of the ocean. When phytoplankton grow under sub-saturating light, the maximum ETR_τ can be scaled down, using the irradiance dependence $ERT_\tau(E)$. However, in this case, net carbon fixation rates will be overestimated, because variable fluorescence does not measure respiration.

9.7. Appendix A - Setting up of bench top-flowthrough FRRF

Note, this protocol is tailored for the mini-FIRe but may be modified for other FRRf instruments (e.g., Chelsea and Turner).

9.7.1. Pre-cruise preparations

All tubing and other components must be cleaned with bleach prior to each fieldwork event (cruise, survey, etc.). Please see section 4.3 (Plumbing) of IOCCG (2019) for additional details. This is especially important for inflow tubing, debubblers, and the flow-through cuvette. All tubing and other components must thoroughly be rinsed with Milli-Q distilled water after being flushed with bleach prior to use.

Consult Appendix I: Pre-Cruise Checklist when packing. Make sure to include:

- Mini-FIRe FRRf instrument and power supply
- Monitor, cable, and power supply
- Acintic Light Source
- Keyboard
- GPS unit
- First-stage debubbler
- Second-stage debubbler
- Sufficient tubing and replacement tubing
- Flow Control valves
- Tool box w/several adapters, connectors, etc.
- Portable power source if necessary

9.7.2. Setting up of instrument on ship

Familiarization with the ship/lab layout beforehand is very helpful to ascertain the most appropriate location for setting up of a flowthrough min-FIRe instrument. A benchtop version is best set up in a wet laboratory, preferably in a cool, dark and a relatively vibration-free location. It is also preferable to place the instrument close to outflow from the ship's seawater flow through system, to ensure that ambient seawater temperatures flowing through are not affected by temperatures in the ship's wet lab. It is also advantageous to have the instrument placed alongside other flow through sensors viz. salinity, temperature and fluorometric sensors that are usually located close to the outflow of the sea flowthrough system generally above a sink. All the seawater that comes out through the ship's intake generally go through a first stage debubbler. More details on Bubbles and debubbling can be found in section 5.2 of IOCCG (2019). Outflow from the first stage debubbler can be regulated with flow control valves. For the mini-FIRe it is best to have a second debubbler to help ensure that the outflow from the stage 1 debubbler is completely stripped of remaining bubbles before it enters the instrument cuvette. Regulation of the flow rate and the amount of time seawater samples spends in the measurement cuvette is controlled by a computer-controlled solenoid valve. Outflow from the measurement cuvette can be drained directly into a sink with the help of tubing.

Once all the plumbing is in place, the monitor and keyboard, the actinic light source and the solenoid control box are to be connected to the rear of the instrument via ports on the rear of the instrument. Once the actinic light source is connected it to be placed above the cuvette chamber. GPS feed either from the ship or from an independent unit can be directly ported to the instrument via a RS-232 serial port on the rear of the instruement. Please see section 3 (Ancillary Measurements for In-Line Systems) of IOCCG (2019), for additional details.

Measurements made by the mini-FIRe are very sensitive to ambient light and hence althought the flow-through cuvette sits inside of the instrument it is covered with an acrylic cover. Please see section 5.5 (Contamination by ambient light) of IOCCG (2019) for additional details.

When the flow-through system is turned on, adjust the flow rate as necessary using the flow control valve. Please see section 5.1 (Flow rate) in IOCC (2019) for additional details. Check for leaks and make sure that there are no air bubbles.

If everything looks good, the instrument can be powered, with the help of a switch located on the bottom left-hand corner of the front panel of the instrument. The instrument is operated via DOS system. Check the date and time on the instrument and correct if necessary using the DOS command, set date and time. There are several programs installed on the mini-FIRe. CONT.exe is the program for continuous underway measurements. This program runs standard dark measurements in addition to periodic light regulated measurements of ETR (see Quick Operation Manual for mini-FIRe Fluorometer).

To operate in flow through mode, type cont in the command line to start the program. All command letters are case-sensitive. Enter the filename in the second line of the leftmost menu entitled Log. The filename must not exceed eight characters and should have the extension .000. Once you have entered the filename, press s to start the program. As per the manual, the program will automatically adjust the gain, process the fluorescence profiles after each acquisition cycle, and save the data. Approximately every twenty minutes, the solenoid valve will kick on and the mini-FIRe will make ambient light adjusted fluorescence measurements on the sample in the cuvette. Upon completion, the solenoid valve will turn on and the water will resume flowing, and the instrument will return to making dark measurements.

Depending on the duration of the cruise, measurements are typically made for the entirety of one sampling day before the program is closed. To stop acquiring data, press ‘s’ again. Press ‘q to quit the program.

The mini-FIRe must be powered off before you plug the thumb drive into the front panel of the instrument. Power on the instrument and copy the data onto the thumb drive. The files will be listed one after the other until completion. The mini-FIRe generates several ASCII file types with the extensions: .COL, .DAT, .PAR, .REC, and .RES. The .PAR file contains the P-E measurements and the .RES file contains the dark measurements. Review the data and discard any points that have been contaminated by bubbles. Please see section 8.4 (Removal of data contaminated by bubbles) in IOCCG (2019) for additional details. Additional details for processing the data are available with the mini-FIRe operational manual.

9.8. References

Abbott MR, Letelier RM. (1998) Decorrelation scales of chlorophyll as observed from bio-optical drifters in the California Current. Deep Sea Research Part II: Topical Studies in Oceanography, 45(8):1639-67.

Abbott MR, Letelier RM. (1999) Algorithm theoretical basis document: chlorophyll fluorescence (MODIS Product Number 20). Ocean Biology Processing Group, NASA's Earth Observing System, 1999.

Behrenfeld MJ, Bale AJ, Kolber ZS, Aiken J, Falkowski PG. (1996) Confirmation of iron limitation of phytoplankton photosynthesis in the equatorial Pacific Ocean. Nature. 383(6600): 508-11.

Behrenfeld MJ, Worthington K, Sherrell RM, Chavez FP, Strutton P, McPhaden M, et al. Controls on tropical Pacific Ocean productivity revealed through nutrient stress diagnostics. Nature. 2006 Aug 31;442(7106):1025-8.

Behrenfeld MJ, Westberry TK, Boss ES, O'Malley RT, Siegel DA, Wiggert JD, et al. (2009) Satellite-detected fluorescence reveals global physiology of ocean phytoplankton. Biogeosciences. 6(5):779-94.

Bibby, T. S., Gorbunov, M. Y., Wyman, K. W., & Falkowski, P. G. (2008). Photosynthetic community responses to upwelling in mesoscale eddies in the subtropical North Atlantic and Pacific Oceans. Deep-Sea Research Part II -Topical Studies in Oceanography, 55(10-13), 1310-1320. doi:10.1016/j.dsr2.2008.01.014

Bilger W. and O. Bjorkman (1990) Role of the xanthophyll cycle in photoprotection elucidated by measurements of light-induced absorption changes, fluorescence and photosynthesis in Hedera canariensis. Photosyn. Res. 25: 173-185.

Boyd PW, Aiken J, Kolber Z (1997) Comparison of radiocarbon and fluorescence based (pump and probe) measurements of phytoplankton photosynthetic characteristics in the Northeast Atlantic Ocean. Marine Ecology Progress Series 149:215-226

Brody SS, Rabinowitch E. (1957) Excitation lifetime of photosynthetic pigments in vitro and in vivo. Science. 125(3247):555.

Cheah W, McMinn A, Griffiths FB, Westwood KJ, Wright SW, Molina E, Webb JP, van den Enden R (2011) Assessing Sub-Antarctic Zone primary productivity from fast repetition rate fluorometry. Deep-Sea Research Part II - Topical Studies in Oceanography 58:2179-2188

Corno G, Letelier RM, Abbott MR, Karl DM (2006) Assessing primary production variability in the North Pacific subtropical gyre: A comparison of fast repetition rate fluorometry and C-14 measurements. Journal of Phycology 42:51-60

Crofts, A.R., Wraight, C.A., 1983. The electrochemical domain of photosynthesis, Biochim. Biophys. Acta. 726, 149-185.

Cullen JJ, Ciotti AM, Davis RF, Neale PJ, editors. Relationship between near-surface chlorophyll and solar-stimulated fluorescence: biological effects. 1997.

Esaias WE, Abbott MR, Barton I, Brown OB, Campbell JW, Carder KL, et al. (1998) An overview of MODIS capabilities for ocean science observations. Ieee T Geosci Remote. 36(4):1250-65.

Estevez-Blanco P, Cermeno P, Espineira M, Fernandez E (2006) Phytoplankton photosynthetic efficiency and primary production rates estimated from fast repetition rate fluorometry at coastal embayments affected by upwelling (Rias Baixas, NW of Spain). Journal of Plankton Research 28:1153-1165

Falkowski, P.G., Koblizek, M., Gorbunov, M., and Kolber, Z., 2004. Development and Application of Variable Chlorophyll Fluorescence Techniques in Marine Ecosystems, in: Papageorgiou, C. and Govingjee (Eds), Chlorophyll a Fluorescence: A signature of Photosynthesis, Springer, Dordrecht, pp. 757-778.

Falkowski, P.G., Raven, J.A., 2007. Aquatic photosynthesis, second edition, Princeton University Press, Princeton.

Falkowski P.G., Lin H., and Gorbunov M.Y. (2017) What limits photosynthetic energy conversion efficiency in nature? Lessons from the oceans – Phil. Trans. Royal Soc. B, 372: 20160376. http://dx.doi.org/10.1098/rstb.2016.0376

Fujiki T, Suzue T, Kimoto H, Saino T (2007) Photosynthetic electron transport in Dunaliella tertiolecta (Chlorophyceae) measured by fast repetition rate fluorometry: relation to carbon assimilation. Journal of Plankton Research 29:199-208

Genty B., J.M. Briantais, and N.R. Baker (1989) The relationship between the quantum yield of photosynthetic electron transport and quenching of chlorophyll fluorescence. Biochim. Biophys. Acta 990: 87-92.

Gorbunov M.Y., Kolber Z., and Falkowski P.G. (1999) Measuring photosynthetic parameters in individual algal cells by Fast Repetition Rate fluorometry. - *Photosynthesis Research*, **62**(2-3): 141-153.

Gorbunov M.Y., Falkowski P.G. and Kolber Z. (2000) Measurement of photosynthetic parameters in benthic organisms *in situ* using a SCUBA-based fast repetition rate fluorometer. - *Limnol. Oceanogr.*, **45**(1):242-245.

Gorbunov M.Y., Z. Kolber, M.P. Lesser, and P.G. Falkowski P.G. (2001) Photosynthesis and photoprotection in symbiotic corals. - *Limnol. Oceanogr.*, **46**(1):75-85.

Gorbunov MY, and Falkowski PG. (2005). Fluorescence Induction and Relaxation (FIRe) Technique and Instrumentation for Monitoring Photosynthetic Processes and Primary Production in Aquatic Ecosystems. In: "Photosynthesis: Fundamental Aspects to Global Perspectives" - Proc. 13th International Congress of Photosynthesis, Montreal, Aug.29 – Sept. 3, 2004. (Eds: A. van der Est and D. Bruce), Allen Press, V.2, pp. 1029-1031.

Gorbunov MY, E Shirsin, E Nikonova, VV Fadeev, and PG Falkowski (2020) The use of multi-spectral Fluorescence Induction and Relaxation technique for physiological and taxonomic analysis of phytoplankton communities. - *Marine Ecology Progress Series*, 644: 1-13. DOI: https://doi.org/10.3354/meps13358.

Gorbunov MY and PG Falkowski (2020) Using chlorophyll fluorescence kinetics to determine photosynthesis in aquatic ecosystems. - *Limnol. Oceanogr.*, doi: 10.1002/lno.11581.

Gordon HR, Brown OB, Evans RH, Brown JW, Smith RC, Baker KS, et al. (1988) A semianalytic radiance model of ocean color. Journal of Geophysical Research: Atmospheres. 93(D9):10909-24.

Gordon HR, Morel AY. In - Water Algorithms. Remote Assessment of Ocean Color for Interpretation of Satellite Visible Imagery: A Review. Lecture Notes on Coastal and Estuarine Studies: Springer-Verlag; 1983. p. 24-67.

Gower JFR, Doerffer R, Borstad GA. (1999) Interpretation of the 685 nm peak in water-leaving radiance spectra in terms of fluorescence, absorption and scattering, and its observation by MERIS. Int J Remote Sens. 20(9):1771-86.

Halsey KH, Milligan AJ, Behrenfeld MJ (2010) Physiological optimization underlies growth rate-

independent chlorophyll-specific gross and net primary production. Photosynthesis Research 103:125-137

Halsey KH, Milligan AJ, Behrenfeld MJ (2011) Linking time-dependent carbon-fixation efficiencies in Dunaliella tertiolecta (chlorophyceae) to underlying metabolic pathways. Journal of phycology 47:66-76

Halsey KH, O'Malley RT, Graff JR, Milligan AJ, Behrenfeld MJ (2013) A common partitioning strategy for photosynthetic products in evolutionarily distinct phytoplankton species. New Phytol 198:1030-1038

Hancke K, Dalsgaard T, Sejr MK, Markager S, Glud RN (2015) Phytoplankton productivity in an Arctic Fjord (West Greenland): Estimating electron requirements for carbon fixation and oxygen production. PloS one 10:e0133275

Herron, H.A. and D. Mauzerall. 1971. The development of photosynthesis in a greening mutant of Chlorella and an analysis of the light saturation curve. Plant Physiol 50: 141–148.

Hughes, D.J., D.A. Campbell, M.A. Doblin, J.C. Kromkamp, E.C. Lawrenz, M. Moore, K. Oxborough, O. Prášil, P.J. Ralph, M.F. Alvarez, and D.J. Suggett (2018a) Roadmaps and Detours: Active Chlorophyll-a Assessments of Primary Productivity Across Marine and Freshwater Systems. Environ. Sci. Technol. 52(21): 12039-12054.

Hughes, D.J., D. Varkey, M.A. Doblin, T. Ingleton, A. Mcinnes, P.J. Ralph, V. van Dongen-Vogels, and D.J. Suggett (2018b) Impact of nitrogen availability upon the electron requirement for carbon fixation in Australian coastal phytoplankton communities. Limnology and Oceanography 63:1891-1910.

Huot Y, Franz BA, Fradette M. (2013) Estimating variability in the quantum yield of Sun-induced chlorophyll fluorescence: a global analysis of oceanic waters. Remote Sens Environ. 132:238-53.

Huot Y, Brown CA, Cullen JJ. (2005) New algorithms for MODIS sun-induced chlorophyll fluorescence and a comparison with present data products. Limnol Oceanogr-Meth. 3:108-30.

IOCCG Protocol Series (2019). Inherent Optical Property Measurements and Protocols: Best Practices for the Collection and Processing of Ship-Based Underway Flow-Through Optical Data. Boss, E., Haëntjens, N., Ackleson, S.G., Balch, B., Chase, A., Dall'Olmo, G., Freeman, S., Liu, Y., Loftin, J., Neary, W., Nelson, N., Novak, M., Slade, W., Proctor, C., Tortell, P., and Westberry. T. IOCCG Ocean Optics and Biogeochemistry Protocols for Satellite Ocean Colour Sensor Validation, Volume 4.0, edited by A. R. Neeley and A. Mannino, IOCCG, Dartmouth, NS, Canada. http://dx.doi.org/10.25607/OBP-664

Jassby, A. D., and T. Platt. (1976) Mathematical formulation of the relationship between photosynthesis and light for phytoplankton. Limnol. Oceanogr. **21**: 540–547. doi:10.4319/lo.1976.21.4.0540

Ko E., Park J., Gorbunov M.Y., Yoo S. (2019) Uncertainties in variable fluorescence and 14C methods to estimate primary productivity: a case study in the coastal waters off the Korean peninsula – Marine Ecology Progress Series, 627, 13-31.

Kolber Z, Zehr J, Falkowski P. Effects of Growth Irradiance and Nitrogen Limitation on

Photosynthetic Energy-Conversion in Photosystem-II. Plant Physiol. 1988 Nov; 88(3):923-9.

Kolber Z, Falkowski PG (1993) Use of Active Fluorescence to Estimate Phytoplankton Photosynthesis in-Situ. Limnology and Oceanography 38:1646-1665

Kolber ZS, Prasil O, Falkowski PG (1998) Measurements of variable chlorophyll fluorescence using fast repetition rate techniques: defining methodology and experimental protocols. Biochimica Et Biophysica Acta-Bioenergetics 1367:88-106

Kromkamp JC, Forster RM (2003) The use of variable fluorescence measurements in aquatic ecosystems: differences between multiple and single turnover measuring protocols and suggested terminology. European Journal of Phycology 38:103-112

Kromkamp JC, Dijkman NA, Peene J, Simis SGH, Gons HJ (2008) Estimating phytoplankton primary production in Lake IJsselmeer (The Netherlands) using variable fluorescence (PAM-FRRF) and C-uptake techniques. European Journal of Phycology 43:327-344

Lakowicz JR. Principles of Fluorescence Spectroscopy. 3rd ed. New York, USA: Springer Science and Business Media, LLC., New York, USA; 2006 2006.

Letelier RM, Abbott MR, Karl DM. (1997) Chlorophyll natural fluorescence response to upwelling events in the Southern Ocean. Geophys Res Lett. 24(4):409-12.

Lawrenz E, Silsbe G, Capuzzo E, Ylostalo P, Forster RM, Simis SGH, Prasil O, Kromkamp JC, Hickman AE, Moore CM, Forget MH, Geider RJ, Suggett DJ (2013) Predicting the Electron Requirement for Carbon Fixation in Seas and Oceans. Plos One 8

Laws EA (1991) Photosynthetic Quotients, New Production and Net Community Production in the Open Ocean. Deep-Sea Research Part a-Oceanographic Research Papers 38:143-167

Lin H, Kuzminov FI, Park J, Lee S, Falkowski PG, Gorbunov MY. (2016) The fate of photons absorbed by phytoplankton in the global ocean. Science. 351(6270):264-7.

Maritorena S, Morel A, Gentili B. (2000) Determination of the fluorescence quantum yield by oceanic phytoplankton in their natural habitat. Appl Optics. 39(36):6725-37.

Melrose DC, Oviatt CA, O'Reilly JE, Berman MS (2006) Comparisons of fast repetition rate fluorescence estimated primary production and C-14 uptake by phytoplankton. Marine Ecology Progress Series 311:37-46

Milligan AJ, Halsey KH, Behrenfeld MJ (2015) Advancing interpretations of 14C-uptake measurements in the context of phytoplankton physiology and ecology. Journal of Plankton Research 37:692-698

Moore CM, Suggett DJ, Holligan PM, Sharples J, Abraham ER, Lucas MI, Rippeth TP, Fisher NR, Simpson JH, Hydes DJ (2003) Physical controls on phytoplankton physiology and production at a shelf sea front: a fast repetition-rate fluorometer based field study. Marine Ecology Progress Series 259:29-45

Moore CM, Suggett DJ, Hickman AE, Kim YN, Tweddle JF, Sharples J, Geider RJ, Holligan PM (2006) Phytoplankton photoacclimation and photoadaptation in response to environmental gradients in a shelf sea. Limnology and Oceanography 51:936-949

Morel A, Prieur L. Analysis of variations in ocean color. Limnol Oceanogr. 1977;22(4):709-22.

Morrison JR. (2003) *In situ* determination of the quantum yield of phytoplankton chlorophyll a fluorescence: A simple algorithm, observations, and a model. Limnol Oceanogr. 48(2):618-31.

Myers, J. and J.R. Graham. 1971. The photosynthetic unit of Chlorella measured by repetitive short flashes. Plant Physiol. 48: 282–286.

Neville RA, Gower JFR. (1977) Passive remote sensing of phytoplankton via chlorophyll α fluorescence. Journal of Geophysical Research. 82(24):3487-93.

Oxborough, K., C.M. Moore, D.J. Suggett, T. Lawson, H.G. Chan, and R.J. Geider. 2012. Direct estimation of functional PSII reaction center concentration and PSII electron flux on a volume basis: A new approach to the analysis of Fast Repetition Rate fluorometry (FRRf) data. Limnol. Oceanogr.: Methods 2012, 10 (3), 142−154.

Parkhill, J.-P., G. Maillet, and J.J. Cullen. 2001. Fluorescence-based maximal quantum yield for PSII as a diagnostic of nutrient stress. J. Phycol., 37: 517–529.

Robinson C, Suggett D, Cherukuru N, Ralph P, Doblin M (2014) Performance of Fast Repetition Rate fluorometry based estimates of primary productivity in coastal waters. Journal of Marine Systems 139:299-310

Schuback N, Schallenberg C, Duckham C, Maldonado MT, Tortell PD (2015) Interacting Effects of Light and Iron Availability on the Coupling of Photosynthetic Electron Transport and CO2-Assimilation in Marine Phytoplankton. PLoS One 10:e0133235

Schuback N, Hoppe CJ, Tremblay JÉ, Maldonado MT, Tortell PD (2017) Primary productivity and the coupling of photosynthetic electron transport and carbon fixation in the Arctic Ocean. Limnology and Oceanography 62:898-921

Sherman J., MY Gorbunov, O. Schofield, and PG Falkowski (2020) Photosynthetic energy conversion efficiency along the West Antarctic Peninsula - Limnol. Oceanogr. doi: 10.1002/lno.11562

Suggett D, Kraay G, Holligan P, Davey M, Aiken J, Geider R (2001) Assessment of photosynthesis in a spring cyanobacterial bloom by use of a fast repetition rate fluorometer. Limnology and Oceanography 46:802-810

Suggett DJ, Oxborough K, Baker NR, MacIntyre HL, Kana TM, Geider RJ (2003) Fast repetition rate and pulse amplitude modulation chlorophyll a fluorescence measurements for assessment of photosynthetic electron transport in marine phytoplankton. European Journal of Phycology 38:371-384

Suggett DJ, Moore CM, Maranon E, Omachi C, Varela RA, Aiken J, Holligan PM (2006) Photosynthetic electron turnover in the tropical and subtropical Atlantic Ocean. Deep-Sea Research Part Ii-Topical Studies in Oceanography 53:1573-1592

Suggett DJ, Prášil O, Borowitzka MA (2010) Chlorophyll a Fluorescence in Aquatic Sciences: Methods and Applications: Methods and Applications. Springer

Zhu Y, Ishizaka J, Tripathy S, Wang S, Mino Y, Matsuno T, Suggett D (2016) Variation of the photosynthetic electron transfer rate and electron requirement for daily net carbon fixation in Ariake Bay, Japan. Journal of oceanography 72:761-776

Zhu Y, Ishizaka J, Tripathy SC, Wang S, Sukigara C, Goes J, Matsuno T, Suggett DJ (2017) Relationship between light, community composition and the electron requirement for carbon fixation in natural phytoplankton. Marine Ecology Progress Series 580:83-100

10. Autonomous Platforms

David P. Nicholson[1], Andrea J. Fassbender[2], Magdalena M. Carranza[3], Ivona Cetinic[4]

[1]*Marine Chemistry and Geochemistry Department, Woods Hole Oceanographic Institution, Massachusetts, USA*
[2]*NOAA Pacific Marine Environmental Laboratory, Washington, USA*
[3]*Monterey Bay Aquarium Research Institute, California, USA*
[4]*Universities Space Research Association, Maryland, USA*

10.1. Introduction

Advances in underwater robotics and biogeochemical sensors have, in recent decades, greatly expanded the ability of oceanographers to observe ocean processes using autonomous systems (Lee et al. 2017). These tools have enabled new approaches for quantifying ocean productivity and hold the promise to vastly improve the spatial and temporal coverage of *in situ* primary productivity and net community productivity estimates. In the last several years, multiple methods relying on measures of biogeochemical properties such as oxygen, carbon, nitrogen, chlorophyll fluorescence, optical backscatter, and irradiance, etc. have been used to estimate rates of productivity in the upper ocean. These emerging applications for autonomous observations complement existing satellite remote sensing and ship-based approaches. Autonomous platforms profile the subsurface water column capturing the vertical structure, such as the deep chlorophyll maximum, often missed by ocean color satellites. However, in the open ocean these applications are still relatively new and vary widely in the type of productivity (net, gross, etc.) captured and methodological assumptions required. Here, we summarize the current state of autonomous platform-based productivity estimates, best practices, and potential for future growth with a focus on routinely deployed chemical and optical sensors and open ocean applications.

Depending on the approach, autonomous estimates of productivity approximate either net community production (NCP), net primary production (NPP) or gross primary production (GPP) and quantify these rates in carbon, oxygen, or nitrogen-based units (Figure 10.1). Some approaches also quantify heterotrophic rates such as community respiration (CR), which is the sum of respiration by autotrophs (R_A) and heterotrophs (R_H). Here, we outline more widespread methodologies used to quantify these metabolic rates, recognizing that these approaches continue to evolve, mature, and expand. First, mass balance approaches to estimating NCP are described, followed by NPP and GPP methods based on optical algorithms and diel budgets, respectively.

10.1.1. Platforms, sensors, and calibration.

Advancements in autonomous sensors and platforms over the past few decades are transforming our ability to observe ocean biogeochemical changes persistently and over a wide range of time scales (Sauzède et al. 2016, Bushinsky et al. 2019, Chai et al. 2020, Bisson et al. 2021). Moorings (Körtzinger et al. 2008, Emerson and Stump, 2010, Weeding and Trull 2014, Fassbender et al. 2016, 2017), wave gliders (Wilson et al. 2014, Chavez et al. 2017), subsurface gliders (Rudnick 2016) floats (D'Asaro 2003, Yang et al. 2017, Williams et al. 2018, Bushinsky et al. 2018, Arteaga et al. 2020, Claustre et al. 2020), and Wire Walkers (Lucas et al. 2013, Omand et al. 2017) are becoming more commonly used to evaluate upper ocean metabolic balances, study the magnitude

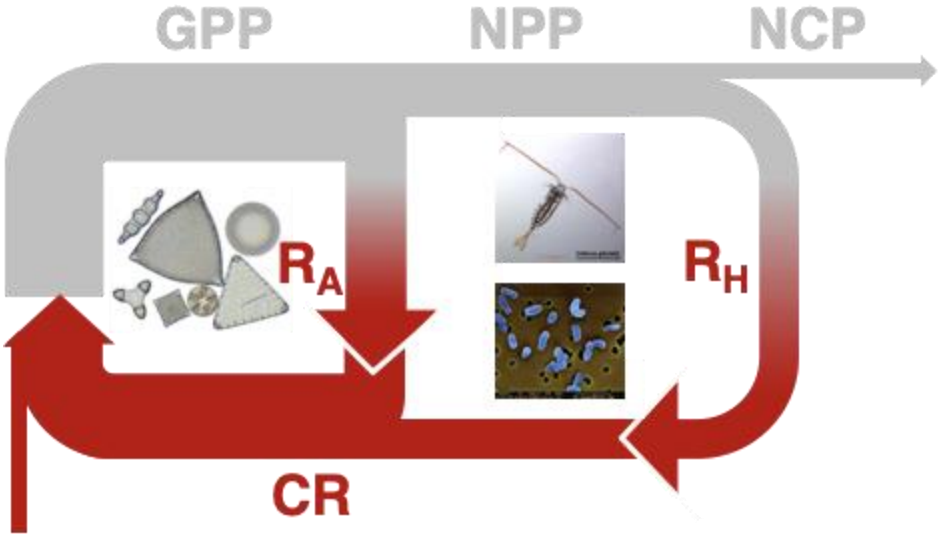

Figure 10.1. Diagram of metabolic rates of in the surface ocean

and phenology of biological processes, and quantify the biological pump. The most mature and widespread chemical and optical sensors used to quantify primary productivity are shown in Table 10.1. These sensors are suitable for long-term deployment based on their robustness and power requirements.

Despite recent advances in sensor technology, biogeochemical sensors require careful calibration and evaluation. So far, no biogeochemical sensors should be considered to have sufficient accuracy and stability for quantitative estimates of biogeochemical rates without careful calibration and validation. Biogeochemical sensors are subject to a range of factors that can reduce accuracy and bias primary productivity estimates. These include aging/degradation of sensor components (both prior to, and during deployment) caused by, for example, reduced intensity of LED light sources with time, biofouling of optical windows, dynamic errors due to finite sensor response times, sensor drift, and inadequate sensor characterization or factory calibration. Best practices for calibration of each sensor type have been documented through several efforts by NASA, SCOR, IOCCG, Argo, and GEOTRACES-led groups who have produced detailed protocols outlining proper calibration procedures and best deployment practices (e.g., Owens and Wong 2009, Boss et al. 2015, 2019, 2020, Bittig et al. 2019).

In addition to individual sensor calibration, sensors that are part of a sensor array require intercalibration to provide consistency between each sensor unit. For example, NAB08 and EXPORTS (Siegel et al. 2021) took the approach of a "gold standard" well-characterized and calibrated sensor, usually deployed aboard ship's CTD (Boss et al. 2015) that is then used for intercalibration via ship-board calibration casts and vicarious intercalibration opportunities. For large-scale programs such as Biogeochemical Argo, ship-based programs such as GO-SHIP and databases such as SOCAT (Bakker et al. 2016) serve as validation datasets.

The ultimate standard for biogeochemical sensors is high-quality discrete measurements taken from research vessels. In many cases, there is a direct correspondence between sensor and

Table 10.1.

Biogeochemical properties routinely deployed aboard autonomous platforms that can be used for estimates of productivity. Modified from Chai et al. 2020.

Property	Symbol	Sensor	Platform	PP measurement
Dissolved oxygen	O_2	Luminescense lifetime optode	All autonomous platforms	NCP/GPP
Partial pressure of carbon dioxide	pCO_2	NDIR / Equilibration based infrared analyzer	Unmanned Surface Vehicles	NCP
Nitrate	NO_3^-	Ultraviolet spectrophotometer	Profiling floats, gliders	NCP
pH	pH	Ion sensitive field-effect transistor	All autonomous platforms	NCP/GPP
Particulate organic carbon	b_{bp}	Optical backscatter	All autonomous platforms	GPP
Particulate organic carbon	c_p	Optical attenuation	floats	
Chlorophyll a	Chl / ChlF	Fluorometer	All autonomous platforms	NPP
Downwelling irradiance and PAR	PAR	Radiometer	Profiling floats, gliders	NPP

shipboard measurements. For example, oxygen optodes are calibrated against shipboard Winkler oxygen titrations. Other sensors measure a property more removed from the quantity of biogeochemical interest. For example, optical backscatter sensors, which measure the intensity of light scattered back to the sensor, are used to estimate particulate organic carbon. Making such connections requires what is termed ‘proxy building’ in which shipboard biogeochemical (BGC) measurements are statistically compared to the related sensor measurement. Such proxy relationships can vary regionally and temporally as a function of a wide range of factors including, for example, phytoplankton community composition and mineral deposition. Similarly, Chl-a concentrations are obtained from float fluorescence data that have been corrected for non-photochemical quenching (NPQ) effects and, in some cases, calibrated against HPLC measurements from two near-surface water samples obtained during float deployments (Johnson et al. 2017a, Haëntjens et al. 2017). Regional, temporal, and depth dependences of the fluorescence to chlorophyll relationship are another challenge for interpreting sensor data used for proxy estimation (Roesler et al. 2017).

10.1.2. Sensor Calibration

Long term deployments of biogeochemical sensors aboard autonomous platforms and moorings (Chai et al 2020) allow for unprecedented insights into the variability of oceanic productivity but can also often suffer from measurement quality degradation due to biofouling and/or instrumental drift over time. Moored instruments, as well as instrumentation that spends substantial time in the euphotic zone, are more susceptible to biofouling. In both cases, post deployment calibration (some platforms are not recoverable), sensor redundancy on the same platform (hard due to the power/weight limitations of the platforms), or intercalibration with other in-situ platforms or ocean color satellites can help with long term drift correction. Profiling floats spend most of the time at great depths, and the transition to faster communication systems (Iridium) has substantially decreased the amount of time floats spend at the surface for data transmission (~20'), greatly reducing bio-fouling effects (Roemmich et al. 2019).

It has been noted that discrepancies in the measured quantities across multiple instruments (in experiments where arrays of autonomous or human guided platforms were deployed) often can be larger than the innate variability of the measured parameter. These discrepancies mostly arise due to the instrument calibration approaches and particle-associated physiology (e.g., for ChlF see (Roesler et al. 2017), and different configurations of the instrument (e.g., angle, wavelength, acceptance angle, etc.). Although no official protocols for intercalibration exist, two recent, large field experiments - NAB08 and EXPORTS - used similar approaches to intercalibration of sensors across different platforms that we outline here. First, a "gold standard" - well characterized and calibrated sensor, usually deployed aboard ship's CTD - is defined (Boss et al. 2015). This sensor is usually the one paired with discrete biogeochemical measurements later used to develop BGC proxies. For the duration of the experiment, 5-10 targeted (and more serendipitous) encounters between the "gold standard" and other instruments are performed. During these planned encounters targeted autonomous platforms are kept at the surface and when within proximity (usually within the visible distance, see Briggs et al. 2011 and Siegel 2021), profiles are simultaneously obtained from both platforms. These encounters can be later used for calibration (checks for the drift, biofouling, etc.) intercalibration (ensuring for the same output in instrument units), and extension of the developed BGC proxies allowing for array-wide calculations of BGC stocks and rates.

Here, BGC proxies refer to mapping properties directly measured by a sensor to a quantity that is more ecologically or biogeochemically relevant. For example, optical backscatter is used to estimate particulate organic carbon (POC) and phytoplankton carbon (C_{phyto}). Likewise, fluorescence at one wavelength (typically 695 nm) induced by excitation at another wavelength (typically 470 nm) is used to estimate Chlorophyll *a*. Such proxy relationships may be seasonally and regionally variable and are most accurate when co-located samples are collected, rather than relying on previously published relationships.

Once deployed, various techniques are used to improve calibration. Often these approaches involve comparing the sensor to known, or calculated reference values. For example, for optical sensors, deep values can be assumed to be below detection limits for downwelling irradiance, chlorophyll, and optical backscatter. These reference values can be used to adjust factory-calibrated dark values. For oxygen, measurements can be compared against climatological values at deep reference levels (Takeshita et. al. 2013). Some platforms are capable of in-air measurement of a known atmospheric oxygen partial pressure. This air-calibration approach is applied to

profiling floats (Johnson et al. 2015, Bittig and Körtzinger 2015, 2017) as well as gliders (Nicholson et al. 2017). Statistical models also are used to predict inorganic carbon and nitrate concentrations at depth (Williams et al. 2016, Carter et. al. 2018, Bittig et al. 2018). Overall, calibration approaches are nuanced, and depend significantly on platform and sensor model.

10.2. Net Community Production

Net community production (NCP) is equal to the gross photosynthesis (GPP) minus the combined autotrophic and heterotrophic respiration (i.e., CR), reflecting the net ecosystem metabolism of both dissolved and particulate organic material (see Section 2.2). While this definition is straight-forward, multiple approaches have been used to quantify NCP providing complementary but often dissimilar information about upper ocean carbon cycling. The general approach is to look at the change over time in the depth-integrated concentration (stock) of a biologically active parameter. When evaluated over a sufficient time period (commonly 1 year), NCP is equivalent to the amount of carbon exported from the depth (or density) horizon evaluated, assuming that the system is in steady state (i.e., there is no secular change in the property used to assess NCP) (Emerson 2014).

The current state of autonomous sensor technology makes it possible to estimate NCP from oxygen (Alkire et al. 2014, Bushinsky and Emerson 2015, Haskell et al. 2019, Huang et al. 2018, Nicholson et al. 2008, Thomalla et al. 2015, Yang et al. 2017), nitrate (NO3: Bif et al. 2019, Haskell et al. 2020, Johnson 2010, Johnson et al. 2017, Plant et al. 2016, Williams et al. 2018), DIC (Fassbender et al. 2016, 2017, Johnson 2010, Körtzinger et al. 2008, Williams et al. 2018) and total alkalinity (TA, Fassbender et al. 2016, 2017, Williams et al. 2018). Chemical sensors are capable of measuring O_2 and NO_3^- directly, however TA is commonly derived from regional TA-salinity relationships or global algorithms (Bittig et al. 2018, Carter et al. 2016, Carter et al. 2018, Lee et al. 2006) while DIC is often computed from TA estimates and measurements of pCO_2 or pH but can also be directly estimated from empirical algorithms (e.g., Bittig et al. 2018). Changes in the stock of a parameter over time, within a specific depth or density interval, reflect the various processes occurring within or influencing that layer of water, some of which are biological in nature. By quantifying all physical processes, the residual term reflects the biological contributions in addition to computational errors.

10.2.1. Underlying Equations

Chemical tracer budgets must account for all upper-ocean fluxes that influence the tracer over the observing period, including physical (Phys), freshwater (FW), and biological (Bio) fluxes. Additionally, DIC and O_2 budgets must account for air-sea exchange processes (Gas). An example equation for the changes in tracer stock over time (t), expressed for DIC, is:

$$\frac{\partial DIC}{\partial t} = \frac{\partial DIC}{\partial t}\Big|_{Gas} + \frac{\partial DIC}{\partial t}\Big|_{Phys} + \frac{\partial DIC}{\partial t}\Big|_{FW} + \frac{\partial DIC}{\partial t}\Big|_{Bio} \quad (10.1)$$

The Gas term accounts for bulk air-sea gas exchange and is parameterized as the difference between observed (obs) and saturated (sat) concentrations (with respect to the atmosphere) of the molecule of interest multiplied by the gas transfer velocity (k), which scales as a function of wind speed (Wanninkhof, 2014).

$$\frac{\partial DIC}{\partial t}\Big|_{Gas} = k([CO_2]_{obs} - [CO_2]_{sat}) \tag{10.2}$$

Observed and saturated concentrations are often calculated from gas partial pressures (e.g., pCO_2 and pO_2) measured in seawater and the atmospheric boundary layer (corrected to the water-vapor-saturated gas partial pressures (Dickson et al. 2007), and the respective solubility constants (Garcia and Gordon 1992, Weiss 1974). When *in situ*, local observations are not available, the wind speed, atmospheric surface pressure, and relative humidity data are retrieved by interpolating reanalysis data to the autonomous asset location. Additionally, the dry air mixing ratio of atmospheric CO_2 can be obtained from NOAA's Marine Boundary Layer dataset (Wanninkhof et al. 2019) while atmospheric surface pO_2 can be calculated using reanalysis data following Bittig and Körtzinger (2015).

Unlike CO_2 (which is highly soluble), the air-sea exchange of O_2 must also account for bubble mediated flux (F_B), which can significantly increase mixed layer O_2 concentrations and leave a lasting (~1 month) signature on the water column (see (Emerson and Bushinsky, 2016) and citations therein).

$$\frac{\partial O_2}{\partial t}\Big|_{Gas} = k([O_2]_{obs} - [O_2]_{sat}) + F_B \tag{10.3}$$

The FW budget term accounts for evaporation and precipitation effects on tracer concentrations based on salinity (Sal) observations, expressed here for DIC:

$$\frac{\partial DIC}{\partial t}\Big|_{FW} = \left(\frac{\partial Sal}{\partial t} - \frac{\partial Sal}{\partial t}\Big|_{Phys}\right) \times \frac{DIC}{Sal}\Big|_{t=0} \tag{10.4}$$

where t = 0 is the DIC to salinity ratio at time zero in the budget integration. The Phys term accounts for tracer supply or removal due to vertical turbulent mixing, as well as vertical advection, expressed here for DIC:

$$\frac{\partial DIC}{\partial t}\Big|_{Phys} = -\left(w + \frac{\partial h}{\partial t}\right)\frac{(DIC_{ML} - DIC_h)}{h} - \frac{1}{h}\left(K_z \frac{\partial DIC}{\partial z}\right)\Big|_h \tag{10.5}$$

where DIC_{ML} is DIC concentration in a mixed layer of depth h, and w, DIC_h, K_z, and $\delta DIC/\delta z$ are the vertical velocity, DIC concentration, eddy diffusivity, and vertical concentration gradient evaluated at the depth of the mixed layer. Horizontal advection and diffusion processes are often omitted, particularly in annual NCP budgets, due to poor constraint on lateral gradients as well as the dominance of vertical processes on seasonal timescales (see discussion below).

After accounting for Gas, FW, and Phys, the residual Bio term (which includes all errors) can be solved by rearranging equation 10.1. For the DIC and TA budgets, the residual biological term reflects both NCP and net calcium carbonate ($CaCO_3$) production.

$$\frac{\partial DIC}{\partial t}\Big|_{Bio} = \frac{\partial DIC}{\partial t}\Big|_{NCP} + \frac{\partial DIC}{\partial t}\Big|_{CaCO_3} \tag{10.6}$$

To differentiate these terms, one must leverage the fact that biological processes influence DIC and TA at well-known stoichiometric ratios. For example, each mole of $CaCO_3$ produced results in

a reduction of one mole of DIC and two moles of TA. Additionally, for organic matter production, one mole of hydrogen phosphate, 18 moles of H^+ and 117 moles of CO_2 are consumed, resulting in a TA increase of 17 moles (Wolf-Gladrow et al. 2007, Anderson and Sarmiento 1994, Brewer and Goldman 1976). Using these relationships and rearranging Eqs. 10.5 and 10.6, one can solve for the DIC and TA budget NCP and $CaCO_3$ terms (Fassbender et al. 2016):

$$\left.\frac{\partial DIC}{\partial t}\right|_{NCP} = \frac{\left.\frac{\partial TA}{\partial t}\right|_{Bio} - 2\left.\frac{\partial DIC}{\partial t}\right|_{Bio}}{-2 + (-17/117)} \tag{10.7}$$

$$\left.\frac{\partial DIC}{\partial t}\right|_{CaCO_3} = \left.\frac{\partial DIC}{\partial t}\right|_{Bio} - \left.\frac{\partial DIC}{\partial t}\right|_{NCP} \tag{10.8}$$

The inclusion of $CaCO_3$ cycling in tracer budget evaluations remains rare (Fassbender et al. 2016, 2017, Williams et al. 2018, Haskell et al. 2020) and provides an integrated (rather than *in situ*) view of $CaCO_3$ production because TA is presently estimated from parameters that are not instantaneously influenced by $CaCO_3$ production (often salinity and temperature). Still, the separation of carbon pools can bring new insight to the role of calcium carbonate minerals in the biological carbon pump (e.g., Marañón et al. 2016).

When networks of chemical sensors are deployed, even more information can be gleaned from tracer budgets (e.g., Johnson 2010, Haskell et al. 2020). For example, by assuming a C:O organic matter conversion ratio of 1.4 (Laws 1991), C:N stoichiometry of 16:117 (Anderson and Sarmiento 1994), and a TA:N stoichiometry of -17:16 (Brewer and Goldman 1976, Wolf-Gladrow et al. 2007), the budgets can be solved in multiple ways to independently deconvolve the $CaCO_3$ and NCP terms. For example, DIC_{NCP} can be determined using the C:O or C:N ratio, which can be subtracted from the overall DIC_{Bio} term to solve for DIC_{CaCO3}:

$$DIC_{CaCO_3} = DIC_{Bio} - (R_{C:O} \times O_{2Bio}) = DIC_{Bio} - (R_{C:N} \times NO^-_{3Bio}) \tag{10.9}$$

Alternatively, TA_{NCP} can be determined using the TA:N ratio to solve for TA_{CaCO3} and DIC_{CaCO3}:

$$TA_{CaCO_3} = 2 \times DIC_{CaCO_3} = TA_{Bio} - (R_{TA:N} \times NO^-_{3Bio}) \tag{10.10}$$

Redundant closing of budgets with different tracer pairings can thus provide quantitative information about potential systematic biases in the tracer methods, which each have different strengths and weaknesses.

10.2.2. Net Community Production Uncertainties

10.2.2.1. Elemental Stoichiometries

A key uncertainty in tracer budget approaches is the use of fixed and often unknown elemental stoichiometries (i.e., $R_{C:O}$, $R_{C:N}$, etc.) for bulk net community production and respiration. With sensor networks, different ratios can be used to convert biological production terms to other elemental quantities, providing some bounds on the error associated with these conversions. For example, the $O_{2\,Bio}$ and $NO_{3^-\,Bio}$ terms provide estimates of net organic matter production that can be converted to units of DIC and compared. Alternatively, the DIC_{NCP} term derived from $O_{2\,Bio}$ can be used with the $NO_{3^-\,NCP}$ term to estimate the C:N ratio of net community metabolism. The recent advent and widespread use of autonomous pH sensors (Martz et al. 2010, Johnson et al. 2016) now makes it

possible to estimate DIC directly (from pH observations and TA estimates), rather than through the C:O (or C:N) conversion, and look at changes in DIC_{NCP} and $NO_{3^- NCP}$ (or $O_{2\,NCP}$) simultaneously to evaluate variability in the C:N (or C:O) ratio over time (Haskell et al. 2020). This is quite useful because most tracer budgets assume a C:N stoichiometry near ~6.6 (Redfield et al. 1963) even though dissolved organic carbon (DOC) production also contributes to NCP and can have a C:N ratio that differs significantly (e.g., DOC $R_{C:N}$ ~10) from Redfield (e.g., Letscher and Moore 2015).

With the advent of more comprehensive sensor networks being deployed on autonomous platforms (e.g., Johnson et al. 2017), upper ocean tracer budgets are becoming more complex and comprehensive. Some investigators are now attempting to differentiate the particulate organic carbon (POC) and dissolved organic carbon (DOC) phases of NCP using solely *in situ* observations on autonomous platforms (Figure 10.2). For example, Alkire et al. (2012) quantified NCP using oxygen and nitrate observations from a Lagrangian profiling float (D'Asaro 2003) in the North Atlantic Ocean. Considering differing elemental stoichiometries for POC and DOC, they estimated the POC and DOC components of NCP. They were then able to subtract the standing stock of POC, derived from float backscattering measurements, from NCP_{POC} term to determine how much of the NCP_{POC} had been exported from the upper ocean during the 1.5-month study period. Similarly, Haskell et al (2020) used nitrate, DIC, and TA budgets to solve for POC, DOC, and $CaCO_3$ production and export for >10 years of biogeochemical profiling float observations in the North Pacific Ocean. The recent combination of nitrate, oxygen, and pH sensors on biogeochemical profiling floats (Johnson et al. 2017), and ongoing efforts with subsurface gliders (Takeshita et al. 2021, Saba et al. 2019), will provide new opportunities to further advance tracer budget methodologies enabling more comprehensive upper ocean carbon cycling studies. In particular, the quantification of all biogenic carbon pools represents a step forward in autonomous carbon cycle analyses that will yield more nuanced understanding of marine ecosystem responses to ocean warming and acidification.

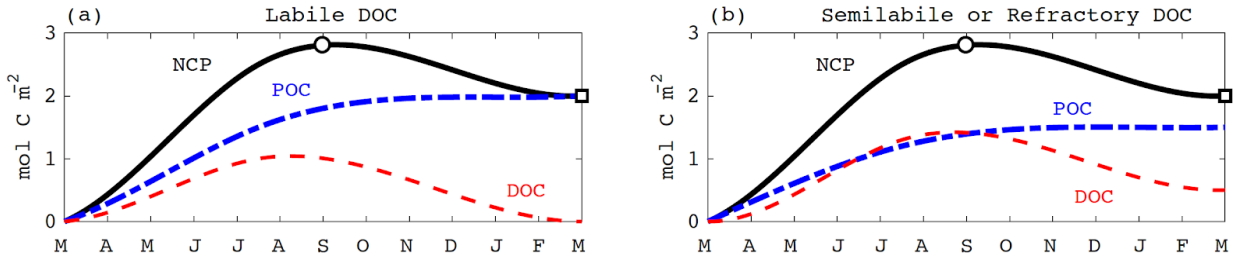

Figure 10.2. Schematic of mixed layer NCP over the course of one year (black line). The blue line shows the POC component of NCP and the red line shows the DOC component of NCP. In the left panel, labile DOC is produced and consumed over the course of the year. In the right panel, a fraction of the DOC produced is recalcitrant and is not remineralized within the year. NCP evaluated from March to September provides a consistent seasonal NCP estimate between scenarios. However, due to heterotrophic respiration of DOC in the later portion of the year, seasonal NCP is not an accurate estimate of annual NCP, which is commonly assumed to be equivalent to the annual export. If the recalcitrant DOC is eventually respired in the upper ocean, it will not contribute to carbon export. These are some of the challenges associated with the omission of DOC cycling in upper ocean carbon budgets, short integration time scales, and the assumption of steady state.

10.2.2.2. Integration Time Scales and Steady State Assumptions

The timescale of integration will determine the dominant physical processes to evaluate or sources of uncertainty in the physical flux estimates if relevant processes are not quantifiable due to lack of appropriate observations. On the shortest scales (~hours-diurnal), wave dynamics, inertial responses to high-frequency atmospheric forcing, convective-driven mixing, and coherent vortices from wave-wind interactions (i.e., Langmuir Circulation) play a dominant role. Atmospheric weather phenomena (on synoptic scales, O(100-1000 km)) and sub-mesoscale ocean dynamics (O(1-10 km), e.g., Levy et al. 2018, Estapa et al. 2015) will introduce variability on scales of a few days. These short-term events can introduce significant variability in physical fluxes and biogeochemical tracers, and if undersampled, produce aliasing effects on long-term means (Monteiro et al. 2015, Whitt et al. 2019). For instance, storm events can lead to short-term deepening of the mixed layer, entraining additional carbon or nutrients into the mixed layer. Such short-term events cannot be estimated from monthly data or averages. The 10-day profiling frequency of most floats will also miss this short-term variability (Xing et al. 2020).

The ocean mesoscale (with spatial scales of O(10-100 km)) introduces variability on sub-seasonal scales of weeks to months. Though mesoscale eddies and the associated geostrophic currents can be estimated from satellite altimetry (i.e., sea surface height anomalies), biogeochemical tracer distributions on these temporal scales are not yet possible from observations at a global scale. Gliders, on the other hand, can return nearly vertical profiles at much higher temporal resolution (~1h) and capture both the high-frequency internal ocean dynamics from submesoscale to mesoscale eddies, as well as influences of atmospheric weather, though glider missions typically only last a few months (i.e., ~3-6 months, Rudnick 2016). Eddies and fronts become a source of uncertainty for physical flux estimates in float-based tracer budgets and can be particularly important during springtime restratification in the midlatitude subtropical gyres (Johnson et al. 2016) or regions with strong horizontal gradients such as western boundary currents. On seasonal to annual scales, seasonal changes in insolation, air-sea buoyancy fluxes and wind forcing (depending on the region) will tend to dominate, but horizontal advection can also be regionally important (e.g., in the Southern Ocean, Rosso et al. 2017).

Practically, in order to use the time-rate of change terms in Eqs.10.1-1.07 it is desirable to conduct work in a Lagrangian reference frame (Alkire et al. 2012, Siegel et al. 2021). Otherwise, difficult-to-resolve lateral advective fluxes and spatial variability can obscure the temporal evolution. When the time-rate of change cannot be determined, often a steady-state assumption is employed by assuming a zero rate of change. Such steady-state estimates can contain significant biases and are most useful when averaged over significant space and time. On annual and longer timescales, the time rate of change term tends to be very small compared to NCP.

10.2.2.3. The Choice of Integration Depth

The depth or density horizon to which upper ocean tracer budgets are integrated often varies depending on the research question of interest. The most common integration depths include the seasonally varying mixed layer (ML), a fixed light level (often the euphotic depth or 1% light level), and the local maximum winter mixed layer. Seasonal ML budgets are often used when observations are limited to the near surface (e.g., moorings) and provide information about the processes influencing air-sea exchange. However, ML budgets do not account for NCP that occurs below the ML in regions of clear waters with deep euphotic zones (e.g., in the subtropical gyres), which can cause an underestimation of total NCP. Additionally, ML budgets do not account for

the fall/winter re-entrainment of biologically respired carbon that may have escaped the warm season mixed layer as particles before being metabolized. Instead, this re-entrained carbon would be interpreted as a physical process, which can lead to an overestimation of NCP. While these two biases are compensating, it is not clear that they are rectified.

Euphotic zone budgets more accurately capture the total net production of biomass in the upper ocean (Buesseler et al. 2020), which provides a constraint on how much carbon is available for export to support mesopelagic food webs. However, quantifying physical contributions to these budgets can be more challenging due to the decoupling of the euphotic depth with the ML depth, which is a physically meaningful horizon at which it is easier to estimate turbulent fluxes. The euphotic depth is also often decoupled from the air-sea exchange interface (i.e., ML) during the warm season, making it more difficult to quantify the biological influence on air-sea gas exchange. Additionally, this horizon is also sensitive to biases caused by seasonal re-entrainment of biologically respired carbon, which can lead to an overestimate of NCP.

The local maximum winter ML is another common depth horizon, which is often preferred in studies targeting questions related to carbon export (Palevsky and Doney 2018). By integrating over this depth horizon, all production and respiration above the export depth is accounted for. However, the production estimate will be lower than the maximum NCP due to the inclusion of deeper depths where net heterotrophy is occurring. This approach therefore provides a lower bound estimate on annual NCP, but a realistic estimate of the amount of carbon exported from the upper ocean annually and thus available for mesopelagic food webs. This horizon is also decoupled from the air-sea exchange interface outside of winter, complicating the quantification of air-sea exchange contributions to the budget.

The depth horizon of integration will also determine the subtleties and uncertainties in the calculation of physical flux terms. Integrating to a fixed depth, implies an estimation of vertical and horizontal advection and turbulent fluxes. An integration to the base of the mixed-layer depth (MLD) should incorporate an assessment of entrainment fluxes due to temporal changes in the MLD, in addition to vertical turbulent diffusion, as well as horizontal advection across a sloping ML (e.g., Levy et al. 2013, Emerson et al. 2008). A depth horizon away from the influence of the seasonally varying surface forcing will minimize errors from vertical diffusion or entrainment. Integration to an isopycnal layer, involves estimates of isopycnal and diapycnal fluxes, which can deviate from horizontal and vertical fluxes in regions where isopycnals outcrop to the surface, e.g., near fronts or eddies.

Due to important differences in the type of information gleaned from tracer budgets evaluated to different integration depths, it is recommended that investigators are very clear about these nuances of their study, justify the choice of integration depth and document associated uncertainties.

10.2.2.4. Air-Sea Exchange Parameterizations

A key source of uncertainty in tracer budgets that include a gaseous component (e.g., O_2 and DIC) comes from the parametrization of air-sea fluxes using a global, bulk equation (Wanninkhof 2014). Oxygen can be particularly challenging, as the air-sea fluxes induced by bubbles and solubility are generally equivalent to or larger than the flux induced by biological activity, particularly during winter and spring (Emerson and Stump 2010, Emerson and Bushinsky 2016). Deconvolving the changes in oxygen caused by physical and biological processes is therefore

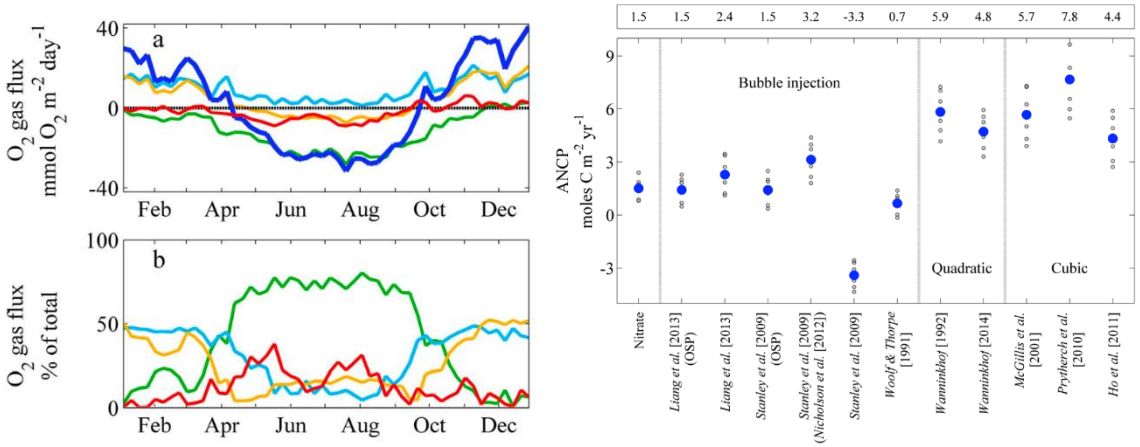

Figure 10.3. From Plant et al. 2016 – left panel, their Fig.9 caption: "(a) Average annual oxygen flux across the air sea boundary using the optimized gas exchange model from Liang et al. [2013]: net (heavy blue), diffusive flux (green), completely dissolving bubble flux (light blue), partially dissolving bubble flux (orange), and oxygen flux due to biology (red). A positive flux is into the ocean. (b) The same as Figure 9 a above but plotted as a percent of the total absolute magnitude.". Right panel, their Figure 8 caption: "Model-derived estimates of ANCP for all years integrated to 35 m depth. Estimates based on nitrate measurements are compared to oxygen-based estimates using various gas flux parameterizations grouped by model type. Individual years are grey. Average of all years are blue and in the top row of values. Parentheses indicate different tunings for the Liang et al. [2013] or Stanley et al. [2009] formulations in this work (OSP) and by Nicholson et al. [2012]."

highly sensitive to the accuracy of the oxygen measurements (Takeshita et al. 2013, Johnson et al. 2015) as well as the gas exchange computation (Emerson and Bushinksy 2016, Plant et al. 2016, Figure 10.3). CO_2 on the other hand is a very soluble gas for which it is generally not necessary to directly parameterize bubbles (Broecker and Peng 1974). However, a different challenge associated with all air-sea flux calculations was recently pointed out by Ho et al. (2020) who identified the potential for significant biases when observations below the sea surface don't capture near surface phenomena such as rain events. This bias was found in underway ship observations and may be more challenging to identify from one autonomous platform. However, presently profiling floats with O_2 air calibration capability do collect O_2 observations all the way to the sea surface, which will make it possible to probe this issue further.

The recent development and commercialization of robust pH sensors for application on autonomous ocean platforms is making it possible to use pH observations and TA estimates to calculate sea surface pCO_2 values with ~3% uncertainty (Williams et al. 2018) and, thus, quantify air-sea CO_2 fluxes. This is now enabling DIC budgets to be constrained on platforms that do not measure pCO_2 directly (e.g., Fassbender et al. 2016, 2017). Additionally, this method has important potential for filling gaps in the global carbon budget (Gray et al. 2018, Bushinsky et al. 2019) and significant effort is being made to validate the methodology in numerous ocean regions (Fay et al. 2018, Takeshita et al. 2019).

10.2.2.5. The impact of ocean physics on NCP estimates

The estimation of physical fluxes requires consideration of the spatio-temporal variability captured by the different types of platforms and frames of reference. Moorings measure ocean variability passing through a fixed location (i.e., from a Eulerian frame of reference). Lagrangian floats are designed to be neutrally buoyant and follow the 3-D movement of water parcels (D'Asaro 2003), providing an ideal frame of reference for tracer budget calculations (Alkire et al.

2012) but they remain specialized platforms that are not widely available. Profiling floats provide quasi-Lagrangian measurements, as they are ballasted to drift along constant pressure rather than isopycnals during their park phase before profiling. Profile data from floats fully capture vertical structure on many scales, though individual floats do not resolve timescales of variability shorter than twice their profile sampling period (~10 days), temporal variability on shorter scales can be assessed statistically on regional/basin to global scales using arrays of floats (e.g., Gille 2012, Carranza et al. 2018). Gliders, like floats, are buoyancy driven but can slowly travel laterally because they have wings. The slow survey speed of gliders (~20 km per day) provides information about spatial variability but it can be difficult to disentangle variations in time versus space unless a coordinated fleet of gliders is deployed (Leonard et al. 2010).

Regardless of integration depth (or density) horizon, any tracer budget analysis requires an assessment of advective and turbulent fluxes in/out of the control volume.

10.2.2.5.1. Advective Fluxes

Though it is possible to estimate large scale currents, both geostrophic and wind-driven components, from satellite altimetry (i.e., sea surface height) and wind data (e.g., from the Ocean Surface Current Analyses Real-time (OSCAR) product; Dohan 2017), estimation of horizontal advective fluxes for biogeochemical tracers is hindered by the lack of information on horizontal gradients in tracer data. Furthermore, the overground speed of gliders is only approximately 20 km per day and a single glider cannot survey quickly enough to capture a synoptic view of ocean variability. Thus, physical advective terms are often neglected from tracer budgets. Horizontal advection can be significant even on short temporal and spatial scales ($\leq$ 1 month, 20 km; Alkire et al. 2014). The role of horizontal advection by geostrophic currents will be important near strong surface currents (e.g., western boundary currents, e.g., Dong and Kelly 2004). Ekman advection, however, can dominate the seasonal cycle of horizontal advection in open ocean areas subject to strong wind forcing (e.g., in the Southern Ocean; Dong et al. 2007). Vertical advection due to wind-driven convergences/divergences in the surface Ekman transport (i.e., Ekman pumping) can be quantified from satellite wind stress curl fields (e.g., Risien and Chelton 2008). Horizontal Ekman advection is typically limited to a fraction of the mixed layer (though in summer, the Ekman depth can be deeper than the MLD), and its effects should be considered if the depth of integration chosen for tracer budget analysis is shallower than the seasonally varying MLD. Ekman pumping effects, however, can be influential below the mixed layer.

10.2.2.5.2. Turbulent Fluxes

In contrast to advective fluxes, biogeochemical tracer gradients are often well constrained by vertical profiles and uncertainty largely stems from estimating the vertical (or diapycnal) eddy diffusivity coefficient (K_z). Turbulent fluxes are often parameterized as an eddy diffusivity coefficient times a gradient (i.e., in analogy to down-gradient molecular diffusion). Turbulence homogenizes properties and momentum cascading energy from large to small eddies. Turbulent billows span scales of order 10-m to mm scales, where they dissipate energy. The most accurate K_Z estimates rely on measurements of turbulent dissipation rates, which require microstructure observations.

Microstructure observations are acquired using very specialized sensors, capable of resolving cm-scale fluctuations of shear or temperature variance, which are typically deployed on free-falling profilers from ships, and require high expertise. Though microstructure sensor technology

is evolving, and reliable estimates are possible from autonomous platforms (e.g., Lien et al. 2016, Nagai et al. 2020, Fer et al. 2014), satellite data transmission remains a challenge and instrument recovery for data acquisition is still necessary. Thus, diapycnal diffusivities from microstructure measurements remain very sparse in the global oceans.

Indirect methods to estimate dissipation rates have leveraged CTD measurements sampled at relatively high vertical resolution (i.e., ~1 m). These so-called fine-scale parameterizations, though more uncertain, allow for estimates of vertical eddy diffusivities, their spatial and seasonal patterns, on regional to global scales (Kunze 2006, Wu et al. 2011, Whalen, et al. 2012). These parameterizations either relate 10-100m scale strain and shear variance from the internal wave field to the associated turbulence dissipation rates (i.e., from breaking internal waves due to shear and convective instabilities), or estimate dissipation rates from the largest scales of turbulent overturns (i.e., Thorpe scales, from m-scale density inversions; Alford and Pinkel 2000, Thompson et al. 2007, Frants et al. 2013). A major shortcoming of any of these dissipation-rate based estimates is that diapycnal eddy diffusivities are related to dissipation rates through the mean stratification indirectly (i.e., $K_\rho = \Gamma\varepsilon/N^2$, Osborn 1972), and thus, the relationship breaks in regions of weak stratification or steep pycnoclines. This implies that estimates of diffusivities in or around the mixed layer, where primary productivity takes place are more challenging.

Approaches to estimating turbulent fluxes across the integration horizon, in order of likely accuracy, include (1) direct measurement of turbulence via microstructure or other measurements; (2) quantitative estimates of temporally/seasonally varying K_z, for example, based on heat and salt budgets (Cronin et al. 2015, Pelland et al. 2017); and (3) use of a constant, canonical value, or values for K_z, such as 10^{-5} m^2 s^{-1} (Bushinsky and Emerson 2015). However, direct or seasonal diffusivity estimates may not always be feasible and in many cases, the uncertainty associated with vertical diffusive flux is smaller than from other sources such as air-sea gas exchange. Uncertainty from these estimates should be propagated through the mass balance equation using a Monte Carlo approach to estimate overall uncertainty in NCP.

Horizontal turbulent fluxes of biogeochemical tracers are difficult to quantify. Though estimates of horizontal eddy diffusivities, $K_н$, are available at the surface from satellite altimetry (Klocker and Abernathy, 2014), surface drifters (Zhurbas et al. 2014), and even for the subsurface from Argo floats (Cole et al. 2015), as well as from combinations of different platforms globally (Roach, et al. 2018); the estimation of turbulent horizontal fluxes of biogeochemical parameters is challenging due to the lack of biogeochemical tracer distributions at the appropriate temporal and spatial scales.

Alternatively, physical flux terms can be estimated from a physical ocean model forced by atmospheric reanalysis data collocated in space and time to float profiles (Plant et al. 2016). This approach requires model optimization (i.e., tunning of model parameters) for the site under consideration to properly capture physical processes. An assessment of the modeled physics can be performed leveraging temperature and salinity data from the CTD sensors on the floats.

10.3. GPP and NPP rate estimates

An emerging approach for calculating ocean primary productivity is to utilize biogeochemical sensor output from platforms such as floats, moorings, or gliders to estimate rates of photosynthetic carbon fixation. Approaches have been applied that estimate either Gross Primary Productivity

(GPP), the total rate of photosynthetic carbon fixation or Net Primary Productivity (NPP), the remaining photosynthetic production of organic carbon by autotrophs once autotrophic respiratory losses are removed.

A variety of approaches have been published in recent years which broadly can be classified into methods that depend on diel dynamics and methods that depend on photosynthetic algorithms. The diel methods rely on changes in stock of carbon, oxygen or nitrogen over the diel period. In this sense, they can be considered analogous to the traditional light/dark bottle incubation approach (see Chapter 5). In contrast, the algorithmic methods employ models of photosynthesis normalized to carbon or chlorophyll, and thus are much more akin to satellite ocean color productivity models (Behrenfeld and Falkowski 1997, Westberry et al. 2008).

10.3.1. Diel productivity approaches

10.3.1.1. Platforms and sensors for diel productivity

Diel PP measurements have been achieved using a range of platforms including gliders, profiling floats, surface drifters and shipboard flow-through systems. For oxygen-based estimates, optode type sensors are preferable due to their proven stability. Slower response optodes are a good match for this application as they are less noisy than fast-response optodes and still have sufficient time to equilibrate with the homogenous mixed layer. The exception would be in a region with very shallow mixed layer depths and a strong oxygen gradient below. For bio-optics, diel cycles have been observed in both particulate beam attenuation (c_p) or b_{bp}. Diel cycles generally are more robust in c_p. Transmissometers, however, are less frequently used on autonomous systems than optical backscatter. Thus, measuring c_p is recommended, when possible, but b_{bp} can be considered as an alternative.

The primary requirement for observing diel cycles is sufficient temporal sampling resolution to resolve the diel cycle. In theory, because the phasing of the 24-hr cycle is known, a priori, the minimum sampling frequency would be twice per day if measurement timing corresponded to near dawn and near dusk. However, this minimal cycling frequency leaves no free degrees of measurement freedom to evaluate the quality of the diel cycle fit or if physical fluxes may have biased an estimate. In general, the 5-8 daily profiles of an open-ocean glider is a more useful minimum sampling frequency. Platforms with higher frequency sampling, such as profiling moorings, Wire Walkers or surface drifters can improve resolution of diel cycles and potentially resolve sub-daily variations, such as morning intensified photosynthetic rates.

10.3.1.2. Diel Productivity: Underlying equations and assumptions

The use of diel signals to estimate primary productivity has a long history in aquatic sciences, appearing in the literature as early as the 1930s (Butcher et al. 1930) and was formalized by Odum (1956). These early applications in rivers were based on large diel changes observed in shallow, riverine systems. Only recently these approaches have been applied to open-ocean systems which often are characterized by small diel amplitudes and are not traditionally samples on diel timescales from research vessels. Such an approach has been demonstrated (Tijssen 1979) using Winkler titrations, yet proved too laborious for common application. The advent of robust sensors on autonomous platforms (Johnson et al. 2009) has greatly expanded the possibility of widespread productivity estimates.

In recent years, autonomous platforms have been used to obtain productivity estimates based on diel signals using oxygen (Barone et al. 2019, Briggs et al. 2018,Nicholson et al. 2015) and bio-

optical estimates of particulate organic carbon (Briggs et al. 2018, Loisel et al. 2011, White et al. 2017). These approaches are based on measuring changes over the diel period in the surface mixed layer and estimate the volumetric primary productivity (GPP_v) averaged over the surface mixed layer. While in theory, the method should be extensible below the mixed layer but still within the euphotic zone, lower rates and higher physical variability in the deep euphotic make it difficult to extract a diel productivity signal. Both approaches estimate GPP_v based on the relationship that the net change in either dissolved oxygen or organic carbon due to biological processes depends on the balance of gross photosynthesis (GPP) and community respiration (CR).

$$\frac{dC}{dt} = GPP(t) + CR(t) \tag{10.11}$$

If one assumes that CR proceeds at an unchanged throughout the 24-hour day, then:

$$GPP_v = \frac{t^{day}}{24}\frac{dC}{dt}^{day} - \frac{dC}{dt}^{night} \tag{10.12}$$

where *tday* is the length of daylight in hours, *dCdtday* represents the rate (per hour) of increase in oxygen or POC during the day due to photosynthetic production, *dCdtnight* is the rate of change due to nighttime respiration. When the photoperiod is close to 12 hours, GPP_v can be approximated as the rate of daytime increase plus twice the rate nighttime decrease. Integrated mixed layer GPP (GPP_{ml}) can then be calculated as the product of GPP_v and mixed layer depth. In practice approaches to calculate oxygen and carbon-based productivity differ and are outlined in detail below.

10.3.1.3. Diel Productivity: Oxygen-based approaches

For dissolved oxygen, several physical processes also can influence dissolved oxygen concentrations, including advective fluxes (F_{adv}), air-sea exchange (F_{as}) and vertical entrainment and mixing (F_v). Eq 10.11 thus can be revised as:

$$\frac{dO_2}{dt} = GPP(t) + CR(t) + F_{Gas} + F_{Phys} \tag{10.13}$$

Generally, air sea flux can be estimated directly, using an air-sea flux parameterization that includes bubble dynamics (Liang et al. 2013, Nicholson et al. 2016) such as described in Sect 10.2.2.4. In general, diel GPP and CR estimates are much less sensitive to air-sea flux estimates than are NCP because of the daily timescale, GPP and CR rates are much higher than air-sea flux (Figure 10.4). Advective and turbulent fluxes are more difficult to estimate (see section 10.2.2.5). The approach to observationally constraining GPP and CR has been to integrate the above equation over the course of a day such that:

$$\frac{dO_2}{dt} = GPP(t) + CR(t) + F_{Gas} + F_{Phys}O_2(t) = \int_{t_o}^{t_1} GPP + CR(t_1 - t_o) + \int_{t_o}^{t_1} F_{Gas} + C \tag{10.14}$$

where C is a constant of integration. If the functional form of GPP is assumed (for example, to be linearly related to PAR, then the theoretical shape of a diel O_2 curve can be statistically fit to observations to estimate the magnitude of GPP and CR as well as the uncertainty of each daily estimate (Barone et al. 2019). A statistical significance test to each daily estimate can help to filter out estimates that are contaminated by physical O_2 fluxes.

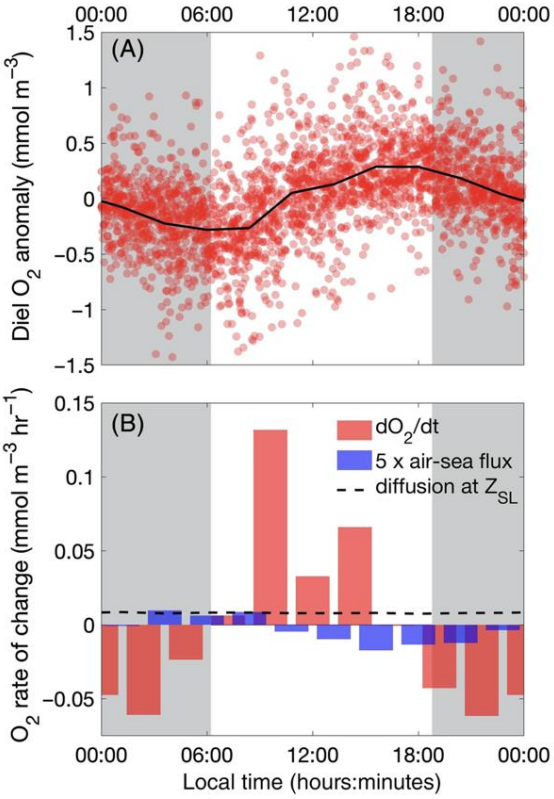

Figure 10.4. Adapted from Barone et al. (2019). These figures represent the aggregate observations from four glider missions. (a) Observed (red dots) and average (black line) O_2 anomaly with respect to the average concentration calculated daily in the surface layer. (b) The average rate of change in O_2 (red bars) and the sea surface flux divided by ZSL (multiplied by 5 to make it visible, blue bars); the dashed line depicts diapycnal O_2 fluxes divided by ZSL assuming $K_z = 10^{-4} m^2 s^{-1}$. The gray background represents the time of day between the average sunset time and the average sunrise time.

Complementary to oxygen-based approaches, diel rates can also be determined from nitrate and DIC (by measuring pCO_2 or pH and assuming alkalinity). This approach has been demonstrated in Monterey Bay (Johnson 2010).

10.3.1.4. Diel Productivity: Optics-based approaches

Diel changes in POC have also been used to calculate GPP using autonomous sensors (Fig 10.5). The most successful applications have used beam transmission rather than backscatter (Briggs et al. 2018, Loisel et al. 2011, White et al. 2017). The first step in this approach is to convert measured beam attenuation to carbon units using a locally appropriate relationship (Sect 10.1.2 above). Once in carbon units, GPP can be estimated using equation 10.12 above.

In interpretation of diel c_p or b_{bp} measurements, several considerations and potential sources of error have been identified. One source of uncertainty is in the conversion of c_p or b_{bp} to carbon concentration. Each responds more sensitively to different size ranges more efficiently and empirical relationships between and c_p or b_{bp} and POC can vary significantly on factors such as community composition, particle size, shape, mineral and chemical composition, etc. (Cetinić

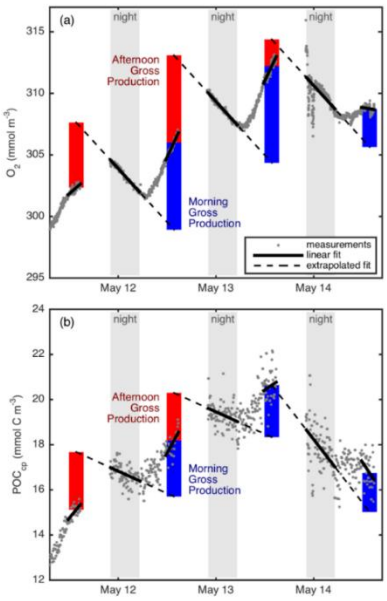

Figure 10.5. (a) Diel O_2 measurements compared to (b) diel POC (derived from c_p) measurements.

et al. 2012, Rasse et al. 2017). While POC-based approaches do not have an air-sea exchange term to contend with, there can be a loss of POC from the mixed layer due to sinking flux. This loss term would lead to a positive bias in the magnitude of CR.

10.3.1.5. Sources of error in Diel Productivity estimates

10.3.1.5.1. Stoichiometry

When estimating GPP from diel O_2, a photosynthetic quotient (PQ) is required to convert to carbon units. Given that GPP is generally much larger than NCP, an O:C ratio for recycled production, such as 1.1 is more appropriate for converting from GPP_{O2} to GPP_C (Laws 1991). Also of note, is diel O_2 methodologies are not sensitive to light dependent reactions such as the Mehler cycle which are 'water-water' reactions with no net oxygen evolution. Thus, a GPP estimate from diel O_2 estimates should be expected to be lower than isotopic approaches (e.g., triple O_2 isotopes, Chapter 7).

10.3.1.5.2. Fluxes due to ocean physics for diel productivity approaches

The diel approach is subject to biases that are introduced by any unresolved fluxes that vary significantly throughout the course of a daily fit. A common example is if the platform crosses a front which results in a large advective flux. Physical processes with a diurnal timescale or less than a day can also interfere with extracting GPP and CR information. For example, mixing can vary on the diel scale due to daily heating, cooling and wind speed variations (Briggs et al. 2018, Nicholson et al. 2015), or surface wave effects. Another physical process that can confound GPP and CR estimates is internal, near-inertial oscillations driven by wind bursts that occur at a frequency near the diurnal period (Gordon et al. 2020), or smaller. The Coriolis frequency is 24 hours at 30°N and 30°S and thus care should be taken when observations are near these latitudes, or towards higher latitudes as the inertial period decreases.

Air-sea gas exchange is also a potential source of bias for O_2-based diel cycles. The rate of air-sea flux is generally small compared to GPP and CR. However, over the timescale of a day, the flux is often consistently in one direction depending on if the water is supersaturated or undersaturated. The air-sea flux term in Eq. X thus can introduce a bias towards GPP or CR. A comparison between GPP and CR requires careful accounting of the air sea flux.

10.3.2. Chlorophyll/irradiance models

Photosynthetic production algorithms offer an alternative approach to estimating rates of ocean productivity. Such approaches are based on photosynthesis versus irradiance relationships and generally have been translated from ocean color remote sensing community and have applied algorithms designed for remote sensed measurements (Behrenfeld et al. 2005, Behrenfeld and Falkowski 1997, Westberry et al. 2008) to *in situ*, sensor-based measurements. Autonomous platforms have the advantage, compared to ocean color remote sensing, of resolving the vertical structure of parameters including chlF, bbp and PAR. Rather than inferring the vertical structure of these parameters from surface properties as satellite algorithms do, profiles of relevant properties can be directly measured. This can result in a simplified application of remote algorithms in which equations to infer vertical structure are replaced by direct observations. These remote sensing approaches predict net primary productivity using quasi-empirical algorithms developed based upon laboratory and field observations of phytoplankton physiology. These can broadly be divided into chlorophyll-based algorithms, such as VGPM and carbon-based algorithms such CbPM.

10.3.2.1. Chlorophyll-based NPP

A chlorophyll-based NPP algorithm fundamentally quantifies net photosynthetic production as the product of chlorophyll concentration and chlorophyll-specific photosynthetic rate, which is parameterized as a function of environmental conditions, including irradiance (*E*), temperature (*T*), day length (t_{day}). For example, the VGPM model seeks to integrate the following equation from the surface to the base of the euphotic zone

$$NPP = \int_0^{z_{eu}} \left(Chl(z) \times P^b_{opt}(z) \times t_{day}\right) dz \tag{10.15}$$

But is limited to surface properties as inputs available via remote sensing.

$$NPP = Chl_{(z=0)} P^b_{opt_{(z=0)}} \times t_{day} \times f(PAR) \times z_{eu} \tag{10.16}$$

where f(par) is the fractional relationship between integrated NPP and maximum NPP if optimal rates (pb_opt) were achieved from surface to z_{eu}. The pb_opt term is a function of temperature and accounts both for direct temperature dependencies of metabolic rates as well as nutrient stress that correlates with higher sea surface temperature. f(par) is an empirical function of surface par, while z_{eu} is based on an empirical relationship to surface chlorophyll (Morel and Berthon 1989).

A profiling autonomous system with optical sensors for chlorophyll and PAR can in theory directly quantify the parameters needed to us equation 10.x and avoid the assumptions and empirical equations that are required to arrive at equation 10.x because chlorophyll profiles and z_{eu} can be measured directly and thus potentially can improve upon uncertainties inherent to remote

sensing algorithms (Jacox et al. 2015). For example, a chlorophyll-based in-situ model was used to estimated NPP from a Seaglider using vertical profiles of irradiance and chlorophyll (Hemsley at al. 2015).

Applying this approach requires attention to several potential pitfalls. The first is the quality of chlorophyll and irradiance measurements. For chlorophyll, fluorometers measure chlorophyll fluorescence, often excited at 470 nm. There is significant variability in converting chlorophyll fluorescence to chlorophyll a concentration based on phytoplankton community structure and physiology (Roesler et al. 2017). Furthermore, non-photochemical quenching lowers quantum yield and contaminates observations during daytime in the upper 10s of meters (Sachmann et al. 2008). Accurately measuring downwelling irradiance and/or PAR is also a challenge on a platform such as a glider and measurements must be corrected for sensor orientation while profiling. Profiles often are not coordinated to local noon, so adjustments for time of day are also necessary.

10.3.2.2. Carbon-based NPP

Carbon-based algorithms, particularly CbPM (Behrenfeld et al. 2005, Westberry et al. 2008), have been applied to estimate NPP from profiling floats (Estapa et al. 2019, Yang et al. 2021). Carbon based algorithms are dependent on equating NPP to the product of phytoplankton carbon stock (C_{phyto}) and specific growth rate (μ):

$$NPP(z) = C_{phyto}(z) \times \mu(z), \text{ where } \mu = f(Chl, C_{phyto}, I, T, t_{day}, \dots) \quad (10.17)$$

Float-based CbPM NPP estimates are somewhat simpler than the full remote sensing algorithm because directly measured profiles of chlorophyll and C_{phyto} and irradiance are used. However, most applications on autonomous platforms to date have been on systems that do not include direct measurements of downwelling irradiance (I). In these cases, surface irradiance from remote sensing products together with chlorophyll-dependent models of diffuse attenuation coefficient (K_d) to calculate irradiance at depth (Estapa et al. 2019, Morel and Maritorena 2001). Validation of Argo float based NPP against ^{14}C PP incubations in the North Atlantic indicate promising, yet mixed results, suggesting the potential for future improvement in in situ NPP algorithms (Yang et al. 2021).

10.4. Recommendations and Future Outlook

Primary productivity estimation approaches using biogeochemical sensor observations from autonomous platforms are rapidly developing. A range of methods from mass balances of carbon, oxygen, and nitrogen, to diel fitting and bio-optical algorithms are targeting a range of metabolic rates, including GPP, NPP and NCP. Due to the diversity of sensors, platforms and strategies used to estimate these rates, we provide generalized recommendations that investigators should keep in mind.

(1) Robust results require the utmost care be taken to calibrate sensors following platform-specific QC best practices. Often this may optimally require collection of discrete samples (POC, O_2, HPLC, etc.) in order to calibrate and validate sensor accuracy.

(2) When applying any of the outlined methods, it is critical to consider the specific study setting and identify the most significant sources of uncertainty. For mass balance approaches, this may include, for example, air-sea flux, or lateral advection. Likewise for optical approaches,

relationships for the conversion of optical properties to more ecologically relevant quantities such as C_{phyto} and Chlorophyll *a* involve inherent uncertainties. Total uncertainty should be reported using Monte Carlo simulation, or other methods.

(3) Governing equations and any assumptions should be clearly documented, including if any mass balance terms were assumed to be zero (e.g., steady-state assumption, or neglecting physical flux terms).

(4) Because methods are not standardized, we recommend archiving and sharing both raw observational datasets as well as code to provide reproducible workflows.

We anticipate that quantification of primary productivity from in situ sensor-based observations will continue to mature and methodologies will become more standardized. Growing observing systems such as Biogeochemical Argo and other multiplatform observing systems have the potential to quantify rates of productivity in situ, on regional to global scales. The merging of in situ observations with remotely sensed ocean color (Bisson et al. 2021, Sauzède et al. 2016) and numerical biogeochemistry and ecosystem models (Wang et al. 2020) could fuel a new generation of global-scale ocean primary productivity products.

10.5. References

Alford, M. H., & Pinkel, R. (2020). Observations of Overturning in the Thermocline: The Context of Ocean Mixing. Journal of Physical Oceanography, 30(5), 805–832. https://doi.org/10.1175/1520-0485(2000)030<0805:oooitt>2.0.co;2

Alkire, M. B. et al. (2012), Estimates of net community production and export using high-resolution, Lagrangian measurements of O2, NO3□, and POC through the evolution of a spring diatom bloom in the North Atlantic, *Deep-Sea Research Part I*, *64*(C), 157–174, doi:10.1016/j.dsr.2012.01.012.

Alkire, M. B., Lee, C., D'Asaro, E., Perry, M. J., Briggs, N., Cetinić, I. and Gray, A. (2014). Net community production and export from Seaglider measurements in the North Atlantic after the spring bloom, J. Geophys. Res. Oceans, 119(9), 6121–6139, doi:10.1002/2014JC010105.

Anderson, L. A. and Sarmiento, J. L. (1994). Redfield ratios of remineralization determined by nutrient data analysis, Glob. Biogeochem. Cycles, 8(1), 65–80, doi:10.1029/93GB03318.

Arteaga, L. A., Boss, E., Behrenfeld, M. J., Westberry, T. K., & Sarmiento, J. L. (2020). Seasonal modulation of phytoplankton biomass in the Southern Ocean. Nature Communications, 1–10. https://doi.org/10.1038/s41467-020-19157-2.

Bakker, D. C., Pfeil, B., Landa, C. S., Metzl, N., O'brien, K. M., Olsen, A., ... & Xu, S. (2016). A multi-decade record of high-quality fCO 2 data in version 3 of the Surface Ocean CO 2 Atlas (SOCAT). Earth System Science Data, 8(2), 383-413.

Barone, B., Nicholson, D., Ferrón, S., Firing, E. and Karl, D. (2019). The estimation of gross oxygen production and community respiration from autonomous time-series measurements in the oligotrophic ocean, Limnol. Oceanogr. Methods, 17(12), 650–664, doi:10.1002/lom3.10340.

Behrenfeld, M. J. and Falkowski, P. G. (1997). Photosynthetic rates derived from satellite-based chlorophyll concentration, Limnol. Oceanogr., 42(1), 1–20, doi:10.2307/2838857.

Behrenfeld, M. J., Boss, E., Siegel, D. A. and Shea, D. M. (2005). Carbon-based ocean productivity and phytoplankton physiology from space, Glob. Biogeochem. Cycles, 19(1), GB1006, doi:10.1029/2004GB002299.

Bif, M. B., Siqueira, L. and Hansell, D. A. (2019). Warm Events Induce Loss of Resilience in Organic Carbon Production in the Northeast Pacific Ocean, Glob. Biogeochem. Cycles, 33(9), 1174–1186, doi:10.1029/2019GB006327.

Bisson, K. M., Boss, E., Werdell, P. J., Ibrahim, A., and Behrenfeld, M. J. (2021). Particulate Backscattering in the Global Ocean: A Comparison of Independent Assessments, Geophys. Res. Lett., 48, e2020GL090909, https://doi.org/10.1029/2020GL090909.

Bittig, H. C. and Körtzinger, A. (2015). Tackling Oxygen Optode Drift: Near-Surface and In-Air Oxygen Optode Measurements on a Float Provide an Accurate *in situ* Reference J. Atmospheric Ocean. Technol., 32(8), 1536–1543, doi:10.1175/JTECH-D-14-00162.1.

Bittig, H. C., & Körtzinger, A. (2017). Update on response times, in-air measurements, and in situ drift for oxygen optodes on profiling platforms. Ocean Science, 13(1), 1-11.

Bittig, H. C., Steinhoff, T., Claustre, H., Fiedler, B., Williams, N. L., Sauzède, R., Körtzinger, A. and Gattuso, J.-P. (2018). An Alternative to Static Climatologies: Robust Estimation of Open Ocean CO2 Variables and Nutrient Concentrations From T, S, and O2 Data Using Bayesian Neural Networks, Front. Mar. Sci., 5, doi:10.3389/fmars.2018.00328.

Bittig, H. C., Maurer, T. L., Plant, J. N., Schmechtig, C., Wong, A. P., Claustre, H., ... & Xing, X. (2019). A BGC-Argo guide: Planning, deployment, data handling and usage. Frontiers in Marine Science, 6, 502.

Boss, E., Guidi, L., Richardson, M. J., Stemmann, L., Gardner, W., Bishop, J. K. B., Anderson, R. F. and Sherrell, R. M. (2015). Optical techniques for remote and in-situ characterization of particles pertinent to GEOTRACES, Prog. Oceanogr., 133, 43–54, doi:10.1016/j.pocean.2014.09.007.

Boss, E., Haëntjens, N., Ackleson, S. G., Balch, B., Chase, A., Dall'Olmo, G., ... & Westberry, T. (2019). IOCCG Ocean Optics and Biogeochemistry Protocols for Satellite Ocean Colour Sensor Validation Inherent Optical Property Measurements and Protocols: Best Practices for the Collection and Processing of Ship-Based Underway Flow-Through Optical Data (v4. 0). IOCCG Ocean Optics and Biogeochemistry Protocols for Satellite Ocean Colour Sensor Validation.

Boss, E., Waite, A. M., Uitz, J., Acinas, S. G., Sosik, H. M., Fennel, K., ... & Karp-Boss, L. (2020). Recommendations for plankton measurements on the GO-SHIP program with relevance to other sea-going expeditions. SCOR Working Group 154 GO-SHIP Report.

Brewer, P. G., & Goldman, J. C. (1976). Alkalinity changes generated by phytoplankton growth 1. Limnology and Oceanography, 21(1), 108-117.

Briggs, N., Perry, M. J., Cetinić, I., Lee, C., D'Asaro, E., Gray, A. M., & Rehm, E. (2011). High-resolution observations of aggregate flux during a sub-polar North Atlantic spring bloom. Deep Sea Research Part I: Oceanographic Research Papers, 58(10), 1031-1039.

Briggs, N., Guðmundsson, K., Cetinić, I., D'Asaro, E., Rehm, E., Lee, C. and Perry, M. J. (2018). A multi-method autonomous assessment of primary productivity and export efficiency in the springtime North Atlantic, Biogeosciences, 15(14), 4515–4532, doi:https://doi.org/10.5194/bg-15-4515-2018.

Buesseler, K. O., Boyd, P. W., Black, E. E., & Siegel, D. A. (2020). Metrics that matter for assessing the ocean biological carbon pump. *PNAS*, 1–9. https://doi.org/10.1073/pnas.1918114117

Bushinsky, S. M. and Emerson, S. (2015). Marine biological production from *in situ* oxygen measurements on a profiling float in the subarctic Pacific Ocean, Glob. Biogeochem. Cycles, 29(12), 2015GB005251, doi:10.1002/2015GB005251.

Bushinsky, S. M., & Emerson, S. R. (2018). Biological and physical controls on the oxygen cycle in the Kuroshio Extension from an array of profiling floats. Deep Sea Research Part I: Oceanographic Research Papers, 141, 51-70.

Bushinsky, S. M., Takeshita, Y., & Williams, N. L. (2019). Observing Changes in Ocean Carbonate Chemistry: Our Autonomous Future. Current Climate Change Reports, 5(3), 207–220. https://doi.org/10.1007/s40641-019-00129-8

Butcher, B. W., Pentelow, F. T. K. and Woodley, J. W. A. (1930). Variations in Composition of River Waters, Int. Rev. Gesamten Hydrobiol. Hydrogr., 24(1–2), 47–80, doi:10.1002/iroh.19300240104.

Carter, B. R., Williams, N. L., Gray, A. R. and Feely, R. A. (2016). Locally interpolated alkalinity regression for global alkalinity estimation, Limnol. Oceanogr. Methods, 14(4), 268–277, doi:10.1002/lom3.10087.

Carter, B. R., Feely, R. A., Williams, N. L., Dickson, A. G., Fong, M. B., & Takeshita, Y. (2018). Updated methods for global locally interpolated estimation of alkalinity, pH, and nitrate. Limnology and Oceanography: Methods, 16(2), 119-131.

Carranza, M. M., Gille, S. T., Franks, P. J. S., Johnson, K. S., Pinkel, R., & Girton, J. B. (2018). When Mixed Layers Are Not Mixed. Storm-Driven Mixing and Bio-optical Vertical Gradients in Mixed Layers of the Southern Ocean. *Journal of Geophysical Research: Oceans*, *123*(10), 7264–7289. https://doi.org/10.1029/2018jc014416

Cetinić, I., Perry, M. J., Briggs, N. T., Kallin, E., D'Asaro, E. A. and Lee, C. M. (2012). Particulate organic carbon and inherent optical properties during 2008 North Atlantic Bloom Experiment, J. Geophys. Res. Oceans, 117(C6), C06028, doi:10.1029/2011JC007771, 2012.

Chai, F., Johnson, K. S., Claustre, H., Xing, X., Wang, Y., Boss, E., et al. (2020). Monitoring ocean biogeochemistry with autonomous platforms. Nature Reviews Earth & Environment, 1(6), 315–326. https://doi.org/10.1038/s43017-020-0053-y

Chavez, F. P., Sevadjian, J., Wahl, C., Friederich, J. and Friederich, G. E. (2017). Measurements of pCO2 and pH from an autonomous surface vehicle in a coastal upwelling system, Deep Sea Res. Part II Top. Stud. Oceanogr., doi:10.1016/j.dsr2.2017.01.001.

Claustre, H., Johnson, K. S. and Takeshita, Y. (2020). Observing the Global Ocean with Biogeochemical-Argo, Annu. Rev. Mar. Sci., 12(1), 23–48, doi:10.1146/annurev-marine-010419-010956.

Cole, S. T., C. Wortham, E. Kunze, and B. Owens (2015), Eddy stirring and horizontal diffusivity from Argo float observations: Geographic and depth variability, *Geophys. Res. Lett.*, *42*, *3989–3997, doi:10.1002/2015GL063827.*

Cronin, M. F., Pelland, N. A., Emerson, S. R., and Crawford, W. R. (2015). Estimating diffusivity from the mixed layer heat and salt balances in the North Pacific. J. Geophys. Res. Oceans 120, 7346–7362. doi: 10.1002/2015JC011010

D'Asaro, E. (2003). Performance of autonomous lagrangian floats. J. Atmos. Oceanic Technol. 20, 896–911.

Dickson, A. G., Sabine, C. L. and Christian, J. R. (2007). Guide to Best Practices for Ocean CO2 Measurements., Report, North Pacific Marine Science Organization. [online] Available from: http://www.oceandatapractices.net/handle/11329/249.

Dohan, K. (2017). Ocean surface currents from satellite data. Journal of Geophysical Research: Oceans, 122(4), 2647–2651. https://doi.org/10.1002/2017jc012961

Dong, S., & Kelly, K. A. (2004). Heat Budget in the Gulf Stream Region: The Importance of Heat Storage and Advection. Journal of Physical Oceanography, 34(5), 1214–1231. https://doi.org/10.1175/1520-0485(2004)034<1214:hbitgs>2.0.co;2

Dong, S., Gille, S. T., & Sprintall, J. (2007). An Assessment of the Southern Ocean Mixed Layer Heat Budget. Journal of Climate, 20(17), 4425–4442. https://doi.org/10.1175/jcli4259.1

Emerson, S. (2014). Annual net community production and the biological carbon flux in the ocean, Glob. Biogeochem. Cycles, 28(1), 2013GB004680, doi:10.1002/2013GB004680, 2014.

Emerson, S. and Bushinsky, S. (2016). The role of bubbles during air-sea gas exchange, J. Geophys. Res. Oceans, doi:10.1002/2016JC011744.

Emerson, S. and Stump, C. (2010) Net biological oxygen production in the ocean—II: Remote *in situ* measurements of O2 and N2 in subarctic pacific surface waters, Deep Sea Res. Part Oceanogr. Res. Pap., 57(10), 1255–1265, doi:10.1016/j.dsr.2010.06.001.

Emerson, S., Stump, C., & Nicholson, D. (2008). Net biological oxygen production in the ocean: Remote in situ measurements of O 2and N 2in surface waters. *Global Biogeochemical Cycles*, *22*(3), n/a-n/a. https://doi.org/10.1029/2007gb003095

Estapa, M. L., D. A. Siegel, K. O. Buesseler, R. H. R. Stanley, M. W. Lomas, and N. B. Nelson (2015), Decoupling of net community and export production on submesoscales in the Sargasso Sea, Global Biogeochem. Cycles, 29, 1266–1282, doi:10.1002/2014GB004913.

Estapa, M. L., Feen, M. L. and Breves, E. (2019). Direct Observations of Biological Carbon Export From Profiling Floats in the Subtropical North Atlantic, Glob. Biogeochem. Cycles, 33(3), 282–300, doi:10.1029/2018GB006098.

Fassbender, A. J., Sabine, C. L. and Cronin, M. F. (2016). Net community production and calcification from 7 years of NOAA Station Papa Mooring measurements, Glob. Biogeochem. Cycles, 30(2), 250–267, doi:10.1002/2015GB005205.

Fassbender, A. J., Sabine, C. L., Cronin, M. F. and Sutton, A. J. (2017). Mixed-layer carbon cycling at the Kuroshio Extension Observatory, Glob. Biogeochem. Cycles, 31(2), 272–288, doi:10.1002/2016GB005547.

Fay, A. R., Lovenduski, N. S., McKinley, G. A., Munro, D. R., Sweeney, C., Gray, A. R., ... & Williams, N. (2018). Utilizing the Drake Passage Time-series to understand variability and change in subpolar Southern Ocean pCO2. Biogeosciences, 15(12), 3841-3855.

Fer, I., Peterson, A. K., & Ullgren, J. E. (2014). Microstructure Measurements from an Underwater Glider in the Turbulent Faroe Bank Channel Overflow. Journal of Atmospheric and Oceanic Technology, 31(5), 1128–1150. https://doi.org/10.1175/jtech-d-13-00221.1

Frants, M., Damerell, G. M., Gille, S. T., Heywood, K. J., MacKinnon, J., & Sprintall, J. (2013). An Assessment of Density-Based Finescale Methods for Estimating Diapycnal Diffusivity in the Southern Ocean. Journal of Atmospheric and Oceanic Technology, 30(11), 2647–2661. https://doi.org/10.1175/jtech-d-12-00241.1

Garcia, H. E. and Gordon, L. I. (1992). Oxygen solubility in seawater: Better fitting equations, Limnol. Oceanogr., 37(6), 1307–1312, doi:10.4319/lo.1992.37.6.1307.

Gille, S. T. (2012). Diurnal variability of upper ocean temperatures from microwave satellite measurements and Argo profiles. *Journal of Geophysical Research*, *117*(C11). https://doi.org/10.1029/2012jc007883

Gordon, C., Fennel, K., Richards, C., Shay, L. K. and Brewster, J. K. (2020). Can ocean community production and respiration be determined by measuring high-frequency oxygen profiles from autonomous floats?, Biogeosciences Discuss., 1–24, doi:https://doi.org/10.5194/bg-2020-119.

Gray, A. R., Johnson, K. S., Bushinsky, S. M., Riser, S. C., Russell, J. L., Talley, L. D., ... & Sarmiento, J. L. (2018). Autonomous biogeochemical floats detect significant carbon dioxide outgassing in the high-latitude Southern Ocean. Geophysical Research Letters, 45(17), 9049-9057.

Haëntjens, N., Boss, E. & Talley, L. D. (2017). Revisiting ocean color algorithms for chlorophyll a and particulate organic carbon in the Southern Ocean using biogeochemical floats. J. Geophys. Res.: Oceans https://doi.org/10.1002/ 2017JC012844.

Haskell, W. Z., Hammond, D. E., Prokopenko, M. G., Teel, E. N., Seegers, B. N., Ragan, M. A., Rollins, N. and Jones, B. H. (2019). Net Community Production in a Productive Coastal Ocean From an Autonomous Buoyancy-Driven Glider, J. Geophys. Res. Oceans, 124(6), 4188–4207, doi:10.1029/2019JC015048.

Haskell, W. Z., Fassbender, A. J., Long, J. S., & Plant, J. N. (2020). Annual net community production of particulate and dissolved organic carbon from a decade of biogeochemical profiling float observations in the Northeast Pacific. Global Biogeochemical Cycles, 34(10), e2020GB006599.

Hemsley, V. S., Smyth, T. J., Martin, A. P., Frajka-Williams, E., Thompson, A. F., Damerell, G., & Painter, S. C. (2015). Estimating oceanic primary production using vertical irradiance and chlorophyll profiles from ocean gliders in the North Atlantic. Environmental science & technology, 49(19), 11612-11621.

Ho, D. T., & Schanze, J. J. (2020). Precipitation-Induced Reduction in Surface Ocean pCO2: Observations From the Eastern Tropical Pacific Ocean. Geophysical Research Letters, 47(15), e2020GL088252.

Huang, Y., Yang, B., Chen, B., Qiu, G., Wang, H. and Huang, B. (2018). Net community production in the South China Sea Basin estimated from *in situ* O2 measurements on an Argo profiling float, Deep Sea Res. Part Oceanogr. Res. Pap., 131, 54–61, doi:10.1016/j.dsr.2017.11.002.

Jacox, M. G., Edwards, C. A., Kahru, M., Rudnick, D. L., & Kudela, R. M. (2015). The potential for improving remote primary productivity estimates through subsurface chlorophyll and irradiance measurement. Deep Sea Research Part II: Topical Studies in Oceanography, 112, 107-116.

Johnson, K. S., Berelson, W. M., Boss, E. S., Chase, Z., Claustre, H., Emerson, S. R., Gruber, N., Kortzinger, A., Perry, M. J. and Riser, S. C. (2009). Observing biogeochemical cycles at global scales with profiling floats and gliders: Prospects for a global array, J. Oceanogr., 22(3).

Johnson, K. S. (2010). Simultaneous measurements of nitrate, oxygen, and carbon dioxide on oceanographic moorings: Observing the Redfield ratio in real time, Limnol. Oceanogr., 55(2), 615–627, doi:10.4319/lo.2010.55.2.0615.

Johnson, K. S., Plant, J. N., Riser, S. C., & Gilbert, D. (2015). Air oxygen calibration of oxygen optodes on a profiling float array. Journal of Atmospheric and Oceanic Technology, 32(11), 2160-2172.

Johnson, L., C. M. Lee, and E. A. D'Asaro (2016), Global Estimates of Lateral Springtime Restratification, *Journal of Physical Oceanography*, *46*(5), 1555–1573, doi:10.1175/JPO-D-15-0163.1.

Johnson, K. S., Plant, J. N., Coletti, L. J., Jannasch, H. W., Sakamoto, C. M., Riser, S. C., ... & Sarmiento, J. L. (2017a). Biogeochemical sensor performance in the SOCCOM profiling float array. Journal of Geophysical Research: Oceans, 122(8), 6416-6436.

Johnson, K. S., Plant, J. N., Dunne, J. P., Talley, L. D. and Sarmiento, J. L. (2017b). Annual nitrate drawdown observed by SOCCOM profiling floats and the relationship to annual net community production, J. Geophys. Res. Oceans, 122(8), 6668–6683, doi:10.1002/2017JC012839.

Klocker, A., & Abernathey, R. (2014). Global patterns of mesoscale eddy properties and diffusivities. Journal of Physical Oceanography, 44(3), 1030-1046.

Körtzinger, A., Send, U., Lampitt, R. S., Hartman, S., Wallace, D. W. R., Karstensen, J., Villagarcia, M. G., Llinás, O. and DeGrandpre, M. D. (2008). The seasonal pCO_2 cycle at 49°N/16.5°W in the northeastern Atlantic Ocean and what it tells us about biological productivity, J. Geophys. Res. Oceans, 113(C4), C04020, doi:10.1029/2007JC004347.

Kunze, E., Firing, E., Hummon, J. M., Chereskin, T. K., & Thurnherr, A. M. (2006). Global Abyssal Mixing Inferred from Lowered ADCP Shear and CTD Strain Profiles. Journal of Physical Oceanography, 36(8), 1553–1576. https://doi.org/10.1175/jpo2926.1

Laws, E. A. (1991). Photosynthetic quotients, new production and net community production in the open ocean, Deep-Sea Res, 38(1), 143–167.

Lee, K., Tong, L. T., Millero, F. J., Sabine, C. L., Dickson, A. G., Goyet, C., Park, G.-H., Wanninkhof, R., Feely, R. A. and Key, R. M. (2006). Global relationships of total alkalinity

with salinity and temperature in surface waters of the world's oceans, Geophys. Res. Lett., 33(19), doi:10.1029/2006GL027207.

Lee, C., Paluszkiewicz, T., Rudnick, D., Omand, M. and Todd, R. (2017). Autonomous Instruments Significantly Expand Ocean Observing: An Introduction to the Special Issue, Oceanography, 30(2), 15–17, doi:10.5670/oceanog.2017.211.

Leonard, N. E., Paley, D. A., Davis, R. E., Fratantoni, D. M., Lekien, F., & Zhang, F. (2010). Coordinated control of an underwater glider fleet in an adaptive ocean sampling field experiment in Monterey Bay. *Journal of Field Robotics*, *27*(6), 718–740. https://doi.org/10.1002/rob.20366

Letscher, R. T., & Moore, J. K. (2015). Preferential remineralization of dissolved organic phosphorus and non-Redfield DOM dynamics in the global ocean: Impacts on marine productivity, nitrogen fixation, and carbon export. Global Biogeochemical Cycles, 29(3), 325-340.

Levy, M., Bopp, L., Karleskind, P., Resplandy, L., Ethe, C., & Pinsard, F. (2013). Physical pathways for carbon transfers between the surface mixed layer and the ocean interior. *Global Biogeochemical Cycles*, *27*(4), 1001–1012. https://doi.org/10.1002/gbc.20092

Lévy, M., Franks, P. J., & Smith, K. S. (2018). The role of submesoscale currents in structuring marine ecosystems. Nature communications, 9(1), 1-16.

Liang, J.-H., Deutsch, C., McWilliams, J. C., Baschek, B., Sullivan, P. P. and Chiba, D. (2013). Parameterizing bubble-mediated air-sea gas exchange and its effect on ocean ventilation, Glob. Biogeochem. Cycles, 27(3), 894–905, doi:10.1002/gbc.20080.

Lien, R.-C., Sanford, T. B., Carlson, J. A., & Dunlap, J. H. (2016). Autonomous microstructure EM-APEX floats. *Methods in Oceanography*, *17*, 282–295. https://doi.org/10.1016/j.mio.2016.09.003

Loisel, H., Vantrepotte, V., Norkvist, K., Mériaux, X., Kheireddine, M., Ras, J., Pujo-Pay, M., Combet, Y., Leblanc, K., Dall'Olmo, G., Mauriac, R., Dessailly, D. and Moutin, T. (2011). Characterization of the bio-optical anomaly and diurnal variability of particulate matter, as seen from scattering and backscattering coefficients, in ultra-oligotrophic eddies of the Mediterranean Sea, Biogeosciences, 8(11), 3295–3317, doi:https://doi.org/10.5194/bg-8-3295-2011.

Lucas, A. J., Pitcher, G. C., Probyn, T. A., & Kudela, R. M. (2013). The influence of diurnal winds on phytoplankton dynamics in a coastal upwelling system off southwestern Africa. Deep Sea Research Part II …, 1–13. https://doi.org/10.1016/j.dsr2.2013.01.016

Maranón, E., Balch, W. M., Cermeno, P., González, N., Sobrino, C., Fernández, A., ... & Pelejero, C. (2016). Coccolithophore calcification is independent of carbonate chemistry in the tropical ocean. Limnology and Oceanography, 61(4), 1345-1357.

Monteiro, P., L. Gregor, and M. Levy (2015), Intraseasonal variability linked to sampling alias in air-sea CO2 fluxes in the Southern Ocean, *Geophysical Research Letters*, doi:10.1002/(ISSN)1944-8007.

Morel, A., & Berthon, J. F. (1989). Surface pigments, algal biomass profiles, and potential production of the euphotic layer: Relationships reinvestigated in view of remote-sensing applications. Limnology and oceanography, 34(8), 1545-1562.

Morel, A. and Maritorena, S. (2001). Bio-optical properties of oceanic waters: A reappraisal, J. Geophys. Res. Oceans, 106(C4), 7163–7180, doi:10.1029/2000JC000319, 2001.

Nagai, T., Quintana, G. M. R., Gómez, G. S. D., Hashihama, F., & Komatsu, K. (2021). Elevated turbulent and double-diffusive nutrient flux in the Kuroshio over the Izu Ridge and in the Kuroshio Extension. *Journal of Oceanography*, *77*(1), 55–74. https://doi.org/10.1007/s10872-020-00582-2

Nicholson, D., Emerson, S. and Eriksen, C. C. (2008) Net community production in the deep euphotic zone of the subtropical North Pacific gyre from glider surveys, Limnol. Oceanogr., 53(5part2), 2226–2236, doi:10.4319/lo.2008.53.5_part_2.2226.

Nicholson, D. P., Stanley, R. H., Barkan, E., Karl, D. M., Luz, B., Quay, P. D., & Doney, S. C. (2012). Evaluating triple oxygen isotope estimates of gross primary production at the Hawaii Ocean Time-series and Bermuda Atlantic Time-series Study sites. Journal of Geophysical Research: Oceans, 117(C5).

Nicholson, D. P., Wilson, S. T., Doney, S. C. and Karl, D. M. (2015). Quantifying subtropical North Pacific gyre mixed layer primary productivity from Seaglider observations of diel oxygen cycles, Geophys. Res. Lett., 42(10), 2015GL063065, doi:10.1002/2015GL063065.

Nicholson, D. P., Khatiwala, S. and Heimbach, P. (2016). Noble gas tracers of ventilation during deep-water formation in the Weddell Sea, IOP Conf. Ser. Earth Environ. Sci., 35(1), 012019, doi:10.1088/1755-1315/35/1/012019.

Nicholson, D. P., & Feen, M. L. (2017). Air calibration of an oxygen optode on an underwater glider. Limnology and Oceanography: Methods, 15(5), 495-502.

Odum, H. T. (1956). Primary production in flowing waters, Limnol. Oceanogr., 1(2), 102–117.

Omand, M., Cetinić, I., & Lucas, A. (2017). Using Bio-Optics to Reveal Phytoplankton Physiology from a Wirewalker Autonomous Platform. Oceanography, 30(2), 128–131. https://doi.org/10.5670/oceanog.2017.233

Osborn, T. R., & Cox, C. S. (1972). Oceanic fine structure. Geophysical Fluid Dynamics, 3(4), 321-345.

Owens, W. B., & Wong, A. P. (2009). An improved calibration method for the drift of the conductivity sensor on autonomous CTD profiling floats by θ–S climatology. Deep Sea Research Part I: Oceanographic Research Papers, 56(3), 450-457.

Palevsky, H. I. and Doney, S. C. (2018). How Choice of Depth Horizon Influences the Estimated Spatial Patterns and Global Magnitude of Ocean Carbon Export Flux, Geophys. Res. Lett., 45(9), 4171–4179, doi:10.1029/2017GL076498, 2018.

Pelland, N. A., Eriksen, C. C., & Cronin, M. F. (2017). Seaglider surveys at Ocean Station Papa: Diagnosis of upper-ocean heat and salt balances using least squares with inequality constraints. Journal of Geophysical Research: Oceans, 122(6), 5140-5168.

Plant, J. N., Johnson, K. S., Sakamoto, C. M., Jannasch, H. W., Coletti, L. J., Riser, S. C. and Swift, D. D. (2016). Net community production at Ocean Station Papa observed with nitrate and oxygen sensors on profiling floats, Glob. Biogeochem. Cycles, 30(6), 2015GB005349, doi:10.1002/2015GB005349, 2016.

Rasse, R., Dall'Olmo, G., Graff, J., Westberry, T. K., van Dongen-Vogels, V. and Behrenfeld, M. J. (2017). Evaluating Optical Proxies of Particulate Organic Carbon across the Surface Atlantic Ocean, Front. Mar. Sci., 4, doi:10.3389/fmars.2017.00367.

Redfield, A. C., Ketchum, B. H., & Richards, F. A. (1963). The influence of organisms on the composition of seawater. The sea, 2, 26-77.

Risien, C., and Chelton, D. (2008). A global climatology of surface wind and wind stress fields from eight years of QuikSCAT scatterometer data. Journal of Physical Oceanography, 38(11), 2379–2413.

Roach, C. J., Balwada, D., & Speer, K. (2018). Global observations of horizontal mixing from Argo float and surface drifter trajectories. Journal of Geophysical Research: Oceans, 123(7), 4560-4575.

Roemmich, D. (2019). On the Future of Argo: A Global, Full-Depth, Multi-Disciplinary Array. Frontiers in Marine Science, 6, 1–28. https://doi.org/10.3389/fmars.2019.00439.

Roesler, C., Uitz, J., Claustre, H., Boss, E., Xing, X., Organelli, E., Briggs, N., Bricaud, A., Schmechtig, C., Poteau, A., D'Ortenzio, F., Ras, J., Drapeau, S., Haëntjens, N. and Barbieux, M. (2017). Recommendations for obtaining unbiased chlorophyll estimates from *in situ* chlorophyll fluorometers: A global analysis of WET Labs ECO sensors, Limnol. Oceanogr. Methods, 15(6), 572–585, doi:10.1002/lom3.10185.

Rosso, I., M. R. Mazloff, A. Verdy, and L. D. Talley (2017), Space and time variability of the Southern Ocean carbon budget, *Journal of Geophysical Research: Oceans*, *9*(6805), 596, doi:10.1017/CBO9780511977817.

Rudnick, D. L. (2016). Ocean Research Enabled by Underwater Gliders, Annu. Rev. Mar. Sci., 8(1), null, doi:10.1146/annurev-marine-122414-033913.

Sackmann, B. S., Perry, M. J., & Eriksen, C. C. (2008). Seaglider observations of variability in daytime fluorescence quenching of chlorophyll-a in Northeastern Pacific coastal waters. Biogeosciences Discussions, 5(4), 2839-2865.

Sauzède, R., Claustre, H., Uitz, J., Jamet, C., Dall'Olmo, G., D'Ortenzio, F., Gentili, B., Poteau, A., and Schmechtig, C. (2016). A neural network-based method for merging ocean color and Argo data to extend surface bio-optical properties to depth: Retrieval of the particulate backscattering coefficient, J. Geophys. Res. Oceans, 121, 2552–2571, https://doi.org/10.1002/2015JC011408.

Siegel, D. A., Cetinić, I., Graff, J. R., Lee, C. M., Nelson, N., Perry, M. J., ... & Zhang, X. (2021). An operational overview of the EXport Processes in the Ocean from RemoTe Sensing (EXPORTS) Northeast Pacific field deployment.

Stanley, R. H., Jenkins, W. J., Lott III, D. E., & Doney, S. C. (2009). Noble gas constraints on air-sea gas exchange and bubble fluxes. Journal of Geophysical Research: Oceans, 114(C11).

Takeshita, Y., Martz, T. R., Johnson, K. S., Plant, J. N., Gilbert, D., Riser, S. C., et al. (2013). A climatology-based quality control procedure for profiling float oxygen data. Journal of Geophysical Research: Oceans, 118(10), 5640–5650. https://doi.org/10.1002/jgrc.20399

Takeshita, Y., Jones, B. D., Johnson, K. S., Chavez, F. P., Rudnick, D. L., Blum, M., Conner, K., Jensen, S., Long, J. S., Maughan, T., Mertz, K. L., Sherman, J. T. and Warren, J. K. (2021). Accurate pH and O2 Measurements from Spray Underwater Gliders, J. Atmos. Ocean. Technol., 38(2), 181–195, doi:10.1175/JTECH-D-20-0095.1.

Thomalla, S. J., Racault, M.-F., Swart, S. and Monteiro, P. M. S. (2015). High-resolution view of the spring bloom initiation and net community production in the Subantarctic Southern Ocean using glider data, ICES J. Mar. Sci., 72(6), 1999–2020, doi:10.1093/icesjms/fsv105.

Thompson, A. F., Gille, S. T., MacKinnon, J. A., & Sprintall, J. (2007). Spatial and Temporal Patterns of Small-Scale Mixing in Drake Passage. Journal of Physical Oceanography, 37(3), 572–592. https://doi.org/10.1175/jpo3021.1

Tijssen, S. B. (1979). Diurnal oxygen rhythm and primary production in the mixed layer of the Atlantic Ocean at 20°N, Neth. J. Sea Res., 13(1), 79–84, doi:10.1016/0077-7579(79)90034-6.

Wang, B., Fennel, K., Yu, L., & Gordon, C. (2020). Assessing the value of biogeochemical Argo profiles versus ocean color observations for biogeochemical model optimization in the Gulf of Mexico. Biogeosciences, 17(15), 4059-4074.

Wanninkhof, R., Asher, W. E., Ho, D. T., Sweeney, C., & McGillis, W. R. (2009). Advances in quantifying air-sea gas exchange and environmental forcing. Annual review of marine science, 1, 213-244.

Wanninkhof, R. (2014). Relationship between wind speed and gas exchange over the ocean revisited, Limnol. Oceanogr. Methods, 12(6), 351–362, doi:10.4319/lom.2014.12.351.

Wanninkhof, R., Pickers, P. A., Omar, A. M., Sutton, A., Murata, A., Olsen, A., ... & Schuster, U. (2019). A surface ocean CO2 reference network, SOCONET and associated marine boundary layer CO2 measurements. Frontiers in Marine Science, 6, 400.

Weeding, B. and Trull, T. W. (2014). Hourly oxygen and total gas tension measurements at the Southern Ocean Time Series site reveal winter ventilation and spring net community production, J. Geophys. Res. Oceans, 119(1), 348–358, doi:10.1002/2013JC009302.

Weiss, R. F. (1974). Carbon dioxide in water and seawater: the solubility of a non-ideal gas, Mar. Chem., 2(3), 203–215, doi:10.1016/0304-4203(74)90015-2.

Westberry, T., Behrenfeld, M. J., Siegel, D. A. and Boss, E. (2008). Carbon-based primary productivity modeling with vertically resolved photoacclimation, Glob. Biogeochem. Cycles, 22(2), GB2024, doi:10.1029/2007GB003078.

Whalen, C. B., L. D. Talley, and J. A. MacKinnon (2012), Spatial and temporal variability of global ocean mixing inferred from Argo profiles, *Geophysical Research Letters*, *39*(18), doi:10.1029/2012GL053196.

White, A. E., Barone, B., Letelier, R. M. and Karl, D. M. (2017). Productivity Diagnosed from the Diel Cycle of Particulate Carbon in the North Pacific Subtropical Gyre, Geophys. Res. Lett., 2016GL071607, doi:10.1002/2016GL071607.

Whitt, D. B., Lévy, M., & Taylor, J. R. (2019). Submesoscales enhance storm-driven vertical mixing of nutrients: insights from a biogeochemical large eddy simulation. Journal of Geophysical Research: Oceans, 124(11), 8140-8165.

Williams, N. L., Juranek, L. W., Johnson, K. S., Feely, R. A., Riser, S. C., Talley, L. D., ... & Wanninkhof, R. (2016). Empirical algorithms to estimate water column pH in the Southern Ocean. Geophysical Research Letters, 43(7), 3415-3422.

Williams, N. L., Juranek, L. W., Feely, R. A., Russell, J. L., Johnson, K. S. and Hales, B. (2018). Assessment of the Carbonate Chemistry Seasonal Cycles in the Southern Ocean From Persistent Observational Platforms, J. Geophys. Res. Oceans, 123(7), 4833–4852, doi:10.1029/2017JC012917.

Wilson, J. M., Severson, R. and Beman, J. M. (2014). Ocean-Scale Patterns in Community Respiration Rates along Continuous Transects across the Pacific Ocean, PLoS ONE, 9(7), e99821, doi:10.1371/journal.pone.0099821.

Wolf-Gladrow, D. A., Zeebe, R. E., Klaas, C., Kortzinger, A., & Dickson, A. G. (2007). Total alkalinity: The explicit conservative expression and its application to biogeochemical processes. Marine Chemistry, 106(1–2), 287–300. https://doi.org/10.1016/j.marchem.2007.01.006.

Wu, L., Jing, Z., Riser, S., & Visbeck, M. (2011). Seasonal and spatial variations of Southern Ocean diapycnal mixing from Argo profiling floats : Nature Geoscience : Nature Publishing Group. Nature Geoscience, 4(6), 363–366. https://doi.org/10.1038/ngeo1156

Xing, X., Wells, M. L., Chen, S., Lin, S. and Chai, F.: Enhanced Winter Carbon Export Observed by BGC-Argo in the Northwest Pacific Ocean, Geophys. Res. Lett., 47(22), doi:10.1029/2020GL089847, 2020.

Yang, B., Emerson, S. R. and Bushinsky, S. M. (2017). Annual net community production in the subtropical Pacific Ocean from *in situ* oxygen measurements on profiling floats, Glob. Biogeochem. Cycles, 31(4), 2016GB005545, doi:10.1002/2016GB005545.

Yang, B., Boss, E. S., Haëntjens, N., Long, M. C., Behrenfeld, M. J., Eveleth, R. and Doney, S. C. (2020). Phytoplankton Phenology in the North Atlantic: Insights From Profiling Float Measurements, Front. Mar. Sci., 7, doi:10.3389/fmars.2020.00139.

Yang, B., Fox, J., Behrenfeld, M. J., Boss, E. S., Haëntjens, N., Halsey, K. H., ... & Doney, S. C. (2021). In situ estimates of net primary production in the western North Atlantic with Argo profiling floats. Journal of Geophysical Research: Biogeosciences, 126(2), e2020JG006116.

Zhurbas, V., Lyzhkov, D., & Kuzmina, N. (2014). Drifter-derived estimates of lateral eddy diffusivity in the world ocean with emphasis on the Indian Ocean and problems of parameterisation. Deep Sea Research Part I: Oceanographic Research Papers, 83, 1-11.